Multimotor transport in constitutive exocytosis

Andrea Serra Marques

ISBN: 978-94-6108-997-7

The studies described in this thesis were performed at the Department of Cell Biology of the Erasmus MC in Rotterdam and at the division of Cell Biology at the Faculty of Science of the Utrecht University in Utrecht, The Netherlands.

This research was supported by Fundação para a Ciência e a Tecnologia (FCT) fellowship awarded to Andrea Serra Marques and by the Netherlands Organization for Scientific Research (NWO) CW ECHO grant awarded to Anna Akhmanova.

Layout and printing by: Gildeprint, The Netherlands

Cover: Colorfull tracking - colored tracks represent maximum intensity projections of Rab6-positive vesicle movements from the Golgi to the cell periphery in a HeLa cell.

© 2015 by Andrea Margarita Afonso Serra Marques

All rights reserved.

Multimotor transport in constitutive exocytosis

Multimotor transport in constitutieve secretie

(met een samenvatting in het Nederlands)

Proefschrift
ter verkrijging van de graad van doctor
aan de Universiteit Utrecht op gezag van de rector magnificus,
prof. dr. G. J. van der Zwaan,
ingevolge het besluit van het college voor promoties
in het openbaar te verdedigen
op woensdag 10 juni 2015 des middags te 2.30 uur

door

Andrea Margarita Afonso Serra Marques

geboren op 1 november 1985
te Caracas, Venezuela

Promotor: Prof. dr. A.S. Akhmanova

I was taught that the way of progress was neither swift nor easy.
Marie Curie

Para os meus Pais e para a minha irmã Teresita

Contents

Scope of the thesis **9**

Chapter 1 Introduction - Mechanisms of microtubule-based membrane transport **11**

- 1 General introduction 13
- 2 Microtubule-based motor proteins 13
  - 2.1 Kinesin superfamily 15
  - 2.2 Dynein 15
  - 2.2.1 Dynactin 18
- 3 General principles of motor-cargo interaction and transport mechanisms of specific cargo 19
  - 3.1 Transmembrane motor receptors 21
  - 3.2 Adaptor proteins and small GTPases 22
  - 3.3 Lipid-binding proteins in motor recruitment 24
  - 3.4 Transport mechanisms of specific cargo 24
    - 3.4.1 Mitochondria 24
    - 3.4.2 Endoplasmic Reticulum (ER) 25
    - 3.4.3 Golgi Apparatus 26
    - 3.4.4 Golgi - ER 26
    - 3.4.5 Post-Golgi carriers 26
    - 3.4.6 Endosomes and lysosomes 27
    - 3.4.7 Other organelles 27
- 4 Regulation of Transport 28
  - 4.1 Control of motor-adaptor attachment 28
  - 4.2 Control of motor-microtubule attachment and motor activity 29
- 5 Bidirectional cargo transport by multiple motors 32

Chapter 2 BICD2, dynactin, and LIS1 cooperate in regulating dynein recruitment to cellular structures **45**

Chapter 3 Bicaudal D family adaptor proteins control the velocity of dynein-based movements **71**

Chapter 4 The kinesin-3 family member KIF13B promotes transport of exocytotic carriers **99**

Chapter 5 KIDINS220 links KIF13B to the Dystrophin Associated Protein Complex **133**

Chapter 6 Characterization of docking and fusion machineries for Rab6-secretory vesicles **151**

Chapter 7 General Discussion **183**
- 7.1 Cargo selection and regulation of transport by adaptor proteins 185
- 7.2 Transport by multiple motors and regulation of transport velocity 187
- 7.3 KIF13B and its possible roles in cortical organization and neuronal function 189
- 7.4 Docking and fusion of Rab6 secretory vesicles with the plasma membrane 191
- 7.5 Future perspectives 192

Summary **201**
Samenvatting **203**
Portfolio **205**
Curriculum vitae **207**
List of publications **209**
Acknowledgements **211**

Scope of the thesis

Intracellular trafficking controls numerous cellular functions by promoting the correct sorting, transport and delivery of cargos in the cell. Multiple regulatory mechanisms acting at different trafficking steps rely on the dynamic microtubule system and associated molecular motors, dynein and kinesins. The aim of this thesis is to dissect the mechanisms underlying cargo selection and cargo transport by adaptor proteins and microtubule motors and investigate possible connections between the docking and fusion machineries essential for the delivery of cellular content.

In **chapter 1** we give an overview of the current knowledge of microtubule-based motors and discuss the general principles of transport of different membrane organelles. In addition, the mechanisms of transport regulation and bidirectional transport by multiple motors are discussed.

In **chapter 2** we show that the adaptor protein BICD2 forms a triple complex with dynein and dynactin both in vivo and in vitro and promotes a stable interaction between dynein and dynactin.

In **chapter 3**, we analyse the effect of different kinesins on the motility of Rab6-positive vesicles by using an inducible dimerization system and show that kinesin-1 and kinesin-3 can differently modulate microtubule plus-end vesicle velocity. Additionally, we demonstrate that the Bicaudal D family proteins BICD2 and BICDR-1 differently regulate the velocity of dynein-based movements and consequently control the distribution of transport carriers.

In **chapter 4** we show that the kinesin-3 family member KIF13B promotes the transport of carriers of constitutive secretion to the cell periphery and study motor distribution on endogenous moving cargo in the context of multimotor transport.

In **chapter 5** we explore the relationship between KIF13B and its newly identified binding partner KIDINS220 and discuss the possible roles of this interaction in podosomes and neurons.

In **chapter 6** we investigate the molecular links between the docking and fusion machineries responsible for the fusion of exocytotic carriers with the plasma membrane. Additionally, we suggest a new function for the EHD endocytic family of proteins in mediating the interplay between the docking and fusion machineries of exocytotic carriers.

In **chapter 7** we discuss the results of the studies described in this thesis and present future research directions in light of the recent technical advances.

1

Introduction

Mechanisms of microtubule-based membrane transport

Andrea Serra-Marques

1. General Introduction

Intracellular trafficking is an essential cellular mechanism, which is required for cell function, homeostasis, morphogenesis, polarity and signaling. During the past decades, an extensive field of research has developed and contributed to a better understanding of how accurate sorting, transport and delivery of different cargoes are regulated. The cytoskeleton, a complex network of filamentous polymers and regulatory proteins consisting of microtubules, actin, intermediate filaments and other filamentous structures, plays a pivotal role in these processes. It is well known that intracellular transport is driven by motor proteins that directionally move cargo either along actin filaments – myosins – or on microtubules – kinesins and dyneins (Vale, 2003). Here, we will focus on the role of microtubule-based transport, discussing the mechanisms of motility of different membrane organelles. We will discuss the key regulatory mechanisms within this specific type of transport, namely motor-cargo and motor-adaptor interaction, motor activity and regulation of bidirectional transport.

2. Microtubule-based motor proteins

Microtubules are filamentous structures consisting of α- and β-tubulin heterodimers that display a dynamic behavior, switching between phases of polymerization (growth) and depolymerization (shrinkage), a phenomenon known as dynamic instability (Akhmanova and Steinmetz, 2008; Kirschner and Mitchison, 1986).

Being polarized structures, microtubules have an end that grows fast and is more dynamic, called the plus end, and an end that grows slow and is less dynamic, called the minus end (Gouveia and Akhmanova, 2010; Summers and Kirschner, 1979). Early studies performed using squid giant axons already suggested that the movement of organelles along microtubules can occur in opposite directions, and later work showed that it is driven by two distinct classes of molecular motors, kinesin and dynein (Hirokawa, 1998; Hirokawa et al., 1989; Vale, 1990). While most kinesins drive transport in the plus end direction, dynein moves cargo towards the minus end of microtubules.

Motor proteins (including myosins, which move along actin filaments) generally consist of a motor domain and a tail domain (Figure 1). The motor domain directly binds to microtubules and to ATP, the energy derived from the hydrolysis of which is converted into mechanical energy and force production required for movement (Vale, 2003; Verhey and Hammond, 2009). The motor domain is connected to the tail domain by a stalk. The tail region, which can also participate in motor regulation, is less conserved and generally mediates the binding to different cargos and adaptor proteins (Schlager and Hoogenraad, 2009; Vale, 2003).

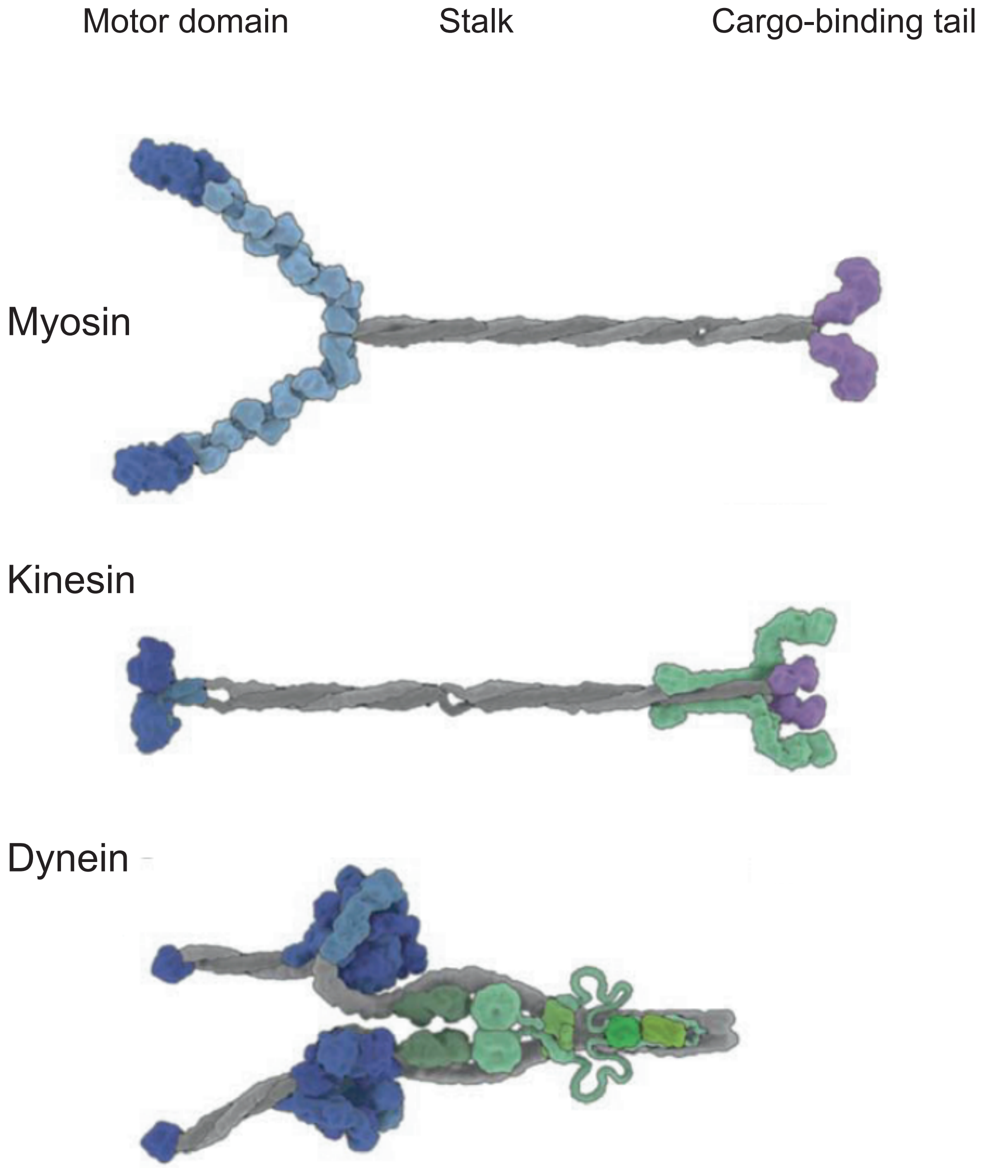
Motor domain
Stalk
Cargo-binding tail
Myosin
Kinesin
Dynein

Figure 1: Representative structures of the three families of cytoskeletal motor proteins.
The motor regions are represented in blue. The cargo-binding regions responsible for cargo attachment are shown in purple. The intermediate chains and additional subunits involved in motor dimerization, processivity and cargo recognition are represented in green. Modified from (Carter, 2013).

2.1 Kinesin superfamily

The kinesin superfamily of proteins comprises more than 40 homologues, which are sub-divided into fifteen families (kinesin-1 to kinesin-14B) according to their phylogeny (Hirokawa et al., 2009; Lawrence et al., 2004; Miki et al., 2005) (Figure 2).

A kinesin motor protein generally consists of a motor domain responsible for movement, a neck linker and a neck coiled coil region important for motor activity, and a stalk and tail regions that regulate dimerization, motor activity and the interaction with cargos and adaptor proteins. The motor domain comprises a P-loop that binds ATP, with the energy from ATP hydrolysis converted into mechanical energy and force production required for the movement along microtubule tracks (Marx et al., 2009; Schnitzer and Block, 1997; Verhey et al., 2011) . Kinesins can be classified into N-kinesins, C-kinesins and M-kinesins, depending on whether the motor domain is located at the N-terminus, C-terminus or in the middle of the protein, respectively. N-kinesins walk towards the plus end of microtubules, while the C-kinesins (kinesin-14 members) move to the microtubule minus ends. M-kinesins, which belong to the kinesin-13 family do not undergo any directional motility and their main funtion is to promote microtubule depolymerization (Hirokawa et al., 2009; Hunter et al., 2003). Multiple studies have shown that the members of kinesin-8, 7, 13 and 14 families can also bind to the plus end of microtubules, where they promote microtubule depolymerization or dampening of microtubule dynamics (Gouveia and Akhmanova, 2010; Jiang and Akhmanova, 2011; Walczak, 2006)

Since their discovery, kinesins have been implicated in the transport of multiple membrane organelles, messenger RNAs (mRNA)s and in the positioning and dynamics of organelles and specialized structures such as the Golgi apparatus and the mitotic spindle (Civelekoglu-Scholey and Scholey, 2010; Gumy et al., 2014; Hirokawa and Noda, 2008; Hirokawa et al., 2009). Different regulatory mechanisms relevant for kinesin-based transport will be discussed later.

2.2 Dynein

Dyneins, in contrast to most of kinesins, are the molecular motors responsible for the transport of cargos to the minus end of microtubules. More than 15 genes encoding dynein heavy chain have been identified in most species, but the majority are axonemal, being involved in the bending of cilia and flagella (Kardon and Vale, 2009). Interestingly, there are only two dyneins known to funtion in the cytoplasm, namely cytoplasmic dynein 1 and cytoplasmic dynein 2. While cytoplasmic dynein 2 is more specialized and mainly engaged in retrograde intraflagellar transport, cytoplasmic dynein 1 (from now on generally called dynein) is involved in many cellular functions, being responsible for most of the minus end directed transport along microtubules (Kardon et al., 2009; Kardon and Vale, 2009). In budding yeast, dynein is important for nuclear positioning

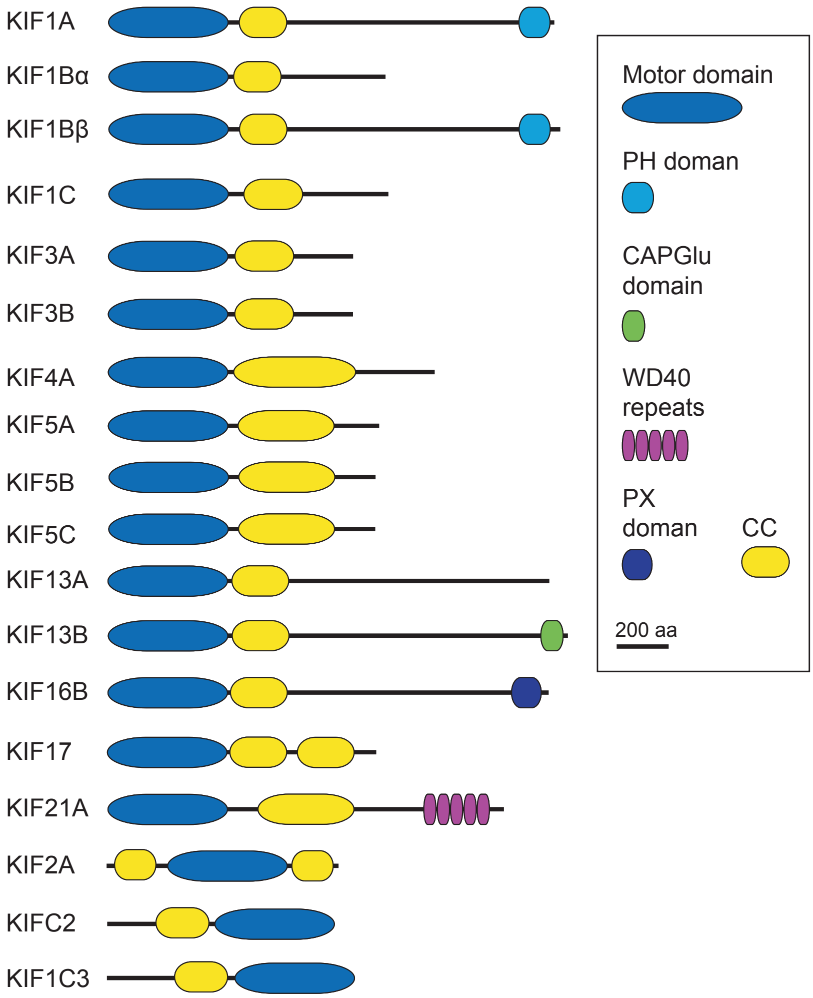
KIF1A
KIF1Bα
KIF1Bβ
KIF1C
KIF3A
KIF3B
KIF4A
KIF5A
KIF5B
KIF5C
KIF13A
KIF13B
KIF16B
KIF17
KIF21A
KIF2A
KIFC2
KIF1C3
Motor domain
PH doman
CAPGlu domain
WD40 repeats
PX doman
CC
200 aa

Figure 2: Schematic representation of the domain structure of the principle kinesins
Kinesins generally contain a motor domain responsible for movement, a neck linker and a neck coiled coil region important for motor activity and a stalk and tail regions that regulate dimerization, motor activity and the interaction with cargos and adaptor proteins. Kinesins with the motor domain at the N-terminus are generally called N-kinesins, while kinesins with the motor domain at the C-terminus or in the middle are called C-kinesins or N-kinesins, respectively. Some kinesins contain specific domains, such as pleckstrin homology (PH) and Phox homology (PX) domains, CAP-Gly domain (a conserved, Gly-rich domain found in several cytoskeleton-associated proteins) and the WD40 repeats. Reproduction of a scheme from (Hirokawa et al., 2009)

during cell division. In animals, it plays varied functions, including transport of multiple cargoes, such as organelles, lipid droplets, mRNA, proteins (Jha and Surrey, 2015; Kardon and Vale, 2009). During cell division, dynein participates in spindle formation and positioning, and in the silencing of the spindle assembly checkpoint prior to the anaphase onset (Griffis et al., 2007; Jha and Surrey, 2015; McGrail and Hays, 1997; Merdes et al., 2000). The size of the dynein motor is one of the most remarkable differences between dynein and kinesin: a typical dynein molecule has a mass of ~1.5 MDa, ~10 times larger than an average kinesin (Vallee et al., 1988). In terms of structure, dynein consists of a stalk, a motor domain and a tail domain. The 15 nm stalk separates the microtubule binding domain from the motor domain. This structure configuration is distinct from kinesin and myosin, where the cytoskeletal polymer-binding site and catalytic site are integrated within a single globular motor domain (Carter et al., 2008).

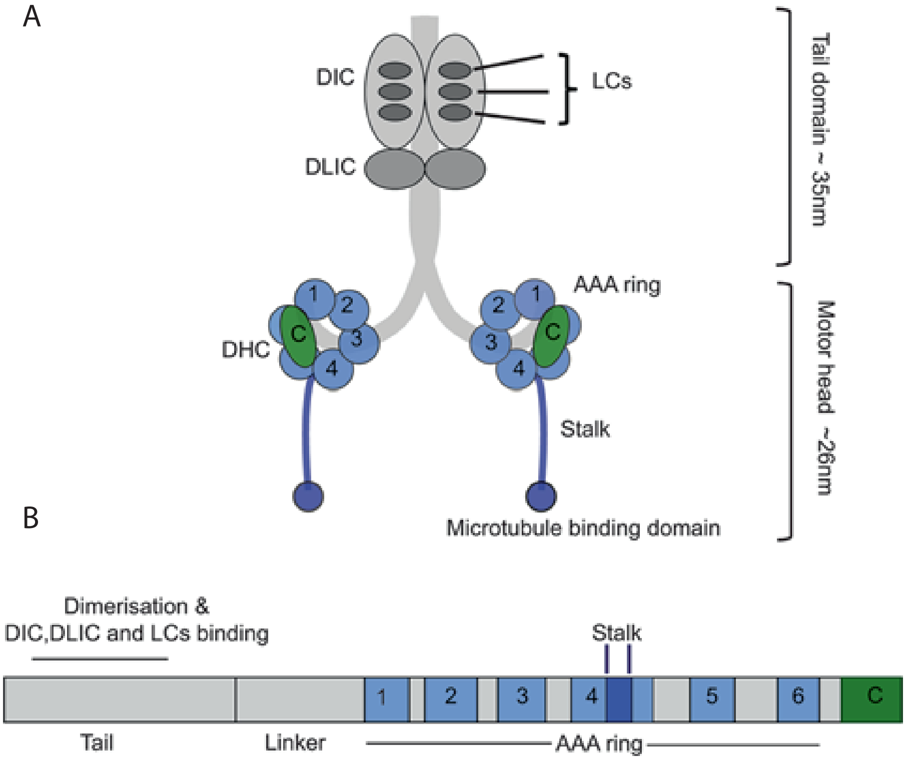
A
DIC
LCs
DLIC
Tail domain ~ 35nm
AAA ring
1
2
3
4
C
DHC
Stalk
Motor head ~26nm
Microtubule binding domain
B
Dimerisation &
DIC,DLIC and LCs binding
Stalk
1
2
3
4
5
6
C
Tail
Linker
AAA ring

Figure 3: Composition and domain structure of cytoplasmic dynein
(**A**) Composition of the dynein complex. Cytoplasmic dynein heavy chains (DHCs), with their motor and tail domains are shown in grey. The motor domain is represented in blue, and the stalk projecting from the motor domain and microtubule binding domain are shown in dark blue. The linker is represented in green. The non-catalytic subunits the dynein intermediate chain (DIC), dynein light intermediate chain (DLIC) and the light chains (LCs) are also shown (**B**) Domain organization of the DHC sequence.
The positions of the dimerization region and of the binding region for the smaller subunits are indicated. Adapted from (Jha and Surrey, 2015)

The motor domain of dynein consists of six AAA+ ATPase domains arranged in a circle; four of these domains (AAA1-4) can bind and hydrolyze ATP. However, mutagenesis studies have revealed that only domains AAA1 and AAA3 are required for motility (with the AAA1 domain being the main site for ATP hydrolysis), while the other domains might have a structural and regulatory role (Cho et al., 2008; Kardon and Vale, 2009; Kon et al., 2004; Reck-Peterson and Vale, 2004).

The coiled coil stalk projects directly from the AAA4 domain and connects the motor domain to the microtubule (Burgess et al., 2003; Gee et al., 1997). A linker, dynein's mechanical element present at the C-terminal of the motor head, also binds to the catalytic ring, and recent studies have shown that ATP hydrolysis promotes linker remodeling and microtubule affinity regulation (Bhabha et al., 2014; Schmidt et al., 2014). The tail domains of two dynein heavy chains (DHC) mediate homodimerization and constitute a scaffold for the five non-catalytic dimeric subunits. The intermediate chain (IC) and light intermediate chain (LIC) bind directly to the tail of the heavy chain, while the smaller light chains, light chain 8 (LC8), light chain 7 (LC7) and T-complex testis specific protein 1 (TCText1), bind to the dynein complex through the intermediate chain (Jha and Surrey, 2015; Kardon and Vale, 2009; Pfister et al., 2006) (Figure 3). Dynein binds to multiple proteins that are essential to adapt the motor to its many cellular functions (Vale, 2003). One of them is the multisubunit protein complex dynactin.

2.2.1 Dynactin

Dynactin is a multisubunit protein complex and one of dynein's key interactors required for most of cytoplasmic dynein activities in the cell (Schroer, 2004). Dynactin serves as a platform for cargo interaction, mediating the association of dynein with some cargos, and it is also involved in the targeting and regulation of dynein processive movement (Kardon and Vale, 2009).

Dynactin is a large complex comprised of 11 different subunits, and its molecular mass is approximately 1 MDa, similar to the size of dynein. The dynactin molecule is asymmetric, and Electron Microscopy (EM) studies revealed that is composed of 2 structural domains – a ~ 10x40 nm rod and a 25-50 nm arm that projects from the rod. (Schroer, 2004). The rod is a short filament of actin-related protein 1 (Arp1), and its main function might be to mediate the association with cargos through the interaction with the βIII spectrin present on the membrane of several cargos. The two ends of the Arp1 filament are composed of additional subunits. The pointed end is composed of ARP11, p62, p25 and p27 and might be involved in cargo binding. The barbed end associates with the heterodimeric actin-capping protein CapZ. The Arp1 filament is bound to a dimer of p150glued, a tetramer of p50 (or dynamitin, because its overexpression dissociates the dynactin complex) and p24 (Figure 4).

The arm projected form the Arp1 filament consists of the N-terminal coiled coil (CC1) of the p150glued dimer, which contains a microtubule-binding cytoskeleton associated protein Gly-rich (CAP-Gly) domain (Kardon and Vale, 2009; Steinmetz and Akhmanova, 2008). p150glued interacts directly with dynein and it promotes dynein processivity, possibly by binding to microtubules through its CAP-Gly domain or the adjacent positively charged regions but might also involve other mechanisms (see below).

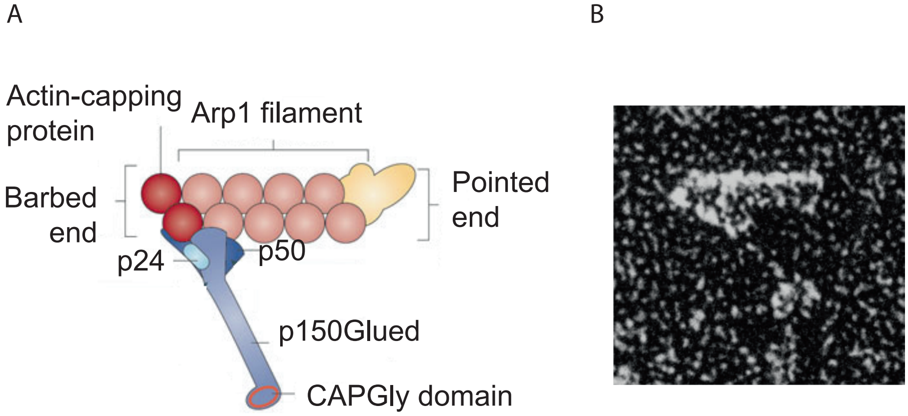

Figure 4: Composition and domain structure of the dynactin complex
The dynactin complex is composed of a rod-like Arp1 filament with a barbed and a pointed end and a p150Glued arm that projects from the rod and contains a microtubule-binding domain at the tip. Additional subunits are associated. The EM structure of the dynactin complex is shown on the right. Scheme modified from (Kardon and Vale, 2009) and EM image from (Schroer, 2004).

3. General principles of motor-cargo interaction and transport mechanisms of specific cargo

In the cell, several trafficking systems rely on the microtubule network for the transport of their membrane compartments. One of the most important transport systems in the cell is the exocytotic pathway, which is intimately connected to the lysosomal and endocytic pathways (Figure 5). New proteins are synthesized in the Endoplasmic Reticulum (ER) and transported to the Golgi apparatus, where they will be sorted and packed into vesicles to be secreted or inserted into the membrane (Bonifacino and Glick, 2004; Pfeffer, 2007). The endocytic system is composed of a group of membrane-enclosed compartments with varied identities that perform specific functions associated with the uptake, recycling and catabolism of different cellular components.

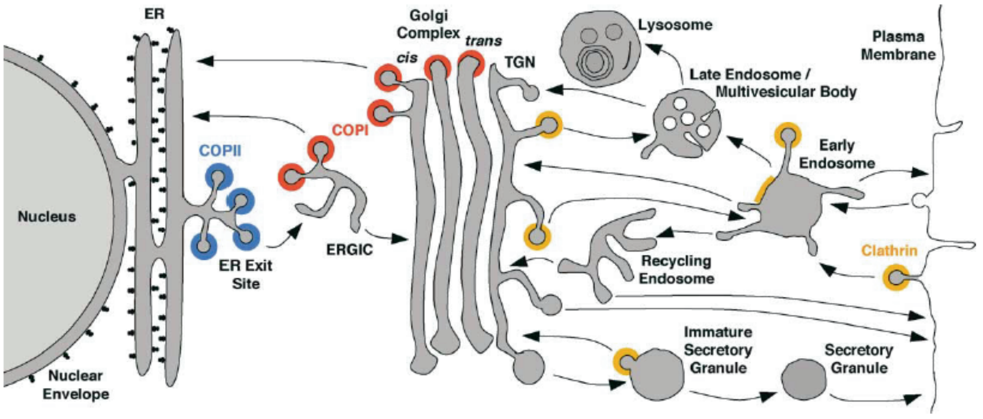
ER
Golgi Complex
cis
trans
TGN
Lysosome
Plasma Membrane
Late Endosome / Multivesicular Body
COPI
COPII
Early Endosome
Nucleus
ERGIC
ER Exit Site
Clathrin
Recycling Endosome
Immature Secretory Granule
Secretory Granule
Nuclear Envelope

Figure 5: Intracellular transport pathways
Schematic representation of the secretory, lysosomal and endocytic pathways. Transport steps are indicated by arrows. Colors indicate the known or presumed locations of COPII (blue), COPI (red), and clathrin (orange). Adapted from (Bonifacino and Glick, 2004).

Early, late and recycling endosomes, as well as lysosomes are the organelles constituting this system, and communication between these organelles is essential to target proteins that were internalized from the plasma membrane for degradation or for recycling of the components back to the cell surface. Several endocytic vesicles deliver internalized content from the plasma membrane into the early endosome, the main sorting platform of the endocytic pathway. From the endosome, cargo is sorted for degradation, where endosomes mature and fuse with the lysosome, or for recycling back to the cell surface or trans-Golgi network (TGN), through recycling endosomes. Vesicles from the TGN can also directly fuse with the early endosome (Bonifacino and Rojas, 2006; Granger et al., 2014; Grant and Donaldson, 2009).

In order to be transported along the cytoskeleton, membranes need to be linked to molecular motors. There are different mechanisms for motor-cargo attachment (Figure 6) and some will be described below.

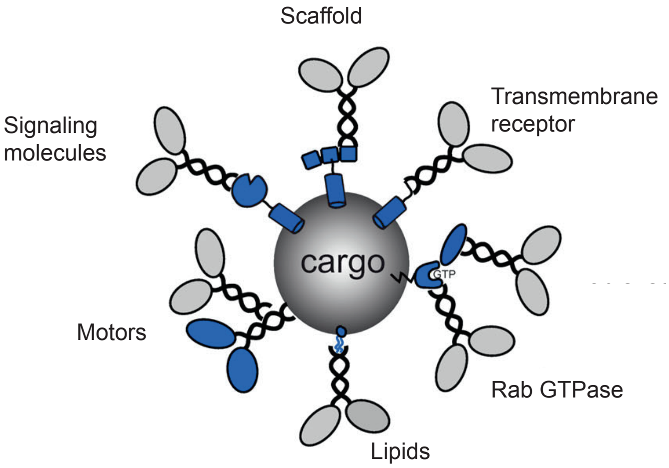

Figure 6: Motor-cargo interaction
Schematic representation of different mechanisms of motor-cargo interaction. Motor proteins can interact with cargos through transmembrane receptors, scaffolding complexes, lipids, Rab GTPases and effectors or by associating with other molecular motors or signaling molecules. Adapted from (Schlager and Hoogenraad, 2009).

3.1. Transmembrane motor receptors

One of the mechanisms of motor-cargo interaction consists of the binding of a motor protein to receptors or membrane proteins present on membrane cargos. The first kinesin receptor identified was kinectin, a transmembrane ER protein reported to anchor KIF5 (Kinesin-1) to membrane vesicles, promoting active transport (Kumar et al., 1995; Toyoshima et al., 1992). Regardless of its early identification, its relevance is still under debate (Hirokawa et al., 2009; Plitz and Pfeffer, 2001). Kinesin-1 has also been suggested to bind directly to the transmembrane amyloid precursor protein (APP), promoting its axonal transport (Kamal et al., 2000; Satpute-Krishnan et al., 2006). However, some studies have contradicted this model and suggested that the c-Jun N-terminal kinase interacting protein (JIP) and the small GTPase Rab3 might be required for the binding of kinesin-1 to APP (Inomata et al., 2003; Lazarov et al., 2005; Szodorai et al., 2009). KIF5B also interacts directly with the neurotrophin receptor p75 during polarized transport in MDCK cells (Jaulin et al., 2007).

Direct interactions between dynein and transmembrane proteins have also been reported. The dynein light chain Tctex-1 was reported to directly interact with the photoreceptor rhodopsin and rhodopsin mutations that cause retinal degeneration impair the binding to dynein (Tai et al., 1999). Tctex-1 was also found to bind neurotrophin Trk receptors, suggesting a role for the dynein motor in the retrograde transport of Trk receptors (Yano et al., 2001). Additionally, the same dynein subunit binds the receptor for the neurotrophic poliovirus CD115, promoting its axonal retrograde transport (Mueller et al., 2002).

Additional interactions between other dynein subunits and transmembrane proteins have been described, but some studies have disputed their relevance (Akhmanova and Hammer, 2010).

3.2. Rab GTPases and adaptor proteins

One of the largest groups of proteins involved in the regulation of intracellular trafficking are the Rab GTPases. They are involved in several steps of vesicle trafficking, including vesicle budding and coat assembly, transport along cytoskeletal tracks and tethering and fusion (Cai et al., 2007; Stenmark, 2009). Interestingly, the number of Rab genes in a certain organism is proportional to the complexity of the genome; the yeast *S. cerevisiae* has 11 Rab genes, *D. melanogaster* has 26, *C. elegans* has 29 and in humans there are more than 60 different Rab proteins (Bock et al., 2001; Stenmark, 2009). Only a subset of Rabs are conserved from yeast to humans (Rab1/Ypt1, Rab5/Ypt5, Rab6/Ypt6, Rab7/Ypt7, and Rab11/Ypt31), and only 17 are shared by *C. elegans*, *D. melanogaster* and humans (Fukuda, 2008). Most of Rab isoforms are only present in higher eukaryotes, and this might reflect the need for more specialized membrane-associated processes in specific cell types. Like all members of the Ras superfamily, Rab GTPases act as molecular switches, alternating between a GTP-bound active state and a GDP-bound inactive state (Stenmark, 2009). They exist in their inactive GDP form in the cytoplasm, associated with the GDP-dissociation inhibitor (GDI), which occludes the hydrophobic C-terminal prenyl anchor of the Rab. With the aid of a GDF (GDI displacement factor), Rabs are recruited and anchored to the membrane via a prenyl group (Dirac-Svejstrup et al., 1997). The membrane-anchored Rab is subsequently activated by a GEF (Guanine nucleotide exchange factor), which catalyzes the replacement of GDP by GTP (Soldati et al., 1994; Ullrich et al., 1994). Once activated, the Rab interacts with downstream effectors and is inactivated when GTP is hydrolyzed, a reaction mediated by a GAP (GTPase-activating protein) (Rybin et al., 1996) (Figure 7).

Despite their wide range of functions, Rabs are key regulators of the attachment of cellular cargos to microtubule motors. Several direct interactions between motors and Rabs have been reported. One of the first direct interactions between a Rab and a kinesin is the interaction between Rab6 and KIF20A (Rab6 kinesin, kinesin-6) (Echard et al., 1998). Another example is the interaction between Rab14 and KIF16B (kinesin 3), required for the transport of fibroblast growth factor receptor 2 (FGFR2)-containing vesicles from the Golgi to the plasma membrane, in a GTP-dependent manner (Ueno et al., 2011). More recently, the interaction between KIF13A and Rab11 was reported and proposed to be required for the transport of recycling endosomes (Delevoye et al., 2014). Despite some examples of direct motor-Rab binding, small GTPases function is often mediated by adaptor proteins. Rab6 has been shown to associate with KIF5B (kinesin-1) through to

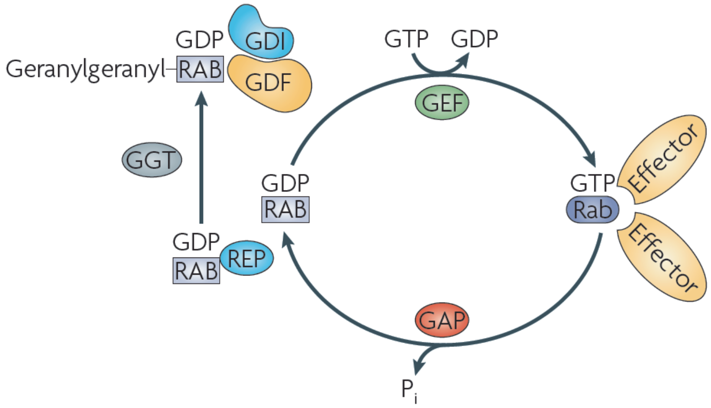

Figure 7: Rab GTPase cycle
The GDP-Rab is recognized by a Rab escort protein (REP) and a geranylgeranyl transferase (GGT) that geranylgeranylates the Rab, which will be consequently recognized by a Rab GDP dissociation inhibitor (GDI). The GDP-Rab/GDI complex is targeted to the membrane through the interaction with a membrane-bound GDI displacement factor (GDF).The conversion from GDP to GTP-bound state is catalyzed by a guanine nucleotide exchange factor (GEF). In the active GTP-bound form, the Rab interacts with multiple effectors. It is converted into an inactive state by the action of a GTPase-activating protein (GAP) that stimulates GTP hydrolysis and release of an inorganic phosphate (Pi). Adapted from (Stenmark, 2009)

the adaptor protein Bicaudal D2 (BICD2), promoting processive transport of exocytotic vesicles from the Golgi to the plasma membrane (Grigoriev et al., 2007). Interestingly, Rab6 also associates with KIF1C (Kinesin-3) through Bicaudal D related protein 1 (BICDR-1), promoting the anterograde transport of Rab6 secretory carriers in the axon of hippocampal neurons (Schlager et al., 2010). The Rab3 effector DENN/MADD mediates the association of Rab3 to KIF1Bβ and KIF1A, promoting the transport of axonal Rab3-containing vesicles in hippocampal neurons (Niwa et al., 2008). Rab11A was reported to regulate the trafficking of recycling endosomes by associating with KIF3B (kinesin-2) through its effector RIP11/FIP5 (Schonteich et al., 2008). The same molecular complex was recently shown to be required for endosome apical transport during epithelial lumen formation (Li et al., 2014). Additionally, the Rab11 effector FIP3 has been shown to bind to kinesin-1, mediating the transport of FIP3-containing vesicles to the cleavage furrow during cytokinesis (Simon and Prekeris, 2008). More recently, Rab11 and KIF16B have been implicated in a new pathway mediating the transcytosis of the transferrin receptor, but the molecular links mediating this process are still not clear (Perez Bay et al., 2013). Rab27B forms a complex with Slp1 and CRMP-2 necessary for the binding to kinesin-1 and the transport of axonal TrKB-containing vesicles (Arimura et al., 2009).

Rab proteins can also associate with the dynein complex to promote transport towards the minus end of microtubules. Rab7 on late endosomes (LE) binds to two effectors, RILP and ORP1L, which promote the binding to the dynactin subunit p150^{glued}, which in turn recruits the dynein complex promoting the transport of late endosomes to the minus end of microtubules (Johansson et al., 2007). Interestingly, the Rab7-RILP- p150^{glued} complex can also associate with the Endoplasmic Reticulum (ER) protein VAP (VAMP [vesicle-associated membrane protein]-associated ER protein). VAP promotes uncoupling of the dynein complex from LE at LE-ER contact sites (in a mechanism dependent of cholesterol levels on the LE membrane), blocking the transport in the minus end direction and facilitating the transport of late endosomes to the plus end of microtubules (Rocha et al., 2009). Rab11 has been shown to bind to the dynein light intermediate chain 1 and 2 (DLIC1 and DLIC2) through the adaptor protein Rab11-FIP3, controlling the transport between sorting endosomes and recycling endosomes (Horgan et al., 2010a, b). Rab6 also associates with dynein, either through the binding to the dynactin subunit p150^{glued} or to the adaptors of the BICD family of proteins, promoting the transport of Rab6 secretory carriers (Hoogenraad et al., 2003; Matanis et al., 2002; Schlager et al., 2010; Short et al., 2002). Additionally, Rab3B has been shown to bind to the dynein subunit Tctex1, regulating the transport of osteoclastic vesicles and bone resorption (Pavlos et al., 2011). More recently, the small GTPase Arf1 was shown to associate with the dynein complex in the Golgi apparatus through the Golgi protein golgin160, contributing for Golgi integrity and possibly for ER to Golgi transport.

3.3. Lipid-binding proteins in motor recruitment

Lipids are important determinants of the identity of different organelles, and lipid composition can also influence motor recruitment to specific organelles. The kinesin-3 family members KIF1A/Unc-104 and KIF1Bβ contain a pleckstrin homology (PH) domain in the tail region, and have been shown to directly interact with PI(4,5)P2-containing synaptic vesicle precursors (Klopfenstein et al., 2002; Klopfenstein and Vale, 2004). KIF16B, another kinesin-3 family member, contains a PX domain that mediates the binding to PI(3)P on early endosomes (Hoepfner et al., 2005). Although lipid binding is important for motor-cargo binding, complementary recruitment mechanisms are often necessary to assure an efficient recruitment and transport of membrane organelles. One example is the aforementioned assembly of the complex KIF1A/1Bβ-Rab3-DENN/MADD necessary for the efficient transport of Rab3-positive synaptic vesicles into axons (Akhmanova and Hammer, 2010; Hirokawa et al., 2009; Niwa et al., 2008).

3.4. Transport mechanisms of specific cargo

3.4.1 Mitochondria

Mitochondria are double membrane organelles whose main function is the synthesis of ATP required for cell function and survival. Their function is particularly relevant in neurons, where high energy supplies are required for synaptic transmission, generation of action potentials and axonal growth (Lin and Sheng, 2015). Mitochondria are clustered in the cell body and transported into dendrites and axons, and even though their transport is dependent on both actin and microtubule cytoskeletons, the rapid and long distance transport is powered by microtubule based motors. Defects in mitochondria funtion and transport are linked to several neurological diseases, supporting their pivotal relevance in the establishment of functional neuronal circuits (Boldogh and Pon, 2007; Mattson et al., 2008). The bidirectional transport of mitochondria in axons and dendrites is powered by kinesins and dynein (Pilling et al., 2006) and their association is often mediated by adaptor proteins. KIF1Bβ (kinesin-3) has been shown to associate with mitochondria and to promote their transport *in vitro* (Nangaku et al., 1994) and studies performed in cells from KIF5B knockout mice revealed that kinesin-1 is essential for the transport of mitochondria to peripheral areas in the cell (Tanaka et al., 1998). The adaptor proteins syntabulin and RabBP2 have also been shown to promote the binding of Kinesin-1 to mitochondria (Hirokawa et al., 2009).

Genetic screens performed in *Drosophila* to uncover genes required for synaptic function identified the small GTPase Miro, anchored to the outer mitochondrial membrane, and the adaptor protein Milton (TRAK) as necessary for kinesin-mediated mitochondria anterograde axonal transport. Kinesin-1 associates with mitochondria through the interaction with TRAK, which in turn binds to Miro (Glater et al., 2006; Guo et al., 2005; Stowers et al., 2002; Wang and Schwarz, 2009) and direct interaction between kinesin-1 and Miro has also been reported (Macaskill et al., 2009). There are two TRAK proteins in mammals, TRAK1 and TRAK 2 (Brickley et al., 2005). A recent study has shown that the two TRAKs differently regulate transport of mitochondria – TRAK1 binds to both kinesin-1 and to dynein, promoting transport into axons, while TRAK2, which adopts a different conformation, predominantly binds to dynein and steers mitochondrial transport into dendrites (van Spronsen et al., 2013). This study shed light on the mechanisms of bidirectional transport of mitochondria, but further studies are required to fully understand how mitochondrial transport is regulated. Kinesin-dependent mitochondria transport has also been reported in non-neuronal cells (Boldogh and Pon, 2007).

3.4.2 Endoplasmic Reticulum

The ER protein kinectin was shown to bind to kinesin-1, what suggested that kinesin-1 was the motor protein involved in the extension of ER tubules (Santama et al., 2004; Toyoshima et al., 1992). Nevertheless, and as discussed by Hirokawa and colleagues (Hirokawa et al., 2009), the relevance of this interaction in ER dynamics is controversial. It was reported that knockdown of KIF5 (kinesin-1) or kinectin does not affect ER structure and dynamics (Plitz and Pfeffer, 2001; Tanaka et al., 1998) , but independent studies have reported that kinesin-1 promotes ER tubule extension towards the cell periphery and that this motility is dependent on the kinesin light chain splice form KLC1B. Additionally, it was shown that dynein drives fast movement of ER tubules towards the center of the cell (Wozniak et al., 2009) and the sliding of ER tubules along microtubules has been observed in different systems (Friedman et al., 2010; Hamada et al., 2014).

3.4.3 Golgi Apparatus

The Golgi apparatus is a dynamic organelle and the combined action of opposite motors is essential for its correct positioning in the cell. The kinesin-6 KIF20A (Rabkinesin 6) has been shown to associate to Golgi apparatus through the interaction with the small GTPase Rab6 (Echard et al., 1998). Additionally, the minus end directed kinesin KIFC3 and dynein have been shown to be required for proper Golgi formation, integrity and positioning (Echard et al., 1998; Harada et al., 1998; Xu et al., 2002; Yadav et al., 2012).

3.4.4 Golgi – Endoplasmic Reticulum

Transport along microtubules of cargo in small vesicles between the Golgi apparatus and the ER is bidirectional (Brown et al., 2014). Anterograde transport from the ER to the Golgi is normally mediated by COPII vesicles, while retrograde Golgi to ER transport is mediated by COPI vesicles. The ER to Golgi transport is powered by dynein, and it was shown that dynactin subunit p150glued interacts with Sec23, a subunit of the COPII complex, on the ER (Watson et al., 2005). Kinesin-1 and kinesin-2 have been reported to specifically promote the plus-end transport and recycling of pre-Golgi vesicles to the ER (Lippincott-Schwartz et al., 1995; Stauber et al., 2006).

3.4.5 Post-Golgi carriers

Post-Golgi carriers also use the microtubule system to reach their target destination. Several kinesins have been implicated in the transport of post-Golgi vesicles in different systems. The kinesin-3 family motor KIF13A is required for the transport of the mannose-6-phosphate receptor (M6PR) from the TGN to the plasma membrane (Nakagawa et al., 2000), and another kinesin-3 motor, KIF13B, has been recently implicated in the anterograde transport of VEGFR2-containing vesicles from the Golgi to the cell surface in epithelial cells during angiogenesis (Yamada et al., 2014). In MDCK cells, the polarized transport of post-Golgi vesicles containing the neurotrophin receptor p75 to the apical membrane is powered by kinesin-1 (Jaulin et al., 2007). Kinesin-1, in coordination with kinesin-3, has also been shown to promote the transport of Rab6 exocytotic vesicles from the Golgi to the plasma membrane. These carriers move bidirectionally along microtubules, and the role of dynein as the main driver of transport to the minus-end of microtubules is well established (Grigoriev et al., 2007; Hoogenraad et al., 2003; Schlager et al., 2014b; Short et al., 2002). It was also recently proposed that the kinesin-5 KIF11/Eg5 is required for the transport of the post-Golgi carriers CARTS (Carriers of the TGN to the cell Surface). A special case of post-Golgi cargo are synaptic vesicle precursors in neurons; as discussed above, kinesin-3 KIF1A (Unc104 in *C.elegans*) is the major motor responsible for their motility, although other kinesins, such as kinesin-1, might also be involved.

3.4.6 Endosomes and Lysosomes

Actin and microtubule motors power the transport and delivery of endocytic organelles to their target compartment, and the involvement of the dynein/dynactin complex has been implicated in multiple trafficking steps within the endocytic pathway. Early studies showed that in blastocysts of mice lacking the dynein heavy chain, endosomes and lysosomes are distributed throughout the cytoplasm and not concentrated in the proximity of the nucleus (Harada et al., 1998). Additionally, the dynein motor has been reported to interact with the mammalian sorting nexin 4 (SNX4) present on early endosomes (EE) and endosomal recycling compartment (ERC) through the linker protein WW domain-containing protein 1 (WWC1), promoting their transport to the juxtanuclear region. WWC1 depletion induces relocation of endocytic cargo to peripheral areas, further supporting the relevance of the dynein motor in the transport of endocytic compartments (Traer et al., 2007).

Concerning kinesin-based motility, the kinesin motors KIF16B, KIF13A, KIF13B (kinesin-3) and KIF3B (kinesin-2) have been implicated in the directional transport of early and recycling endosomes and lysosomes (Delevoye et al., 2014; Granger et al., 2014; Hoepfner et al., 2005; Kanai et al., 2014; Perez Bay et al., 2013; Schonteich et al., 2008). Interestingly, kinesin-1 and dynein also interact with ARF6 on recycling endosomes through their interaction with the adaptor proteins JIP3 and JIP4, controlling the bidirectional transport of endosomes to the intercellular bridge during cytokinesis (Montagnac et al., 2009). More recently, the adaptor protein Hook was identified as a factor required for both dynein and kinesin-mediated early endosome movement in the fungus *Aspergillus nidulans* (Bielska et al., 2014; Zhang et al., 2014). Most of motor protein-endosome interactions are mediated by GTPases associated with specific endocytic compartments, a classic mechanism of motor-cargo interaction. For more details on motor – endosome interactions mediated by GTPases please see section 3.2.

3.4.7 Other organelles

Several other organelles within the cell depend on the microtubule network for their efficient transport to the target destination. The motility of peroxisomes, the site of long-chain fatty acid catabolism, can be controlled by myosin, but dynein and kinesin can also transport peroxisomes both *in vivo* and *in vitro* (Kural et al., 2005; van der Zand and Tabak, 2013). The trafficking of phagosomes, specialized organelles responsible for the internalization and degradation of pathogenic elements, and lipid droplets, the regulators of lipid homeostasis, also depends on the bidirectional transport driven by kinesin-1 and dynein (Al-Haddad et al., 2001; Blocker et al., 1997; Welte et al., 2005). These two opposing microtubule motors have also been implicated in the transport of mRNAs assembled into ribonucleoprotein particles (mRNPs) from the cell body to specific locations in different cell types, regulating the local translation of specific mRNAs (Bullock, 2011; Gumy et al., 2013; Kanai et al., 2004). Although not discussed here, both kinesin (in this case kinesin-2) and dynein are essential for intraflagellar transport.

4. Regulation of transport

Microtubule-based transport is a multi-step process, where several factors must be tightly and simultaneously regulated. Motor activity, motor-cargo and motor-adaptor attachment, cytoskeletal organization, microtubule modifications and interaction between motors are all different layers of regulation that will ensure that a cargo is correctly loaded, transported and delivered at the appropriate target destination.

4.1 Control of motor-adaptor attachment

We have previously discussed different mechanisms of motor-cargo attachment, which in many cases is mediated by a small GTPase and/or adaptor proteins (section 3.2). GTPases normally bind to their effectors in the GTP-bound state, and for that reason the regulation of the GTP/GDP cycle is essential. For example, the kinesin KIF16B binds to the active GTP-bound Rab14, an interaction essential for the transport of fibroblast growth factor receptor 2 (FGFR2)-containing vesicles and early embryonic development (Ueno et al., 2011).

Signaling molecules can also regulate motor-adaptor interactions. One example is the association of the adaptor protein JIP1 with kinesin-1. JIP proteins also participate in the assembly of JNK signaling complexes by recruiting MAPKKK, MAPKK and JNK, and it has been shown that activation of MAPKKK or MAPKK induces kinesin release from cargo. This shows that JIP proteins not only directly link kinesin to cargo, but also control kinesin-cargo association by recruiting JNK pathway kinases (which are also transported by kinesin-1) (Horiuchi et al., 2007). Interestingly, it has been proposed that local activation of JNK induces a shift from kinesin to dynein-based motility, an effect that might be caused by the release of kinesin from cargo or from microtubules (Verhey and Hammond, 2009).

Calcium signaling has also been implicated in motor-cargo association. In neurons, KIF17 binds to the scaffold protein Mint-1 to promote the transport of the NMDA receptor subunit 2B (NR2B), and subsequent studies have shown that the Ca2+/calmodulin-dependent protein kinase II (CaMKII) regulates the dissociation of KIF17 from Mint. An increase in Ca2+ levels upon neuronal excitation induces activation of CaMKII, which in turn phosphorylates the tail of KIF17, disrupting the association between KIF17 and Mint-1 and releasing the kinesin from the transported cargo (Guillaud et al., 2003; Guillaud et al., 2008). CaMKII has also been implicated in the control of the association between KIF4 and the nuclear enzyme poly (ADPribose) polymerase-1 (PARP-1), contributing for the regulation of neuronal survival during brain development (Midorikawa et al., 2006). The small GTPase Miro is a calcium sensor that regulates kinesin-mediated mitochondria transport. The binding of calcium to Miro induces conformational changes on the molecule that might result in the dissociation of the kinesin from mitochondria surface or in the binding of Miro to the motor domain, preventing kinesin-microtubule association (Macaskill et al., 2009; Wang and Schwarz, 2009). Additionally, phosphorylation of KLCs of a kinesin-1 motor by the protein kinase glycogen synthase kinase 3β (GSK3β) was shown to decrease the association of kinesin-1 with membrane-bounded organelles promoting delivery of cargo to specific subcellular domains (Morfini et al., 2002). In *Drosophila*, the kinase UNC-51 binds to and phosphorylates the kinesin heavy chain adaptor protein UNC-76, which in turn binds to the synaptic vesicle protein synaptotagmin-1. This is an example of a phosphorylation-dependent association of a kinesin with a cargo-adaptor protein (Toda et al., 2008).

Different kinesins can interact with different adaptor proteins, and this allows multiple regulatory mechanisms for the motor-cargo coupling and also motor-microtubule association. For cytoplasmic dynein, even though there are only a few isoforms of each subunit, the complexity of these mechanisms is even higher. This is due to the huge number of adaptor proteins that can associate with the dynein complex. Dynactin and Lis1-NudE/NudEL form a complex with dynein and their concerted action, either together or in different combinations, is required for dynein recruitment to cargo (Kardon and Vale, 2009).

4.2 Control of motor-microtubule attachment and motor activity

Once dynein and kinesin associate with their cargos, other factors come into play to control the correct transport of the cargo along microtubules. One important step is the attachment of the motor to microtubules. There are different studies showing that post translational modifications of tubulin subunits can influence the dynamics and affinity of kinesins for microtubules. For instance, kinesin-1 motility shows preference for the acetylated and detyrosinated microtubules in non-polarized cells (Dunn et al., 2008; Reed et al., 2006). In neurons, populations of microtubules with different modifications seem to control polarized trafficking: tyrosinated microtubules, more abundant in dendrites, might contribute to preventing kinesin-1 from entering the dendrites, while detyrosinated microtubules present in axons might help to direct kinesin-1 into this compartment (Konishi and Setou, 2009; Verhey and Hammond, 2009). An important question is whether tubulin modifications affect motor binding directly. A recent *in vitro* study with modified tubulins showed that kinesin velocity and processivity can be affected by the composition of the tubulin C-terminal tails, the major sites of tubulin modifications: kinesin-1 motility was increased by polyglutamylation, while kinesin-2 motility was favored by α-tubulin detyrosination (Sirajuddin et al., 2014). Tubulin detyrosination caused a moderate increase in the landing rate of kinesin-1 *in vitro*, while tubulin acetylation had little effect on the motility parameters of this kinesin, despite the fact that this motor shows strong preference for acetylated microtubules in cells, suggesting that additional factors might be involved (Kaul et al., 2014).

Despite the high similarity between the motor domain of different kinesins, their affinity for microtubule modifications is variable (Verhey and Hammond, 2009), suggesting that other regions within the kinesin molecule might influence the selectivity for specific microtubules. Not only post-translational modifications but also specific microtubule associated proteins (MAP) can influence transport. For instance, the *Drosophila* homologue of MAP7 (Ensconsin) has been shown to promote the recruitment of kinesin-1 to microtubules and to work as an "activator" of kinesin-1 mediated transport (Barlan et al., 2013; Sung et al., 2008). There are also studies showing that the binding of the motor domain to microtubules can be regulated by adaptor proteins. As discussed previously, the GTPase and calcium sensor Miro, which is essential for mitochondria transport, was proposed to associate with the motor domain of kinesin-1 upon calcium binding, preventing its interaction with microtubules (Wang and Schwarz, 2009).

Kinesin motors, when not bound to cargo, are maintained in an inactive state by an autoinhibitory mechanism that allows the motor to be activated with controlled precision, both spatially and temporary. Autoinhibition as a regulatory mechanism was first described for kinesin-1, which exists in two distinct conformations - an extended active conformation and a folded inactive conformation where the tail region can interact with the motor domain and inhibit microtubule binding and ADP release from the nucleotide pocket (Verhey and Hammond, 2009; Verhey et al., 2011). Autoinhibitory mechanisms have been proposed for other kinesins as well, and release of autoinhibition has been shown to be mediated by cargo binding and phosphorylation (Verhey and Hammond, 2009).

In the case of dynein, several studies have suggested that intramolecular interactions contribute to the binding of the motor to microtubules and to its processivity (Vallee et al., 2012). ATP hydrolysis is coupled to dynein movement, being essential for the regulation of microtubule affinity. After ATP hydrolysis, the linker, which works as a lever and is essential for generation of movement, changes its conformation, and the dynein's microtubule binding domain (MTBD) detaches from the microtubule. Once the nucleotide binding domain is free or bound to ADP, the MTBD associates again with the microtubule (Carter, 2013; Roberts et al., 2013; Schmidt et al., 2014). LIS1, an adaptor protein that can directly bind to the dynein motor domain, was shown to operate like a "clutch" that uncouples microtubule binding from ATPase cycles (Huang et al., 2012).

As mentioned above, dynactin, which binds to DIC, is also required for dynein processivity, determined by the number of steps that the motor takes before detaching from the microtubule (Jha and Surrey, 2015), and dynein's function strictly depends on dynactin association. The microtubule-binding domain of p150glued, which consists of the CAP-Gly domain with some adjacent sequences, was proposed to work as an additional tether increasing the affinity of dynein for the microtubule (King and Schroer, 2000). However, studies in *Drosophila* and budding yeast have shown that the CAP-Gly domain is not required for dynactin-induced dynein motility (Kardon et al., 2009; Kim et al., 2007). Recent *in vitro* work showed that the coiled coil regions of p150glued promote and regulate vertebrate dynein processivity in a complex manner (Jha and Surrey, 2015; Tripathy et al., 2014).

The interaction between dynein and dynactin appears to be tightly regulated in cells. Our laboratory has shown that an N-terminal fragment of BICD2 (BICD2-N) stabilizes the dynein-dynactin complex biochemically (Splinter et al., 2012). The same effect was observed by other groups who reconstituted the complex *in vitro* (McKenney et al., 2014; Schlager et al., 2014a). Interestingly, the facilitation of dynein-dynactin interaction by BICD2-N remarkably increased dynein's processivity *in vitro* (McKenney et al., 2014; Schlager et al., 2014a), an effect also induced by other adaptor proteins, such as Spindly, Rab11-FIP3 and Hook3 (McKenney et al., 2014). The current model is that adaptor proteins enhance dynein-dynactin interaction upon cargo binding, thus promoting dynein processivity. Interestingly, a recent study has shown that single dynein molecules were inhibited and non-processive, with their motor heads stacked together. When the motor heads were separated by a rigid rod, dynein started moving processively along microtubules. Furthermore, assembly of dynein molecules on a cargo empowered them to move unidirectionally and generate force cooperatively. This work thus suggests that dynein in the cell is inhibited by intramolecular head-to-head association, becoming active upon cargo binding (Torisawa et al., 2014). Interestingly, BICD2 and the related adaptor protein BICDR-1 were shown to regulate the dynein-based motility of Rab6-secretory vesicles in cells, with BICDR-1 inducing a remarkable increase of speed (Schlager et al., 2014b). In light of these recent studies, it is tempting to speculate that the binding of different cargo and adaptor proteins to dynein might induce conformational changes in the motor domains, promoting the dissociation of the motor heads and increasing dynein motility.

5. Bidirectional cargo transport by multiple motors

As discussed in the sections above, many cellular organelles are bidirectionally transported by kinesins and dynein along microtubules, and the correct cellular distribution of cargos within the cell strongly depends on the balance of these movements (Figure 8).

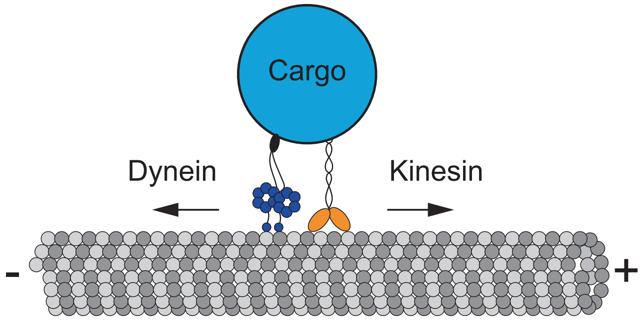

Figure 8: Bidirectional transport
Membrane cargos in the cell are transported bidirectionally along microtubules, with kinesin powering movement to plus end of microtubules and dynein to the minus end.

Through the years, several studies have been performed to dissect this mechanism of transport, and varied models and *in vitro* reconstitution experiments have successfully recapitulated bidirectional transport of cargos in cells. To explain bidirectional transport, two main models have emerged: the "tug-of-war" or "mechanical competition" model and the "coordination" or "co-dependence" model (Hancock, 2014; Welte, 2004) (Figure 9). Both models account for the presence of different types of motors with opposite polarities on a cargo, but differ when it comes to explaining how these motors act to power transport in different directions. In the "tug-of-war" model, the net force generated by opposite polarity motors will determine the direction in which the motor will be transported, while in the "coordination" model, opposite motors do not generate force against each other. Results supporting both models have been described in the literature. Early studies performed in *Drosophila* suggested that a tug-of-war mechanism could be responsible for the bidirectional transport of lipid droplets (Welte et al., 1998). It was also shown that directional switching of endosomes involves a phase of slower velocity coincident with vesicle elongation. This suggested that a tug-of-war between opposite motors was promoting the bidirectional movement and fission of endosomes (Soppina et al., 2009). Furthermore, more recent studies have shown that intracellular cargo and artificial beads associated with dynein and kinesin had lower stall forces compared with beads bound only to kinesin. This suggests that motors attached to the same cargo exert opposing forces and mechanically compete with each other, fitting with the tug-of-war model (Blehm et al., 2013). Despite experimental evidence supporting this model, several other studies have suggested that opposite motors need to cooperate in order to promote bidirectional transport (the "coordination" or "co-dependence" model). In a tug-of-war situation, when one motor is "switched off", the other should freely transport cargo in the opposite direction, but several studies have shown that interfering with the function of one motor can impair transport in both directions (Hancock, 2014). For instance, kinesin-1 and dynein strongly require each other for bidirectional transport of peroxisomes in Drosophila S2 cells (Ally et al., 2009). Furthermore, the depletion of kinesin light chain 1 and 2 (KLC1 and KLC2) in mouse hippocampal neurons impairs bidirectional transport of prion protein (PrPc) vesicles; the inhibition of KLCs caused a decrease in the percentage of anterograde moving vesicles and a higher frequency of paused vesicles, but also a reduction in the percentage of retrograde moving particles (Encalada et al., 2011). Additionally, it was shown that in dorsal root ganglia (DRG) neurons, depletion of the dynein subunit p150Glued caused a significant decrease of lysosomes motility in both anterograde and retrograde direction, and an increase of the non-motile fraction (Moughamian and Holzbaur, 2012).

As previously described, adaptor proteins can influence motor activity by controlling the binding to motor proteins, and several studies have emerged proposing adaptor proteins to be essential regulators of bidirectional transport (Hancock, 2014). One example is the aforementioned recent study demonstrating that kinesin-1 drives the transport of mitochondria into axons of hippocampal neurons. Importantly, the anterograde transport of mitochondria also requires dynein and the adaptor protein TRAK1, which binds to both dynein and kinesin and might help to coordinate their activities (van Spronsen et al., 2013).

Taken together, cellular cargos are transported by sets of multiple motors, which move along differentially modified microtubules, with adaptors proteins and MAPs providing additional levels of complexity. A combination of *in vivo* and *in vitro* reconstitution experiments and computational models will be essential to address the basic mechanisms governing bidirectional transport of different cargos in biological systems.

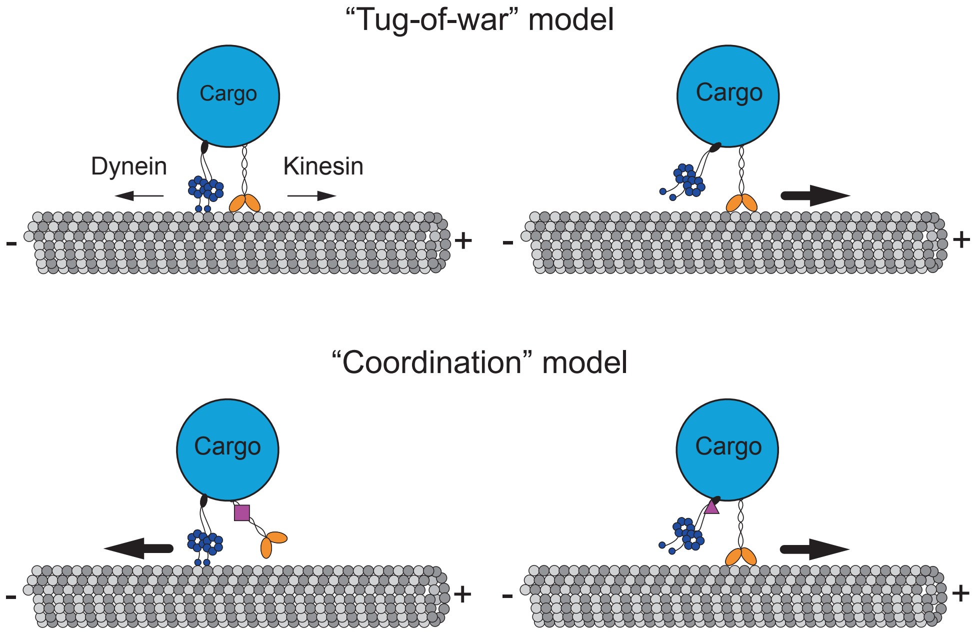
"Tug-of-war" model
Cargo
Dynein
Kinesin
Cargo
-
+
-
+
"Coordination" model
Cargo
Cargo
-
+
-
+

Figure 9: Regulation of bidirectional transport
There are two main models to explain bidirectional transport. In the tug-of-war model, kinesin and dynein exert opposite forces and the "strongest" motors will win, promoting transport independently of the opposite motor. In the "coordination" model, motors do not compete but rather cooperate to drive transport. This process is normally mediated by adaptor proteins (pink) that regulate interactions between motors.

References

Akhmanova, A., Hammer, J.A., 3rd, 2010. Linking molecular motors to membrane cargo. Current opinion in cell biology 22, 479-487.

Akhmanova, A., Steinmetz, M.O., 2008. Tracking the ends: a dynamic protein network controls the fate of microtubule tips. Nature reviews. Molecular cell biology 9, 309-322.

Al-Haddad, A., Shonn, M.A., Redlich, B., Blocker, A., Burkhardt, J.K., Yu, H., Hammer, J.A., 3rd, Weiss, D.G., Steffen, W., Griffiths, G., Kuznetsov, S.A., 2001. Myosin Va bound to phagosomes binds to F-actin and delays microtubule-dependent motility. Molecular biology of the cell 12, 2742-2755.

Ally, S., Larson, A.G., Barlan, K., Rice, S.E., Gelfand, V.I., 2009. Opposite-polarity motors activate one another to trigger cargo transport in live cells. The Journal of cell biology 187, 1071-1082.

Arimura, N., Kimura, T., Nakamuta, S., Taya, S., Funahashi, Y., Hattori, A., Shimada, A., Menager, C., Kawabata, S., Fujii, K., Iwamatsu, A., Segal, R.A., Fukuda, M., Kaibuchi, K., 2009. Anterograde transport of TrkB in axons is mediated by direct interaction with Slp1 and Rab27. Developmental cell 16, 675-686.

Barlan, K., Lu, W., Gelfand, V.I., 2013. The microtubule-binding protein ensconsin is an essential cofactor of kinesin-1. Current biology : CB 23, 317-322.

Bhabha, G., Cheng, H.C., Zhang, N., Moeller, A., Liao, M., Speir, J.A., Cheng, Y., Vale, R.D., 2014. Allosteric communication in the Dynein motor domain. Cell 159, 857-868.

Bielska, E., Schuster, M., Roger, Y., Berepiki, A., Soanes, D.M., Talbot, N.J., Steinberg, G., 2014. Hook is an adapter that coordinates kinesin-3 and dynein cargo attachment on early endosomes. The Journal of cell biology 204, 989-1007.

Blehm, B.H., Schroer, T.A., Trybus, K.M., Chemla, Y.R., Selvin, P.R., 2013. In vivo optical trapping indicates kinesin's stall force is reduced by dynein during intracellular transport. Proceedings of the National Academy of Sciences of the United States of America 110, 3381-3386.

Blocker, A., Severin, F.F., Burkhardt, J.K., Bingham, J.B., Yu, H., Olivo, J.C., Schroer, T.A., Hyman, A.A., Griffiths, G., 1997. Molecular requirements for bi-directional movement of phagosomes along microtubules. The Journal of cell biology 137, 113-129.

Bock, J.B., Matern, H.T., Peden, A.A., Scheller, R.H., 2001. A genomic perspective on membrane compartment organization. Nature 409, 839-841.

Boldogh, I.R., Pon, L.A., 2007. Mitochondria on the move. Trends in cell biology 17, 502-510.

Bonifacino, J.S., Glick, B.S., 2004. The mechanisms of vesicle budding and fusion. Cell 116, 153-166.

Bonifacino, J.S., Rojas, R., 2006. Retrograde transport from endosomes to the trans-Golgi network. Nature reviews. Molecular cell biology 7, 568-579.

Brickley, K., Smith, M.J., Beck, M., Stephenson, F.A., 2005. GRIF-1 and OIP106, members of a novel gene family of coiled-coil domain proteins: association in vivo and in vitro with kinesin. The Journal of biological chemistry 280, 14723-14732.

Brown, A.K., Hunt, S.D., Stephens, D.J., 2014. Opposing microtubule motors control motility, morphology and cargo segregation during ER-to-Golgi transport. Biology open 3, 307-313.

Bullock, S.L., 2011. Messengers, motors and mysteries: sorting of eukaryotic mRNAs by cytoskeletal transport. Biochemical Society transactions 39, 1161-1165.

Burgess, S.A., Walker, M.L., Sakakibara, H., Knight, P.J., Oiwa, K., 2003. Dynein structure and power stroke. Nature 421, 715-718.

Cai, H., Reinisch, K., Ferro-Novick, S., 2007. Coats, tethers, Rabs, and SNAREs work together to mediate the intracellular destination of a transport vesicle. Developmental cell 12, 671-682.

Carter, A.P., 2013. Crystal clear insights into how the dynein motor moves. Journal of cell science 126, 705-713.

Carter, A.P., Garbarino, J.E., Wilson-Kubalek, E.M., Shipley, W.E., Cho, C., Milligan, R.A., Vale, R.D., Gibbons, I.R., 2008. Structure and functional role of dynein's microtubule-binding domain. Science 322, 1691-1695.

Cho, C., Reck-Peterson, S.L., Vale, R.D., 2008. Regulatory ATPase sites of cytoplasmic dynein affect processivity and force generation. The Journal of biological chemistry 283, 25839-25845.

Civelekoglu-Scholey, G., Scholey, J.M., 2010. Mitotic force generators and chromosome segregation. Cellular and molecular life sciences : CMLS 67, 2231-2250.

Delevoye, C., Miserey-Lenkei, S., Montagnac, G., Gilles-Marsens, F., Paul-Gilloteaux, P., Giordano, F., Waharte, F., Marks, M.S., Goud, B., Raposo, G., 2014. Recycling endosome tubule morphogenesis from sorting endosomes requires the kinesin motor KIF13A. Cell reports 6, 445-454.

Dirac-Svejstrup, A.B., Sumizawa, T., Pfeffer, S.R., 1997. Identification of a GDI displacement factor that releases endosomal Rab GTPases from Rab-GDI. The EMBO journal 16, 465-472.

Dunn, S., Morrison, E.E., Liverpool, T.B., Molina-Paris, C., Cross, R.A., Alonso, M.C., Peckham, M., 2008. Differential trafficking of Kif5c on tyrosinated and detyrosinated microtubules in live cells. Journal of cell science 121, 1085-1095.

Echard, A., Jollivet, F., Martinez, O., Lacapere, J.J., Rousselet, A., Janoueix-Lerosey, I., Goud, B., 1998. Interaction of a Golgi-associated kinesin-like protein with Rab6. Science 279, 580-585.

Encalada, S.E., Szpankowski, L., Xia, C.H., Goldstein, L.S., 2011. Stable kinesin and dynein assemblies drive the axonal transport of mammalian prion protein vesicles. Cell 144, 551-565.

Friedman, J.R., Webster, B.M., Mastronarde, D.N., Verhey, K.J., Voeltz, G.K., 2010. ER sliding dynamics and ER-mitochondrial contacts occur on acetylated microtubules. The Journal of cell biology 190, 363-375.

Fukuda, M., 2008. Regulation of secretory vesicle traffic by Rab small GTPases. Cellular and molecular life sciences : CMLS 65, 2801-2813.

Gee, M.A., Heuser, J.E., Vallee, R.B., 1997. An extended microtubule-binding structure within the dynein motor domain. Nature 390, 636-639.

Glater, E.E., Megeath, L.J., Stowers, R.S., Schwarz, T.L., 2006. Axonal transport of mitochondria requires milton to recruit kinesin heavy chain and is light chain independent. The Journal of cell biology 173, 545-557.

Gouveia, S.M., Akhmanova, A., 2010. Cell and molecular biology of microtubule plus end tracking proteins: end binding proteins and their partners. International review of cell and molecular biology 285, 1-74.

Granger, E., McNee, G., Allan, V., Woodman, P., 2014. The role of the cytoskeleton and molecular motors in endosomal dynamics. Seminars in cell & developmental biology 31, 20-29.

Grant, B.D., Donaldson, J.G., 2009. Pathways and mechanisms of endocytic recycling. Nature reviews. Molecular cell biology 10, 597-608.

Griffis, E.R., Stuurman, N., Vale, R.D., 2007. Spindly, a novel protein essential for silencing the spindle assembly checkpoint, recruits dynein to the kinetochore. The Journal of cell biology 177, 1005-1015.

Grigoriev, I., Splinter, D., Keijzer, N., Wulf, P.S., Demmers, J., Ohtsuka, T., Modesti, M., Maly, I.V., Grosveld, F., Hoogenraad, C.C., Akhmanova, A., 2007. Rab6 regulates transport and targeting of exocytotic carriers. Developmental cell 13, 305-314.

Guillaud, L., Setou, M., Hirokawa, N., 2003. KIF17 dynamics and regulation of NR2B trafficking in hippocampal neurons. The Journal of neuroscience : the official journal of the Society for Neuroscience 23, 131-140.

Guillaud, L., Wong, R., Hirokawa, N., 2008. Disruption of KIF17-Mint1 interaction by CaMKII-dependent phosphorylation: a molecular model of kinesin-cargo release. Nature cell biology 10, 19-29.

Gumy, L.F., Katrukha, E.A., Kapitein, L.C., Hoogenraad, C.C., 2013. New insights into mRNA trafficking in axons. Developmental neurobiology.

Gumy, L.F., Katrukha, E.A., Kapitein, L.C., Hoogenraad, C.C., 2014. New insights into mRNA trafficking in axons. Developmental neurobiology 74, 233-244.

Guo, X., Macleod, G.T., Wellington, A., Hu, F., Panchumarthi, S., Schoenfield, M., Marin, L., Charlton, M.P., Atwood, H.L., Zinsmaier, K.E., 2005. The GTPase dMiro is required for axonal transport of mitochondria to Drosophila synapses. Neuron 47, 379-393.

Hamada, T., Ueda, H., Kawase, T., Hara-Nishimura, I., 2014. Microtubules contribute to tubule elongation and anchoring of endoplasmic reticulum, resulting in high network complexity in Arabidopsis. Plant physiology 166, 1869-1876.

Hancock, W.O., 2014. Bidirectional cargo transport: moving beyond tug of war. Nature reviews. Molecular cell biology 15, 615-628.

Harada, A., Takei, Y., Kanai, Y., Tanaka, Y., Nonaka, S., Hirokawa, N., 1998. Golgi vesiculation and lysosome dispersion in cells lacking cytoplasmic dynein. The Journal of cell biology 141, 51-59.

Hirokawa, N., 1998. Kinesin and dynein superfamily proteins and the mechanism of organelle transport. Science 279, 519-526.

Hirokawa, N., Noda, Y., 2008. Intracellular transport and kinesin superfamily proteins, KIFs: structure, function, and dynamics. Physiological reviews 88, 1089-1118.

Hirokawa, N., Noda, Y., Tanaka, Y., Niwa, S., 2009. Kinesin superfamily motor proteins and intracellular transport. Nature reviews. Molecular cell biology 10, 682-696.

Hirokawa, N., Pfister, K.K., Yorifuji, H., Wagner, M.C., Brady, S.T., Bloom, G.S., 1989. Submolecular domains of bovine brain kinesin identified by electron microscopy and monoclonal antibody decoration. Cell 56, 867-878.

Hoepfner, S., Severin, F., Cabezas, A., Habermann, B., Runge, A., Gillooly, D., Stenmark, H., Zerial, M., 2005. Modulation of receptor recycling and degradation by the endosomal kinesin KIF16B. Cell 121, 437-450.

Hoogenraad, C.C., Wulf, P., Schiefermeier, N., Stepanova, T., Galjart, N., Small, J.V., Grosveld, F., de Zeeuw, C.I., Akhmanova, A., 2003. Bicaudal D induces selective dynein-mediated microtubule minus end-directed transport. The EMBO journal 22, 6004-6015.

Horgan, C.P., Hanscom, S.R., Jolly, R.S., Futter, C.E., McCaffrey, M.W., 2010a. Rab11-FIP3 binds dynein light intermediate chain 2 and its overexpression fragments the Golgi complex. Biochemical and biophysical research communications 394, 387-392.

Horgan, C.P., Hanscom, S.R., Jolly, R.S., Futter, C.E., McCaffrey, M.W., 2010b. Rab11-FIP3 links the Rab11 GTPase and cytoplasmic dynein to mediate transport to the endosomal-recycling compartment. Journal of cell science 123, 181-191.

Horiuchi, D., Collins, C.A., Bhat, P., Barkus, R.V., Diantonio, A., Saxton, W.M., 2007. Control of a kinesin-cargo linkage mechanism by JNK pathway kinases. Current biology : CB 17, 1313-1317.

Huang, J., Roberts, A.J., Leschziner, A.E., Reck-Peterson, S.L., 2012. Lis1 acts as a “clutch” between the ATPase and microtubule-binding domains of the dynein motor. Cell 150, 975-986.

Hunter, A.W., Caplow, M., Coy, D.L., Hancock, W.O., Diez, S., Wordeman, L., Howard, J., 2003. The kinesin-related protein MCAK is a microtubule depolymerase that forms an ATP-hydrolyzing complex at microtubule ends. Molecular cell 11, 445-457.

Inomata, H., Nakamura, Y., Hayakawa, A., Takata, H., Suzuki, T., Miyazawa, K., Kitamura, N., 2003. A scaffold protein JIP-1b enhances amyloid precursor protein phosphorylation by JNK and its association with kinesin light chain 1. The Journal of biological chemistry 278, 22946-22955.

Jaulin, F., Xue, X., Rodriguez-Boulan, E., Kreitzer, G., 2007. Polarization-dependent selective transport to the apical membrane by KIF5B in MDCK cells. Developmental cell 13, 511-522.

Jha, R., Surrey, T., 2015. Regulation of processive motion and microtubule localization of cytoplasmic dynein. Biochemical Society transactions 43, 48-57.

Jiang, K., Akhmanova, A., 2011. Microtubule tip-interacting proteins: a view from both ends. Current opinion in cell biology 23, 94-101.

Johansson, M., Rocha, N., Zwart, W., Jordens, I., Janssen, L., Kuijl, C., Olkkonen, V.M., Neefjes, J., 2007. Activation of endosomal dynein motors by stepwise assembly of Rab7-RILP-p150Glued, ORP1L, and the receptor betaIII spectrin. The Journal of cell biology 176, 459-471.

Kamal, A., Stokin, G.B., Yang, Z., Xia, C.H., Goldstein, L.S., 2000. Axonal transport of amyloid precursor protein is mediated by direct binding to the kinesin light chain subunit of kinesin-I. Neuron 28, 449-459.

Kanai, Y., Dohmae, N., Hirokawa, N., 2004. Kinesin transports RNA: isolation and characterization of an RNA-transporting granule. Neuron 43, 513-525.

Kanai, Y., Wang, D., Hirokawa, N., 2014. KIF13B enhances the endocytosis of LRP1 by recruiting LRP1 to caveolae. The Journal of cell biology 204, 395-408.

Kardon, J.R., Reck-Peterson, S.L., Vale, R.D., 2009. Regulation of the processivity and intracellular localization of Saccharomyces cerevisiae dynein by dynactin. Proceedings of the National Academy of Sciences of the United States of America 106, 5669-5674.

Kardon, J.R., Vale, R.D., 2009. Regulators of the cytoplasmic dynein motor. Nature reviews. Molecular cell biology 10, 854-865.

Kaul, N., Soppina, V., Verhey, K.J., 2014. Effects of alpha-tubulin K40 acetylation and detyrosination on kinesin-1 motility in a purified system. Biophysical journal 106, 2636-2643.

Kim, H., Ling, S.C., Rogers, G.C., Kural, C., Selvin, P.R., Rogers, S.L., Gelfand, V.I., 2007. Microtubule binding by dynactin is required for microtubule organization but not cargo transport. The Journal of cell biology 176, 641-651.

King, S.J., Schroer, T.A., 2000. Dynactin increases the processivity of the cytoplasmic dynein motor. Nature cell biology 2, 20-24.

Kirschner, M., Mitchison, T., 1986. Beyond self-assembly: from microtubules to morphogenesis. Cell 45, 329-342.

Klopfenstein, D.R., Tomishige, M., Stuurman, N., Vale, R.D., 2002. Role of phosphatidylinositol(4,5) bisphosphate organization in membrane transport by the Unc104 kinesin motor. Cell 109, 347-358.

Klopfenstein, D.R., Vale, R.D., 2004. The lipid binding pleckstrin homology domain in UNC-104 kinesin is necessary for synaptic vesicle transport in Caenorhabditis elegans. Molecular biology of the cell 15, 3729-3739.

Kon, T., Nishiura, M., Ohkura, R., Toyoshima, Y.Y., Sutoh, K., 2004. Distinct functions of nucleotide-binding/hydrolysis sites in the four AAA modules of cytoplasmic dynein. Biochemistry 43, 11266-11274.

Konishi, Y., Setou, M., 2009. Tubulin tyrosination navigates the kinesin-1 motor domain to axons. Nature neuroscience 12, 559-567.

Kumar, J., Yu, H., Sheetz, M.P., 1995. Kinectin, an essential anchor for kinesin-driven vesicle motility. Science 267, 1834-1837.

Kural, C., Kim, H., Syed, S., Goshima, G., Gelfand, V.I., Selvin, P.R., 2005. Kinesin and dynein move a peroxisome in vivo: a tug-of-war or coordinated movement? Science 308, 1469-1472.

Lawrence, C.J., Dawe, R.K., Christie, K.R., Cleveland, D.W., Dawson, S.C., Endow, S.A., Goldstein, L.S., Goodson, H.V., Hirokawa, N., Howard, J., Malmberg, R.L., McIntosh, J.R., Miki, H., Mitchison, T.J., Okada, Y., Reddy, A.S., Saxton, W.M., Schliwa, M., Scholey, J.M., Vale, R.D., Walczak, C.E., Wordeman, L., 2004. A standardized kinesin nomenclature. The Journal of cell biology 167, 19-22.

Lazarov, O., Morfini, G.A., Lee, E.B., Farah, M.H., Szodorai, A., DeBoer, S.R., Koliatsos, V.E., Kins, S., Lee, V.M., Wong, P.C., Price, D.L., Brady, S.T., Sisodia, S.S., 2005. Axonal transport, amyloid precursor protein, kinesin-1, and the processing apparatus: revisited. The Journal of neuroscience : the official journal of the Society for Neuroscience 25, 2386-2395.

Li, D., Kuehn, E.W., Prekeris, R., 2014. Kinesin-2 mediates apical endosome transport during epithelial lumen formation. Cellular logistics 4, e28928.

Lin, M.Y., Sheng, Z.H., 2015. Regulation of mitochondrial transport in neurons. Experimental cell research.

Lippincott-Schwartz, J., Cole, N.B., Marotta, A., Conrad, P.A., Bloom, G.S., 1995. Kinesin is the motor for microtubule-mediated Golgi-to-ER membrane traffic. The Journal of cell biology 128, 293-306.

Macaskill, A.F., Rinholm, J.E., Twelvetrees, A.E., Arancibia-Carcamo, I.L., Muir, J., Fransson, A., Aspenstrom, P., Attwell, D., Kittler, J.T., 2009. Miro1 is a calcium sensor for glutamate receptor-dependent localization of mitochondria at synapses. Neuron 61, 541-555.

Marx, A., Hoenger, A., Mandelkow, E., 2009. Structures of kinesin motor proteins. Cell motility and the cytoskeleton 66, 958-966.

Matanis, T., Akhmanova, A., Wulf, P., Del Nery, E., Weide, T., Stepanova, T., Galjart, N., Grosveld, F., Goud, B., De Zeeuw, C.I., Barnekow, A., Hoogenraad, C.C., 2002. Bicaudal-D regulates COPI-independent Golgi-ER transport by recruiting the dynein-dynactin motor complex. Nature cell biology 4, 986-992.

Mattson, M.P., Gleichmann, M., Cheng, A., 2008. Mitochondria in neuroplasticity and neurological disorders. Neuron 60, 748-766.

McGrail, M., Hays, T.S., 1997. The microtubule motor cytoplasmic dynein is required for spindle orientation during germline cell divisions and oocyte differentiation in Drosophila. Development 124, 2409-2419.

McKenney, R.J., Huynh, W., Tanenbaum, M.E., Bhabha, G., Vale, R.D., 2014. Activation of cytoplasmic dynein motility by dynactin-cargo adapter complexes. Science 345, 337-341.

Merdes, A., Heald, R., Samejima, K., Earnshaw, W.C., Cleveland, D.W., 2000. Formation of spindle poles by dynein/dynactin-dependent transport of NuMA. The Journal of cell biology 149, 851-862.

Midorikawa, R., Takei, Y., Hirokawa, N., 2006. KIF4 motor regulates activity-dependent neuronal survival by suppressing PARP-1 enzymatic activity. Cell 125, 371-383.

Miki, H., Okada, Y., Hirokawa, N., 2005. Analysis of the kinesin superfamily: insights into structure and function. Trends in cell biology 15, 467-476.

Montagnac, G., Sibarita, J.B., Loubery, S., Daviet, L., Romao, M., Raposo, G., Chavrier, P., 2009. ARF6 Interacts with JIP4 to control a motor switch mechanism regulating endosome traffic in cytokinesis. Current biology : CB 19, 184-195.

Morfini, G., Szebenyi, G., Elluru, R., Ratner, N., Brady, S.T., 2002. Glycogen synthase kinase 3 phosphorylates kinesin light chains and negatively regulates kinesin-based motility. The EMBO journal 21, 281-293.

Moughamian, A.J., Holzbaur, E.L., 2012. Dynactin is required for transport initiation from the distal axon. Neuron 74, 331-343.

Mueller, S., Cao, X., Welker, R., Wimmer, E., 2002. Interaction of the poliovirus receptor CD155 with the dynein light chain Tctex-1 and its implication for poliovirus pathogenesis. The Journal of biological chemistry 277, 7897-7904.

Nakagawa, T., Setou, M., Seog, D., Ogasawara, K., Dohmae, N., Takio, K., Hirokawa, N., 2000. A novel motor, KIF13A, transports mannose-6-phosphate receptor to plasma membrane through direct interaction with AP-1 complex. Cell 103, 569-581.

Nangaku, M., Sato-Yoshitake, R., Okada, Y., Noda, Y., Takemura, R., Yamazaki, H., Hirokawa, N., 1994. KIF1B, a novel microtubule plus end-directed monomeric motor protein for transport of mitochondria. Cell 79, 1209-1220.

Niwa, S., Tanaka, Y., Hirokawa, N., 2008. KIF1Bbeta- and KIF1A-mediated axonal transport of presynaptic regulator Rab3 occurs in a GTP-dependent manner through DENN/MADD. Nature cell biology 10, 1269-1279.

Pavlos, N.J., Cheng, T.S., Qin, A., Ng, P.Y., Feng, H.T., Ang, E.S., Carrello, A., Sung, C.H., Jahn, R., Zheng, M.H., Xu, J., 2011. Tctex-1, a novel interaction partner of Rab3D, is required for osteoclastic bone resorption. Molecular and cellular biology 31, 1551-1564.

Perez Bay, A.E., Schreiner, R., Mazzoni, F., Carvajal-Gonzalez, J.M., Gravotta, D., Perret, E., Lehmann Mantaras, G., Zhu, Y.S., Rodriguez-Boulan, E.J., 2013. The kinesin KIF16B mediates apical transcytosis of transferrin receptor in AP-1B-deficient epithelia. The EMBO journal 32, 2125-2139.

Pfeffer, S.R., 2007. Unsolved mysteries in membrane traffic. Annual review of biochemistry 76, 629-645.

Pfister, K.K., Shah, P.R., Hummerich, H., Russ, A., Cotton, J., Annuar, A.A., King, S.M., Fisher, E.M., 2006. Genetic analysis of the cytoplasmic dynein subunit families. PLoS genetics 2, e1.

Pilling, A.D., Horiuchi, D., Lively, C.M., Saxton, W.M., 2006. Kinesin-1 and Dynein are the primary motors for fast transport of mitochondria in Drosophila motor axons. Molecular biology of the cell 17, 2057-2068.

Plitz, T., Pfeffer, K., 2001. Intact lysosome transport and phagosome function despite kinectin deficiency. Molecular and cellular biology 21, 6044-6055.

Reck-Peterson, S.L., Vale, R.D., 2004. Molecular dissection of the roles of nucleotide binding and hydrolysis in dynein's AAA domains in Saccharomyces cerevisiae. Proceedings of the National Academy of Sciences of the United States of America 101, 1491-1495.

Reed, N.A., Cai, D., Blasius, T.L., Jih, G.T., Meyhofer, E., Gaertig, J., Verhey, K.J., 2006. Microtubule acetylation promotes kinesin-1 binding and transport. Current biology : CB 16, 2166-2172.

Roberts, A.J., Kon, T., Knight, P.J., Sutoh, K., Burgess, S.A., 2013. Functions and mechanics of dynein motor proteins. Nature reviews. Molecular cell biology 14, 713-726.

Rocha, N., Kuijl, C., van der Kant, R., Janssen, L., Houben, D., Janssen, H., Zwart, W., Neefjes, J., 2009. Cholesterol sensor ORP1L contacts the ER protein VAP to control Rab7-RILP-p150 Glued and late endosome positioning. The Journal of cell biology 185, 1209-1225.

Rybin, V., Ullrich, O., Rubino, M., Alexandrov, K., Simon, I., Seabra, M.C., Goody, R., Zerial, M., 1996. GTPase activity of Rab5 acts as a timer for endocytic membrane fusion. Nature 383, 266-269.

Santama, N., Er, C.P., Ong, L.L., Yu, H., 2004. Distribution and functions of kinectin isoforms. Journal of cell science 117, 4537-4549.

Satpute-Krishnan, P., DeGiorgis, J.A., Conley, M.P., Jang, M., Bearer, E.L., 2006. A peptide zipcode sufficient for anterograde transport within amyloid precursor protein. Proceedings of the National Academy of Sciences of the United States of America 103, 16532-16537.

Schlager, M.A., Hoang, H.T., Urnavicius, L., Bullock, S.L., Carter, A.P., 2014a. In vitro reconstitution of a highly processive recombinant human dynein complex. The EMBO journal 33, 1855-1868.

Schlager, M.A., Hoogenraad, C.C., 2009. Basic mechanisms for recognition and transport of synaptic cargos. Molecular brain 2, 25.

Schlager, M.A., Kapitein, L.C., Grigoriev, I., Burzynski, G.M., Wulf, P.S., Keijzer, N., de Graaff, E., Fukuda, M., Shepherd, I.T., Akhmanova, A., Hoogenraad, C.C., 2010. Pericentrosomal targeting of Rab6 secretory vesicles by Bicaudal-D-related protein 1 (BICDR-1) regulates neuritogenesis. The EMBO journal 29, 1637-1651.

Schlager, M.A., Serra-Marques, A., Grigoriev, I., Gumy, L.F., Esteves da Silva, M., Wulf, P.S., Akhmanova, A., Hoogenraad, C.C., 2014b. Bicaudal d family adaptor proteins control the velocity of Dynein-based movements. Cell reports 8, 1248-1256.

Schmidt, H., Zalyte, R., Urnavicius, L., Carter, A.P., 2014. Structure of human cytoplasmic dynein-2 primed for its power stroke. Nature.

Schnitzer, M.J., Block, S.M., 1997. Kinesin hydrolyses one ATP per 8-nm step. Nature 388, 386-390.

Schonteich, E., Wilson, G.M., Burden, J., Hopkins, C.R., Anderson, K., Goldenring, J.R., Prekeris, R., 2008. The Rip11/Rab11-FIP5 and kinesin II complex regulates endocytic protein recycling. Journal of cell science 121, 3824-3833.

Schroer, T.A., 2004. Dynactin. Annual review of cell and developmental biology 20, 759-779.

Short, B., Preisinger, C., Schaletzky, J., Kopajtich, R., Barr, F.A., 2002. The Rab6 GTPase regulates recruitment of the dynactin complex to Golgi membranes. Current biology : CB 12, 1792-1795.

Simon, G.C., Prekeris, R., 2008. Mechanisms regulating targeting of recycling endosomes to the cleavage furrow during cytokinesis. Biochemical Society transactions 36, 391-394.

Sirajuddin, M., Rice, L.M., Vale, R.D., 2014. Regulation of microtubule motors by tubulin isotypes and post-translational modifications. Nature cell biology.

Soldati, T., Shapiro, A.D., Svejstrup, A.B., Pfeffer, S.R., 1994. Membrane targeting of the small GTPase Rab9 is accompanied by nucleotide exchange. Nature 369, 76-78.

Soppina, V., Rai, A.K., Ramaiya, A.J., Barak, P., Mallik, R., 2009. Tug-of-war between dissimilar teams of microtubule motors regulates transport and fission of endosomes. Proceedings of the National Academy of Sciences of the United States of America 106, 19381-19386.

Splinter, D., Razafsky, D.S., Schlager, M.A., Serra-Marques, A., Grigoriev, I., Demmers, J., Keijzer, N., Jiang, K., Poser, I., Hyman, A.A., Hoogenraad, C.C., King, S.J., Akhmanova, A., 2012. BICD2, dynactin, and LIS1 cooperate in regulating dynein recruitment to cellular structures. Molecular biology of the cell 23, 4226-4241.

Stauber, T., Simpson, J.C., Pepperkok, R., Vernos, I., 2006. A role for kinesin-2 in COPI-dependent recycling between the ER and the Golgi complex. Current biology : CB 16, 2245-2251.

Steinmetz, M.O., Akhmanova, A., 2008. Capturing protein tails by CAP-Gly domains. Trends in biochemical sciences 33, 535-545.

Stenmark, H., 2009. Rab GTPases as coordinators of vesicle traffic. Nature reviews. Molecular cell biology 10, 513-525.

Stowers, R.S., Megeath, L.J., Gorska-Andrzejak, J., Meinertzhagen, I.A., Schwarz, T.L., 2002. Axonal transport of mitochondria to synapses depends on milton, a novel Drosophila protein. Neuron 36, 1063-1077.

Summers, K., Kirschner, M.W., 1979. Characteristics of the polar assembly and disassembly of microtubules observed in vitro by darkfield light microscopy. The Journal of cell biology 83, 205-217.

Sung, H.H., Telley, I.A., Papadaki, P., Ephrussi, A., Surrey, T., Rorth, P., 2008. Drosophila ensconsin promotes productive recruitment of Kinesin-1 to microtubules. Developmental cell 15, 866-876.

Szodorai, A., Kuan, Y.H., Hunzelmann, S., Engel, U., Sakane, A., Sasaki, T., Takai, Y., Kirsch, J., Muller, U., Beyreuther, K., Brady, S., Morfini, G., Kins, S., 2009. APP anterograde transport requires Rab3A GTPase activity for assembly of the transport vesicle. The Journal of neuroscience : the official journal of the Society for Neuroscience 29, 14534-14544.

Tai, A.W., Chuang, J.Z., Bode, C., Wolfrum, U., Sung, C.H., 1999. Rhodopsin's carboxy-terminal cytoplasmic tail acts as a membrane receptor for cytoplasmic dynein by binding to the dynein light chain Tctex-1. Cell 97, 877-887.

Tanaka, Y., Kanai, Y., Okada, Y., Nonaka, S., Takeda, S., Harada, A., Hirokawa, N., 1998. Targeted disruption of mouse conventional kinesin heavy chain, kif5B, results in abnormal perinuclear clustering of mitochondria. Cell 93, 1147-1158.

Toda, H., Mochizuki, H., Flores, R., 3rd, Josowitz, R., Krasieva, T.B., Lamorte, V.J., Suzuki, E., Gindhart, J.G., Furukubo-Tokunaga, K., Tomoda, T., 2008. UNC-51/ATG1 kinase regulates axonal transport by mediating motor-cargo assembly. Genes & development 22, 3292-3307.

Torisawa, T., Ichikawa, M., Furuta, A., Saito, K., Oiwa, K., Kojima, H., Toyoshima, Y.Y., Furuta, K., 2014. Autoinhibition and cooperative activation mechanisms of cytoplasmic dynein. Nature cell biology 16, 1118-1124.

Toyoshima, I., Yu, H., Steuer, E.R., Sheetz, M.P., 1992. Kinectin, a major kinesin-binding protein on ER. The Journal of cell biology 118, 1121-1131.

Traer, C.J., Rutherford, A.C., Palmer, K.J., Wassmer, T., Oakley, J., Attar, N., Carlton, J.G., Kremerskothen, J., Stephens, D.J., Cullen, P.J., 2007. SNX4 coordinates endosomal sorting of TfnR with dynein-mediated transport into the endocytic recycling compartment. Nature cell biology 9, 1370-1380.

Tripathy, S.K., Weil, S.J., Chen, C., Anand, P., Vallee, R.B., Gross, S.P., 2014. Autoregulatory mechanism for dynactin control of processive and diffusive dynein transport. Nature cell biology 16, 1192-1201.

Ueno, H., Huang, X., Tanaka, Y., Hirokawa, N., 2011. KIF16B/Rab14 molecular motor complex is critical for early embryonic development by transporting FGF receptor. Developmental cell 20, 60-71.

Ullrich, O., Horiuchi, H., Bucci, C., Zerial, M., 1994. Membrane association of Rab5 mediated by GDP-dissociation inhibitor and accompanied by GDP/GTP exchange. Nature 368, 157-160.

Vale, R.D., 1990. Microtubule-based motor proteins. Current opinion in cell biology 2, 15-22.

Vale, R.D., 2003. The molecular motor toolbox for intracellular transport. Cell 112, 467-480.

Vallee, R.B., McKenney, R.J., Ori-McKenney, K.M., 2012. Multiple modes of cytoplasmic dynein regulation. Nature cell biology 14, 224-230.

Vallee, R.B., Wall, J.S., Paschal, B.M., Shpetner, H.S., 1988. Microtubule-associated protein 1C from brain is a two-headed cytosolic dynein. Nature 332, 561-563.

van der Zand, A., Tabak, H.F., 2013. Peroxisomes: offshoots of the ER. Current opinion in cell biology 25, 449-454.

van Spronsen, M., Mikhaylova, M., Lipka, J., Schlager, M.A., van den Heuvel, D.J., Kuijpers, M., Wulf, P.S., Keijzer, N., Demmers, J., Kapitein, L.C., Jaarsma, D., Gerritsen, H.C., Akhmanova, A., Hoogenraad, C.C., 2013. TRAK/Milton motor-adaptor proteins steer mitochondrial trafficking to axons and dendrites. Neuron 77, 485-502.

Verhey, K.J., Hammond, J.W., 2009. Traffic control: regulation of kinesin motors. Nature reviews. Molecular cell biology 10, 765-777.

Verhey, K.J., Kaul, N., Soppina, V., 2011. Kinesin assembly and movement in cells. Annu Rev Biophys 40, 267-288.

Walczak, C.E., 2006. Kinesin-8s: motoring and depolymerizing. Nature cell biology 8, 903-905.

Wang, X., Schwarz, T.L., 2009. The mechanism of Ca2+ -dependent regulation of kinesin-mediated mitochondrial motility. Cell 136, 163-174.

Watson, P., Forster, R., Palmer, K.J., Pepperkok, R., Stephens, D.J., 2005. Coupling of ER exit to microtubules through direct interaction of COPII with dynactin. Nature cell biology 7, 48-55.

Welte, M.A., 2004. Bidirectional transport along microtubules. Current biology : CB 14, R525-537.

Welte, M.A., Cermelli, S., Griner, J., Viera, A., Guo, Y., Kim, D.H., Gindhart, J.G., Gross, S.P., 2005. Regulation of lipid-droplet transport by the perilipin homolog LSD2. Current biology : CB 15, 1266-1275.

Welte, M.A., Gross, S.P., Postner, M., Block, S.M., Wieschaus, E.F., 1998. Developmental regulation of vesicle transport in Drosophila embryos: forces and kinetics. Cell 92, 547-557.

Wozniak, M.J., Bola, B., Brownhill, K., Yang, Y.C., Levakova, V., Allan, V.J., 2009. Role of kinesin-1 and cytoplasmic dynein in endoplasmic reticulum movement in VERO cells. Journal of cell science 122, 1979-1989.

Xu, Y., Takeda, S., Nakata, T., Noda, Y., Tanaka, Y., Hirokawa, N., 2002. Role of KIFC3 motor protein in Golgi positioning and integration. The Journal of cell biology 158, 293-303.

Yadav, S., Puthenveedu, M.A., Linstedt, A.D., 2012. Golgin160 recruits the dynein motor to position the Golgi apparatus. Developmental cell 23, 153-165.

Yamada, K.H., Nakajima, Y., Geyer, M., Wary, K.K., Ushio-Fukai, M., Komarova, Y., Malik, A.B., 2014. KIF13B regulates angiogenesis through Golgi to plasma membrane trafficking of VEGFR2. Journal of cell science 127, 4518-4530.

Yano, H., Lee, F.S., Kong, H., Chuang, J., Arevalo, J., Perez, P., Sung, C., Chao, M.V., 2001. Association of Trk neurotrophin receptors with components of the cytoplasmic dynein motor. The Journal of neuroscience : the official journal of the Society for Neuroscience 21, RC125.

Zhang, J., Qiu, R., Arst, H.N., Jr., Penalva, M.A., Xiang, X., 2014. HookA is a novel dynein-early endosome linker critical for cargo movement in vivo. The Journal of cell biology 204, 1009-1026.

2

BICD2, dynactin and LIS1 cooperate in regulating dynein recruitment to cellular structures

Daniël Splinter[a,*], David S. Razafsky[b,*], Max A. Schlager[c], Andrea Serra-Marques[d],
Ilya Grigoriev[a,d], Jeroen Demmers[e], Nanda Keijzer[c], Kai Jiang[d], Ina Poser[f], Anthony A. Hyman[f],
Casper C. Hoogenraad[c,d], Stephen J. King[b,†] and Anna Akhmanova[a,d]

[a]Department of Cell Biology, Erasmus Medical Centre, 3000 CA Rotterdam, Netherlands
[c]Department of Neuroscience, Erasmus Medical Centre, 3000 CA Rotterdam, Netherlands
[e]Proteomics Centre, Erasmus Medical Centre, 3000 CA Rotterdam, Netherlands
[b]Division of Molecular Biology and Biochemistry, University of Missouri–Kansas City, Kansas City, MO 64110
[d]Cell Biology, Faculty of Science, Utrecht University, 3584 CH Utrecht, Netherlands
[f]Max Planck Institute of Molecular Cell Biology and Genetics, 01307 Dresden, Germany

Molecular Biology of the Cell 2012 Nov;23(21):4226-41

BICD2, dynactin, and LIS1 cooperate in regulating dynein recruitment to cellular structures

Daniël Splinter[a,*], David S. Razafsky[b,*], Max A. Schlager[c], Andrea Serra-Marques[d], Ilya Grigoriev[a,d], Jeroen Demmers[e], Nanda Keijzer[c], Kai Jiang[d], Ina Poser[f], Anthony A. Hyman[f], Casper C. Hoogenraad[c,d], Stephen J. King[b,†], and Anna Akhmanova[a,d]
[a]Department of Cell Biology, [c]Department of Neuroscience, and [e]Proteomics Centre, Erasmus Medical Centre, 3000 CA Rotterdam, Netherlands; [b]Division of Molecular Biology and Biochemistry, University of Missouri–Kansas City, Kansas City, MO 64110; [d]Cell Biology, Faculty of Science, Utrecht University, 3584 CH Utrecht, Netherlands; [f]Max Planck Institute of Molecular Cell Biology and Genetics, 01307 Dresden, Germany

ABSTRACT **Cytoplasmic dynein is the major microtubule minus-end–directed cellular motor. Most dynein activities require dynactin, but the mechanisms regulating cargo-dependent dynein–dynactin interaction are poorly understood. In this study, we focus on dynein–dynactin recruitment to cargo by the conserved motor adaptor Bicaudal D2 (BICD2). We show that dynein and dynactin depend on each other for BICD2-mediated targeting to cargo and that BICD2 N-terminus (BICD2-N) strongly promotes stable interaction between dynein and dynactin both in vitro and in vivo. Direct visualization of dynein in live cells indicates that by itself the triple BICD2-N–dynein–dynactin complex is unable to interact with either cargo or microtubules. However, tethering of BICD2-N to different membranes promotes their microtubule minus-end–directed motility. We further show that LIS1 is required for dynein-mediated transport induced by membrane tethering of BICD2-N and that LIS1 contributes to dynein accumulation at microtubule plus ends and BICD2-positive cellular structures. Our results demonstrate that dynein recruitment to cargo requires concerted action of multiple dynein cofactors.**

Monitoring Editor
Xueliang Zhu
Chinese Academy of Sciences

Received: Mar 14, 2012
Revised: Aug 24, 2012
Accepted: Aug 30, 2012

INTRODUCTION

Cytoplasmic dynein is a motor responsible for moving a large variety of cargoes to the minus ends of microtubules (MTs; Kardon and Vale, 2009). The majority of dynein-dependent transport processes require dynactin, a protein complex that stimulates dynein processivity and participates in cargo binding (Holleran *et al.*, 1998; Schroer, 2004). Dynein and dynactin directly bind to each other through the interaction between the dynactin subunit p150^{Glued} and the dynein intermediate chain (DIC; Karki and Holzbaur, 1995; Vaughan and Vallee, 1995; King *et al.*, 2003). Although dynein and dynactin can be isolated from brain extracts, the purified complexes are not strongly bound to each other (Bingham *et al.*, 1998). Several studies suggest that the two complexes exist as separate pools that only transiently come together to induce motility (Quintyne *et al.*, 1999; Quintyne and Schroer, 2002; Habermann *et al.*, 2001). This notion is supported by imaging studies in budding yeast, which suggest that the dynein–dynactin interaction is tightly regulated (Woodruff *et al.*, 2009; Markus and Lee, 2011). Therefore it appears that additional factors must be present in cells to regulate the dynein–dynactin association and thus dynein-dependent cargo transport.

One well-studied adaptor for MT motors is the evolutionary conserved coiled-coil protein Bicaudal D (BicD; Claussen and Suter, 2005). In *Drosophila*, BicD controls movement of messenger

---

This article was published online ahead of print in MBoC in Press (http://www.molbiolcell.org/cgi/doi/10.1091/mbc.E12-03-0210) on September 5, 2012.

*These authors contributed equally to this article.

[†]Present address: Burnett School of Biomedical Sciences, University of Central Florida, Orlando, FL 32827.

Address correspondence to: Anna Akhmanova (a.akhmanova@uu.nl), Stephen J. King (stephen.king@ucf.edu).

Abbreviations used: AL, annulate lamellae; BICD, Bicaudal D; BICD2-C, Bicaudal D2 C-terminus; BICD2-FL, Bicaudal D2 full-length protein; BICD2-N, Bicaudal D2 N-terminus; DHC, dynein heavy chain; DIC, dynein intermediate chain; DLIC, dynein light intermediate chain; GFP, green fluorescent protein; HA, hemagglutinin; IP, immunoprecipitation; MT, microtubule; NE, nuclear envelope.

© 2012 Splinter *et al.* This article is distributed by The American Society for Cell Biology under license from the author(s). Two months after publication it is available to the public under an Attribution–Noncommercial–Share Alike 3.0 Unported Creative Commons License (http://creativecommons.org/licenses/by-nc-sa/3.0).
"ASCB®," "The American Society for Cell Biology®," and "Molecular Biology of the Cell®" are registered trademarks of The American Society of Cell Biology.

ribonucleoproteins and lipid droplets during development (Bullock *et al.*, 2006; Clark *et al.*, 2007; Larsen *et al.*, 2008; Dienstbier *et al.*, 2009; Bianco *et al.*, 2010). The mammalian homologues of fly BicD, Bicaudal D1 (BICD1) and BICD2, participate in vesicle transport: their C-terminal cargo-binding segment associates with the small GTPase Rab6, which is present at the Golgi and exocytotic vesicles (Hoogenraad *et al.*, 2001; Matanis *et al.*, 2002; Short *et al.*, 2002; Grigoriev *et al.*, 2007). The fly BicD also binds to Rab6 (Coutelis and Ephrussi, 2007; Januschke *et al.*, 2007) and in addition participates in clathrin-mediated membrane trafficking (Li *et al.*, 2010). Furthermore, BicD homologues in mammals, flies, and worms are involved in MT-dependent nuclear positioning (Swan *et al.*, 1999; Fridolfsson *et al.*, 2010; Splinter *et al.*, 2010). In mammalian cells this function depends on the recruitment of BICD2 to the nuclear envelope (NE) through the interaction between BICD2 C-terminus (BICD2-C) and the nucleoporin RanBP2 (Splinter *et al.*, 2010). In flies, BicD-C binds to Egalitarian and FMRP, which in turn associate with mRNAs (Dienstbier *et al.*, 2009), and with the clathrin heavy chain (Li *et al.*, 2010), in line with the view that the C-terminal domain is the cargo-binding part of the BicD molecule.

Studies in flies, worms, and mammals have shown that BicD homologues participate in several transport pathways, which depend on cytoplasmic dynein and kinesin-1 (Claussen and Suter, 2005; Dienstbier *et al.*, 2009; Fridolfsson *et al.*, 2010; Splinter *et al.*, 2010; Aguirre-Chen *et al.*, 2011). The N-terminal portion of BICD (BICD-N) is responsible for the recruitment of dynein and dynactin: our previous study showed that when the N-terminal fragment of BICD2 is artificially tethered to cargoes, it induces their dynein-dependent transport to MT minus ends (Hoogenraad *et al.*, 2003). These observations were confirmed for *Drosophila* BicD using mRNA transport as a model (Dienstbier *et al.*, 2009). Owing to the potent and conserved capacity to induce dynein-based motility, BICD adaptors thus represent a good model with which to dissect the molecular mechanisms of dynein targeting and activation.

RESULTS

BICD2-N forms a triple complex with dynein and dynactin in cells

To characterize the binding of BICD2 to dynein and dynactin, we investigated their interactions by immunoprecipitation (IP). HeLa cells were transfected with constructs expressing green fluorescent protein (GFP)-tagged BICD2 full length (GFP-BICD2-FL), GFP-BICD2-N, GFP-BICD2-C (Figure 1A), or GFP alone as a negative control, and lysates of these cells were used for IP with anti-GFP antibodies (Figure 1B, left). When GFP-BICD2-N was pulled down from HeLa cells, both dynein and dynactin were efficiently precipitated, whereas a much weaker coprecipitation was observed with GFP-BICD2-FL and no interaction was seen with GFP-BICD2-C or GFP (Figure 1B). To determine whether BICD2 preferentially binds to dynein or dynactin, we performed IPs of endogenous dynein and dynactin using DIC and p150$^{\text{Glued}}$ antibodies and found that GFP-BICD2-N was efficiently coprecipitated with both complexes (Figure 1B, middle and right). Remarkably, whereas dynein and dynactin displayed very little coprecipitation in control GFP-expressing cells or in cells expressing GFP-BICD2-C, coprecipitation of the two complexes was significantly increased in cells overexpressing GFP-BICD2-N (Figure 1B, middle and right, vertical arrows). Expression of GFP-BICD2-FL also increased coprecipitation of dynein with dynactin, but the effect was weaker than that observed with GFP-BICD2-N (Figure 1B, middle).

To obtain an independent confirmation of these observations, we performed IP with anti-GFP antibodies from HeLa cells stably expressing endogenous levels of C-terminally tagged GFP fusions of dynein/dynactin subunits generated by BAC TransgeneOmics (Poser *et al.*, 2008). For these experiments, we used stable cell lines expressing GFP-tagged dynein heavy chain (DHC), dynein IC 2 (DIC2), dynein light intermediate chain 1 (DLIC1), or p50 (also known as dynamitin or dynactin 2). We transfected these four cell lines with constructs encoding hemagglutinin (HA)-tagged BICD2-FL or BICD2-N. As a control, we used HA-tagged GRASP-1 (Hoogenraad *et al.*, 2010), an endosomal coiled-coil adaptor protein that does not interact with dynein or dynactin. The same stable cell lines that were not transfected with any additional constructs were used as another control. We found that all three GFP-tagged dynein subunits coprecipitated endogenous DIC, indicating that they were incorporated into the dynein complex (Figure 1C). The three dynein subunits weakly coprecipitated HA–BICD2-FL and strongly coprecipitated BICD2-N (Figure 1C). Of importance, although coprecipitation of dynactin with the three dynein subunits was weak in control cells, it was strongly enhanced in cells expressing BICD2-N (Figure 1C, vertical arrows below the blots). p50-GFP coprecipitated p150$^{\text{Glued}}$, suggesting that it was incorporated into dynactin, and it also coprecipitated BICD2-N (Figure 1C, bottom right). p50-GFP did not coprecipitate dynein from control cells, but a significant amount of coprecipitated dynein was observed in BICD2-N–expressing cells (Figure 1C, vertical arrow). Taken together, the results of IP of endogenous and GFP-tagged dynein and dynactin subunits indicate that high levels of BICD2-N stabilize the interaction between dynein and dynactin. The interaction of dynein and dynactin with BICD2-FL was much weaker, suggesting that it is inhibited by the C-terminal part of BICD2, as proposed previously (Hoogenraad *et al.*, 2001, 2003).

BICD2-N forms a triple complex with dynein and dynactin in vitro

Strong association of BICD2-N with both dynein and dynactin correlates with its capacity to induce minus end–directed movement. When BICD2-N is artificially tethered to mitochondria and peroxisomes by a fusion with a *Listeria monocytogenes* ActA-derived membrane-targeting sequence (MTS), these organelles are relocated to centrosomes, where they form a distinct cluster with a compact accumulation of peroxisomes surrounded by mitochondria (Hoogenraad *et al.*, 2003). We generated a series of deletion mutants of the original BICD2-N fragment and used the peroxisome/mitochondria relocalization assay to map the minimal dynein–dynactin interaction domain of BICD2 (Supplemental Figure S1A). We found that the BICD2-N region located between residues 25 and 400 (BICD2-Nsh, the "short" version of BICD2-N; Supplemental Figure S1A) was sufficient to potently target peroxisomes and mitochondria to the centrosome (Supplemental Figure S1B and unpublished data).

Next we purified BICD2-Nsh fragment from *Escherichia coli* and examined its capacity to promote dynein-dynactin association in vitro. Dynein and dynactin were purified from bovine brain as described previously (Bingham *et al.*, 1998; Mallik *et al.*, 2005; Supplemental Figure S1, C and D). Mass spectrometry–based characterization of the two complexes showed that they are not significantly contaminated with each other (Table S1, A and B). Next we analyzed the complexes using sucrose density gradient centrifugation. When analyzed separately, purified dynein and dynactin were present in successive fractions corresponding to ~20S (Figure 2A). In addition, when dynein and dynactin were mixed together prior to the analysis, they were still present in the same fractions, indicating that the two complexes do not stably bind each other after

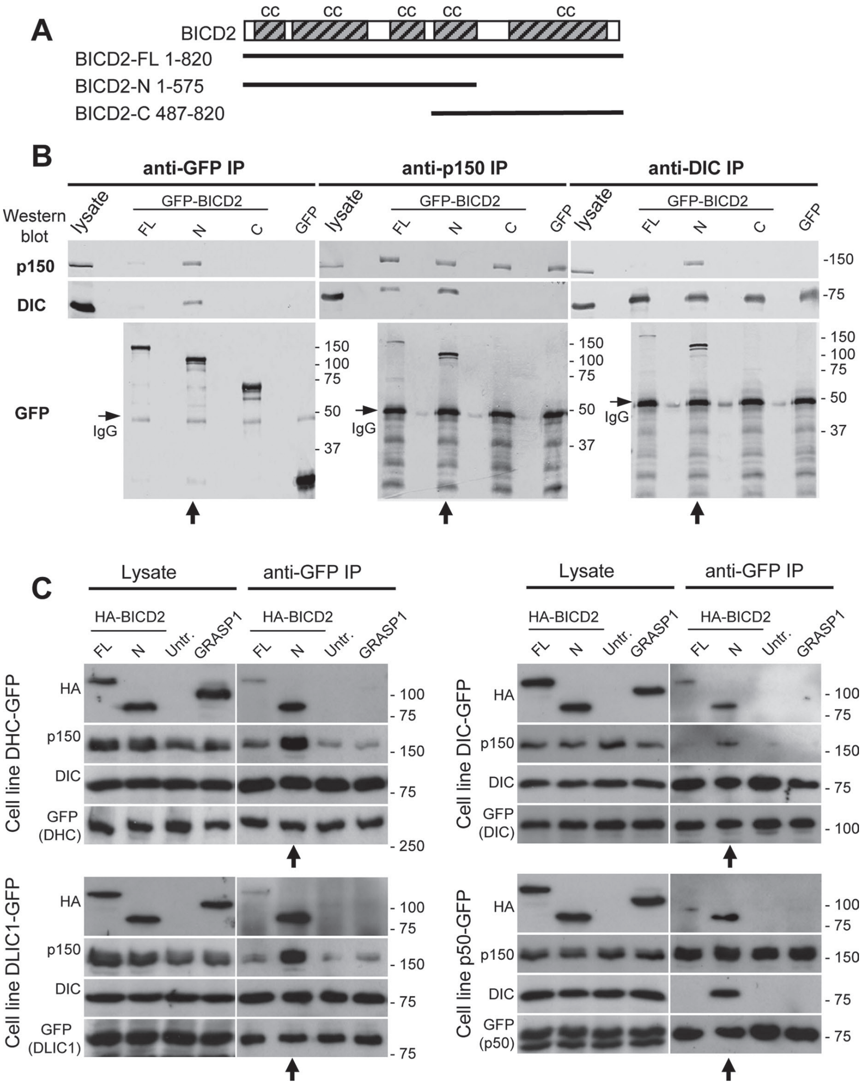
A
BICD2
CC
CC
CC
CC
CC
BICD2-FL 1-820
BICD2-N 1-575
BICD2-C 487-820
B
anti-GFP IP
anti-p150 IP
anti-DIC IP
Western blot
lysate
GFP-BICD2
FL
N
C
GFP
p150
DIC
GFP
IgG
-150
-75
- 150
- 100
- 75
- 50
- 37
C
Lysate
anti-GFP IP
HA-BICD2
FL
N
Untr.
GRASP1
Cell line DHC-GFP
Cell line DIC-GFP
Cell line DLIC1-GFP
Cell line p50-GFP
HA
p150
DIC
GFP (DHC)
GFP (DIC)
GFP (DLIC1)
GFP (p50)
- 100
- 75
- 150
- 250

FIGURE 1: BICD2-N overexpression stabilizes the dynein–dynactin complex in cells. (A) Scheme of BICD2 structure and GFP-BICD2 fusions. (B, C) IP assays with antibodies against GFP, dynactin (p150^{Glued}), and dynein (DIC) were performed with extracts from control HeLa cells transiently overexpressing the indicated GFP-BICD2 fusions or GFP alone (B) or HeLa cells stably expressing GFP-tagged dynein or dynactin subunits either alone (untr.) or in combination with transiently overexpressed, HA-tagged BICD2 or GRASP1 fusions (C). Western blotting was performed with the indicated antibodies. From 1 to 2% of the cell lysate used for the IP and 25% of the IP sample were loaded on gel. In panel B, lanes where GFP-BICD2-N is present show enhanced coprecipitation of dynein and dynactin (vertical arrows below the blots). Bands corresponding to the heavy chain of the antibody used for IP are visible in Western blots with GFP antibodies shown in B (immunoglobulin G, horizontal arrows). In panel C, BICD2-N is coprecipitated with dynein and dynactin and enhances coprecipitation of the two complexes with each other (vertical arrows below the blots). Note that coimmunoprecipitation of dynactin with DIC might be weak because the antibody used, DIC 74.1, can inhibit the interaction between dynein and dynactin.

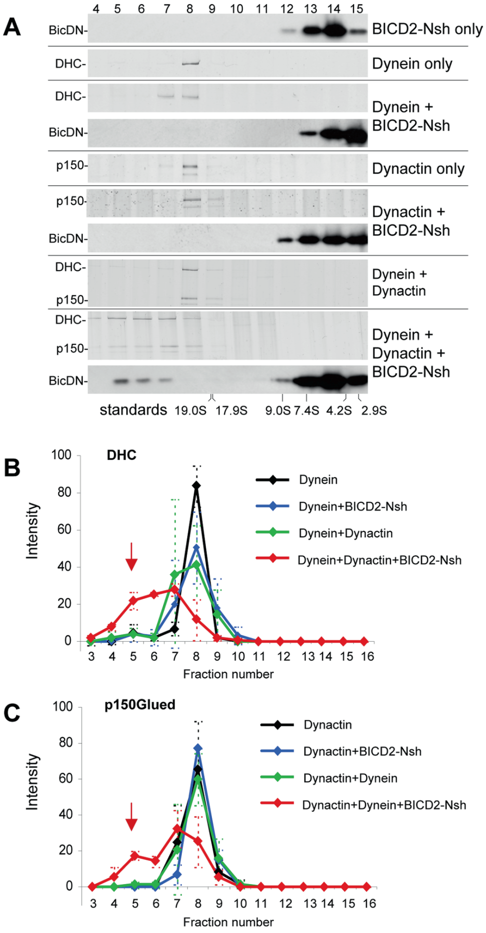

FIGURE 2: Purified BICD2-N, dynein, and dynactin form a triple complex in vitro. Dynein, dynactin, or their combinations with or without BICD2-Nsh (as shown on the right) were sedimented on 10–40% linear sucrose gradients. After centrifugation, equal fractions were collected from the bottom of the gradients and subjected to SDS–PAGE (fraction numbers on top). Dynein and dynactin were found in fractions corresponding to ~20S as determined by silver staining to identify DHC or p150^{Glued}. The position of BICD2-Nsh was determined by Western blotting with anti-BICD2 antibodies. Positions of sucrose density standards are shown at the bottom. Representative gels are shown in A, and quantifications of DHC and p150^{Glued} in different conditions, determined from three independent experiments, are shown in B and C; error bars represent SD. Incubation of dynein and dynactin with the excess of BICD2-Nsh caused a shift of dynein and dynactin and a portion of the BICD2-Nsh protein to denser gradient fractions, indicating that a stable triple complex was present (red arrows in B and C).

purification. The much smaller BICD2-Nsh molecules were found in the lighter fractions at the top of the gradient (Figure 2A). of interest, when we combined dynein, dynactin, and BICD2-Nsh, a considerable proportion of all three components shifted to higher-density fractions, indicating that they had formed a stable supercomplex (Figure 2, A–C). No shift in sedimentation was seen when BICD2-Nsh was added to either dynein or dynactin alone (Figure 2, B and C), indicating that a stable interaction requires the presence of all three components: BICD2-N, dynein, and dynactin. The fact that BICD2-Nsh did not bind to dynein or dynactin alone also showed that the observed interaction is not simply the result of unspecific binding of coiled-coil domains of BICD2, dynein, and dynactin.

We next attempted to identify direct BICD2-N binding partners from the multiple subunits that comprise dynein and dynactin. An N-terminally biotinylated version of BICD2-N was purified from HEK293 cells (Supplemental Figure S1E) and mixed with purified dynein and dynactin, and the resulting complexes were cross-linked with very low doses of the chemical cross-linking reagent Bis[sulfosuccinimidyl] glutarate. The cross-linked complexes were solubilized in denaturing conditions so that only the cross-linked proteins would retain the association with BICD2-N. Subsequently, the biotinylated BICD2-N (together with any cross-linked polypeptides) was isolated by streptavidin pull-down and subjected to mass spectrometry analysis. Of interest, only a small subset of dynein and dynactin subunits was recovered: these included the dynactin p150^{Glued} subunit, DHC, and DLICs (Supplemental Table S1C). The presence of both DHC and DLICs together is not surprising because these dynein subunits are known to bind to each other very tightly and to form a stable subcomplex even in the presence of chaotropic agents (King *et al.*, 2002). Taken together, these data suggest that BICD2-N simultaneously binds p150^{Glued} and either DHC or DLICs.

The cross-linking experiment suggests that the Arp1 filament subcomplex of dynactin is not directly involved in the formation of the triple complex with BID2-N and dynein. Of interest, unlike most other dynein-mediated processes, BICD2-N–dependent organelle relocalization was not inhibited by overexpression of the p50/dynamitin subunit of dynactin, which is known to dissociate p150^{Glued} from the Arp1 filament (Hoogenraad *et al.*, 2003; Melkonian *et al.*, 2007). These results suggest that when BICD2-N is directly tethered to membranes, it might induce their dynein-mediated relocalization in the absence of Arp1 recruitment. We tested this idea by inducing formation of the mitochondria/peroxisome cluster by expressing BICD2-N-MTS and staining it for dynein and dynactin subunits. We found that the overexpression of p50/dynamitin did not block the strong accumulation of dynein and p150^{Glued} at the BICD2-N-MTS–induced mitochondrial cluster but completely removed Arp1 (Supplemental Figure S2). These data are in line with the view that the Arp1 filament of dynactin does not directly participate in BICD2-N–dependent dynein–dynactin interaction and support our data indicating that BICD2-N binds to dynactin through the p150^{Glued}-containing shoulder/sidearm subcomplex.

BICD2-N overexpression causes dynein detachment from cargo and MTs

The finding that BICD2-N stabilizes dynein–dynactin association was unexpected because overexpressed BICD2-N acts as a potent dynein inhibitor (Hoogenraad *et al.*, 2001; Teuling *et al.*, 2008), whereas improved binding to dynactin is supposed to enhance dynein targeting to structures that contain dynactin-interacting proteins such as spectrin (Holleran *et al.*, 1996; Muresan *et al.*, 2001). To investigate directly what happens to dynein when it forms a triple complex

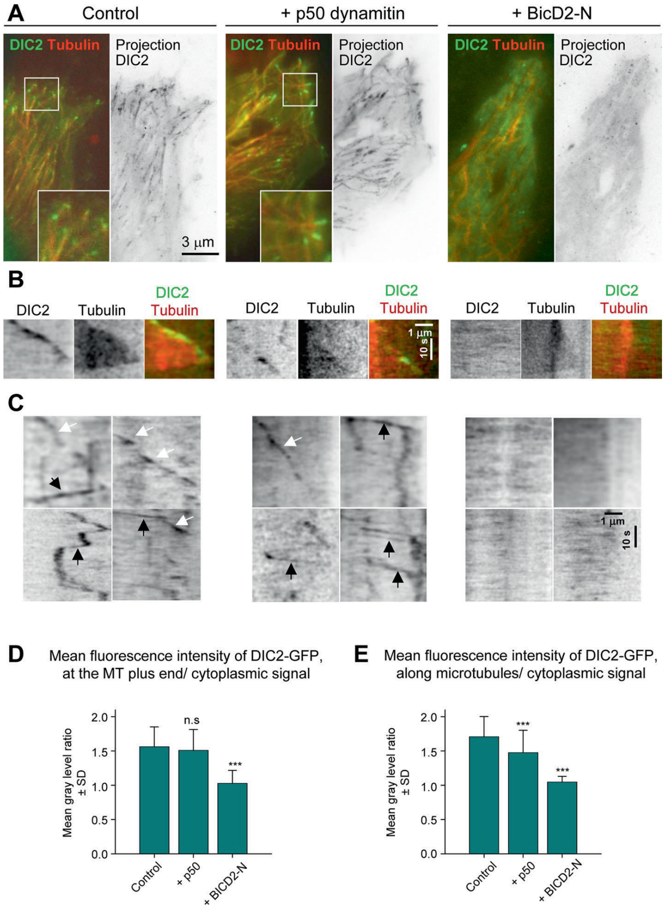
A
Control
+ p50 dynamitin
+ BicD2-N
DIC2 Tubulin
Projection DIC2
3 μm
B
DIC2
Tubulin
DIC2 Tubulin
1 μm
10 s
C
D
Mean fluorescence intensity of DIC2-GFP, at the MT plus end/ cytoplasmic signal
E
Mean fluorescence intensity of DIC2-GFP, along microtubules/ cytoplasmic signal
Mean gray level ratio ± SD
2.0
1.5
1.0
0.5
0.0
n.s
***
Control
+ p50
+ BICD2-N

FIGURE 3: BICD2-N overexpression removes cytoplasmic dynein from MTs. HeLa cells stably expressing DIC2-GFP from a GFP-tagged BAC were transfected with either mCherry–α-tubulin alone or in combination with either HA-tagged p50 or BICD2-N, and simultaneous two-color live-cell imaging with 500-ms interval was performed using TIRF microscopy with high penetration depth. Five consecutive frames were averaged. Control stainings showed 100% cotransfection of mCherry–α-tubulin with HA-tagged fusions. (A) Representative images of DIC2-GFP (green) and mCherry–α-tubulin (red) are shown on the left, and projections of sequential frames (181 (control), 221 (p50), and 117 (BicD-N) are shown on the right. Insets show enlargements of the boxed areas. (B, C) Kymographs illustrating DIC2-GFP displacement at MT tips (B) and along MT lattice (C). In C, rapid particle movements along MTs are indicated by black arrows and the slower movements associated with the growing MT tips by white arrows. (D, E) Quantification of the mean DIC2-GFP signal at the MT plus ends or along MTs normalized by the cytoplasmic signal (a value of 1 indicates absence of enrichment along MTs). Error bars indicate SD; ~30–70 MTs were analyzed in five to seven cells per condition. Values significantly different from control are indicated (Mann–Whitney *U* test, $**p < 0.01$, $***p < 0.001$).

with BICD2-N and dynactin, we examined the localization of GFP-tagged dynein subunits in live cells expressing HA–BICD2-N, using mCherry-α-tubulin as a cotransfection marker (Figure 3). For comparison, in these experiments we used a broadly applied and highly potent dynein inhibitor, p50/dynamitin (Echeverri *et al.*, 1996). HA-tagged versions of both BICD2-N and p50 were used to allow visualization of GFP-fused dynein subunits together with mCherry–α-tubulin.

DIC2-GFP, DHC-GFP, and DLIC1-GFP behaved very similarly in these experiments, and therefore only the results with DIC2-GFP will be discussed in detail. DIC2-GFP was diffusely present in the cytosol, and, in addition, GFP-positive foci and comets were visible (Figure 3A and Supplemental Movie S1). Maximum-intensity projections showed that most of these mobile structures colocalized with MTs. Kymograph analysis along individual MT tracks showed that the comet-like labeling represented growing MT tips, a dynein localization described previously (Vaughan *et al.*, 1999; Kobayashi and Murayama, 2009; Figure 3B and Supplemental Movie S1). In addition to these slowly moving structures (average velocity of 0.2–0.3 μm/s, which corresponds to the average rate of MT polymerization), we also observed GFP-positive foci that moved rapidly along MTs in both plus- and minus-end directions with velocities in the range of 1–2 μm/s (see Figure 3C for representative kymographs). Plus end–directed motility episodes likely represented dynein traveling as a passenger on a bidirectionally moving cargo. Cotransfection of HA-p50 had no strong effect on this localization pattern (Figure 3, A and B, and Supplemental Movie S1). Measurements of the ratio of DIC2-GFP signal along the MTs and in the surrounding cytoplasm showed clear enrichment of the DIC2-GFP on MTs in control and HA-p50 transfected cells (Figure 3, D and E). HA-p50 overexpression caused no significant loss of dynein from MT tips, but the number of DIC2-GFP foci moving along MTs was reduced (Figure 3E), in agreement with the fact that p50 acts as a dynein inhibitor.

Unexpectedly, the overexpression of HA–BICD2-N caused a dramatic redistribution of both MT-associated pools of DIC2-GFP into the cytosol: we observed no DIC2-GFP particles moving along MTs to either plus or minus ends (Figure 3, A, C, and E, and Supplemental Movie S1). The fact that dynein bound to BICD2-N and dynactin is removed from different motile cargoes suggests that BICD2-N occludes an essential interaction site used by multiple dynein adaptors and that additional binding sites present on different dynein and dynactin subunits are not sufficient to target the triple BICD-N–dynein–dynactin complex to cellular structures.

Moreover, BICD2-N expression abolished dynein accumulation at MT ends (Figure 3, A, B, and D, and Supplemental Movie S1), an effect that could be confirmed by staining of fixed DIC2-GFP–expressing cells with a MT plus-end marker EB1 (Supplemental Figure S3A). This result was surprising because the published data suggest that in mammalian cells dynein is targeted to MT tips by dynactin, which binds to MT plus ends through the interaction of the CAP-Gly domain of p150$^{\text{Glued}}$ with CLIP-170 and EB1 (Vaughan *et al.*, 1999, 2002; Lansbergen *et al.*, 2004). To test whether this view is correct, we performed live imaging of GFP-tagged dynein subunits and the dynactin subunit p50 (Figure 4 and Supplemental Movie S2). After knockdown of p150$^{\text{Glued}}$, dynein became much more diffuse: it no longer accumulated at MT tips, and the number of motile dynein foci was strongly reduced, indicating that dynein recruitment to MT tips and motile cargo is indeed dynactin dependent (Figure 4, A, C, and E, and Supplemental Movie S2; see Supplemental Figure S4 for illustration of p150$^{\text{Glued}}$ knockdown efficiency). In contrast, dynactin (detected with p50-GFP) was still observed at MT plus ends in DHC-depleted cells, although the number of labeled MT ends, as well as the number of particles moving along the MTs, was decreased (Figure 4, B, D, and F, and Supplemental Movie S3; see Supplemental Figure S4 for illustration of DHC knockdown efficiency). We thus showed in live cells that in the mammalian system dynein interaction with MT tips is dynactin dependent, whereas dynactin binds to MT plus ends in a dynein-independent manner.

On the basis of all these observations, one could expect that an enhanced interaction between dynein and dynactin induced by BICD2-N would promote dynein recruitment to MT ends. Yet the opposite was true, suggesting that the triple complex formed by BICD2-N, dynactin, and dynein is not competent to interact with MTs. In line with this view, we never observed any enrichment of BICD2-N at the growing MT tips even when this protein was expressed at very low levels (unpublished data), indicating that in spite of its high affinity for dynein and dynactin, BICD2-N cannot be recruited by these complexes to MT ends. It is possible that by binding to dynein and dynactin, BICD2-N induces a conformational change in one or both complexes that is incompatible with their binding to MT ends. Of importance, endogenous dynactin could still be detected at the MT tips in BICD2-N–expressing cells (Supplemental Figure S3B), indicating that a pool of free dynactin that is not bound to BICD2-N and dynein can associate with MT ends. Taken together, our results indicate that dynein targeting to MT tips is more complex than previously believed and that the inhibition of dynein activity by BICD2-N (Hoogenraad *et al.*, 2001; Teuling *et al.*, 2008) is due to dynein sequestration from the normal sites of its activity.

Detailed analysis of BICD2-N–induced cargo movement

The described results suggest that BICD2-N does not simply stabilize dynein–dynactin binding, but that it also affects the properties of the complex. To analyze whether binding to BICD2-N and dynactin within the triple complex affects characteristic properties of dynein movement, we used a regulated heterodimerization system, which allowed us to recruit BICD2-N and associated proteins to different cargoes and measure parameters of their movement by high-resolution live-cell imaging. The heterodimerization system that we used was based on the fact that FKBP12 and FRAP (mTOR) proteins bind to each other with high affinity in the presence of rapamycin (Pollock *et al.*, 2000). Two copies of the rapamycin-binding domain of the human FKBP12 protein (FKBP) were fused to the N-terminus of different cargo-targeting proteins, and a copy of the FRAP domain, which binds to the FKBP12-rapamycin complex (FRB), was added to the C-terminus of the HA–BICD2-N fusion (Figure 5A). A modified version of the FRB domain that can bind to FKBP in the presence of nonimmunosuppressive rapamycin analogue AP21967 (rapalog) was used in these experiments to avoid effects on the endogenous mTOR/FRAP pathway (Pollock *et al.*, 2000).

Our first goal was to compare the parameters of motility induced by BICD2-N to movement of a natural BICD2 cargo, Rab6-positive exocytotic vesicles (Matanis *et al.*, 2002; Grigoriev *et al.*, 2007). To achieve this, we fused FKBP to the N-terminus of GFP-tagged Rab6A (Figure 5A). FKBP2-GFP-Rab6A bound to the Golgi and cytoplasmic vesicles, which moved from the Golgi toward the cell periphery and fused with the plasma membrane, very similar to GFP-Rab6A (Grigoriev *et al.*, 2007; Figure 5B, left, and Supplemental Movie S4).

When HA–BICD2-N–FRB was coexpressed with FKBP2-GFP-Rab6A in the absence of rapalog, strong dispersion of the Golgi apparatus was observed, in line with the fact that BICD2-N diffusely present in the cell inhibits dynein function (Hoogenraad *et al.*, 2001; Figure 5B, middle). The addition of rapalog, which induces FKBP–FRB interaction, caused relocalization of all FKBP2-GFP-Rab6A–positive structures to the cell center, which occurred within 15–25 min (Figure 5B, right, and Supplemental Movie S5). When this experiment was carried out using a red (mStrawberry)-tagged Rab6A in HeLa cells expressing DIC2-GFP, we observed that the diffuse pool of dynein, induced by HA–BICD2-N–FRB overexpression, was recruited to Rab6-positive membranes (Figure 5C and Supplemental Movies S6 and S7).

To be able to distinguish unambiguously MT plus- and minus-end–directed vesicle movements, we used rapid two-color imaging of MRC5-SV human lung fibroblasts in which MTs were visualized with mCherry–α-tubulin (Shaner *et al.*, 2004). The extremely sparse MT network in this cell type permitted us to observe movement of individual vesicles along individual MTs, the plus ends of which could be distinguished by the presence of growth episodes (Figure 5D, and Supplemental Movie S8). Rapid high resolution imaging in MRC5 cells showed that HA-BICD2-N–mediated relocalization of Rab6 membranes to the cell center proceeded in a bidirectional manner: vesicles moving along MTs were frequently switching between MT plus-end and minus-end–directed runs. However, in contrast to control cells, where plus-end–directed vesicle motion predominated, BICD2-N recruitment strongly increased the frequency of MT minus-end–directed movements (Figure 5, E and F, and Supplemental Movie S9). In spite of the significant recruitment of dynein to Rab6A-positive membranes, the velocity of plus- and minus-end–directed movement was the same in the absence of HA–BICD2-N–FRB fusion and after rapalog-induced HA–BICD-N–FRB tethering to Rab6A vesicles (Figure 5G and Supplemental Figure S5).

To further investigate the velocities of BICD-N–induced movement, we used another cargo, Rab3C, which, in contrast to Rab6A, does not associate with endogenous BICD1/2. Rab3C-positive membranes were dispersed through the cytoplasm and showed only infrequent MT-based movements (Figure 6, A–C). Recruitment of HA–BICD2-N–FRB to Rab3C vesicles increased the frequency of their movement, with velocities that were similar to those of Rab6A vesicles (Figure 6, B–D). Our results show that the BICD2-N–dynein–dynactin complex artificially attached either to its cognate or to foreign cargo is fully functional for motility. They also suggest that an artificial increase in the number of dynein motors on the cargo through BICD-N–mediated recruitment has no consequences for the velocity of minus-end–directed movement or for the velocity of kinesin-dependent motility in the opposite direction. These data support the view that motors of opposite polarity on the same cargo do not affect each other's velocity and that cargo velocity is not dependent on the number of associated motors (Shubeita *et al.*, 2008).

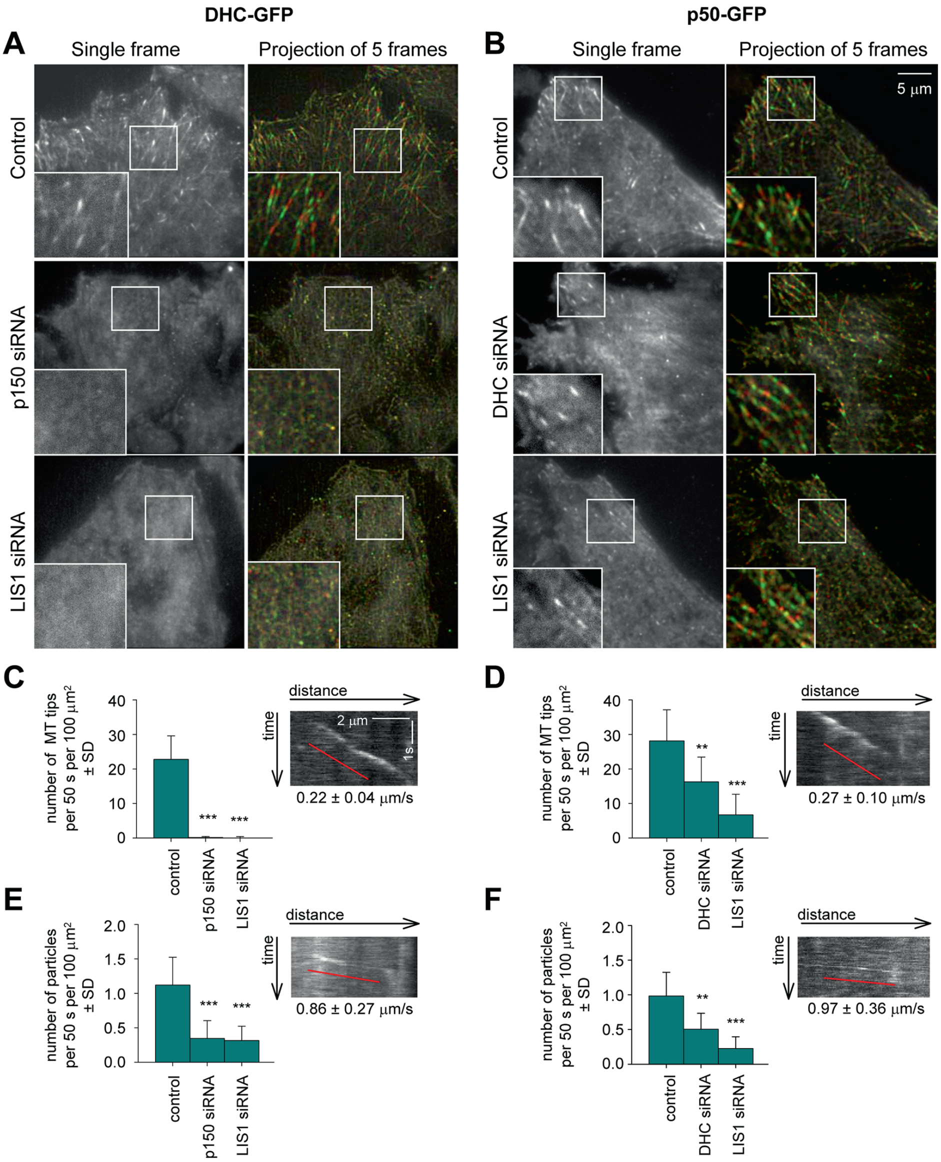
DHC-GFP
p50-GFP
A
Single frame
Projection of 5 frames
B
Single frame
Projection of 5 frames
5 µm
Control
p150 siRNA
LIS1 siRNA
Control
DHC siRNA
LIS1 siRNA
C
number of MT tips per 50 s per 100 µm² ± SD
40
30
20
10
0
***
***
control
p150 siRNA
LIS1 siRNA
distance
time
2 µm
1s
0.22 ± 0.04 µm/s
D
number of MT tips per 50 s per 100 µm² ± SD
40
30
20
10
0
**
***
control
DHC siRNA
LIS1 siRNA
distance
time
0.27 ± 0.10 µm/s
E
number of particles per 50 s per 100 µm² ± SD
2.0
1.5
1.0
0.5
0.0
***
***
control
p150 siRNA
LIS1 siRNA
distance
time
0.86 ± 0.27 µm/s
F
number of particles per 50 s per 100 µm² ± SD
2.0
1.5
1.0
0.5
0.0
**
***
control
DHC siRNA
LIS1 siRNA
distance
time
0.97 ± 0.36 µm/s

FIGURE 4: Dynactin and LIS1 are required for dynein localization to MTs. HeLa cells stably expressing DHC-GFP or p50-GFP from a GFP-tagged BACs were transfected with the indicated siRNAs and used for live-cell imaging with 500-ms interval. Five consecutive frames were averaged. (A, B) Single frames (left) and projections of five consecutive frames (right). Right, odd frames (frames 1, 3 and 5) are shown in green and even frames (frames 2 and 4) are shown in red. (C–F) Analysis of DHC-GFP and p50-GFP dynamics. Quantification of the density of GFP-positive MT ends (C,D) (recognized as comet-like structures with velocity less than 0.5 µm/s) and rapidly moving particles (E, F) (average velocity more than 0.5 µm/s) in different conditions. Plots are represented in the same way as in Figure 3D. Insets show representative kymographs from control cells. Ten cells were analyzed per condition.

LIS1 is required for BICD-N–induced dynein motility

Dynein-mediated organelle motility in cells depends on a number of cofactors, such as the well-known dynein binding protein LIS1 (Vallee *et al.*, 2001). LIS1 was previously implicated in BicD-dependent nuclear positioning (Swan *et al.*, 1999; Bolhy *et al.*, 2011), but it is unclear whether it is required for other BICD-dependent dynein transport routes. We investigated whether LIS1 was present in the complex of BICD2-N, dynein, and dynactin isolated from cells and found that this indeed was the case (Figure 7A).

To test whether LIS1 is needed for BICD2-N–induced motility, we performed RNA interference–mediated LIS1 knockdown. LIS1 could be efficiently depleted from HeLa cells using small interfering RNAs (siRNAs) without affecting the expression of dynein and dynactin (Supplemental Figure S4). As a cargo for this experiment, we used endosomes decorated by FKBP2-VAMP2-GFP (Figure 7B). The advantage of using endosomes as readout is that when dynein is perturbed, endosomes accumulate at the cell margin, whereas other organelles, such as mitochondria or peroxisomes, acquire a more central localization. Dynein-mediated shift to the central cytoplasm regions is thus more apparent for endosomes than for other organelles. Cotransfection of cells with HA–BICD2-N–FRB and FKBP2-VAMP2-GFP resulted in peripherally located endosomes that could be detected with antibodies against transferrin receptor (Figure 7D). The addition of rapalog induced rapid and

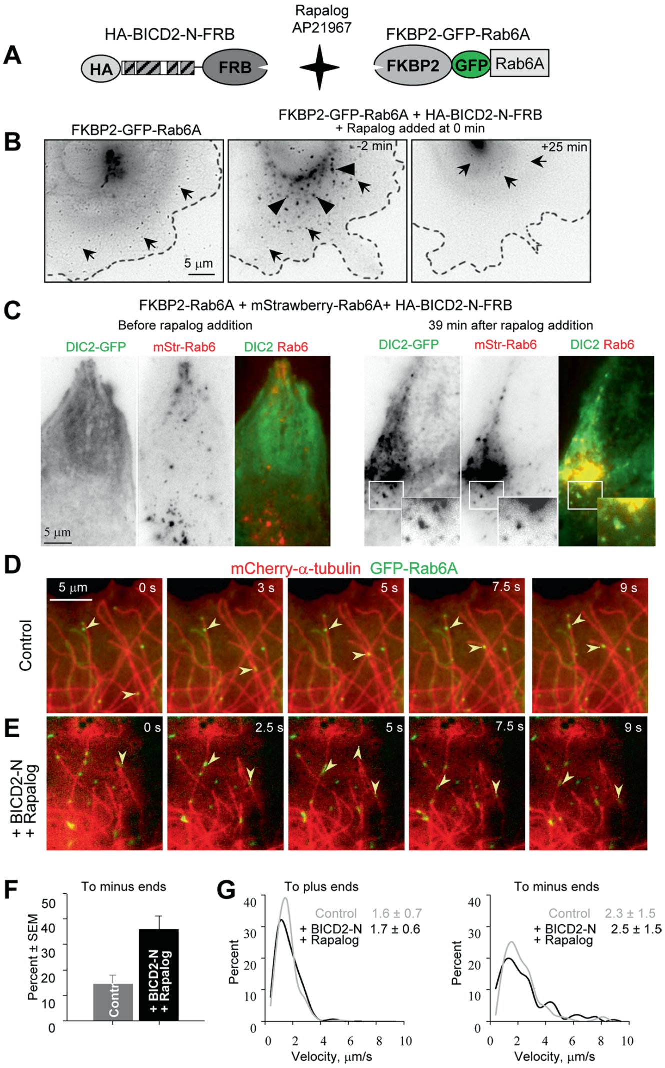
A
HA-BICD2-N-FRB
HA
FRB
Rapalog
AP21967
FKBP2-GFP-Rab6A
FKBP2
GFP
Rab6A
B
FKBP2-GFP-Rab6A
FKBP2-GFP-Rab6A + HA-BICD2-N-FRB
+ Rapalog added at 0 min
-2 min
+25 min
5 µm
C
FKBP2-Rab6A + mStrawberry-Rab6A+ HA-BICD2-N-FRB
Before rapalog addition
39 min after rapalog addition
DIC2-GFP
mStr-Rab6
DIC2 Rab6
5 µm
D
mCherry-α-tubulin GFP-Rab6A
Control
5 µm
0 s
3 s
5 s
7.5 s
9 s
E
+ BICD2-N
+ Rapalog
0 s
2.5 s
5 s
7.5 s
9 s
F
To minus ends
Percent ± SEM
50
40
30
20
10
0
Control
+ BICD2-N
+ Rapalog
G
To plus ends
Percent
40
30
20
10
0
0 2 4 6 8 10
Velocity, µm/s
Control 1.6 ± 0.7
+ BICD2-N 1.7 ± 0.6
+ Rapalog
To minus ends
Control 2.3 ± 1.5
+ BICD2-N 2.5 ± 1.5
+ Rapalog

FIGURE 5: Motility of Rab6A vesicles after BICD2-N recruitment. (A) Scheme of the regulated heterodimerization constructs used to attach BICD2-N to Rab6A-positive membranes. (B) Live image of an MRC5-CV cell expressing FKBP2-GFP-Rab6A alone (left) or together with HA–BICD2-N–FRB (middle and right). The cell shown in the middle and right was treated with 1 µM rapalog AP21967; time relative to the moment of drug addition is indicated. Individual Rab6A vesicles are indicated by arrows and dispersed Golgi fragments by arrowheads. Images were processed by applying Unsharp Mask and Blur filters (Photoshop); contrast is inverted. Cell outlines are indicated by stippled lines. (C) HeLa cells stably expressing DIC-GFP were transiently transfected with FKBP2-Rab6A, mStrawberry-Rab6A, and HA–BICD2-N–FRB and imaged using wide-field microscopy with a 500-ms exposure before and after rapalog addition. Contrast is inverted in single-color frames; in the overlay, DIC-GFP is shown in green and mStrawberry-Rab6A in red. Insets show enlargements of the boxed areas. (D, E) Visualization of Rab6A vesicle movement along MTs. (D) Simultaneous live imaging of FKBP2-GFP-Rab6A (green) and mCherry–α-tubulin (red) in a transiently transfected MRC5 cell; time is indicated. (E) The same as in D, but in a cell cotransfected with HAxBICD2-NxFRB, starting at 47.5 s after rapalog addition. Images were processed by applying Blur filter (Photoshop). Arrowheads indicate vesicles moving toward MT plus ends (D) or minus ends (E). (F, G) Analysis of Rab6 vesicle movement within an ~15-µm-broad area at the cell periphery. Percentage of minus-end–directed movements (F) and averages (in µm/s) and the distributions of movement velocities (G) to MT plus and minus ends in MRC5-CV cells expressing FKBP2-GFP-Rab6A alone or together with HA–BICD2-N–FRB and after rapalog addition. In the latter case, measurements were performed within 25 min after rapalog was added. Approximately 30 cells were analyzed for each condition. The individual distributions and the number of measurements for G are shown in Supplemental Figure S5.

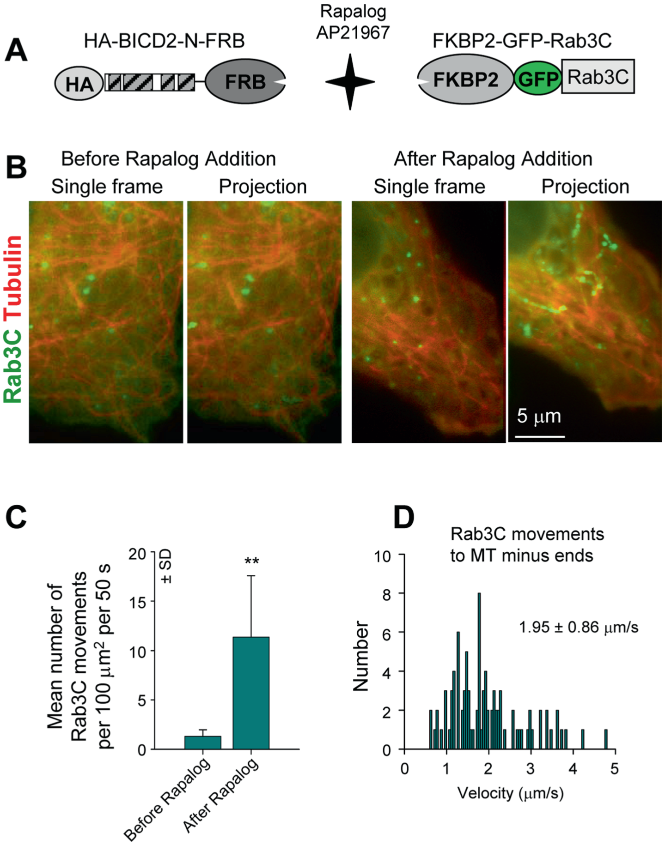

FIGURE 6: Motility of Rab3C vesicles after BICD2-N recruitment. (A) Scheme of the regulated heterodimerization constructs used to attach BICD2-N to Rab3C-positive membranes. (B) Simultaneous live imaging of FKBP2-GFP-Rab3C (green) and mCherry–α-tubulin (red) in a transiently transfected MRC5-CV cell coexpressing HA–BICD2-N–FRB before and after rapalog addition; single frames are shown on the left, and projections of 40 frames are shown on the right. Imaging was performed with 100-ms interval/exposure using wide-field microscopy. Five consecutive frames were averaged. (C) Quantification of the number of FKBP2-GFP-Rab3C particle movements with length >1 μm. Ten cells were analyzed. (D) Distribution of FKBP2-GFP-Rab3C movement velocities to MT minus ends in MRC5-CV cells coexpressing HA–BICD2-N–FRB after rapalog addition. Approximately 90 events in 10 cells were analyzed.

dramatic clustering of endosomes in the pericentrosomal region; this clustering was strongly blocked by depletion of DHC and p150$^{\text{Glued}}$ (Figure 7, C and D). Depletion of LIS1 also prevented formation of a tight pericentrosomal cluster of endosomes; however, in contrast to DHC depletion, more endosomes were present in central cell regions and around the nucleus, suggesting that dynein inhibition might be incomplete (Figure 7, C and D). These data suggest that dynein recruitment, activation, or motility is perturbed in the absence of LIS1.

Next we used HeLa cells expressing GFP-tagged dynein subunits to investigate dynein behavior and found that, very similar to dynactin depletion, LIS1 knockdown caused dynein distribution to become much more diffuse (Figure 4A, bottom, and Supplemental Movie S2). MT plus-end accumulation of dynein was abolished, whereas p50-GFP was still detected at MT plus ends (Figure 4, A–D, and Supplemental Movie S3). The fact that the accumulation of dynein depends not only on dynactin but also on LIS1 suggests that dynein targeting to MT ends in mammalian cells is complex and might in some aspects resemble the LIS1-dependent and dynactin-independent pathway described in budding yeast (Sheeman *et al.*, 2003; Markus *et al.*, 2009, 2011) and in some aspects resemble the LIS1-independent and p150-dynactin–dependent pathway described in filamentous fungi such as *Aspergillus nidulans* and *Ustilago maydis* (Zhang *et al.*, 2003; Lenz *et al.*, 2006; Egan *et al.*, 2012; Yao *et al.*, 2012). In addition, the number of rapid bidirectional movements of DHC-GFP was strongly reduced, similar to p150$^{\text{Glued}}$-depleted cells (Figure 4E). The number of p50-GFP (dynactin) particles displaying rapid bidirectional movements was also reduced by LIS1 and DHC knockdown (Figure 4F), supporting the inhibitory effect of LIS1 depletion on all dynein-based motility.

Dynein and dynactin require each other and LIS1 for efficient recruitment by BICD2 to the nuclear envelope and Rab6-positive membranes

The highly diffuse localization of dynein in LIS1-depleted cells suggested that LIS1 might contribute to dynein recruitment to different cargoes. We set out to test this hypothesis by focusing on membrane structures associated with endogenous BICD2. In G1 and S phases of the cell cycle, BICD2 is predominantly localizes to Rab6-positive membranes and participates in their dynein-mediated movement, whereas in G2 it associates with RanBP2 at the nuclear pores and recruits dynein and dynactin to the NE to ensure proper positioning of the nucleus during mitotic entry (Matanis *et al.*, 2002; Short *et al.*, 2002; Splinter *et al.*, 2010). Strong BICD2-dependent accumulation of endogenous dynein and dynactin at the NE and cytoplasmic stacks of nuclear pores known as annulate lamellae (AL; Kessel, 1992; Daigle *et al.*, 2001) could be observed in G2 cells in which MTs were depolymerized with nocodazole (Splinter *et al.*, 2010). To observe this accumulation, we fixed cells with cold methanol because this fixation procedure permits detection of endogenous dynein (Figure 8A; Splinter *et al.*, 2010). We note that the pool of BICD2 associated with Rab6 membranes is lost in these conditions, and therefore little BICD2 staining is visible in methanol-fixed cells that are not in the G2 phase (Figure 8A; Splinter *et al.*, 2010). Depletion of dynein (DHC) or p150$^{\text{Glued}}$, the large subunit of dynactin, had no

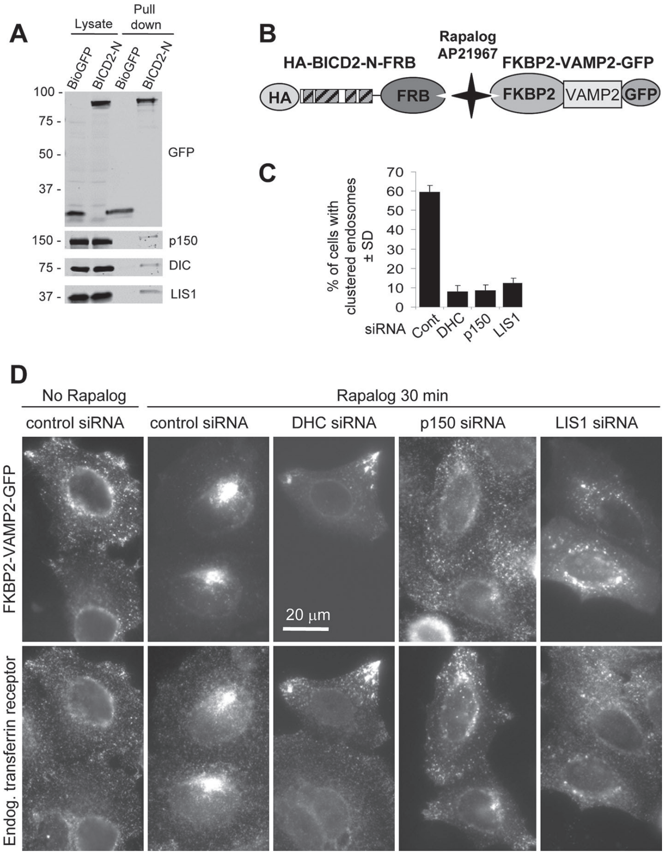

FIGURE 7: BICD2-N-dependent motility requires LIS1. (A) Streptavidin pull-down assays with Bio–GFP or Bio–GFP–BICD2-N were analyzed with the indicated antibodies. Two percent of the cell lysate used for the IP and 25% of the IP sample were loaded on gel. (B) Scheme of the regulated heterodimerization constructs used to attach BICD2-N to endosomes. (C, D) HeLa cells were transfected with different siRNAs; 2 d later, cells were cotransfected with HA–BICD2-N–FRB and FKBP2-GFP-VAMP2; after one additional day in culture, cells were treated with rapalog, fixed, and stained for transferrin receptor. (C) Percentage of HA–BICD2-N–FRB– and FKBP2-GFP-VAMP2–coexpressing HeLa cells with endosomes fully clustered in the cell center, 30 min after rapalog addition. Approximately100 cells were analyzed in three independent experiments. (D) Representative images of HA–BICD2-N–FRB– and FKBP2-GFP-VAMP2–coexpressing cells in different conditions.

effect on the recruitment of BICD2 to the NE (Figure 8, A–C). However, not only did the depletion of dynactin block efficient recruitment of dynein (Figure 8, C and G), as could be expected based on the cargo-targeting function of dynactin, but the reverse was also true: dynactin did not accumulate at the BICD2-decorated NE after dynein knockdown (Figure 8, B and F). Furthermore, consistent with the hypothesis that LIS1 is required for dynein recruitment to BICD2-bound cargoes, depletion of LIS1 prevented BICD2-dependent targeting of dynein and dynactin to the NE in G2 cells (Figure 8, D and H).

Next we tested whether dynein and dynactin require each other and LIS1 for recruitment to Rab6 membranes. Because Rab6 and Rab6-bound BICD2 pool are not preserved in methanol-fixed cells and anti-dynein antibodies did not work in our hands with other fixations, we used DIC2-GFP–expressing cells. After nocodazole-mediated MT disassembly, DIC2-GFP was strongly recruited to the dispersed Golgi fragments and vesicles positive for endogenous BICD2 and Rab6 (Figure 9A). This recruitment was completely abolished when either p150^{Glued} or LIS1 was depleted (Figure 9, B and C). Endogenous dynactin (visualized with staining against p150^{Glued}) was also strongly recruited to BICD2-positive structures in G1 and S cells, which could be recognized by the absence of BICD2 staining on the NE (Figure 9D). Depletion of both dynein (DHC) and LIS1 abolished this recruitment (Figure 9, E and F). Taken together, these data are fully in line with our biochemical observations, which indicate that dynein, dynactin, and BICD2-N form a complex only when all three components are present (Figure 2). These data also suggest that LIS1 is needed for recruitment of the dynein motor complex to different subcellular structures associated with BICD2.

DISCUSSION

How cytoplasmic dynein, the most ubiquitous MT minus-end–directed motor, is recruited to the numerous cellular cargoes is still poorly understood. The vast literature on this subject suggests that multiple dynein and dynactin subunits can interact with a wide range of receptors on various cargoes (Holleran *et al.*, 1996; Tai *et al.*, 1999; Muresan *et al.*, 2001; Kardon and Vale, 2009; Rocha *et al.*, 2009; Cai *et al.*, 2010; Tan *et al.*, 2011; Zhang *et al.*, 2011). Understanding of dynein targeting is further complicated by the existence of highly conserved dynein cofactors, such as LIS1 and NudE/EL, which are required for a broad set of dynein-dependent processes and have been reported to contribute to subcellular dynein recruitment (Guo *et al.*, 2006; Stehman *et al.*, 2007; Vergnolle and Taylor, 2007; Lam *et al.*, 2010; Bolhy *et al.*, 2011; Egan *et al.*, 2012). The picture that emerges from these studies suggests that dynein, either alone or acting in a complex with dynactin and other cofactors, can be targeted to different organelles in a multitude of different ways through various interaction interfaces. In this study, we attempted to dissect the molecular basis of dynein recruitment by one particular motor adaptor, the conserved protein BICD2. We found that the N-terminal fragment of BICD2, which binds to dynein, does not form a stable complex with the motor unless dynactin is also present. Of importance, within the triple complex with BICD2-N, the association of dynein and dynactin is stabilized.

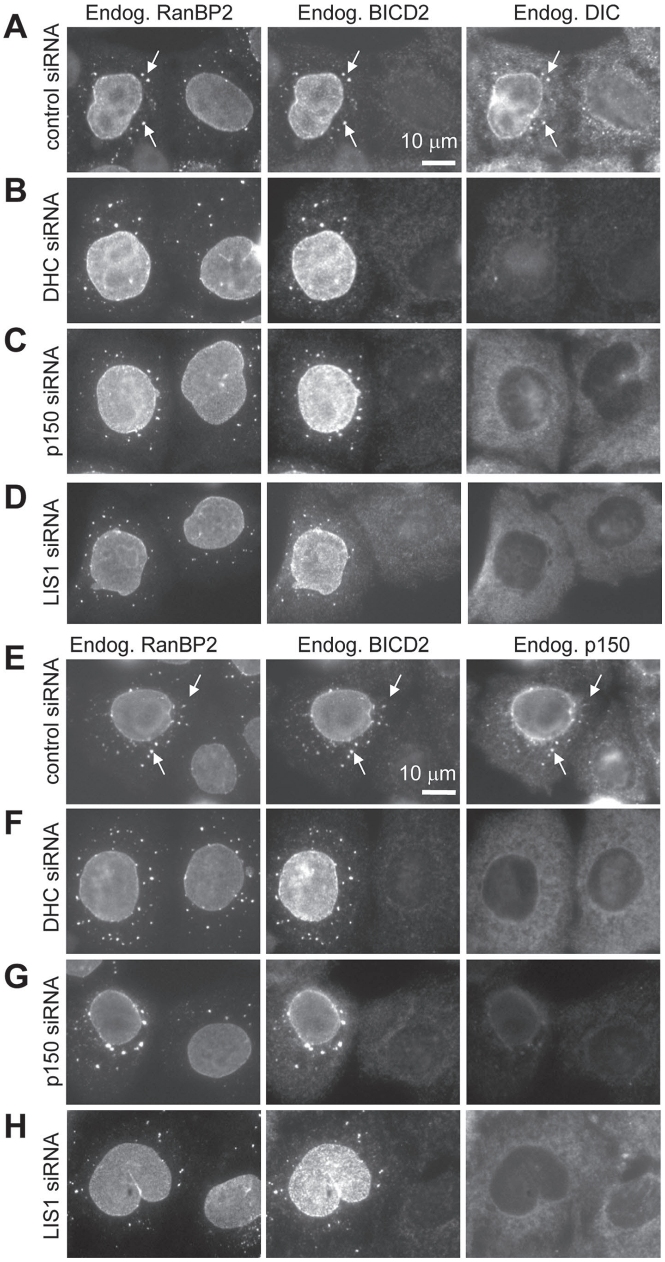

FIGURE 8: Dynein and dynactin are mutually dependent on the G2-specific recruitment to the NE and AL. HeLa cells were transfected with the indicated siRNAs; 3 d later, the cells were treated for 5 h with 10 μM nocodazole, fixed with cold methanol, and stained with the antibodies against the nucleoporin RanBP2, BICD2. and DIC (A–D) or RanBP2, BICD2, and p150^{Glued} (E–H). AL (stacks of nuclear pores in the ER membranes localized in the cytoplasm) are indicated by arrows. Note that methanol fixation preferentially preserves the nuclear pore–bound pool of BICD2 present in G2 cells but not the cytosolic and Rab6-bound BICD2 pool in G1 and S cells, as described previously (Splinter *et al.*, 2010).

The general importance of this interaction mode is emphasized by the fact that in the absence of the C-terminal cargo-binding domain of BICD2, BICD2-N expression effectively suppresses multiple dynein-mediated cellular transport routes, including those that do not depend on BICD2 (Hoogenraad *et al.*, 2001; Teuling *et al.*, 2008). We showed that the triple BICD2-N–dynein–dynactin complex is not competent to stably interact with cellular organelles, as reflected by its highly diffuse localization pattern. This result was surprising: for example, we showed that the Arp1 filament of dynactin is not directly engaged in the BICD2–dynactin interaction, and yet, apparently, the triple BICD2-N–dynein–dynactin complex could not be efficiently targeted to membranes by the interaction between Arp1 and its partners such as spectrin (Holleran *et al.*, 1996). Thus it seems that in spite of being a very large protein assembly, the dynein–dynactin complex occupied by one adaptor molecule cannot efficiently interact with other adaptors through potentially distinct interaction interfaces. This suggests that dynein–dynactin is likely to be targeted to each cargo/subcellular site through a multiple set of interactions, and although some of them might be very specific, others must be common to different pathways. Stabilization of the intrinsically weak dynein–dynactin interaction might be an important theme in this generic targeting process. In connection with this, it is interesting to note that the BICD2-N interaction mode with dynein and dynactin might be evolutionarily conserved because the N-terminal coiled-coil domain of BICD2 shares some similarity with the coiled-coil segments in other MT motor adaptors, the HAP domains of HAP1 and TRAK/Milton proteins (Stowers *et al.*, 2002).

Overexpressed BICD2-N prevented dynein not only from binding to cargo, but also from association with MTs and MT tips. This result was unexpected because we

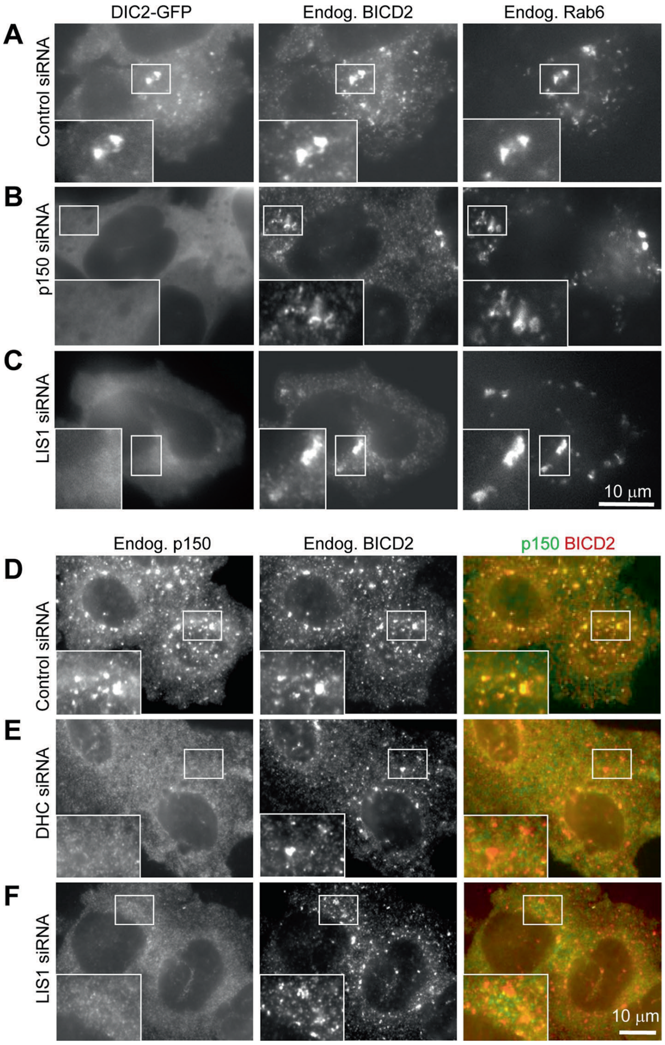

FIGURE 9: LIS1 is required for BICD2-dependent recruitment of dynein and dynactin to the NE. (A–C) HeLa cells stably expressing DIC2-GFP (A–C) or control HeLa cells (D, E) were transfected with the indicated siRNAs; 3 d later, cells were treated for 1 h with 10 μM nocodazole, fixed with 4% paraformaldehyde, and stained with the antibodies against BICD2 and Rab6 (A–C) or BICD2 and p150Glued (D–F). Paraformaldehyde fixation preserves the pool of BICD2 associated with Rab6 membranes.

showed that BICD2-N stabilizes the interaction between dynein and dynactin, and dynactin promotes dynein binding to MT plus ends (Vaughan *et al.*, 1999; Figure 4, A and C), as well as processive dynein motility along MTs (King and Schroer, 2000). It is possible that, depending on conditions, dynein and dynactin might exist in functionally different complexes, which are either capable or incapable of MT interaction and motility. We propose that when the triple BICD2-N–dynein–dynactin complex is not bound to cargo, it exists in an inactive conformation that is incompatible with MT binding. Tethering to cargo activates normal motility of dynein within the BICD2-N–dynein–dynactin complex, possibly due to interaction with additional cargo-associated dynein cofactors.

Of importance, dynactin is still present at MT ends in BICD2-N–expressing cells. Given that BICD2-N does not bind to dynein or dynactin alone and dynactin can bind to MT tips independently of dynein, it is likely that a pool of free dynactin can still recycle on MT plus ends without recruiting BICD2-N. However, if dynactin recruits dynein, the association of the two complexes might create a high-affinity binding site for BICD2-N, which would then cause a conformational change of the triple complex, resulting in its release from MT tips into the cytoplasm. Existence of functionally distinct dynein conformations is supported by studies of dynein offloading from the MT plus ends to the cell cortex in budding yeast (Markus *et al.*, 2009; Markus and Lee, 2011).

The complexity of dynein recruitment and activation is accentuated by the fact that it requires additional cofactors, such as LIS1. We found that in the absence of LIS1, dynein became diffuse in live cells, very similar to the result of dynactin depletion. This applied not only to the cargo-bound dynein, but also to the MT tip–associated dynein pool, indicating that similar to budding yeast, LIS1 participates in promoting dynein targeting to MT plus ends (Sheeman *et al.*, 2003; Markus *et al.*, 2009, 2011). It is important to note here that the pathways responsible for MT tip recruitment of dynein and dynactin in yeast and mammals show clear differences: for example, dynactin depends on dynein and the LIS1 homologue Pac1 for MT-end localization in budding yeast (Woodruff *et al.*, 2009; Markus *et al.*, 2011) but not in mammalian cells.

By immunofluorescence cell staining, we showed that LIS1 depletion inhibited recruitment of dynein and dynactin to endogenous BICD2 cargoes, Rab6-positive membranes, and nuclear pores. These observations are in line with the general importance of LIS1 in dynein-mediated organelle transport, in agreement with findings by Lam *et al.* (2010). These results suggest that in addition to participation in dynein-mediated force generation (McKenney *et al.*, 2010; Yi *et al.*, 2011), LIS1 might also be required for some generic aspects of dynein recruitment or recycling. This conclusion is consistent with the recently published work in *A. nidulans*, which showed that in this fungus the LIS1 homologue is absent from moving cargo and is needed for dynein recruitment or motility initiation but not for the actual dynein-mediated movement (Egan *et al.*, 2012). In our in vitro experiments, we used dynein and dynactin that contained no significant amount of copurified LIS1, suggesting that the formation of the triple BICD2-N–dynein–dynactin complex in the cell-free system does not require equimolar amounts of LIS1. We cannot exclude, however, that catalytic amounts of LIS1 are necessary to induce conformational changes within the complex and that the inability to undergo such changes prevents BICD2-dependent recruitment of dynein and dynactin to cargo in LIS1-depleted cells.

The complete understanding of LIS1 function in dynein-mediated processes would likely require detailed investigation of its functional interplay with NudE/EL proteins, which are also needed for a broad variety of dynein-mediated transport pathways (Kardon and Vale, 2009), strongly cooperate with LIS1 but might compete with dynactin (McKenney *et al.*, 2010, 2011), and act in a nonredundant manner with BICD2 in at least some dynein-targeting processes (Bolhy *et al.*, 2011). Taken together, these findings emphasize the concept that dynein-induced motility cannot be explained by simple pairwise interactions of individual dynein or dynactin subunits with receptor molecules but instead rely on cooperative assembly and possibly sequential activation of large multiprotein complexes on cargoes.

MATERIALS AND METHODS

Antibodies

We used mouse monoclonal antibodies against GFP (Roche, Indianapolis, IN), $p150^{Glued}$ and PEX1 (BD Biosciences, Heidelberg, Germany), DIC (74.1, Chemicon, Temecula, CA; and 74-1, sc-13525, Santa Cruz Biotech, Heidelberg, Germany), HA tag (Covance, Berkeley, CA), Arp1 (a gift of T. Schroer, Johns Hopkins University, Baltimore, MD), LIS1 (antibody 201, a gift of O. Reiner, Weizmann Institute of Science, Rehovot, Israel), Rab6 (a gift of A. Barnekow, University of Münster, Münster, Germany), and transferrin receptor (Boehringer Mannheim, Mannheim, Germany); rabbit antibodies against BICD2 (antibody 2293; Hoogenraad *et al.*, 2001), GFP (Abcam, Cambridge, MA), HA tag (Y-11, sc-805; Santa Cruz Biotech), and DHC (R-325, sc-9115; Santa Cruz Biotech), goat antibodies against RanBP2 (Pichler *et al.*, 2002; a gift of F. Melchior, Deutschen Krebsforschungszentrums–Zentrum für Molekulare Biologie der Universität Heidelberg, Heidelberg, Germany), and secondary goat and donkey Alexa 350, Alexa 488, and Alexa 594 anti-mouse, anti-goat, and anti-rabbit antibodies (Invitrogen, Carlsbad, CA).

Expression constructs, cell culture, transfection, and immunofluorescence staining

All BICD2 constructs are based on the mouse BICD2 cDNA (AJ250106; Hoogenraad *et al.*, 2001). We used the following previously described constructs: Bio–GFP–BICD2-N (Grigoriev *et al.*, 2007), GFP-BICD2-N-MTS (Hoogenraad *et al.*, 2003), and mCherry–α-tubulin (Shaner *et al.*, 2004), a gift of R. Tsien (University of California, San Diego, La Jolla, CA). HA–BICD2–N-FRB and FKBP2-GFP-Rab6 were generated in pEGFP-C by PCR-based technology. FKBP2-GFP-Rab3C and FKBP2-VAMP2-GFP were generated in a similar manner using GFP-Rab3C (van Vlijmen *et al.*, 2008) or VAMP2 fused to a pH-sensitive form of GFP through the lumenal domain (synapto-pHluorin; Sankaranarayanan and Ryan, 2001). Plasmids encoding heterodimerization domains FRB and FKBP2 and the rapamycin-derived heterodimerizer AP21967 were obtained from Ariad (Cambridge, MA). GFP- and mStrawberry-Rab6A constructs were described previously (Grigoriev *et al.*, 2007).

HeLa and MRC5-SV cells were cultured and transfected using PolyFect (Qiagen, Valencia, CA) or FuGENE 6 (Roche) as described previously (Grigoriev *et al.*, 2007). HeLa cells stably expressing GFP-tagged DHC, DIC2, and p50 subunits were generated as a part of a BAC TransgeneOmics project and described previously (Poser *et al.*, 2008). Cells were fixed and stained essentially as described before (Hoogenraad *et al.*, 2003). A 10-min fixation with cold (–20°C) methanol alone was used to visualize dynein, and a combination of fixation with cold methanol (10 min) followed by 4% paraformaldehyde (PFA) in phosphate-buffered saline for 10 min at room temperature was used for staining of dynactin and EB1/EB3 at MT plus ends; fixation with 4% PFA in phosphate-buffered saline for 10 min was used to visualize endosomes and Rab6-positive membranes. MitoTracker red CMXRos (Invitrogen) was applied to cells and fixed for 10 min with 4% PFA in medium (Hoogenraad *et al.*, 2003). To visualize dynein and dynactin at the NE, cells were treated with 10 µm nocodazole (Sigma-Aldrich, St. Louis, MO) for 5 h prior to fixation.

The siRNA transfections were performed as described previously (Splinter *et al.*, 2010) using ON-TARGETplus SMARTpool siRNAs directed against human $p150^{Glued}$, DHC, and LIS1 (Dharmacon, Lafayette, CO).

Immunoprecipitation from HeLa cells

HeLa cells were cultured as described previously (Grigoriev *et al.*, 2007); 70% confluent HeLa cells were transfected with constructs expressing different GFP or HA fusions using either Lipofectamine 2000 (Invitrogen) or polyethyleneimine (molecular weight, 25,000; Polysciences, Warrington, PA). One day after transfection, cells were lysed in a buffer containing 20 mM Tris-HCl, pH 8.0, 100 mM KCl, 1% Triton X-100, and protease inhibitors (Complete, Roche), and immunoprecipitations were performed as described previously (Hoogenraad *et al.*, 2001). Streptavidin pull-downs of Bio–GFP–BICD2-N for Western blotting were performed as described previously (Grigoriev *et al.*, 2007).

Protein purifications

BICD2-Nsh (residues 25–400 of mouse BICD2) was cloned into PET28a and purified with a two-step chromatography protocol using HiTrap Chelating HP resin for the oligohistidine tag, followed by anion exchange chromatography with MonoQ resin (GE Healthcare, Piscataway, NJ). Bio–GFP–BICD2-N (Grigoriev *et al.*, 2007) was purified from HEK293T cells. Seventy percent confluent HEK293T cells were cotransfected with the constructs Bio-GFP-TEV–BICD2-N and BirA using Lipofectamine 2000. One day after transfection, cells were lysed in a buffer containing 20 mM Tris-HCl, 100 mM KCl, 1% Triton X-100, and protease inhibitors (Complete, Roche). Proteins were isolated using Mutein beads (Roche) according to the protocol of the manufacturer, and the purified protein was concentrated with 3-kDa Vivaspin columns (Satorius, Göttingen, Germany). Bovine brain dynactin and cytoplasmic dynein were purified as previously described (Bingham *et al.*, 1998; Mallik *et al.*, 2005).

Sucrose gradients

Different combinations of 0.05 mM dynein, 0.05 mM dynactin, and/or 0.80 mM BICD2-Nsh were incubated for 180 min on ice and then layered onto 10–40% sucrose gradients. After centrifugation, equal-size fractions were collected from the bottom of the gradients and subjected to SDS–PAGE. Dynein and dynactin were found in fractions corresponding to ~20S, as determined by silver staining the fractions to identify the DHC or dynactin $p150^{Glued}$ subunit. Because BICD2-Nsh comigrates with the DLICs and the p50/dynamitin, we determined the position of BICD2-Nsh in the sucrose gradients by probing a Western blot with antibodies to BICD2.

Analysis of BICD2-N–binding partners in dynein and dynactin by cross-linking

Bio-GFP–tagged BICD2-N was incubated with equimolar amounts of bovine brain dynein and dynactin for 3 h on ice in a buffer containing 80 mM 1,4-piperazinediethanesulfonic acid, 1 mM $MgCl_2$, 1 mM ethylene glycol tetraacetic acid, 50 mM NaCl 1 mM dithiothreitol, 0.5 mM ATP, and 0.05% nonyl phenoxylpolyethoxylethanol, pH 6.8. Bis[sulfosuccinimidyl] glutarate (Pierce, Rockford, IL) was added in an end concentration of 0.5 mM and quenched after 30 min with NH_4HCO_3. Formed complexes were denatured with 0.5% SDS, followed by 5 min at 65°C in a buffer containing 20 mM Tris-HCl, pH 8.0, 400 mM KCl, and 0.5% Triton X-100. Streptavidin pull-down was performed as described previously (Grigoriev *et al.*, 2007).

Mass spectrometry–based protein identification

Mass spectrometry analysis was performed essentially as described previously (Grigoriev *et al.*, 2007). Peak lists were automatically created from raw data files using the Mascot Distiller software, version 2.0 (MatrixScience, Boston, MA). The Mascot search algorithm, version 2.0 (MatrixScience) was used for searching against the NCBInr database (release date, NCBInr_20080502.fasta; taxonomy *Bos taurus*). The peptide tolerance was typically set to 2 Da and the fragment ion tolerance to 0.8 Da. Only doubly and triply charged peptides were searched for. A maximum number of two missed cleavages by trypsin were allowed, and carbamidomethylated cysteine and oxidized methionine were set as fixed and variable modifications, respectively. The Mascot score cutoff value for a positive protein hit was set to 100. Individual peptide tandem mass spectrometry spectra with Mowse scores of <40 were checked manually and either interpreted as valid identifications or discarded.

Image acquisition, processing, and analysis

Images of fixed cells were collected with a Leica DMRBE microscope equipped with a PL Fluotar 100×/1.3 numerical aperture (NA) oil objective, FITC/EGFP filter 41012 (Chroma Technology, Bellows Falls, VT), and Texas red filter 41004 (Chroma) and an ORCA-ER-1394 charge-coupled device (CCD) camera (Hamamatsu, Hamamatsu, Japan). Twelve-bit images were projected onto the CCD chip at a magnification of 0.1 μm/pixel. Images of fixed samples were prepared using Photoshop (Adobe, San Jose, CA) by converting them to 8 bits and using linear adjustment of Levels; no image filtering was performed.

Live-cell imaging was performed on an Eclipse Ti-E inverted research microscope with perfect focus system (Nikon, Melville, NY) equipped with a Nikon CFI Apo total internal reflection fluorescence (TIRF) 100×/1.49 NA oil objective and a QuantEM 512SC electron-multiplying CCD camera (Roper Scientific, Tucson, AZ) and controlled with MetaMorph 7.5 software (Molecular Devices, Sunnyvale, CA). The 16-bit images were projected onto the CCD chip with intermediate lens, 2.5×, at a magnification of 0.065 μm/pixel. The microscope was equipped with a Nikon TI-TIRF-E motorized TIRF illuminator. For regular imaging we used a mercury lamp (HBO-103W/2; Osram, Munich, Germany) for excitation or 491-nm, 50-mW Calypso (Cobolt, Solna, Sweden) and 561-nm, 50-mW Jive (Cobolt) lasers. We used an ET-GFP filter set (Chroma) for imaging of proteins tagged with GFP and an ET-mCherry filter set (Chroma) for imaging of proteins tagged with mCherry. For simultaneous imaging of green and red fluorescence we used an ET-mCherry/GFP filter set (Chroma) together with a DualView (DV2l Roper) equipped with a 565dcxr dichroic filter (Chroma) and a HQ530/30m emission filter (Chroma). To keep cells at 37°C, we used a stage-top incubator (INUG2E-ZILCS; Tokai Hit, Fujinomiya, Japan).

Image analysis was performed using MetaMorph. Live-cell images were prepared for publication using Photoshop. Details of image adjustment are indicated in the figure legends. Statistical analysis was performed using a nonparametric Mann–Whitney *U* test in Statistica for Windows and SigmaPlot (Systat Software, San Jose, CA).

ACKNOWLEDGMENTS

We thank J. Raaijmakers and R. Medema for the help with siRNA-mediated depletion experiments; T. Schroer, F. Melchior, A. Barnekow, O. Reiner, and R. Tsien for the gift of materials; and Karel Bezstarosti for technical assistance. This work was supported by the Dutch Ministry of Economic Affairs (BSIK). A.A. is supported by the Netherlands Organization for Scientific Research (NWO-ALW VICI), Netherlands Organization for Health Research and Development (ZonMw-TOP) grants, a Foundation for Fundamental Research on Matter program grant, and a Human Frontier Science Program grant. S.J.K. is supported by the National Institutes of Health (RO1 NS48501) and the University of Missouri Research Board. C.C.H is supported by the Netherlands Organization for Scientific Research (NWO-ALW, NWO-ECHO), the Netherlands Organization for Health Research and Development (ZonMw-VIDI, ZonMw-TOP), the European Science Foundation (European Young Investigators Award), and a Human Frontier Science Program Career Development Award (HFSP-CDA). The work of I.P. and A.A.H. is supported by the European Community's Seventh Framework Program (FP7/2007-2013) under Grant Agreement 241548 (MitoSys Project).

REFERENCES

Aguirre-Chen C, Bulow HE, Kaprielian Z (2011). *C. elegans* bicd-1, homolog of the *Drosophila* dynein accessory factor Bicaudal D, regulates the branching of PVD sensory neuron dendrites. Development 138, 507–518.

Bianco A, Dienstbier M, Salter HK, Gatto G, Bullock SL (2010). Bicaudal-D regulates fragile X mental retardation protein levels, motility, and function during neuronal morphogenesis. Curr Biol 20, 1487–1492.

Bingham JB, King SJ, Schroer TA (1998). Purification of dynactin and dynein from brain tissue. Methods Enzymol 298, 171–184.

Bolhy S, Bouhlel I, Dultz E, Nayak T, Zuccolo M, Gatti X, Vallee R, Ellenberg J, Doye V (2011). A Nup133-dependent NPC-anchored network tethers centrosomes to the nuclear envelope in prophase. J Cell Biol 192, 855–871.

Bullock SL, Nicol A, Gross SP, Zicha D (2006). Guidance of bidirectional motor complexes by mRNA cargoes through control of dynein number and activity. Curr Biol 16, 1447–1452.

Cai Q, Lu L, Tian JH, Zhu YB, Qiao H, Sheng ZH (2010). Snapin-regulated late endosomal transport is critical for efficient autophagy-lysosomal function in neurons. Neuron 68, 73–86.

Clark A, Meignin C, Davis I (2007). A dynein-dependent shortcut rapidly delivers axis determination transcripts into the *Drosophila* oocyte. Development 134, 1955–1965.

Claussen M, Suter B (2005). BicD-dependent localization processes: from *Drosophilia* development to human cell biology. Ann Anat 187, 539–553.

Coutelis JB, Ephrussi A (2007). Rab6 mediates membrane organization and determinant localization during *Drosophila* oogenesis. Development 134, 1419–1430.

Daigle N, Beaudouin J, Hartnell L, Imreh G, Hallberg E, Lippincott-Schwartz J, Ellenberg J (2001). Nuclear pore complexes form immobile networks and have a very low turnover in live mammalian cells. J Cell Biol 154, 71–84.

Dienstbier M, Boehl F, Li X, Bullock SL (2009). Egalitarian is a selective RNA-binding protein linking mRNA localization signals to the dynein motor. Genes Dev 23, 1546–1558.

Echeverri CJ, Paschal BM, Vaughan KT, Vallee RB (1996). Molecular characterization of the 50-kD subunit of dynactin reveals function for the complex in chromosome alignment and spindle organization during mitosis. J Cell Biol 132, 617–633.

Egan MJ, Tan K, Reck-Peterson SL (2012). Lis1 is an initiation factor for dynein-driven organelle transport. J Cell Biol 197, 971–982.

Fridolfsson HN, Ly N, Meyerzon M, Starr DA (2010). UNC-83 coordinates kinesin-1 and dynein activities at the nuclear envelope during nuclear migration. Dev Biol 338, 237–250.

Grigoriev I *et al.* (2007). Rab6 regulates transport and targeting of exocytotic carriers. Dev Cell 13, 305–314.

Guo J, Yang Z, Song W, Chen Q, Wang F, Zhang Q, Zhu X (2006). Nudel contributes to microtubule anchoring at the mother centriole and is involved in both dynein-dependent and -independent centrosomal protein assembly. Mol Biol Cell 17, 680–689.

Habermann A, Schroer TA, Griffiths G, Burkhardt JK (2001). Immunolocalization of cytoplasmic dynein and dynactin subunits in cultured macrophages: enrichment on early endocytic organelles. J Cell Sci 114, 229–240.

Holleran EA, Karki S, Holzbaur EL (1998). The role of the dynactin complex in intracellular motility. Int Rev Cytol 182, 69–109.

Holleran EA, Tokito MK, Karki S, Holzbaur EL (1996). Centractin (ARP1) associates with spectrin revealing a potential mechanism to link dynactin to intracellular organelles. J Cell Biol 135, 1815–1829.

Hoogenraad CC, Akhmanova A, Howell SA, Dortland BR, De Zeeuw CI, Willemsen R, Visser P, Grosveld F, Galjart N (2001). Mammalian Golgi-associated Bicaudal-D2 functions in the dynein-dynactin pathway by interacting with these complexes. EMBO J 20, 4041–4054.

Hoogenraad CC *et al.* (2010). Neuron specific Rab4 effector GRASP-1 coordinates membrane specialization and maturation of recycling endosomes. PLoS Biol 8, e1000283.

Hoogenraad CC, Wulf P, Schiefermeier N, Stepanova T, Galjart N, Small JV, Grosveld F, de Zeeuw CI, Akhmanova A (2003). Bicaudal D induces selective dynein-mediated microtubule minus end-directed transport. EMBO J 22, 6004–6015.

Januschke J, Nicolas E, Compagnon J, Formstecher E, Goud B, Guichet A (2007). Rab6 and the secretory pathway affect oocyte polarity in *Drosophila*. Development 134, 3419–3425.

Kardon JR, Vale RD (2009). Regulators of the cytoplasmic dynein motor. Nat Rev Mol Cell Biol 10, 854–865.

Karki S, Holzbaur EL (1995). Affinity chromatography demonstrates a direct binding between cytoplasmic dynein and the dynactin complex. J Biol Chem 270, 28806–28811.

Kessel RG (1992). Annulate lamellae: a last frontier in cellular organelles. Int Rev Cytol 133, 43–120.

King SJ, Schroer TA (2000). Dynactin increases the processivity of the cytoplasmic dynein motor. Nat Cell Biol 2, 20–24.

King SJ, Bonilla M, Rodgers ME, Schroer TA (2002). Subunit organization in cytoplasmic dynein subcomplexes. Protein Sci 11, 1239–1250.

King SJ, Brown CL, Maier KC, Quintyne NJ, Schroer TA (2003). Analysis of the dynein-dynactin interaction in vitro and in vivo. Mol Biol Cell 14, 5089–5097.

Kobayashi T, Murayama T (2009). Cell cycle-dependent microtubule-based dynamic transport of cytoplasmic dynein in mammalian cells. PLoS One 4, e7827.

Lam C, Vergnolle MA, Thorpe L, Woodman PG, Allan VJ (2010). Functional interplay between LIS1, NDE1 and NDEL1 in dynein-dependent organelle positioning. J Cell Sci 123, 202–212.

Lansbergen G *et al.* (2004). Conformational changes in CLIP-170 regulate its binding to microtubules and dynactin localisation. J Cell Biol 166, 1003–1014.

Larsen KS, Xu J, Cermelli S, Shu Z, Gross SP (2008). BicaudalD actively regulates microtubule motor activity in lipid droplet transport. PLoS ONE 3, e3763.

Lenz JH, Schuchardt I, Straube A, Steinberg G (2006). A dynein loading zone for retrograde endosome motility at microtubule plus-ends. EMBO J 25, 2275–2286.

Li X, Kuromi H, Briggs L, Green DB, Rocha JJ, Sweeney ST, Bullock SL (2010). Bicaudal-D binds clathrin heavy chain to promote its transport and augments synaptic vesicle recycling. EMBO J 29, 992–1006.

Mallik R, Petrov D, Lex SA, King SJ, Gross SP (2005). Building complexity: an in vitro study of cytoplasmic dynein with in vivo implications. Curr Biol 15, 2075–2085.

Markus SM, Lee WL (2011). Regulated offloading of cytoplasmic dynein from microtubule plus ends to the cortex. Dev Cell 20, 639–651.

Markus SM, Plevock KM, St Germain BJ, Punch JJ, Meaden CW, Lee WL (2011). Quantitative analysis of Pac1/LIS1-mediated dynein targeting: Implications for regulation of dynein activity in budding yeast. Cytoskeleton (Hoboken) 68, 157–174.

Markus SM, Punch JJ, Lee WL (2009). Motor- and tail-dependent targeting of dynein to microtubule plus ends and the cell cortex. Curr Biol 19, 196–205.

Matanis T *et al.* (2002). Bicaudal-D regulates COPI-independent Golgi-ER transport by recruiting the dynein-dynactin motor complex. Nat Cell Biol 4, 986–992.

McKenney RJ, Vershinin M, Kunwar A, Vallee RB, Gross SP (2010). LIS1 and NudE induce a persistent dynein force-producing state. Cell 141, 304–314.

McKenney RJ, Weil SJ, Scherer J, Vallee RB (2011). Mutually exclusive cytoplasmic dynein regulation by nude-LIS1 and dynactin. J Biol Chem 286, 39615–39622.

Melkonian KA, Maier KC, Godfrey JE, Rodgers M, Schroer TA (2007). Mechanism of dynamitin-mediated disruption of dynactin. J Biol Chem 282, 19355–19364.

Muresan V, Stankewich MC, Steffen W, Morrow JS, Holzbaur EL, Schnapp BJ (2001). Dynactin-dependent, dynein-driven vesicle transport in the absence of membrane proteins: a role for spectrin and acidic phospholipids. Mol Cell 7, 173–183.

Pichler A, Gast A, Seeler JS, Dejean A, Melchior F (2002). The nucleoporin RanBP2 has SUMO1 E3 ligase activity. Cell 108, 109–120.

Pollock R, Issner R, Zoller K, Natesan S, Rivera VM, Clackson T (2000). Delivery of a stringent dimerizer-regulated gene expression system in a single retroviral vector. Proc Natl Acad Sci USA 97, 13221–13226.

Poser I *et al.* (2008). BAC TransgeneOmics: a high-throughput method for exploration of protein function in mammals. Nat Methods 5, 409–415.

Quintyne NJ, Schroer TA (2002). Distinct cell cycle-dependent roles for dynactin and dynein at centrosomes. J Cell Biol 159, 245–254.

Quintyne NJ, Gill SR, Eckley DM, Crego CL, Compton DA, Schroer TA (1999). Dynactin is required for microtubule anchoring at centrosomes. J Cell Biol 147, 321–334.

Rocha N, Kuijl C, van der Kant R, Janssen L, Houben D, Janssen H, Zwart W, Neefjes J (2009). Cholesterol sensor ORP1L contacts the ER protein VAP to control Rab7-RILP-p150 Glued and late endosome positioning. J Cell Biol 185, 1209–1225.

Sankaranarayanan S, Ryan TA (2001). Calcium accelerates endocytosis of vSNAREs at hippocampal synapses. Nat Neurosci 4, 129–136.

Schroer TA (2004). Dynactin. Annu Rev Cell Dev Biol 20, 759–779.

Shaner NC, Campbell RE, Steinbach PA, Giepmans BN, Palmer AE, Tsien RY (2004). Improved monomeric red, orange and yellow fluorescent proteins derived from *Discosoma* sp. red fluorescent protein. Nat Biotechnol 22, 1567–1572.

Sheeman B, Carvalho P, Sagot I, Geiser J, Kho D, Hoyt MA, Pellman D (2003). Determinants of *S. cerevisiae* dynein localization and activation: implications for the mechanism of spindle positioning. Curr Biol 13, 364–372.

Short B, Preisinger C, Schaletzky J, Kopajtich R, Barr FA (2002). The Rab6 GTPase regulates recruitment of the dynactin complex to Golgi membranes. Curr Biol 12, 1792–1795.

Shubeita GT, Tran SL, Xu J, Vershinin M, Cermelli S, Cotton SL, Welte MA, Gross SP (2008). Consequences of motor copy number on the intracellular transport of kinesin-1-driven lipid droplets. Cell 135, 1098–1107.

Splinter D *et al.* (2010). Bicaudal D2, dynein and kinesin-1 associate with nuclear pore complexes and regulate centrosome and nuclear positioning during mitotic entry. PLoS Biol 8, e1000350.

Stehman SA, Chen Y, McKenney RJ, Vallee RB (2007). NudE and NudEL are required for mitotic progression and are involved in dynein recruitment to kinetochores. J Cell Biol 178, 583–594.

Stowers RS, Megeath LJ, Gorska-Andrzejak J, Meinertzhagen IA, Schwarz TL (2002). Axonal transport of mitochondria to synapses depends on milton, a novel *Drosophila* protein. Neuron 36, 1063–1077.

Swan A, Nguyen T, Suter B (1999). Drosophila Lissencephaly-1 functions with Bic-D and dynein in oocyte determination and nuclear positioning. Nat Cell Biol 1, 444–449.

Tai AW, Chuang JZ, Bode C, Wolfrum U, Sung CH (1999). Rhodopsin's carboxy-terminal cytoplasmic tail acts as a membrane receptor for cytoplasmic dynein by binding to the dynein light chain Tctex-1. Cell 97, 877–887.

Tan SC, Scherer J, Vallee RB (2011). Recruitment of dynein to late endosomes and lysosomes through light intermediate chains. Mol Biol Cell 22, 467–477.

Teuling E, van Dis V, Wulf PS, Haasdijk ED, Akhmanova A, Hoogenraad CC, Jaarsma D (2008). A novel mouse model with impaired dynein/dynactin function develops amyotrophic lateral sclerosis (ALS)-like features in motor neurons and improves lifespan in SOD1-ALS mice. Hum Mol Genet 17, 2849–2862.

Vallee RB, Tai C, Faulkner NE (2001). LIS1: cellular function of a disease-causing gene. Trends Cell Biol 11, 155–160.

van Vlijmen T, Vleugel M, Evers M, Mohammed S, Wulf PS, Heck AJ, Hoogenraad CC, van der Sluijs P (2008). A unique residue in rab3c determines the interaction with novel binding protein Zwint-1. FEBS Lett 582, 2838–2842.

Vaughan KT, Vallee RB (1995). Cytoplasmic dynein binds dynactin through a direct interaction between the intermediate chains and p150Glued. J Cell Biol 131, 1507–1516.

Vaughan KT, Tynan SH, Faulkner NE, Echeverri CJ, Vallee RB (1999). Colocalization of cytoplasmic dynein with dynactin and CLIP-170 at microtubule distal ends. J Cell Sci 112, 1437–1447.

Vaughan PS, Miura P, Henderson M, Byrne B, Vaughan KT (2002). A role for regulated binding of p150(Glued) to microtubule plus ends in organelle transport. J Cell Biol 158, 305–319.

Vergnolle MA, Taylor SS (2007). Cenp-F links kinetochores to Ndel1/Nde1/Lis1/dynein microtubule motor complexes. Curr Biol 17, 1173–1179.

Woodruff JB, Drubin DG, Barnes G (2009). Dynein-driven mitotic spindle positioning restricted to anaphase by She1p inhibition of dynactin recruitment. Mol Biol Cell 20, 3003–3011.

Yao X, Zhang J, Zhou H, Wang E, Xiang X (2012). In vivo roles of the basic domain of dynactin p150 in microtubule plus-end tracking and dynein function. Traffic 13, 375–387.

Yi JY, Ori-McKenney KM, McKenney RJ, Vershinin M, Gross SP, Vallee RB (2011). High-resolution imaging reveals indirect coordination of opposite motors and a role for LIS1 in high-load axonal transport. J Cell Biol 195, 193–201.

Zhang J, Li S, Fischer R, Xiang X (2003). Accumulation of cytoplasmic dynein and dynactin at microtubule plus ends in *Aspergillus nidulans* is kinesin dependent. Mol Biol Cell 14, 1479–1488.

Zhang J, Yao X, Fischer L, Abenza JF, Penalva MA, Xiang X (2011). The p25 subunit of the dynactin complex is required for dynein-early endosome interaction. J Cell Biol 193, 1245–1255.

Supplemental Materials.
Supplemental Figures and Tables

Supplemental Table S1. Identification of BICD2-N binding subunits of dynein and dynactin by mass spectrometry. All proteins identified with a significant score and not present in the background controls are listed.

A. Mass spectrometry analysis of purified bovine dynactin

Score	NCBI GI number	Description	Da	Coverage (%)	Unique Peptides
3890	**gi|149642611**	dynactin 1 (p150Glued)	137458	45.2	41
1478	**gi|5031569**	ARP1	42701	54.5	16
1185	**gi|77736063**	dynactin 2 (p50)	44495	35.7	14
1177	**gi|119914141**	cytoplasmic dynein heavy chain	548197	5.8	19
933	**gi|28603770**	capping protein beta	34176	27.6	12
822	**gi|61316470**	capping protein alpha 2	33073	55.6	9
712	**gi|73953656**	dynactin p62	54023	29.3	9
262	**gi|115497348**	cytoplasmic dynein intermediate chain 2	68734	9.5	3
178	**gi|119892302**	kinesin family member 21A	187179	1.5	2
151	**gi|115497064**	dynactin 3 (p22)	21292	15.1	3
130	**gi|115497256**	dynactin 6 (p27)	21061	14.2	2
68	**gi|164420721**	dynactin 5 (p24)	20698	8.2	2
63	**gi|76640631**	dynein light intermediate chain 2	54392	2.4	1

B. Mass spectrometry analysis of purified bovine dynein

Score	NCBI GI number	Description	Da	Coverage (%)	Unique Peptides
16600	**gi|119914141**	cytoplasmic dynein heavy chain	548197	50.5	199
1593	**gi|114051407**	cytoplasmic dynein light intermediate chain 1	56800	49.6	22
956	**gi|76640631**	cytoplasmic dynein light intermediate chain 2	54392	32.3	14
840	**gi|11276091**	cytoplasmic dynein intermediate chain 1	73222	22.7	10
732	**gi|74004544**	cytoplasmic dynein intermediate chain 2	69215	27.7	9
321	**gi|18777767**	cytoplasmic dynein light chain roadblock type 1	10983	74.0	4
108	**gi|5730085**	cytoplasmic dynein, light chain Tctex	12672	14.2	1
75	**gi|157074188**	ARP1	42382	2.7	1
47	**gi|77736063**	dynactin 2 (p50)	44495	2.2	1

C. Mass spectrometry analysis of Bio-GFP-BICD2-N-dynein-dynactin complex after cross-linking with low doses of Bis[sulfosuccinimidyl] glutarate and isolated by pull-down with streptavidin beads in denaturing conditions

Score	NCBI GI number	Description	Da	Coverage (%)	Unique Peptides
8026	**gi|119914141**	Cytoplasmic dynein heavy chain	548197	29.3	124
718	**gi|149642611**	Dynactin 1 (p150Glued)	137458	8.4	9
513	**gi|18139547**	BICD2	93562	8.9	7
366	**gi|114051407**	Cytoplasmic dynein light intermediate chain 1	56800	12.6	7
365	**gi|76640631**	Cytoplasmic dynein light intermediate chain 2	54392	15.2	6

Splinter et al., Suppl. Figure S1

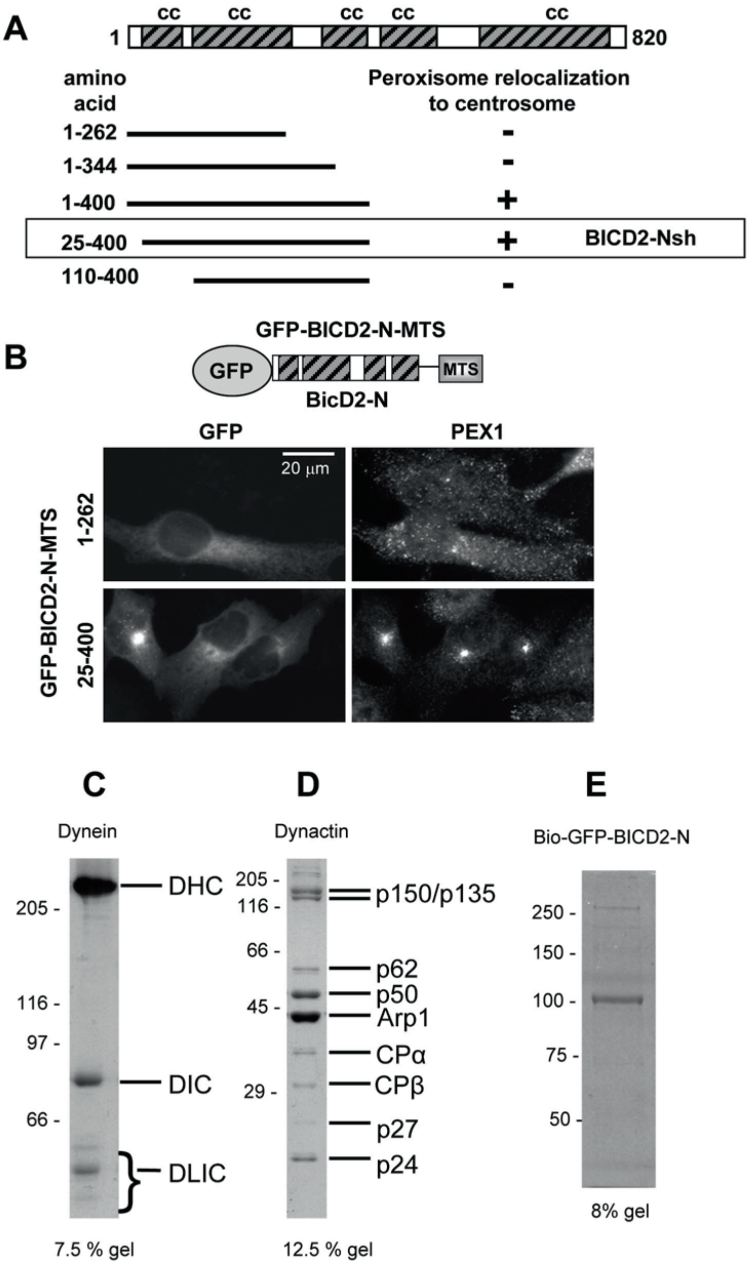
A
cc
cc
cc
cc
cc
1
820
amino acid
Peroxisome relocalization to centrosome
1-262 -
1-344 -
1-400 +
25-400 + BICD2-Nsh
110-400 -
B
GFP-BICD2-N-MTS
GFP
MTS
BicD2-N
GFP
PEX1
20 µm
GFP-BICD2-N-MTS
1-262
25-400
C
Dynein
DHC
205 -
116 -
97 -
DIC
66 -
DLIC
7.5 % gel
D
Dynactin
205 -
116 -
p150/p135
66 -
p62
p50
45 -
Arp1
CPα
29 -
CPβ
p27
p24
12.5 % gel
E
Bio-GFP-BICD2-N
250 -
150 -
100 -
75 -
50 -
8% gel

Supplemental Figure S1. Mapping of the minimal dynein-interacting domain of BICD2 and characterization of the purified protein complexes.

(A,B) Mapping of the minimal dynein-interacting domain of BICD2 using peroxisome/mitochondria relocalization assay. In this assay, BICD2-N fragments are targeted to the cytosolic side of the peroxisomes and mitochondria using the *Listeria monocytogenes* ActA-derived membrane-targeting sequence (MTS) and the distribution of the organelles is assessed by immunofluorescent staining (Hoogenraad *et al.*, 2003). When dynein motors are recruited to the organelles, these organelles form a tight pericentrosomal cluster. **(A)** A scheme of BICD2 fragments used and a summary of their effect on peroxisome localization when fused to MTS. The shortest construct, which potently relocalized is indicated by a box. **(B)** A scheme of GFP-BICD2-N-MTS constructs and representative images showing HeLa cells transfected with different BICD2-N-MTS fusions and stained for the peroxisome marker PEX1. Peroxisomes are relocated to the pericentrosomal region by the GFP-BICD2-N-MTs fusion containing amino acids 25-400 of BICD2, but not by the fusion containing amino acids 1-262.

(C,D) Coomassie-stained gels of dynein (7.5% acrylamide) **(C)** and dynactin (12.5% acrylamide) **(D)** complexes are shown with individual subunits identified.

(E) Coomassie-stained gel showing BICD2-N purified from HEK293 cells.

Splinter et al., Suppl. Figure S2

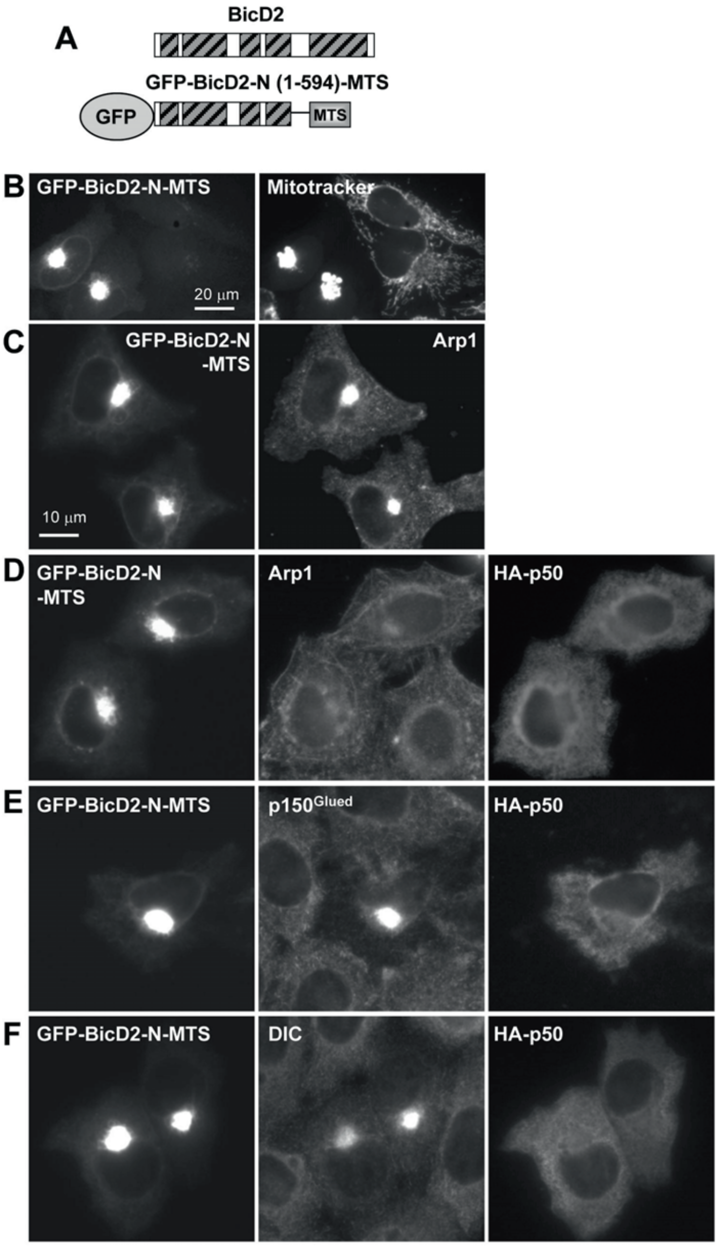
A
BicD2
GFP-BicD2-N (1-594)-MTS
GFP
MTS
B
GFP-BicD2-N-MTS
Mitotracker
20 μm
C
GFP-BicD2-N -MTS
Arp1
10 μm
D
GFP-BicD2-N -MTS
Arp1
HA-p50
E
GFP-BicD2-N-MTS
p150Glued
HA-p50
F
GFP-BicD2-N-MTS
DIC
HA-p50

Supplemental Figure S2. Overexpression of p50/dynamitin removes Arp1 but not dynein or p150Glued from the mitochondrial cluster induced by BICD2-N expression.

(A) A scheme of GFP-BICD2-N-MTS construct.

(B-F) HeLa cells were transfected either with GFP-BICD2-N-MTS alone **(B,C)** or together with HA-p50/dynamitin **(D-F)**, fixed with cold methanol (for dynein staining), with cold methanol followed by 4% paraformaldehyde (for dynactin subunits) or with 4% paraformaldehyde in culturing medium (to visualize mitochondria). Cells were stained with the indicated antibodies against dynein or dynactin subunits, HA tag, or MitoTracker Red CMXRos.

Splinter et al., Suppl. Figure S3

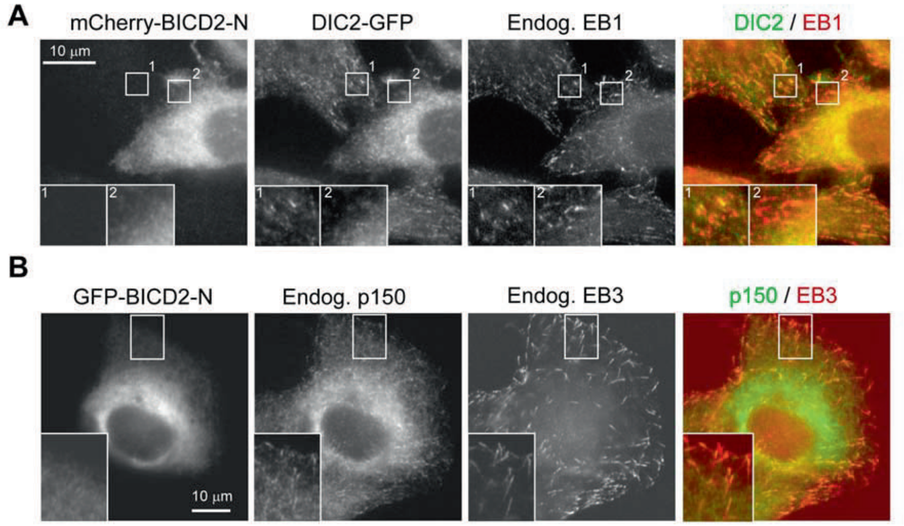
A
mCherry-BICD2-N
DIC2-GFP
Endog. EB1
DIC2 / EB1
10 µm
1
2
B
GFP-BICD2-N
Endog. p150
Endog. EB3
p150 / EB3
10 µm

Supplemental Figure S3. BICD2-N displaces dynein but not dynactin from MT tips.
(A) HeLa cells stably expressing DIC2-GFP (green) were transfected with mCherry-BICD2-N and stained for endogenous EB1, a marker of growing MT plus ends (red). Insets show enlargements of the boxed areas indicated by numbers. Note that DIC2-GFP is diffuse in mCherry-BICD2-N expressing cell but is present at the EB1-positive MT plus ends in surrounding cells.
(B) HeLa cells were transfected with GFP-BICD2-N and stained for endogenous $p150^{Glued}$ (green) and EB3 (red). EB3 is an EB1 family member, which similar to EB1 marks growing MT plus ends. Insets show enlargements of the boxed areas. $p150^{Glued}$ is still detectable at the EB3-positive MT tips in the GFP-BICD2-N-expressing cell.

Splinter et al., Suppl. Figure S4

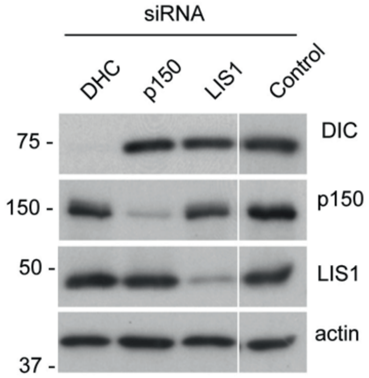
siRNA
DHC
p150
LIS1
Control
75 -
150 -
50 -
37 -
DIC
p150
LIS1
actin

Supplemental Figure S4. Characterization of DHC, p150^{Glued} and LIS1 siRNAs. HeLa cells were transfected with the indicated siRNAs and Western blots were performed with the indicated antibodies 3 days after transfection.

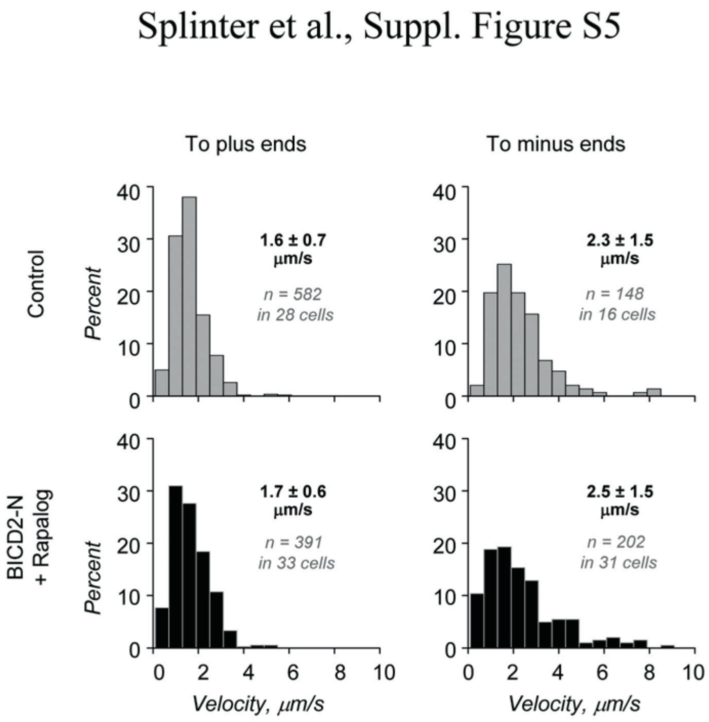

Supplemental Figure S5. Rab6A vesicle movement velocities in the absence of BICD2-N and after BICD2-N recruitment.

Distributions of movement velocities to MT plus and minus ends in MRC5-SV cells expressing FKBP2-GFP-Rab6A alone or together with HA-BICD2-N-FRB, after rapalog addition.

3

Bicaudal D Family adaptor proteins control the velocity of dynein-based movements

Max A. Schlager[1, 3], Andrea Serra-Marques[2, 3], Ilya Grigoriev[2], Laura F. Gumy[2],
Marta Esteves da Silva[2], Phebe S. Wulf[2], Anna Akhmanova[2] and Casper C. Hoogenraad[1, 2]

[1] Department of Neuroscience, Erasmus Medical Center, Rotterdam, the Netherlands
[2] Cell Biology, Faculty of Science, Utrecht University, Utrecht, the Netherlands
[3] Co-first author

Cell Reports 2014 September 11;8(5):1248-56

Bicaudal D Family Adaptor Proteins Control the Velocity of Dynein-Based Movements

Max A. Schlager,[1,3] Andrea Serra-Marques,[2,3] Ilya Grigoriev,[2] Laura F. Gumy,[2] Marta Esteves da Silva,[2] Phebe S. Wulf,[2] Anna Akhmanova,[2,*] and Casper C. Hoogenraad[1,2,*]
[1]Department of Neuroscience, Erasmus Medical Center, Rotterdam, the Netherlands
[2]Cell Biology, Faculty of Science, Utrecht University, Utrecht, the Netherlands
[3]Co-first author
*Correspondence: a.akhmanova@uu.nl (A.A.), c.hoogenraad@uu.nl (C.C.H.)
http://dx.doi.org/10.1016/j.celrep.2014.07.052
This is an open access article under the CC BY-NC-ND license (http://creativecommons.org/licenses/by-nc-nd/3.0/).

SUMMARY

Cargo transport along microtubules is driven by the collective function of microtubule plus- and minus-end-directed motors (kinesins and dyneins). How the velocity of cargo transport is driven by opposing teams of motors is still poorly understood. Here, we combined inducible recruitment of motors and adaptors to Rab6 secretory vesicles with detailed tracking of vesicle movements to investigate how changes in the transport machinery affect vesicle motility. We find that the velocities of kinesin-based vesicle movements are slower and more homogeneous than those of dynein-based movements. We also find that Bicaudal D (BICD) adaptor proteins can regulate dynein-based vesicle motility. BICD-related protein 1 (BICDR-1) accelerates minus-end-directed vesicle movements and affects Rab6 vesicle distribution. These changes are accompanied by reduced axonal outgrowth in neurons, supporting their physiological importance. Our study suggests that adaptor proteins can modulate the velocity of dynein-based motility and thereby control the distribution of transport carriers.

INTRODUCTION

Intracellular transport allows cells to quickly and accurately direct a large variety of subcellular components to specific sites. Transport vesicles usually contain both kinesin and dynein motors and display typical back-and-forth movements along microtubules (MTs). The correct cellular distribution of cargos strongly depends on the balance of these bidirectional movements (Welte, 2010). An important question is, what determines the velocity of a cargo that is driven by motors of opposite polarity? One possibility is that the velocity directly reflects the number of engaged motors. However, results obtained by inferring the motor number from measurements of the forces that drive individual cargos do not support this hypothesis (Shubeita et al., 2008). The size of the cargo (and thus the drag it exerts), as well as additional motors present on the same cargo, might affect the velocity of its movement (Bieling et al., 2010; Erickson et al., 2011; Pan et al., 2006). Finally, various adaptor proteins and cofactors that link motors to cargo have been implicated in regulating cargo movement (Akhmanova and Hammer, 2010; Jolly and Gelfand, 2011; Schlager and Hoogenraad, 2009).

Cytoplasmic dynein is a versatile motor that is known to associate with a large number of adaptor proteins (Kardon and Vale, 2009), but the effect of these proteins on dynein properties, including the rate of translocation, is still poorly understood (Allan, 2011). A well-studied group of dynein adaptors is the evolutionarily conserved Bicaudal D (BICD) family. BICD is an essential factor in *Drosophila* oogenesis and embryogenesis that functions by controlling dynein-mediated mRNA transport (Bullock et al., 2006; Claussen and Suter, 2005). Mammals possess two BICD homologs, BICD1 and BICD2 (Hoogenraad et al., 2001; Matanis et al., 2002), as well as two more distantly related proteins named BICDR-1 and BICDR-2 (Schlager et al., 2010). Mammalian BICD family proteins have been implicated in Rab6 secretory vesicle trafficking (Grigoriev et al., 2007; Matanis et al., 2002) and nuclear positioning (Splinter et al., 2010). Recent studies identified various mutations in the human *BICD2* gene in patients with dominant congenital spinal muscular atrophy (Lipka et al., 2013).

Although they are primarily known as dynein adaptors, BICD family proteins have also been shown to bind to kinesins. BICD2 interacts with kinesin-1 (KIF5) family members, and BICDR-1 binds to kinesin-3 KIF1C (Grigoriev et al., 2007; Matanis et al., 2002). This suggests that BICD proteins play a complex regulatory role in cargo movement. In this study, we investigate this role using Rab6 vesicles as a model system. We show that BICD2 and BICDR-1 interact with dynein-dynactin through the same highly conserved domain and yet differentially affect Rab6 vesicle movement. We demonstrate that BICDR-1 strongly increases Rab6 vesicle speed in the MT minus-end direction and provide data indicating that the proper control of Rab6 vesicle trafficking is important for neuronal development.

RESULTS AND DISCUSSION

Kinesin Family Members Alter the Velocity of MT Plus-End-Directed Rab6 Vesicle Movements

The opposing MT-based motors dynein and kinesin have previously been implicated in Rab6 vesicle motility (Grigoriev et al., 2007; Matanis et al., 2002; Schlager et al., 2010). Since several kinesins, including KIF5B and KIF1C, and cytoplasmic dynein bind to BICD family proteins (Grigoriev et al., 2007; Matanis et al., 2002; Schlager et al., 2010), and the activities of dynein and kinesin motors appear to be closely interlinked (Jolly and Gelfand, 2011), we first set out to determine the influence of kinesin motors on Rab6 transport. We used the FRB-FKBP dimerization system in combination with the cell-permeable rapamycin analog AP21967 (rapalog) to trigger binding of the dimeric motor domains (MDCs) of KIF5B or KIF1C to Rab6 vesicles (Figure 1A; Kapitein et al., 2010; Splinter et al., 2012) and investigated vesicle motility (Figure S1A). To distinguish the direction of Rab6 vesicle movements, we performed two-color imaging in MRC5-SV human lung fibroblasts in which the MT cytoskeleton is very sparse and can be easily visualized with mCherry-tagged α-tubulin (Figure 1B). In these conditions, MT plus ends can be distinguished by the presence of growth episodes, allowing identification of the direction of Rab6 vesicle movement (Splinter et al., 2012). We found that rapalog-induced KIF5B-MDC recruitment to Rab6 vesicles (Figures 1C and S1B–S1D) significantly decreased the mean speed of Rab6 vesicles in the MT plus-end direction, from ~1.7 μm/s to ~1.3 μm/s, and consequently the percentage of rapid events (Figures 1D and 1F). Conversely, KIF1C-MDC recruitment increased the velocity of Rab6 vesicles toward the MT plus ends to ~2.0 μm/s, and in this case the proportion of events that displayed high speed was higher (Figures 1D and 1F). These data show that the recruitment of distinct kinesins can differentially modulate MT plus-end-directed vesicle velocity. Interestingly, recruitment of either kinesin resulted in a marked narrowing of the velocity distribution profiles (Figure 1D), as was apparent from their reduced variances (Figure 1E). In contrast, recruitment of the rigor mutant KIF5B-MDC-T92N (Nakata and Hirokawa, 1995) arrests Rab6 vesicles on MTs (Movie S1; Figure S1E), showing that the results we observe are due to the recruitment of a kinesin with specific properties to the vesicles. Altogether, these results suggest that when the population of motors on the vesicles becomes more homogeneous, because of recruitment of an excess of one particular motor, the velocities of movement become more homogeneous as well. We conclude that it is the nature of the motors, rather than their number, that determines vesicle velocity.

In spite of the significant changes in Rab6 vesicle velocities in the MT plus-end direction, the velocity of minus-end-directed movement (~2.4 μm/s, ~1.5 times higher than the velocity of plus-end-directed movements) was largely unaffected by kinesin tethering to Rab6 vesicles (Figures 1D–1F). Thus, an increase in the number of kinesin motors on the Rab6 cargo had no major consequences for the velocity of dynein-dependent motility. These data are in line with the view that opposite-polarity motors on the same cargo do not directly affect each other's motility, but rather alter the number of runs occurring in each direction (Kapitein et al., 2010; Splinter et al., 2012; Xu et al., 2012). However, we cannot exclude the possibility that endogenous full-length motors bound to cargos by their native linkage mechanisms behave differently from the truncated motors used in the inducible trafficking assay.

Dynein Drives Rapid Rab6 Vesicle Movements

To analyze in more detail the effect of different MT-based motors on Rab6 vesicle velocity, we performed small interfering RNA (siRNA)-mediated depletion of KIF5B, KIF1C, KIF1B (the close homolog of KIF1C), dynein heavy chain (DHC), and combinations thereof. The depletion efficiency was ~70%–90% (Figures S2A–S2C). We performed the experiments in HeLa cells because we were not able to achieve efficient knockdown in MRC5-SV cells. Due to the extremely high density of the MT system in HeLa cells, we could not unambiguously trace individual vesicles along individual MTs. Therefore, MT plus-end- and minus-end-directed runs were analyzed together. Using maximum intensity projections, we identified episodes of vesicle motility and measured their velocities (Figures S1A and S2D). None of the analyzed motor depletions led to a complete inhibition of the overall transport of Rab6 vesicles from the Golgi to the cell periphery (Figures S2D and S2E). The knockdown of single kinesin proteins caused a mild increase in the mean velocity of Rab6 vesicles to ~1.7 μm/s (Figures S2D and S2E). Simultaneous depletion of all three kinesins resulted in a stronger effect (mean velocity of ~2.2 μm/s; Figures S2D and S2E).

We next tested the contribution of dynein to Rab6 vesicle movement. Depletion of DHC decreased the average velocity of vesicle movement to ~1.2 μm/s (Figures S2D and S2E) and reversed the effect of kinesin depletion (Figures S2D–S2F). These data strongly suggest that the rapid Rab6 vesicle movements are dynein-based, which is consistent with the observation that rapid Rab6 movements in MRC5-SV cells are predominantly MT minus-end-directed (Figures 1D, S2D, and S2E). When kinesins were depleted, rapid dynein movements started to predominate, increasing the average speed of Rab6 vesicles, whereas the depletion of dynein led to a relatively larger proportion of the slower kinesin-driven movements. It is also interesting to point out that velocities of dynein-based Rab6 vesicle movements display much broader distribution profiles (higher variance) than the kinesin-driven ones (Figures S2D and S2E). This heterogeneity might be due to the fact that dynein requires multiple adaptors and regulatory factors for its motility (Allan, 2011; Kardon and Vale, 2009).

BICD2 and BICDR-1 Interact with Dynein and Dynactin in a Similar Fashion

To explore the role of adaptor proteins in regulating dynein-driven cargo movement, we focused on the BICD family of proteins. Since both BICD2 and BICDR-1 interact with the dynein complex (Grigoriev et al., 2007; Matanis et al., 2002; Schlager et al., 2010) and colocalize with dynein on vesicles (Figures 2A and 2B; Movies S2 and S3), we first set out to compare the interactions of two BICD family members with the dynein complex in more detail. We performed immunoprecipitation experiments with extracts of HeLa cells stably expressing GFP-tagged DHC (Poser et al., 2008). Apart from some minor experimental variations, DHC consistently coprecipitated both BICD2 and BICDR-1 in equal amounts (Figure 2C). We confirmed this observation by additional immunoprecipitation experiments using antibodies specific for the endogenous dynein intermediate chain (DIC) (Figure 2D). Taken together, these results suggest

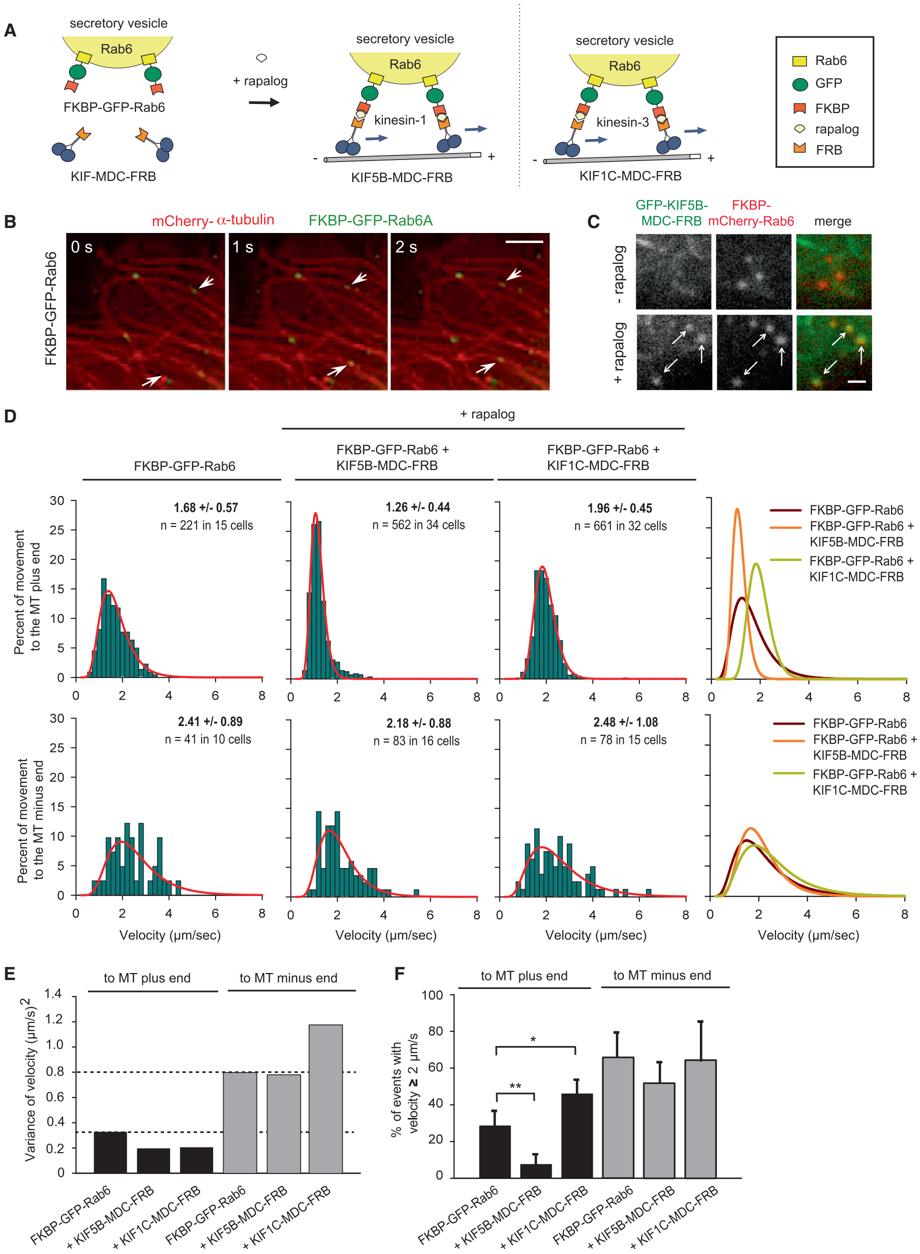

(legend on next page)

that BICD2 and BICDR-1 interact with the dynein motor equally well.

Next, we set out to map the dynein interaction site of BICD2 and BICDR-1 proteins more precisely. Various members of the BICD protein family are very similar in structure: they are coiled coil proteins with a cargo-binding site located in the C terminus and motor-binding sites in the N-terminal half of the molecule (Hoogenraad et al., 2001, 2003; Liu et al., 2013; Schlager et al., 2010; Splinter et al., 2012). By comparing the amino acid sequences of *Drosophila* and mouse BICD family members, we found a highly conserved region in the N terminus of these proteins (Figures 2E and S3). This domain shows homology to the HAP1_N conserved region (Pfam protein database: *pf04849*) and could be involved in the interaction with dynein and dynactin (Hoogenraad et al., 2001, 2003). Interestingly, a conserved alanine residue present in the center of this region is substituted by valine in the *Drosophila* hypomorphic mutant *BicD*^{PA66} (Oh et al., 2000) and is conserved in BICD family members and other adaptor proteins, such as HAP1 and TRAK1/2. Adjacent to this conserved alanine, mouse BICD family members have an additional alanine residue (Figure 2E). We hypothesized that the mutation of these alanine residues might affect the interaction of BICD family members with the dynein-dynactin complex. To test this, we generated BICD2 and BICDR-1 mutants, BICD2-A43V-A44V (BICD2-A/V) and BICDR-1-A116V-A117V (BICDR-1-A/V), respectively (Figure 2E). We found that the amount of A/V mutant BICD2 and BICDR-1 that coprecipitated with the dynein complex was dramatically reduced compared with the wild-type proteins (Figure 2F). This result was confirmed by a reverse immunoprecipitation (Figures 2G and 2H), indicating that the A/V mutations interfere with the ability of both BICD2 and BICDR-1 to bind to dynein and dynactin. These data show that BICD2 and BICDR-1 interact with dynein and dynactin through the same conserved N-terminal domain.

Despite the strong similarities between BICD2 and BICDR-1 in biochemical assays, their cellular distribution is markedly distinct (Schlager et al., 2010). HeLa cells expressing BICD2 showed a diffuse staining pattern with a small accumulation around the centrosome, whereas BICDR-1 showed a strong pericentrosomal accumulation (Figure 2I). Consistent with the biochemical data, the intensity of the A/V mutants at the pericentrosomal region was strongly reduced (Figures 2I and 2J). Together, these results demonstrate that the mutation of these alanine residues affects the interaction of BicD proteins with the dynein-dynactin complex.

BICD Adaptors Control the Velocity of Dynein-Based Movements

BICD2 and BICDR-1 expression also differentially affected the Rab6 vesicle distribution in HeLa cells (Figures 3A and 3B). Whereas overexpression of BICD2 only resulted in a very small recruitment of endogenous Rab6 vesicles to the centrosome, expression of BICDR-1 caused a strong pericentrosomal accumulation of Rab6 vesicles (Figures 3A and 3B). To directly test the effect of BICD proteins on Rab6 vesicle motility, we transiently expressed either BICD2 or BICDR-1 in HeLa cells stably expressing GFP-Rab6 and analyzed the movement of Rab6 vesicles. The expression of BICD2 increased the mean Rab6 vesicle velocity from ~1.5 μm/s to ~1.9 μm/s, while BICDR-1 caused a much larger increase, to ~3.3 μm/s (Figures 3C and 3G; Movie S4). Kymograph analysis of individual vesicle tracks revealed that the increase in velocity was not caused by altered motor switching, but was mainly due to the fact that long processive runs occurred with a higher speed (Figures 3D and 3F). The BICDR-1-induced increase in Rab6 vesicle velocity was also observed in several other cell types, including MRC5-SV and Vero cells (Figure 3E). We next tested the contribution of dynein to the BICDR-1-mediated increase in Rab6 vesicle velocity. Depletion of DHC in BICDR-1-expressing HeLa cells decreased the number of motile Rab6 vesicles and reduced the average velocity from 3.3 μm/s to 2.0 μm/s (Figure 3I). Moreover, expression of the BICDR-1 A/V mutant showed decreased Rab6 vesicle motility compared with BICDR-1 wild-type (Figures S4A and S4B). These data indicate that the BICDR-1-induced increase in Rab6 vesicle motility is dynein based, which is consistent with the BICDR-1-mediated accumulation of Rab6 in the pericentrosomal region (Figures 3A and 3B).

To further prove that the increase in vesicle velocity induced by BICDR-1 expression is due to modulation of dynein motility, we switched back to MRC5-SV expressing mCherry-α-tubulin. Quantitative single-particle tracking revealed that BICDR-1 expression markedly increased the mean Rab6 vesicle speed in the MT minus-end direction, from ~2.3 μm/s to ~3.6 μm/s (Figure 3H). The velocity of plus-end-directed movements was also increased from ~1.6 μm/s in control cells to ~2.2 μm/s (Figure 3H). This could be caused by a change in the set of vesicle-associated kinesin motors, for example, by the enhanced recruitment of a more rapid kinesin such as KIF1C, which is known to interact with BICDR-1 (Schlager et al., 2010). These data demonstrate that BICDR-1 induces a strong increase in Rab6 vesicle velocity, predominantly in the MT minus-end direction.

Figure 1. Distinct Kinesin Motors Differentially Alter Rab6 Vesicle Motility

(A) Inducible Rab6 secretory-vesicle trafficking assay. Fusions of FRB with the motor domain and coiled-coil dimerization region of kinesin-1 (KIF5-MDC-FRB) and kinesin-3 (KIF1C-MDC-FRB) are recruited to FKBP-GFP-Rab6 upon addition of rapalog.

(B) Simultaneous live imaging of FKBP-GFP-Rab6 vesicles (green, arrows) and mCherry-α-tubulin (red) in a transiently transfected MRC5-SV cell; time is indicated in seconds. Imaging of FKBP-GFP-Rab6 in MRC5-SV cells expressing HA-KIF5B-T92N-MDC-FRB is shown in Movie S1. Scale bar, 3 μm.

(C) Representative stills of a small region of a cell transfected with GFP-KIF5B-MDC-FRB and FKBP-mCherry-Rab6 before (−) and after (+) rapalog addition. Arrows indicate Rab6 vesicles. Images are related to Figures S1B–S1D. Scale bar, 1 μm.

(D) Analysis of Rab6 vesicle movement along MTs within the cell upon rapalog-induced recruitment of either KIF5-MDC-FRB or KIF1C-MDC-FRB.

(E) Variance in velocity of Rab6 vesicle movements toward either the MT plus or minus end upon recruitment of the indicated motor constructs.

(F) Percentage of Rab6 vesicle movement events in the direction of either the MT plus or minus end with a velocity of ≥2 μm/s (average ± SD). $^{*}p < 0.01$, $^{**}p < 0.001$, Mann-Whitney U test.

See also Figure S2.

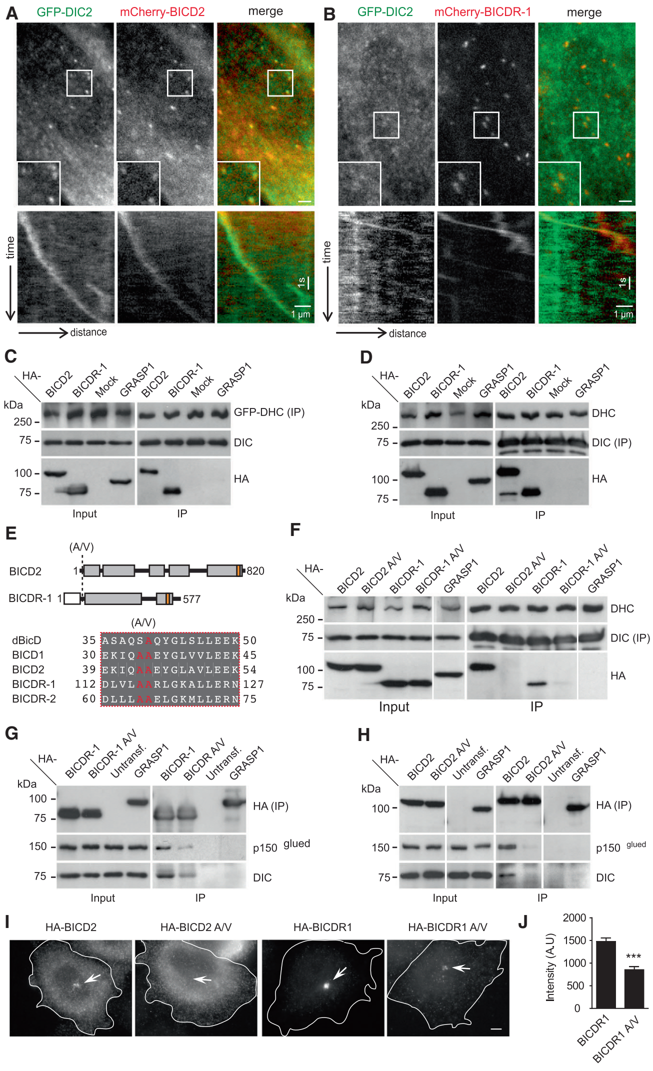
A
GFP-DIC2
mCherry-BICD2
merge
B
GFP-DIC2
mCherry-BICDR-1
merge
time
distance
1s
1 µm
C
HA-
BICD2
BICDR-1
Mock
GRASP1
kDa
250
75
100
GFP-DHC (IP)
DIC
HA
Input
IP
D
DHC
DIC (IP)
E
(A/V)
BICD2
BICDR-1
820
577
dBicD 35 ASAQSAQYGLSLLEEK 50
BICD1 30 EKIQAAEYGLVVLEEK 45
BICD2 39 EKIQAAEYGLAVLEEK 54
BICDR-1 112 DLVLAARLGKALLERN 127
BICDR-2 60 DLLLAAELGKMLLERN 75
F
BICD2 A/V
BICDR-1 A/V
G
Untransf.
HA (IP)
p150 glued
H
I
HA-BICD2
HA-BICD2 A/V
HA-BICDR1
HA-BICDR1 A/V
J
Intensity (A.U)
2000
1500
1000
500
0
***
BICDR1
BICDR1 A/V

Figure 2. Identification of the Conserved Binding Site for Dynein-Dynactin in the N Terminus of BICD Family Proteins

(A and B) HeLa cells stably expressing GFP-DIC2 were transfected with mCherry-BICD2 (A) or mCherry-BICDR-1 (B). The images correspond to one frame of Movies S2 and S3. Kymographs are shown to illustrate the movement of vesicles labeled with GFP-DIC2 and the indicated transfected constructs. Scale bars, 2 μm.

(C) Immunoprecipitations with anti-GFP antibodies from extracts of HeLa cells stably expressing GFP-DHC, transfected with the indicated constructs and probed for DHC, DIC, or hemagglutinin (HA).

(D) Immunoprecipitations with antibodies against DIC from extracts of HeLa cells transfected with the indicated constructs and probed for DHC, DIC, or HA.

(E) Schematic overview of BICD2/BICDR-1 and a section of a sequence alignment of *Drosophila* BicD (dBicD, NP_724056.1), mouse BICD1 (NP_033883), BICD2 (NP_084067), BICDR-1 (NP_001074277), and BICDR-2 (NP_722479). The dashed red line and red letters indicate the site of the dBicD-A40V ($BicD^{PA66}$), BICD2-A116V-A117V (BICD2 A/V), and BICDR-1-A43V-A44V (BICDR-1 A/V) mutations.

(F) Immunoprecipitations with antibodies against DIC from extracts of HeLa cells transfected with the indicated constructs and probed for DHC, DIC, or HA.

(G) Immunoprecipitations with anti-HA antibodies from extracts of HeLa cells transfected with the indicated constructs and probed for DIC, p150Glued, or HA.

(H) Immunoprecipitations with anti-HA antibodies from extracts of HeLa cells transfected with the indicated constructs and probed for DIC, p150Glued, or HA.

(I) Representative image of a HeLa cell overexpressing HA-BICD2, HA-BICD2 A/V, HA-BICDR-1 A/V, or HA-BICDR-1 stained for HA. Solid lines indicate the cell edge, and arrows indicate the centrosome region. Scale bar, 5 μm.

(J) Quantification of the intensity of HA-BICDR-1 and HA-BICDR-1 A/V signal at the centrosome (average ± SEM; HA-BICDR-1, n = 41 cells; HA-BICDR-1 A/V, n = 45 cells; n = 2 independent experiments). ***$p < 0.0001$, t test.

See also Figure S3.

BICD Adaptors Control the Distribution of Rab6 Vesicles and Axonal Outgrowth

BICDR-1 is primarily found in the brain, is expressed in hippocampal and dorsal root ganglion (DRG) neurons, and is required for neural development in zebrafish (Schlager et al., 2010). To test its cellular effect in neuronal systems, we transiently expressed BICD2 and BICDR-1 in developing hippocampal and adult DRG neurons and analyzed the Rab6 vesicle distribution. BICD2 did not affect the distribution of Rab6 vesicles in the neuronal cell body and axons (Figures 4A and 4C). In contrast, BICDR-1 expression induced a strong accumulation of Rab6 vesicles in the cell bodies and led to a ∼3-fold decrease in the number of axonal Rab6 vesicles Figures 4A–4D). Interestingly, BICDR-1 expression in hippocampal and DRG neurons showed a marked reduction in axon outgrowth compared with control cells (Figures 4E–4H). The total axon length was decreased by ∼50% in BICDR-1 expressing neurons, but no difference was observed in GFP-BICD2- or GFP-expressing neurons (Figures 4F and 4H). These results

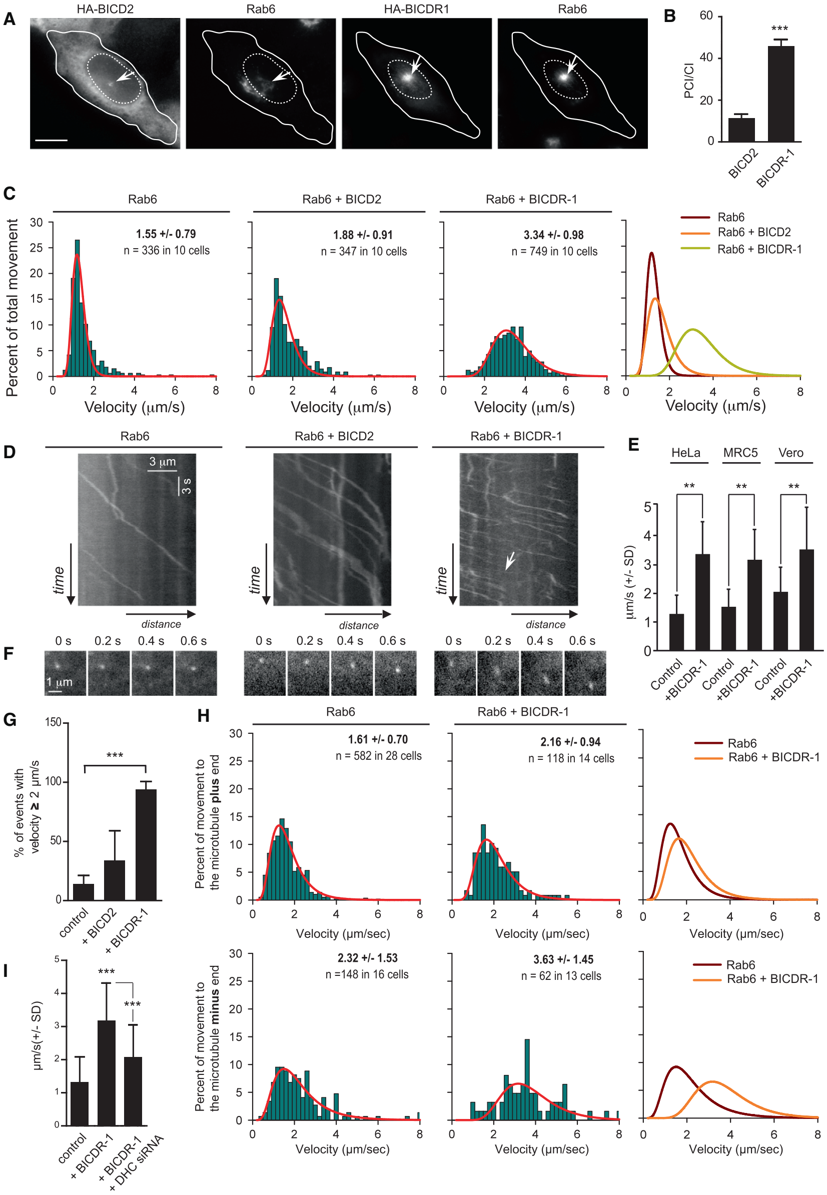

Figure 3. BICDR-1 Increases Rab6 Vesicle Velocity in the MT Minus-End Direction
(A) Representative image of a HeLa cell overexpressing HA-BICD2 or HA-BICDR-1, stained for HA and endogenous Rab6. Solid lines indicate the cell edge, dashed lines indicate the nucleus, and arrows indicate the centrosome region. Scale bar, 10 µm.

(legend continued on next page)

suggest that the observed axon phenotype is due to BICDR-1-induced loss of Rab6 secretory vesicles from the neurites. In agreement with this interpretation, DRG neurons transfected with both Rab6A- and Rab6B-shRNA showed a 50% reduction of total axon length compared with control cells and single Rab6A- or Rab6B-depleted neurons (Figures 4I and 4J), suggesting that Rab6A and Rab6B have an important function in axon outgrowth. These data are consistent with previous results obtained in hippocampal neurons (Schlager et al., 2010) and show that BICDR-1 influences Rab6 vesicle distribution, an effect that is accompanied by altered axonal elongation in both young and adult neurons.

It is interesting to speculate about the possible molecular mechanisms that underlie the observed differences between BICDR-1 and BICD2. One possibility is that the two adaptors interact with different kinesins, which would differentially influence dynein-dependent movements. However, the depletion of various kinesin combinations in BICD2-overexpression did not increase vesicle velocities to the levels observed with BICDR-1 expression (Figures S4C–S4F). Another possibility is that BICDR-1 recruits higher-order assemblies of dynein-dynactin to Rab6 vesicles compared with BICD2, thereby leading to the observed increase in Rab6 vesicle velocity. In vitro studies have shown that changing the number of dynein motors allows robust dynein-driven motion (Derr et al., 2012; Mallik et al., 2005). Moreover, increased minus-end-directed transport of cytoplasmic mRNA in *Drosophila* embryos has been reported to depend on the dosage of BICD and dynein motors (Bullock et al., 2006). Nevertheless, it seems unlikely that the increase in Rab6 vesicle velocity is caused by the enhanced recruitment of dynein-dynactin to Rab6 vesicles, since both BICD2 and BICDR-1 precipitated dynein and dynactin equally well and the interaction could be disrupted by the mutation of the same protein domain. Furthermore, direct imaging of GFP-tagged dynein provided no clear indications of enhanced recruitment by BICDR-1 as compared with BICD2 (Figures 2A and 2B).

One other possibility is that BICDR-1 directly regulates the dynein-dynactin complex and enhances dynein motor activity. Several recent results point to a regulatory mechanism whereby alterations in the dynein tail influence the motor domains (Vallee et al., 2012). In vitro work has shown that dynein cofactors such as Lis1 and NudE can alter the properties of dynein, including its mechanochemical cycle and processivity (Huang et al., 2012; McKenney et al., 2010). The idea that multiple adaptors and regulatory factors are involved in controlling dynein-based motility is consistent with the broad minus-end-directed velocity distribution profiles. However, the mechanistic details underlying the contributions of different adaptors and accessory factors to dynein motor velocity remain an unresolved issue that requires future work.

EXPERIMENTAL PROCEDURES

DNA Constructs, siRNAs, and Cell Lines

Details regarding the BICD2, BICDR-1, Rab6, kinesin constructs, and siRNAs used in this work are provided in Supplemental Experimental Procedures. The HeLa cell lines stably expressing GFP-DIC2 and GFP-DHC were a gift from Dr. Anthony Hyman.

Primary Hippocampal Neuron and DRG Neuron Cultures

Primary hippocampal cultures were prepared from embryonic day 18 (E18) rat brains and transfected using Lipofectamine 2000 (Invitrogen). DRG neurons were isolated from adult female Sprague Dawley rats (3 months old) and transfected using a Microporator (Invitrogen). For details, see Supplemental Experimental Procedures.

Image Acquisition and Live-Cell Imaging

Images of fixed cells were collected with a Leica DMRBE microscope equipped with an ORCA-ER-1394 CCD camera (Hamamatsu) or Nikon Eclipse 80i microscope equipped with a Photometrics CoolSNAP HQ2 CCD camera. Live-cell imaging was performed on a total internal reflection fluorescence inverted research microscope (Nikon Eclipse Ti-E; Nikon) at 37°C in standard culture medium in a closed chamber with 5% CO_2 (Tokai Hit). For details, see Supplemental Experimental Procedures.

SUPPLEMENTAL INFORMATION

Supplemental Information includes Supplemental Experimental Procedures, four figures, and four movies and can be found with this article online at http://dx.doi.org/10.1016/j.celrep.2014.07.052.

AUTHOR CONTRIBUTIONS

M.A.S. cloned the DNA constructs, designed and performed biochemical experiments, and edited the manuscript. A.S.-M. designed and performed knockdown and imaging experiments, analyzed the results, and edited the manuscript. I.G. performed imaging experiments and analyzed the results. L.F.G. performed the DRG neuron experiments and analyzed the results. M.E.d.S. performed the hippocampal neuron experiments and analyzed the results. P.S.W. assisted with cloning the DNA constructs. A.A. and C.C.H. supervised the research and wrote the manuscript.

(B) Ratio of pericentrosomal (PCI) versus cytoplasmic (CI) Rab6 fluorescence intensity in cells overexpressing either HA-BICD2 or HA-BICDR-1 (average ± SEM; HA-BICD2, n = 44; HA-BICDR-1, n = 41 cells). ***$p < 0.0001$, Mann-Whitney test.

(C) Histograms of Rab6 vesicle speeds in HeLa cells stably expressing GFP-Rab6 and transfected for the indicated constructs. GFP-Rab6 motility in HeLa cells in the absence or presence of BICDR-1 is shown in Movie S4.

(D) Kymographs illustrating the movements of GFP-Rab6 vesicles in untransfected cells or cells transfected with the indicated constructs. Scale bar, 3 μm.

(E) Average speed (± SD) of GFP-Rab6 vesicles toward the cell center in HeLa, MRC5-SV, or Vero cells transfected with either a control construct or BICDR-1. **$p < 0.001$, Mann-Whitney U test.

(F) Time-lapse images of GFP-Rab6 vesicles in HeLa cells transfected with either BICD2 or BICDR-1. Time is in seconds.

(G) Overexpression of BICD2 and BICDR-1 led to an increase in the percentage of Rab6 vesicle movement $\geq 2\ \mu$m/s (average ± SD). ***$p < 0.001$, unpaired t test.

(H) Histograms of vesicle speeds toward the MT plus or minus end in MRC5-SV cells transfected with GFP-Rab6A and BICDR-1 when indicated. The indicated values correspond to mean ± SD.

(I) Average speed (± SD) of GFP-Rab6 vesicles in HeLa transfected with a control construct, BICDR-1, or BICDR-1 and DHC siRNA. ***$p < 0.0001$, Mann-Whitney U test.

See also Figure S4.

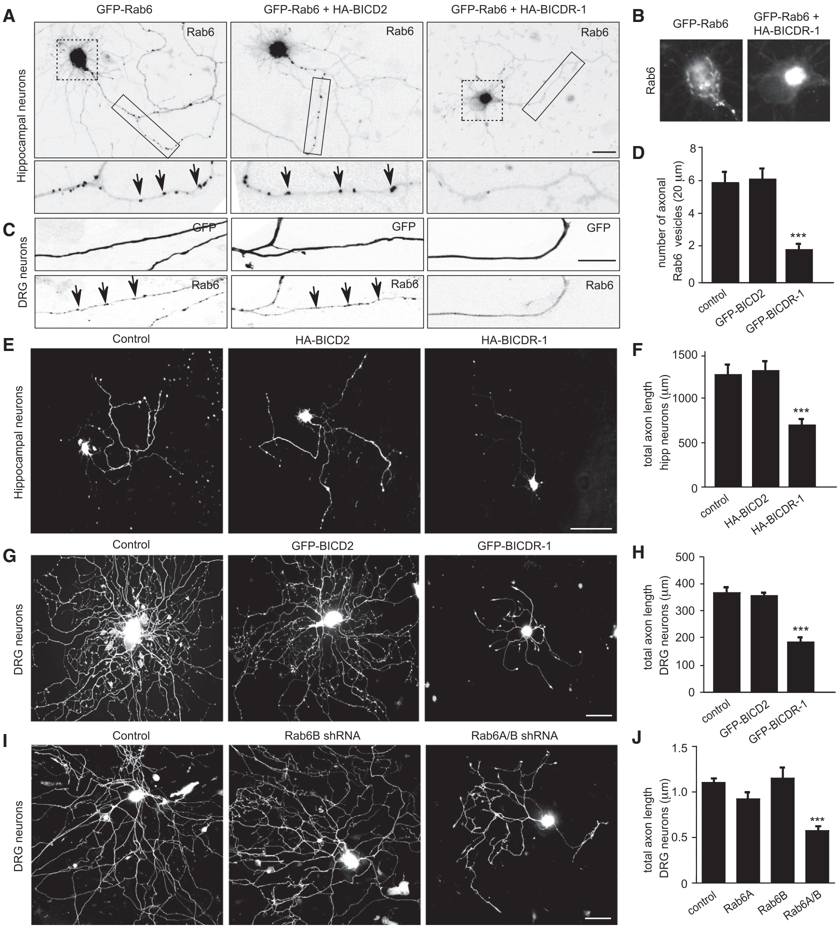
A
GFP-Rab6
GFP-Rab6 + HA-BICD2
GFP-Rab6 + HA-BICDR-1
Rab6
Rab6
Rab6
Hippocampal neurons
B
GFP-Rab6
GFP-Rab6 + HA-BICDR-1
Rab6
C
DRG neurons
GFP
GFP
GFP
Rab6
Rab6
Rab6
D
number of axonal Rab6 vesicles (20 μm)
8
6
4
2
0
***
control
GFP-BICD2
GFP-BICDR-1
E
Control
HA-BICD2
HA-BICDR-1
Hippocampal neurons
F
total axon length hipp neurons (μm)
1500
1000
500
0
***
control
HA-BICD2
HA-BICDR-1
G
Control
GFP-BICD2
GFP-BICDR-1
DRG neurons
H
total axon length DRG neurons (μm)
500
400
300
200
100
0
***
control
GFP-BICD2
GFP-BICDR-1
I
Control
Rab6B shRNA
Rab6A/B shRNA
DRG neurons
J
total axon length DRG neurons (μm)
1.5
1.0
0.5
0
***
control
Rab6A
Rab6B
Rab6A/B

Figure 4. Proper Rab6 Vesicle Distribution Is Important for Axon Elongation in Neurons

(A) Representative images of hippocampal neurons expressing GFP-Rab6, HA-BICD2, or HA-BICDR-1. Scale bar, 20 μm. Enlarged boxed areas correspond to a region of the axon and arrows indicate Rab6 vesicles.

(B) Enlargement of the cell body of the neurons presented in (A) (dashed-line boxes).

(C) Representative images of axons of DRG neurons expressing GFP to highlight neuronal morphology, TagRFP-Rab6, and HA-BICD2 or HA-BICDR-1. Arrows indicate Rab6 vesicles. Scale bar, 10 μm.

(D) Quantification of the number of TagRFP-Rab6 vesicles in axons of DRG neurons transfected with the indicated constructs. Error bars indicate SEM. ***$p < 0.001$, t test.

(E and G) Representative images of hippocampal neurons at 4 days in vitro (DIV4) and DRG neurons at DIV2 transfected with TagBFP and the indicated constructs. Scale bar, 100 μm.

(F and H) Quantification of axon length in TagBFP (control) and HA-BICD2 or HA-BICDR-1 cotransfected hippocampal neurons (DIV4; n = 31–37 cells, n = 3 independent experiments) or GFP (control), GFP-BICDR-1, and GFP-BICD2 transfected DRG neurons (DIV1; n = 53–87 cells; n = 3 independent experiments). Error bars indicate SEM. ***$p < 0.001$, t test.

(I) Representative images of DRG neurons (DIV4) transfected with GFP and the indicated constructs. Scale bar, 100 μm.

(J) Quantification of axon length in GFP and pSuper (control), Rab6A-shRNA, Rab6B-shRNA, or Rab6A/B-shRNA cotransfected DRG neurons (DIV4; n = 31–40 cells; n = 3 independent experiments). Error bars indicate SEM. ***$p < 0.001$, t test.

ACKNOWLEDGMENTS

We thank Drs. Ina Poser and Anthony Hyman for sharing HeLa cells stably expressing GFP-tagged DHC and DIC2. This work was supported by Fundação para a Ciência e a Tecnologia fellowships (A.S.-M. and M.E.S.), the Netherlands Organization for Scientific Research (NWO-ALW-VICI; A.A. and C.C.H.), the Netherlands Organization for Health Research and Development (ZonMW-TOP; A.A. and C.C.H.), the European Science Foundation (EURYI; C.C.H.), the EMBO Young Investigators Program (YIP; C.C.H.), the Research Programme of the Foundation for Fundamental Research on Matter (FOM; A.A. and C.C.H.), a Het Prinses Beatrix Spierfonds grant (PBF; C.C.H.), and an FP7 EU Marie Curie postdoctoral fellowship (L.F.G.).

Received: April 10, 2013
Revised: June 8, 2014
Accepted: July 28, 2014
Published: August 28, 2014

REFERENCES

Akhmanova, A., and Hammer, J.A., 3rd. (2010). Linking molecular motors to membrane cargo. Curr. Opin. Cell Biol. *22*, 479–487.

Allan, V.J. (2011). Cytoplasmic dynein. Biochem. Soc. Trans. *39*, 1169–1178.

Bieling, P., Kronja, I., and Surrey, T. (2010). Microtubule motility on reconstituted meiotic chromatin. Curr. Biol. *20*, 763–769.

Bullock, S.L., Nicol, A., Gross, S.P., and Zicha, D. (2006). Guidance of bidirectional motor complexes by mRNA cargoes through control of dynein number and activity. Curr. Biol. *16*, 1447–1452.

Claussen, M., and Suter, B. (2005). BicD-dependent localization processes: from Drosophilia development to human cell biology. Ann. Anat. *187*, 539–553.

Derr, N.D., Goodman, B.S., Jungmann, R., Leschziner, A.E., Shih, W.M., and Reck-Peterson, S.L. (2012). Tug-of-war in motor protein ensembles revealed with a programmable DNA origami scaffold. Science *338*, 662–665.

Erickson, R.P., Jia, Z., Gross, S.P., and Yu, C.C. (2011). How molecular motors are arranged on a cargo is important for vesicular transport. PLoS Comput. Biol. *7*, e1002032.

Grigoriev, I., Splinter, D., Keijzer, N., Wulf, P.S., Demmers, J., Ohtsuka, T., Modesti, M., Maly, I.V., Grosveld, F., Hoogenraad, C.C., and Akhmanova, A. (2007). Rab6 regulates transport and targeting of exocytotic carriers. Dev. Cell *13*, 305–314.

Hoogenraad, C.C., Akhmanova, A., Howell, S.A., Dortland, B.R., De Zeeuw, C.I., Willemsen, R., Visser, P., Grosveld, F., and Galjart, N. (2001). Mammalian Golgi-associated Bicaudal-D2 functions in the dynein-dynactin pathway by interacting with these complexes. EMBO J. *20*, 4041–4054.

Hoogenraad, C.C., Wulf, P., Schiefermeier, N., Stepanova, T., Galjart, N., Small, J.V., Grosveld, F., de Zeeuw, C.I., and Akhmanova, A. (2003). Bicaudal D induces selective dynein-mediated microtubule minus end-directed transport. EMBO J. *22*, 6004–6015.

Huang, J., Roberts, A.J., Leschziner, A.E., and Reck-Peterson, S.L. (2012). Lis1 acts as a "clutch" between the ATPase and microtubule-binding domains of the dynein motor. Cell *150*, 975–986.

Jolly, A.L., and Gelfand, V.I. (2011). Bidirectional intracellular transport: utility and mechanism. Biochem. Soc. Trans. *39*, 1126–1130.

Kapitein, L.C., Schlager, M.A., van der Zwan, W.A., Wulf, P.S., Keijzer, N., and Hoogenraad, C.C. (2010). Probing intracellular motor protein activity using an inducible cargo trafficking assay. Biophys. J. *99*, 2143–2152.

Kardon, J.R., and Vale, R.D. (2009). Regulators of the cytoplasmic dynein motor. Nat. Rev. Mol. Cell Biol. *10*, 854–865.

Lipka, J., Kuijpers, M., Jaworski, J., and Hoogenraad, C.C. (2013). Mutations in cytoplasmic dynein and its regulators cause malformations of cortical development and neurodegenerative diseases. Biochem. Soc. Trans. *41*, 1605–1612.

Liu, Y., Salter, H.K., Holding, A.N., Johnson, C.M., Stephens, E., Lukavsky, P.J., Walshaw, J., and Bullock, S.L. (2013). Bicaudal-D uses a parallel, homodimeric coiled coil with heterotypic registry to coordinate recruitment of cargos to dynein. Genes Dev. *27*, 1233–1246.

Mallik, R., Petrov, D., Lex, S.A., King, S.J., and Gross, S.P. (2005). Building complexity: an in vitro study of cytoplasmic dynein with in vivo implications. Curr. Biol. *15*, 2075–2085.

Matanis, T., Akhmanova, A., Wulf, P., Del Nery, E., Weide, T., Stepanova, T., Galjart, N., Grosveld, F., Goud, B., De Zeeuw, C.I., et al. (2002). Bicaudal-D regulates COPI-independent Golgi-ER transport by recruiting the dynein-dynactin motor complex. Nat. Cell Biol. *4*, 986–992.

McKenney, R.J., Vershinin, M., Kunwar, A., Vallee, R.B., and Gross, S.P. (2010). LIS1 and NudE induce a persistent dynein force-producing state. Cell *141*, 304–314.

Nakata, T., and Hirokawa, N. (1995). Point mutation of adenosine triphosphate-binding motif generated rigor kinesin that selectively blocks anterograde lysosome membrane transport. J. Cell Biol. *131*, 1039–1053.

Oh, J., Baksa, K., and Steward, R. (2000). Functional domains of the Drosophila bicaudal-D protein. Genetics *154*, 713–724.

Pan, X., Ou, G., Civelekoglu-Scholey, G., Blacque, O.E., Endres, N.F., Tao, L., Mogilner, A., Leroux, M.R., Vale, R.D., and Scholey, J.M. (2006). Mechanism of transport of IFT particles in C. elegans cilia by the concerted action of kinesin-II and OSM-3 motors. J. Cell Biol. *174*, 1035–1045.

Poser, I., Sarov, M., Hutchins, J.R., Hériché, J.K., Toyoda, Y., Pozniakovsky, A., Weigl, D., Nitzsche, A., Hegemann, B., Bird, A.W., et al. (2008). BAC TransgeneOmics: a high-throughput method for exploration of protein function in mammals. Nat. Methods *5*, 409–415.

Schlager, M.A., and Hoogenraad, C.C. (2009). Basic mechanisms for recognition and transport of synaptic cargos. Mol. Brain *2*, 25.

Schlager, M.A., Kapitein, L.C., Grigoriev, I., Burzynski, G.M., Wulf, P.S., Keijzer, N., de Graaff, E., Fukuda, M., Shepherd, I.T., Akhmanova, A., and Hoogenraad, C.C. (2010). Pericentrosomal targeting of Rab6 secretory vesicles by Bicaudal-D-related protein 1 (BICDR-1) regulates neuritogenesis. EMBO J. *29*, 1637–1651.

Shubeita, G.T., Tran, S.L., Xu, J., Vershinin, M., Cermelli, S., Cotton, S.L., Welte, M.A., and Gross, S.P. (2008). Consequences of motor copy number on the intracellular transport of kinesin-1-driven lipid droplets. Cell *135*, 1098–1107.

Splinter, D., Tanenbaum, M.E., Lindqvist, A., Jaarsma, D., Flotho, A., Yu, K.L., Grigoriev, I., Engelsma, D., Haasdijk, E.D., Keijzer, N., et al. (2010). Bicaudal D2, dynein, and kinesin-1 associate with nuclear pore complexes and regulate centrosome and nuclear positioning during mitotic entry. PLoS Biol. *8*, e1000350.

Splinter, D., Razafsky, D.S., Schlager, M.A., Serra-Marques, A., Grigoriev, I., Demmers, J., Keijzer, N., Jiang, K., Poser, I., Hyman, A.A., et al. (2012). BICD2, dynactin, and LIS1 cooperate in regulating dynein recruitment to cellular structures. Mol. Biol. Cell *23*, 4226–4241.

Vallee, R.B., McKenney, R.J., and Ori-McKenney, K.M. (2012). Multiple modes of cytoplasmic dynein regulation. Nat. Cell Biol. *14*, 224–230.

Welte, M.A. (2010). Bidirectional transport: matchmaking for motors. Curr. Biol. *20*, R410–R413.

Xu, J., Shu, Z., King, S.J., and Gross, S.P. (2012). Tuning multiple motor travel via single motor velocity. Traffic *13*, 1198–1205.

SUPPLEMENTARY INFORMATION

Manuscript "Bicaudal D (BICD) family adaptor proteins control the velocity of dynein-based movements" by Schlager et al.,

SUPPLEMENTAL VIDEO LEGENDS

Supplemental video 1, related to Figure 1B.
Dynamics of FKBP-GFP-Rab6 (green) and mKate-α-tubulin (red) in control MRC5 cells and cells co-transfected with KIF5B-T92N-MDC-FRB (rigor mutant). Total time: 450 seconds. 1 frame per second. ~30x sped up.

Supplemental video 2, related to Figure 2A.
Colocalization of GFP-DIC2 and mCherry-BICD2 on moving vesicles in HeLa cells. Total time: 15 seconds. 10 frames per second. ~3x sped up.

Supplemental video 3, related to Figure 2B.
Colocalization of GFP-DIC2 and mCherry-BICDR-1 on moving vesicles in HeLa cells. Total time: 15 seconds. 10 frames per second. ~3x sped up.

Supplemental video 4, related to Figure 4.
GFP-Rab6 motility in control HeLa cells (control, left and middle) and BICDR-1-expressing HeLa cells (BICDR-1, right). Total time: 57.85 seconds. 1.1 frames per second. ~27x sped up.

SUPPLEMENTARY FIGURES

Schlager et al., Supplemental Figure 1

A

	Constructs	Cell line	total number of cells	total number of tracks	average velocity	SD (µm/s)	Variance (SD^2)	No. of tracks with velocity ≥ 2	% of tracks with velocity ≥ 2 µm/s
Fig. 1D	FKBP-GFP-Rab6 (to plus ends)	MRC5	15	221	1.68	0.57	0.32	63	28.51
	FKBP-GFP-Rab6 + KIF5B-MDC-FRB (to plus ends)	MRC5	34	562	1.26	0.44	0.19	42	7.47
	FKBP-GFP-Rab6 + KIF1C-MDC-FRB (to plus ends)	MRC5	32	616	1.96	0.45	0.20	283	45.94
	FKBP-GFP-Rab6 (to minus ends)	MRC5	10	41	2.41	0.89	0.79	27	65.85
	FKBP-GFP-Rab6 + KIF5B-MDC-FRB (to minus ends)	MRC5	16	83	2.18	0.88	0.77	43	51.81
	FKBP-GFP-Rab6 + KIF1C-MDC-FRB (to minus ends)	MRC5	15	78	2.48	1.08	1.17	50	64.10
Fig. 3C	GFP-Rab6	HeLa	10	336	1.55	0.79	0.62	48	14.29
	GFP-Rab6 + BICD2	HeLa	10	347	1.88	0.91	0.83	118	34.01
	GFP-Rab6 + BICDR-1	HeLa	10	749	3.34	0.98	0.96	704	93.99
Fig. 3H	GFP-Rab6 (to plus ends)	MRC5	28	582	1.61	0.70	0.49	148	25.43
	GFP-Rab6 + BICDR-1 (to plus ends)	MRC5	14	118	2.16	0.94	0.88	64	54.24
	GFP-Rab6 (to minus ends)	MRC5	16	148	2.32	1.53	2.34	78	52.70
	GFP-Rab6 + BICDR-1 (to minus ends)	MRC5	13	62	3.63	1.45	2.10	55	88.71
Fig. S2D	GFP-Rab6	HeLa	20	1348	1.45	0.68	0.46	206	15.28
	GFP-Rab6 + KIF5B KD	HeLa	10	848	1.68	0.68	0.46	231	27.24
	GFP-Rab6 + KIF1B KD	HeLa	9	842	1.65	0.94	0.88	202	23.99
	GFP-Rab6 + KIF1C KD	HeLa	13	844	1.70	0.88	0.77	227	26.90
	GFP-Rab6 + KIF5B, 1B, 1C KD	HeLa	11	840	2.25	1.30	1.69	426	50.71
	GFP-Rab6 + DHC KD	HeLa	9	848	1.22	0.61	0.37	62	7.31
	GFP-Rab6 + DHC, KIF5B, 1B, 1C KD	HeLa	14	783	1.46	0.59	0.35	138	17.53
Fig. S4A	GFP-Rab6 + mCherry-BicD2	HeLa	10	558	2.13	1.17	1.37	240	43.01
	GFP-Rab6 + mCherry-BicD2 A/V	HeLa	12	876	1.80	1.00	1.00	275	31.39
	GFP-Rab6 + mCherry-BicDR-1	HeLa	11	898	3.25	1.50	2.25	837	93.21
	GFP-Rab6 + mCherry-BicDR-1 A/V	HeLa	11	799	2.76	1.15	1.32	591	73.97
Fig. S4E	GFP-Rab6	HeLa	20	1348	1.45	0.68	0.46	206	15.28
	GFP-Rab6 + BicD2	HeLa	13	503	2.02	0.80	0.64	230	45.73
	GFP-Rab6 + BicD2 + KIF5B KD	HeLa	8	711	2.20	1.24	1.54	370	52.04
	GFP-Rab6 + BicD2 + KIF5B, 1B KD	HeLa	11	500	2.60	1.06	1.12	349	69.80
	GFP-Rab6 + BicD2 + KIF5B, 1C KD	HeLa	11	476	2.47	0.98	0.96	311	65.34
	GFP-Rab6 + BicD2 + KIF1B, 1C KD	HeLa	12	500	2.40	1.10	1.21	285	57.00

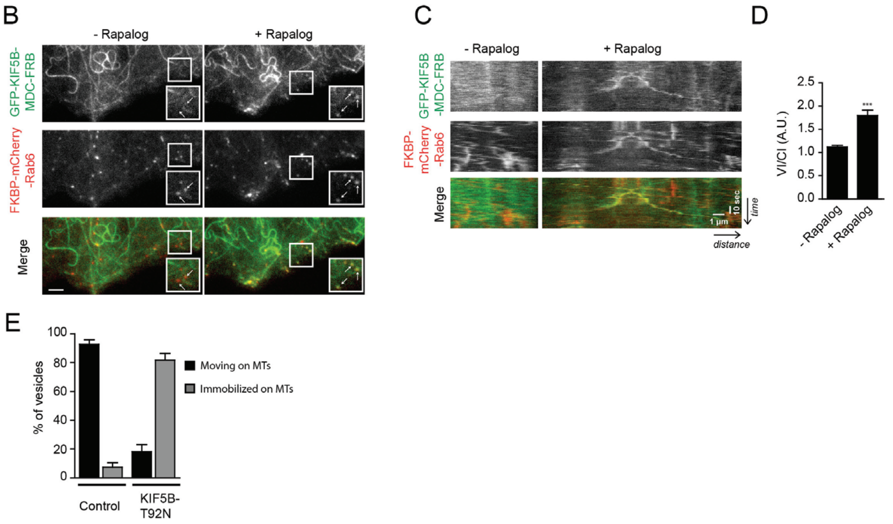

Figure S1, related to Figure 1. Summary of velocity measurements and rapalog induced recruitment of kinesin to Rab6 vesicles

(A) Overview of Rab6 vesicle velocity measured under various conditions in HeLa and MRC5 cells. Related to Fig. 1D, 3C, 3H, S2D, S4A and S4E.

(B) Representative stills of a movie of a cell transfected with GFP-KIF5B-MDC-FRB and FKBP-mCherry-Rab6, before (-) and after (+) addition of rapalog. Arrows highlight Rab6 vesicles before and after recruitment of kinesin. Scale bar: 3 μm.

(C) Kymographs illustrating movements of FKBP-mCherry-Rab6 vesicles before (-rapalog) and after (+ rapalog) recruitment of GFP-KIF5B-MDC-FRB. Scale bar: 1 μm.

(D) Ratio of vesicle fluorescence intensity (VI) versus cytoplasmic KIF5B fluorescence intensity (CI) in cells overexpressing GFP-KIF5B-MDC-FRB and FKBP-mCherry-Rab6, before (-) and after (+) addition of rapalog (average ± S.E.M.; before, *n*=24 vesicles in 3 cells; after, *n*=24 vesicles in 3 cells). *** $p<0.0001$, t-test.

(E) Percentage of vesicles moving and immobilized on microtubules in cells expressing mKate-α-tubulin and FKBP-GFP-Rab6 (control) or in cells co-transfected with KIF5B-T92N-MDC-FRB and treated with rapalog (KIF5B-T92N) (average ± S.E.M.; control, n=120 vesicles in 4 cells; KIF5B-T92N, n=151 in 4 cells). *** $p<0.0001$, unpaired t-test.

Schlager et al., Supplemental Figure 2

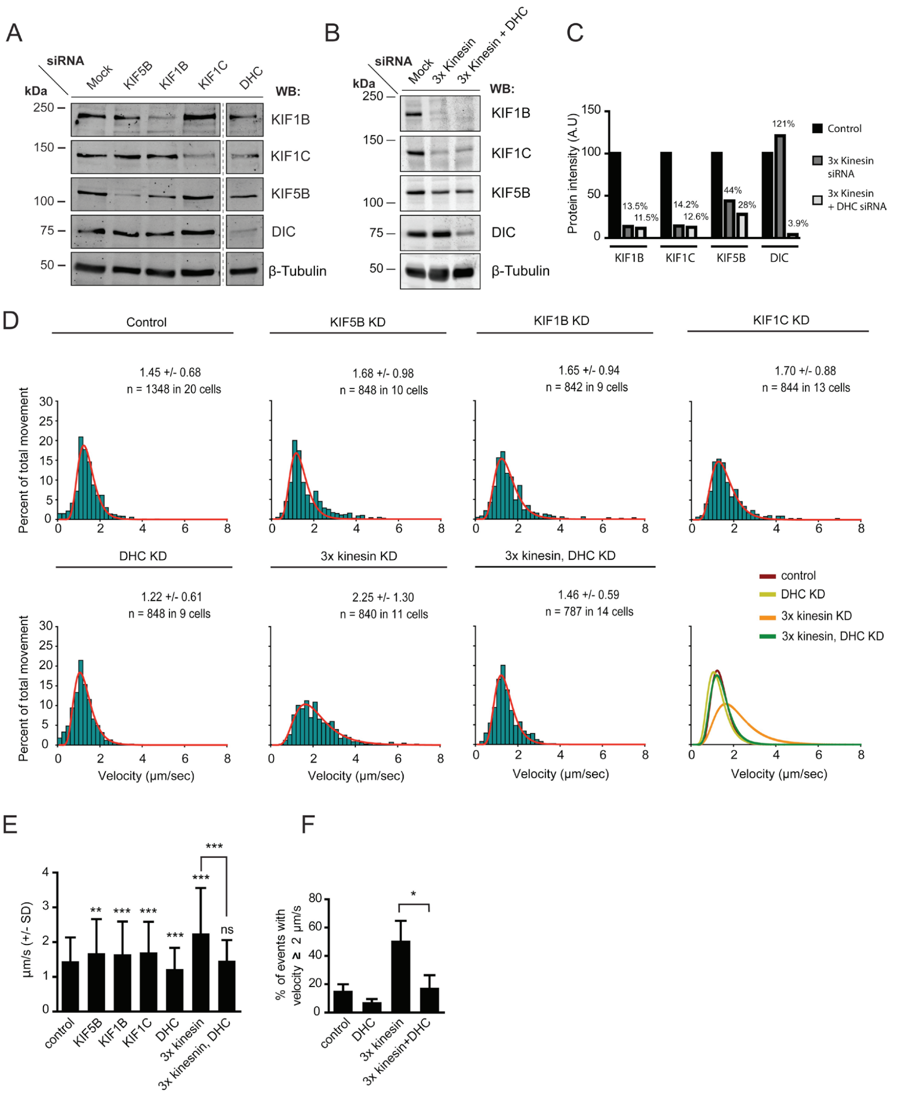

Figure S2, related to Figure 1. KIF5B, KIF1B and KIF1C cooperate to control Rab6-vesicles motility

(A) Western blots showing depletion of KIF5B (kinesin-1), KIF1B (kinesin-3), KIF1C (kinesin-3) and dynein intermediate chain (DIC) in HeLa cells three days after transfection with the indicated siRNAs. DHC, dynein heavy chain. β-tubulin serves as loading control. Note that DIC is co-depleted with DHC, as published previously (Levy and Holzbaur, 2008; Raaijmakers et al., 2013; Splinter et al., 2012)

(B) Western blots showing depletion of KIF5B (kinesin-1), KIF1B (kinesin-3), KIF1C (kinesin-3) and DIC in HeLa cells simultaneously transfected with siRNAs against KIF5B, 1B and 1C (3x kinesin KD) or KIF5B, 1B and 1C and DHC (3x kinesin + DHC KD) three days after siRNA transfection. β-tubulin serves as loading control.

(C) Quantification of protein levels present in the blots shown in B.

(D) Histograms of vesicle speeds in HeLa cells stably expressing GFP-Rab6A and transfected with the indicated siRNA. Values indicated correspond to mean ± S.D.

(E) Mean velocity of all conditions represented in (D). Values indicated correspond to the mean ± S.D. ** $p<0.001$, *** $p<0.0001$, Mann-Whitney U test.

(F) Percentage of events with high velocity (>2 μm/sec) of the indicated conditions represented in (D). Values indicated correspond to the percentages of high velocity tracks. * $p<0.0001$, unpaired t-test.

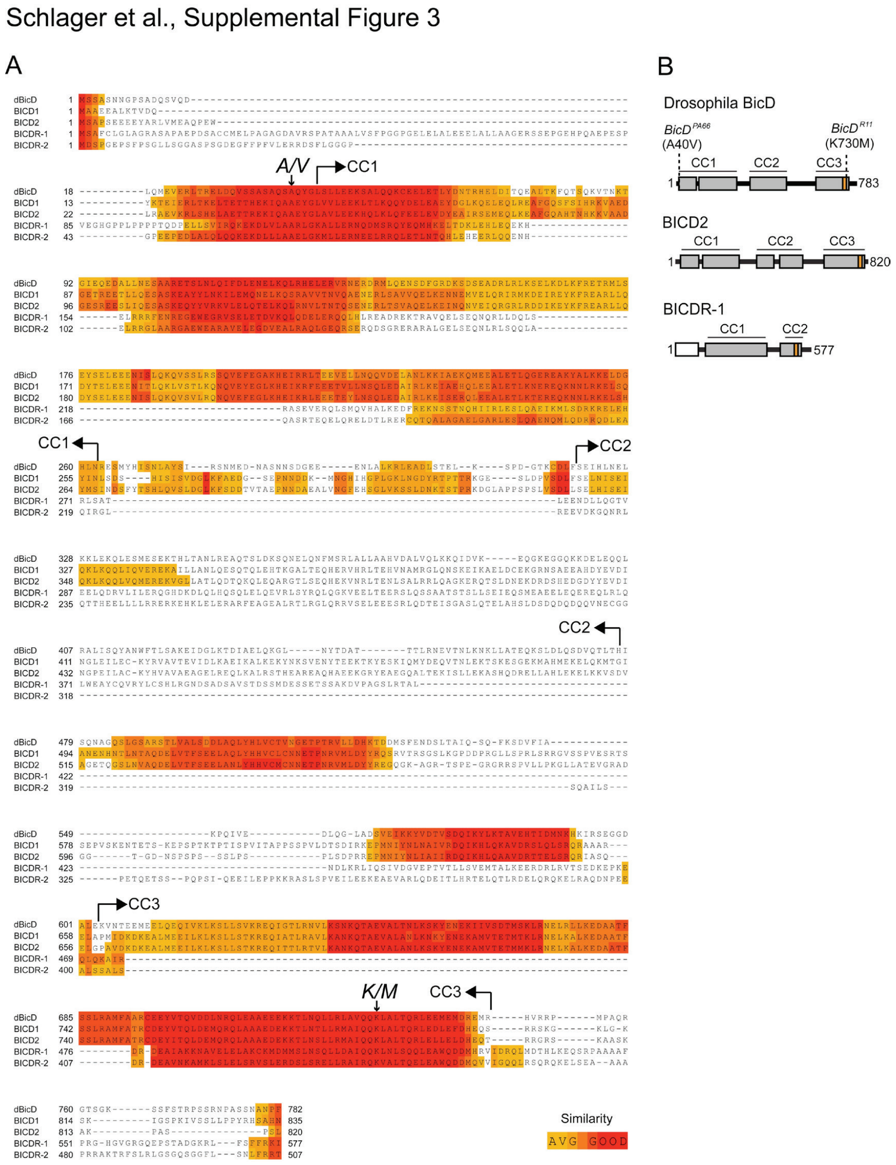
Schlager et al., Supplemental Figure 3
A
dBicD
BICD1
BICD2
BICDR-1
BICDR-2
A/V
CC1
CC1
CC2
CC2
CC3
K/M
CC3
Similarity
AVG
GOOD
B
Drosophila BicD
BicD^PA66
(A40V)
BicD^R11
(K730M)
CC1
CC2
CC3
1
783
BICD2
CC1
CC2
CC3
1
820
BICDR-1
CC1
CC2
1
577

Figure S3, related to Figure 2. Sequence alignment of BICD family proteins

(A) Sequence alignment of segments of the *Drosophila* BicD (dBicD, NP_724056.1), mouse BICD1 (NP_033883), BICD2 (NP_084067), BICDR-1 (NP_001074277) and BICDR-2 (NP_722479). Colors indicate the level of similarity. Vertical arrows indicate sites of mutations corresponding to the known *Drosophila* mutants: A/V indicates A40V (*BicD*^{PA66}) and K/M indicates K730M (*BicD*^{r11}).

(B) Schematic overview of *Drosophila* BicD (dBicD), mouse BICD2 and BICDR-1. Proteins were aligned according to their homology to the alanine at position 40 in dBicD. Grey blocks indicate coiled coils (CC1-CC3). The orange blocks indicate the conserved Rab6 interaction domain and the dashed lines indicate the amino acid positions corresponding to the mutations in *Drosophila* alleles *BicD*^{PA66} (A40V) and *BicD*^{R11} (K730M).

Schlager et al., Supplemental Figure 4

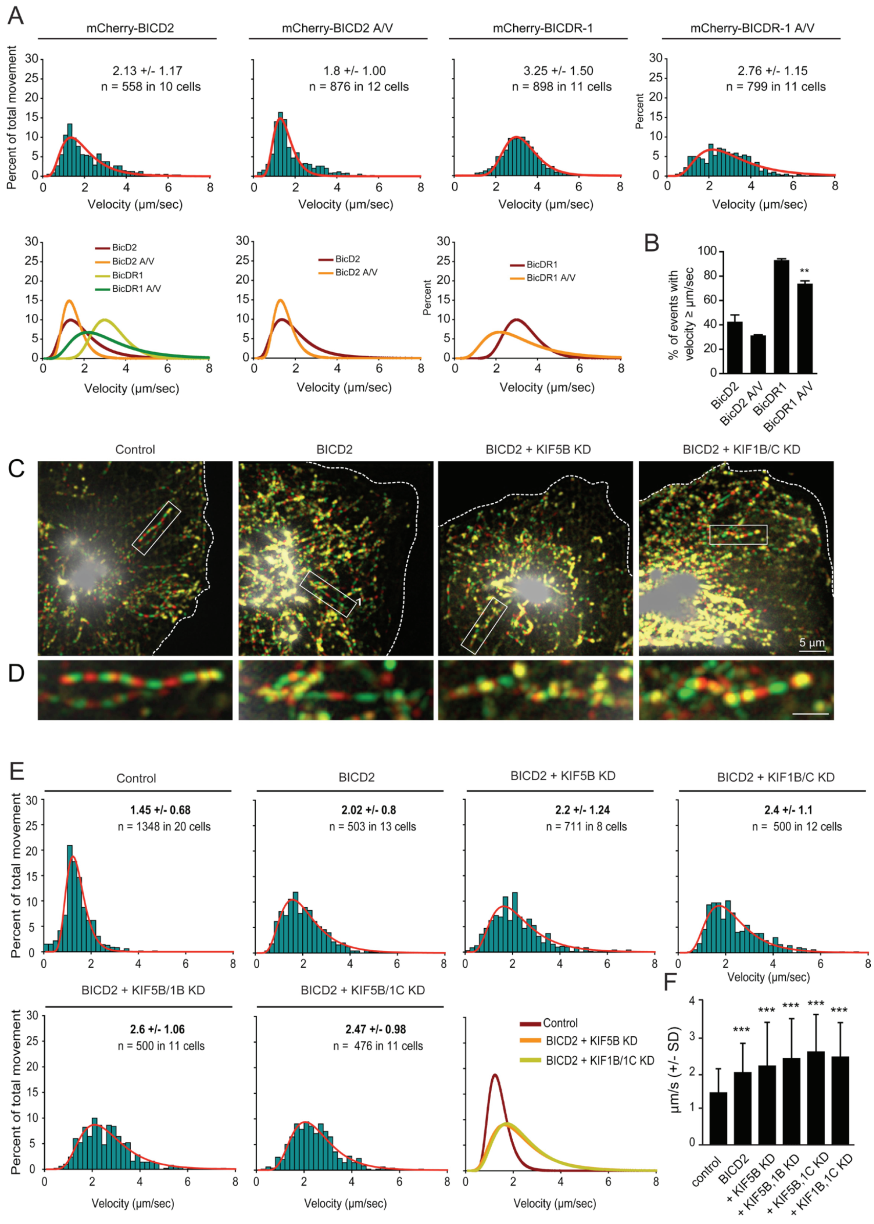

Figure S4, related to Figure 3. BICDR-1 A/V mutant reduces Rab6-vesicle motility and kinesin motors have no strong effect on Rab6 vesicle velocity in BICD2-overexpressing cells.

(A) Histograms of vesicle speeds in HeLa cells stably expressing GFP-Rab6A and transfected with mCherry-BICD2, mCherry-BICD2 A/V, mCherry-BICDR-1 or mCherry-BICDR-1 A/V. Values indicated correspond to the mean ± S.D.

(B) Percentage of events with high velocity (>2 μm/sec) of the conditions represented in (A). Values indicated correspond to the percentages of high velocity tracks. ** $p<0.0001$, unpaired t-test.

(C-D) HeLa cell stably expressing GFP-Rab6A were transfected either with HA-BicD2 or HA-BicD2 and the indicated siRNA(s). The maximum projections of 100 frames of the movies were colorized using the “Time-lapse Series Painter” plug-in for ImageJ. Enlargements of the boxed areas (D) are shown. Scale bar: 5 μm.

(E) Histograms of vesicle speeds in HeLa cells stably expressing GFP-Rab6A and transfected either with HA-BICD2 or HA-BICD2 and the indicated siRNA(s). Values indicated correspond to the mean ± S.D.

(F) Mean velocity of all conditions represented in (C). Values indicated correspond to the mean ± S.D. *** $p<0.0001$, Mann-Whitney U test.

EXPERIMENTAL PROCEDURES

Antibodies and reagents

The following primary and secondary antibodies were used in this study: mouse monoclonal antibodies against Rab6A/Rab6A' (Matanis et al., 2002); rabbit anti-GFP (Abcam), mouse anti-dynein IC74 (Chemicon), rabbit anti-dynein heavy chain (DHC), rabbit anti-HA, rabbit anti-KIF5B, mouse anti-Dynein IC1/2 and mouse anti-β-tubulin (Santa Cruz), mouse anti-HA (Covance), rabbit anti-KIF1Bβ (Bethyl), rabbit anti-KIF1C (Cytoskeleton). For immunofluorescence experiments we used Alexa488-, and Alexa568-conjugated secondary antibodies (Invitrogen). For Western blotting we used HRP-conjugated secondary antibodies (Dako) or IRDye 800CW goat anti-rabbit and anti-mouse antibodies, which were detected using Odyssey Infrared Imaging system (Li-Cor Biosciences).

Expression constructs, siRNAs and cell lines

HA-BICD2 (wildtype and A/V), HA-BICDR-1 (wild type and A/V), mCherry-BICD2, mCherry-BICDR-1 and GFP-Rab6 constructs for mammalian expression were prepared by a PCR-based strategy using the following cDNAs: BICD2 (Hoogenraad et al., 2001), BICDR-1 (Schlager et al., 2010) and Rab6A (Matanis et al., 2002). Subsequently PCR products were subcloned in pGW1-, pβactin- or pEGFP-expression vectors (Hoogenraad et al., 2005). FKBP-GFP-Rab6 and mCherry-α-tubulin (Splinter et al., 2012), GRASP-1 (Hoogenraad et al., 2010) and KIF1C-MDC-FRB and KIF5B-MDC-FRB (Kapitein et al., 2010) constructs were described previously. Plasmid enconding mKate-α-tubulin was obtained from Evrogen. The KIF5B-T92N-MDC-FBR construct was prepared by a PCR based strategy using the previously mentioned KIF5B-MDC-FRB. Plasmids encoding heterodimerisation domains FRB and FKBP2 and the rapamycin-derived heterodimeriser AP21967 (rapalog) were obtained from Ariad. The siRNAs used in this study were synthesized by Ambion and were directed against the following sequences: KIF5B GCCTTATGCATTTGATCGG (siRNA 118426); KIF1B was a pool of three siRNAs: GGGATATAATGTCTGTATT (siRNA 118461); CCAGTATTATTAACCCAAA (siRNA 118459); GGAAGCTCCAAAGTCCTTC (siRNA 118460); KIF1C, GGATAGCAAACAGGAAAAA (siRNA 18395); DHC 5'-CGTACTCCCGTGATTGATG (siRNA 118309). Rab6A- and Rab6B-shRNA constructs were described before (Schlager et al., 2010). The HeLa cell lines stably expressing GFP-DIC2 and GFP-DHC are a gift from Dr. Anthony Hyman (Poser et al., 2008).

Protein Sequence analysis

Protein sequences were aligned using the t-coffee program (Poirot et al., 2003) and the primary structure was analyzed using Prediction of coiled coil Regions in proteins (Coils; www.ch.embnet.org/software/COILS_form.html).

Immunoprecipitation

HeLa cells were cultured in DMEM/Ham's-F10 (50/50%) medium containing 10% FCS and 1% penicillin/streptomycin and were transfected using either Lipofectamine2000 (Invitrogen) according to the manufacturers guidelines or Polyethylenimine (PEI; Mw 25.000; Polysciences) at a 3:1 PEI:DNA ratio (w/w). Cells were harvested 24 hours after transfection, by scraping the cells in ice-cold PBS and lysing cell pellets in the lysis buffer (25 mM Tris-HCl, pH 8.0, 100 mM NaCl, 1.0% Triton X-100, and protease inhibitors; Roche). Supernatant and pellet fractions were separated by centrifugation at 13,200 rpm for 5 minutes. Supernatants were mixed with an equal amount of lysis buffer, protein-A-agarose beads (GE Healthcare), and 3 μg of mouse anti-GFP (Roche), mouse anti-HA (Covance) or mouse anti-IC74 (Millipore). Samples were incubated 4 hours while rotating at 4°C, centrifuged at 2000 rpm and pellets were washed 5-7 times with the wash buffer (25 mM Tris-HCl, pH 8.0, 100 mM NaCl, 0.1 % NP40). Samples were eluted in SDS sample buffer, equally loaded onto SDS-PAGE gels and subjected to Western blotting on polyvinylidene difluoride membrane. Blots were blocked with 2% bovine serum albumin/0.05% Tween 20 in PBS and incubated with primary antibodies at 4°C overnight. Blots were washed with 0.05% Tween 20 in PBS three times for 10 min at room temperature and incubated with either anti-rabbit or anti-mouse IgG antibody conjugated to horseradish peroxidase (Dako). Blots were developed with enhanced chemiluminescent Western blotting substrate (Pierce).

Transfection and immunofluorescence of cultured HeLa, Vero and MRC5 cells

HeLa, Vero and MRC5 cells were cultured in DMEM/Ham's F10 (50/50%) medium containing 10% FCS and 1% penicillin/streptomycin. One day before transfection, cells were plated at 1:20 in Lab-tek chamber slides (Nunc) or on glass coverslips. Cells were transfected with Superfect transfection reagent (Qiagen) or Fugene 6 (Roche) according to the manufacturers protocol and incubated overnight. Stable GFP-Rab6A HeLa clones were selected with fluorescence activated cell sorting (FACS) and cultured in the presence of 0.4 mg/ml G418 (Roche) (Grigoriev et al., 2007). Cells were transfected with 10 nM siRNAs with HiPerFect (Qiagen) and analyzed 3 days after transfection. Rapalog (AP21967; Ariad Pharmaceuticals) was dissolved to 1 mM in ethanol and added to the medium at a final concentration of 20 nM. Cells were either mounted for live imaging or fixed in 4% paraformaldehyde for 10 min at room temperature followed by 5 min in 0.1% Triton X-100 in PBS. Slides were blocked in 0.5% BSA/0.02% glycine in PBS and labeled with primary antibody either for 2 hours at room temperature or overnight at 4°C. Slides were washed three times with 0.05% Tween20 in PBS, labeled with secondary antibodies for 1 hour at room temperature, washed three times with 0.05% Tween20 in PBS and mounted using Vectashield mounting medium (Vector laboratories) (Hoogenraad et al., 2000).

Primary hippocampal neuron cultures and transfection

Primary hippocampal cultures were prepared from embryonic day 18 (E18) rat brains (Hoogenraad et al., 2005). Cells were plated on coverslips coated with poly-L-lysine (30 μg/ml) and laminin (2 μg/ml) at a density of 75,000/well. Hippocampal cultures were grown in Neurobasal medium (NB) supplemented with B27, 0.5 mM glutamine, 12.5 μM glutamate and penicillin/streptomycin. One day after plating, hippocampal neurons were transfected using Lipofectamine 2000 (Invitrogen). Briefly, DNA (3.6 μg /well) was mixed with 3 μl Lipofectamine 2000 in 200 μl NB, incubated for 30 minutes and then added to the neurons in NB at 37°C in 5% CO_2 for 45 min. Next, neurons were washed with NB and transferred in the original medium at 37°C in 5% CO_2 for 3 days.

Dissociated DRG neuron culture

DRG neurons were isolated from adult female Sprague Dawley rats (3 months old). The neurons were dissociated with collagenase type IV (Sigma) and 0.1% trypsin (Sigma). Dissociated neurons were plated on coverslips coated with poly-d-lysine (20 μg/ml), 1 μg/ml laminin and cultured in dissociated DRG culture medium (DMEM

(Lonza), 1% FBS (Invitrogen), penicillin-streptomycin-fungizone (1×) (Sigma), and NGF (20 ng/mL) (Sigma), and kept at 37°C in 5% CO2. Dissociated adult DRG neurons were transfected using a Microporator (Invitrogen), which electroporates within a micropipette tip. Approximately 100.000 cells were transfected per reaction in a volume of 10 µl. Transfected cells were plated and cultured as described above, but without antibiotics for the first 24 hours after electroporation.

Image acquisition and time-lapse live cell imaging

Images of fixed cells were collected with a Leica DMRBE microscope equipped with PLFluotar 40x 1.0 N.A., HCX PL Apo. 63x 1.3 N.A. and PLFluotar 100x 1.3 N.A. oil objectives, FITC/EGFP filter 41012 (Chroma), Texas Red filter 41004 (Chroma), DAPI filter 31000 (Chroma) and an ORCA-ER- 1394 CCD camera (Hamamatsu). Images were projected onto the 12-bit CCD chip at a magnification of 0.1 µm/pixel. Alternatively, we used a Nikon Eclipse 80i microscope equipped with a Plan Fluor 10x N.A. 0.30 objective, Chroma ET-GFP (49002) filter and a Photometrics CoolSNAP HQ2 CCD camera. Live cell imaging was performed on an inverted research microscope Nikon Eclipse Ti-E (Nikon) with perfect focus system (PFS) (Nikon), equipped with Nikon CFI Apo TIRF 100x 1.49 N.A. oil objective (Nikon), Photometrics Evolve 512 EMCCD (Roper Scientific) and controlled with MetaMorph 7.7.5 software (Molecular Devices). The 16-bit images were projected onto the CCD chip with intermediate lens 2.5X (Nikon C mount adapter 2.5X) at a magnification of 0.063 µm/pixel. To keep cells at 37°C we used stage top incubator (model INUBG2E-ZILCS Tokai Hit). The microscope was equipped with TIRF-E motorized TIRF illuminator modified by Roper Scientific France/PICT-IBiSA, Institut Curie. For regular imaging we used mercury lamp HBO-103W/2 (Osram) for excitation or 491nm 100mW Calypso (Cobolt) and 561nm 100mW Jive (Cobolt) lasers. We used ET-GFP filter set (Chroma) for imaging of proteins tagged with GFP; ET-mCherry filter set (Chroma) for imaging of proteins tagged with mCherry. For simultaneous imaging of green and red fluorescence we used triple-band TIRF polychroic ZT405/488/561rpc (Chroma) and triple-band laser emission filter ZET405/488/561m (Chroma), mounted in the metal cube (Chroma, 91032) together with Optosplit III beamsplitter (Cairn Research Ltd, UK) equipped with double emission filter cube configured with ET525/50m, ET630/75m and T585LPXR (Chroma).

Image Analysis and Quantification

Analysis of pericentrosomal versus cytoplasmic Rab6. Ratios of pericentrosomal versus cytoplasmic intensities were determined by measuring the mean gray value of a 34 μm^2 area around the centrosome and an area of equal size in the cytoplasm using ImageJ (http://rsb.info.nih.gov/ij/index.html). The location of the centrosome was determined using the BICD signal. Centrosomal Rab6 intensities were measured in cells where the centrosome was clearly separated from the Golgi apparatus. Ratios were averaged over multiple cells and experiments and a statistical analysis was performed using a Mann Whitney test. .

Analysis of BICDR-1 intensity at the centrosome. The intensity of HA-BICDR-1 and HA-BICDR-1 A/V proteins at the centrosome was determined by measuring the mean gray value around the centrosome using ImageJ (http://rsb.info.nih.gov/ij/index.html). Intensities were normalized by the area and averaged over multiple cells and experiments and a statistical analysis was performed with Student's t test assuming a two-tailed and unequal variation.

Analysis of KIF5B fluorescence intensity on Rab6 vesicles. Ratios of vesicle versus cytoplasmic KIF5B intensities were determined by measuring the mean gray value of an area around the centrosome and an area of equal size in the cytoplasm next to the vesicle using ImageJ (http://rsb.info.nih.gov/ij/index.html). The vesicle position was determined using the Rab6 signal. Ratios were averaged over multiple vesicles and cells and a statistical analysis was performed with Student's t test assuming a two-tailed and unequal variation.

Analysis of Rab6 vesicle velocities. Images of live cells were prepared in MetaMorph software (Molecular Devices) and Adobe Photoshop. Linear adjustment of "Levels" and Unsharp Mask and Gaussian Blur filtering were applied to some images using Adobe Photoshop. Analysis of velocities was performed by computing the mean value for each cell and then averaging the values for cells within a certain category (such as treatment with a particular siRNA); n for each measurement corresponds to the number of velocity events counted in the indicated number of cells over 2-3 independent experiments. The total number of velocity events with velocity higher than 2 µm/sec per cell was calculated and the percentages extracted. The variance is calculated by the average of the squared differences from the mean (SD^2). To evaluate the statistical significance of the observed differences we used the two-tailed Mann-Whitney U test (GraphPad Prism 5 for Windows), a nonparametric alternative to the t-test for independent samples, because many of the measured parameters did not show normal distribution. The test was used to evaluate the hypothesis that the given parameter measured in cells treated with a certain siRNA and/or overexpression construct is the same as in control cells. The results of statistical analysis are indicated in the legend to each figure.

Analysis of Rab6 vesicle velocities in axons. Movies of axons labeled with Rab6-TagRFP or GFP-Rab6 and acquired on the spinning disk confocal microscope were imported into ImageJ software. Maximum intensity projections of those movies contained easily visible tracks corresponding to movement episodes marked by Rab6-TagRFP or GFP-Rab6. Kymographs were built along those curves. On the kymographs single movement episodes were distinguished as bright tilted straight lines. The length and the duration of each growth episode were measured as horizontal and vertical projections of those lines, respectively. The movement velocity was calculated as a ratio of those values.

Analysis of axonal outgrowth. Axon lengths were measured using a fluorescent fill (GFP or mRFP) that highlights neuronal morphology. Images of dissociated DRG and hippocampal neurons were analyzed with ImageJ software. The drawing tool was used to trace and measure the length of the longest neurite per DRG from the axon hillock to the growth cone. The NeuronJ plugin was used to trace and measure the length of the primary axon of hippocampal neurons, from the soma to the tip together with all its branches.

REFERENCES

Grigoriev, I., Splinter, D., Keijzer, N., Wulf, P.S., Demmers, J., Ohtsuka, T., Modesti, M., Maly, I.V., Grosveld, F., Hoogenraad, C.C., *et al.* (2007). Rab6 regulates transport and targeting of exocytotic carriers. Dev Cell *13*, 305-314.

Hoogenraad, C.C., Akhmanova, A., Grosveld, F., De Zeeuw, C.I., and Galjart, N. (2000). Functional analysis of CLIP-115 and its binding to microtubules. J Cell Sci *113 (Pt 12)*, 2285-2297.

Hoogenraad, C.C., Akhmanova, A., Howell, S.A., Dortland, B.R., De Zeeuw, C.I., Willemsen, R., Visser, P., Grosveld, F., and Galjart, N. (2001). Mammalian Golgi-associated Bicaudal-D2 functions in the dynein-dynactin pathway by interacting with these complexes. EMBO J *20*, 4041-4054.

Hoogenraad, C.C., Milstein, A.D., Ethell, I.M., Henkemeyer, M., and Sheng, M. (2005). GRIP1 controls dendrite morphogenesis by regulating EphB receptor trafficking. Nat Neurosci *8*, 906-915.

Hoogenraad, C.C., Popa, I., Futai, K., Martinez-Sanchez, E., Wulf, P.S., van Vlijmen, T., Dortland, B.R., Oorschot, V., Govers, R., Monti, M., *et al.* (2010). Neuron specific Rab4 effector GRASP-1 coordinates membrane specialization and maturation of recycling endosomes. PLoS Biol *8*, e1000283.

Kapitein, L.C., Schlager, M.A., van der Zwan, W.A., Wulf, P.S., Keijzer, N., and Hoogenraad, C.C. (2010). Probing intracellular motor protein activity using an inducible cargo trafficking assay. Biophys J *99*, 2143-2152.

Levy, J.R., Holzbaur E.L. (2008). Dynein drives nuclear rotation during forward progression of motile fibroblasts. J Cell Sci 121(Pt 19), 3187-95.

Matanis, T., Akhmanova, A., Wulf, P., Del Nery, E., Weide, T., Stepanova, T., Galjart, N., Grosveld, F., Goud, B., De Zeeuw, C.I., *et al.* (2002). Bicaudal-D regulates COPI-independent Golgi-ER transport by recruiting the dynein-dynactin motor complex. Nat Cell Biol *4*, 986-992.

Poirot, O., O'Toole, E., and Notredame, C. (2003). Tcoffee@igs: A web server for computing, evaluating and combining multiple sequence alignments. Nucleic Acids Res *31*, 3503-3506.

Poser, I., Sarov, M., Hutchins, J.R., Heriche, J.K., Toyoda, Y., Pozniakovsky, A., Weigl, D., Nitzsche, A., Hegemann, B., Bird, A.W., *et al.* (2008). BAC TransgeneOmics: a high-throughput method for exploration of protein function in mammals. Nat Methods *5*, 409-415.

Raaijmakers, J.A., Tanenbaum, M.E., and Medema, R.H. (2013). Systematic dissection of dynein regulators in mitosis. J Cell Biol *201*, 201-215.

Schlager, M.A., Kapitein, L.C., Grigoriev, I., Burzynski, G.M., Wulf, P.S., Keijzer, N., de Graaff, E., Fukuda, M., Shepherd, I.T., Akhmanova, A., *et al.* (2010). Pericentrosomal targeting of Rab6 secretory vesicles by Bicaudal-D-related protein 1 (BICDR-1) regulates neuritogenesis. EMBO J *29*, 1637-1651.

Splinter, D., Razafsky, D.S., Schlager, M.A., Serra-Marques, A., Grigoriev, I., Demmers, J., Keijzer, N., Jiang, K., Poser, I., Hyman, A.A., *et al.* (2012). BICD2, dynactin, and LIS1 cooperate in regulating dynein recruitment to cellular structures. Mol Biol Cell *23*, 4226-4241.

4

The kinesin-3 family member KIF13B promotes transport of exocytotic carriers

Andrea Serra-Marques[1], Qingyang Liu[1,2], Eugene Katrukha[1], Ilya Grigoriev[1], A. F. Maarten Altelaar[2], Albert J. R. Heck[2], Lukas C. Kapitein[1], Lotte B. Pedersen[3], and Anna Akhmanova[1]

[1] Cell Biology, Faculty of Science, Utrecht University, Utrecht, The Netherlands.
[2] Biomolecular Mass Spectrometry and Proteomics, Bijvoet Center for Biomolecular Research, Utrecht Institute for Pharmaceutical Sciences and The Netherlands Proteomics Centre, Utrecht University, Utrecht, The Netherlands.
[3] Department of Biology, Section of Cell and Developmental Biology, University of Copenhagen, Copenhagen, Denmark.

Abstract

Constitutive secretion is mediated by vesicles, which bud off the trans-Golgi, move to the cell periphery and fuse with the plasma membrane. These vesicles are abundantly labeled with the small GTPase Rab6. Recent work has identified CARTS (carriers of the TGN to the cell surface) as a specific type of exocytotic vesicles containing the secreted cargo pancreatic adenocarcinoma up-regulated factor (PAUF), and we confirmed that PAUF indeed represents one of the cargos of Rab6 vesicles. The transport of Rab6 vesicles depends on several kinesins, including kinesin-1 KIF5B and kinesin-3 family members KIF1C and KIF1B, but the depletion of these three motors does not arrest the motility of Rab6 vesicles, suggesting that additional kinesins might be involved. Here, we show that kinesin-3 KIF13B, previously implicated in the transport of endosomes, also contributes to Rab6 vesicle transport. KIF13B prominently accumulates on Rab6/PAUF-positive vesicles, and the depletion of this motor results in a reduced number of Rab6 vesicle movements towards the plasma membrane. KIF13B recruitment to Rab6 vesicles cannot be explained by an interaction of the motor with the two Rabs present on the vesicles, Rab6 and Rab8, because it does not bind to these Rabs. To find potential links between KIF13B and secretory carriers, we have used mass spectrometry to identify KIF13B binding partners. We have depleted the most prominent of these partners, including hDlg1, utrophin, KIDINS220 and angiomotin and found that none of them was essential to localize the kinesin to Rab6 vesicles, indicating that additional work will be necessary to determine the mechanism of KIF13B recruitment to secretory carriers. We have also examined in detail the localization of KIF13B on the individual carriers and found that during directional vesicle runs, KIF13B was located at the front of the vesicle. The ability to visualize motors present on the moving cargo with high resolution opens interesting possibilities for investigating the mechanisms underlying multimotor cargo transport.

Introduction

The secretory pathway is of fundamental importance for the homeostasis of the cell, and its correct functioning depends on the fine communication between different organelles. Rab GTPases are known identity markers of membrane compartments (Chavrier et al., 1990; Grosshans et al., 2006; Hutagalung and Novick, 2011). The small GTPase Rab6 is known to decorate the Golgi apparatus and participate in the transport between the Golgi, ER, plasma membrane and endosomes (Girod et al., 1999; Martinez et al., 1997; Martinez et al., 1994; Utskarpen et al., 2006; White et al., 1999). Rab6 is also present on cytoplasmic vesicles that move along microtubules (Grigoriev et al., 2007; Jasmin et al., 1992; White et al., 1999; Young et al., 2005). These vesicles predominantly correspond to exocytotic carriers capable of fusing with the plasma membrane (Grigoriev et al., 2007; Grigoriev et al., 2011).

Cytoplasmic Rab6 vesicles move along microtubules in both the plus and minus-end direction. Rab6 directly binds to the adaptor proteins BICD1/2 and BICDR-1, which recruit the dynein complex, responsible for the transport of vesicles to the minus end of microtubules (Grigoriev et al., 2007; Matanis et al., 2002; Schlager et al., 2010). In addition, Rab6 can also interact with dynein and dynactin subunits directly (Bergbrede et al., 2009; Short et al., 2002; Wanschers et al., 2008), and might play a role in the activation of the dynein motor by dissociating dynein from its co-factor Lis1 (Yamada et al., 2013).

The regulation of plus-end directed transport of Rab6 vesicles is also complex. Kinesin-1 family member KIF5B promotes the transport of Rab6 vesicles (Grigoriev et al., 2007). It is currently unknown how KIF5B binds to Rab6 vesicles, but an interaction with BICD2 might contribute to KIF5B recruitment or control of its activity (Grigoriev et al., 2007). The BICD2-related adaptor BICDR-1 binds to the kinesin-3 family motor KIF1C, which also contributes to Rab6 vesicle motility (Schlager et al., 2010). However, simultaneous siRNA-mediated depletion of KIF5B, KIF1C and its close homologue KIF1B was not sufficient to completely block the microtubule plus-end directed motility of Rab6 vesicles in HeLa cells (Grigoriev et al., 2007; Schlager et al., 2014). These observations suggest the involvement of additional kinesins in the transport of Rab6-positive carriers.

Wakana and colleagues have recently described a new class of Golgi derived carriers called CARTS (Carriers of the TGN to the cell surface), which co-localize with Rab6 and Rab8 and contain a protein cargo called PAUF (pancreatic adenocarcinoma up-regulated factor) (Wakana et al., 2012). These vesicular carriers move along microtubules, and it was proposed that the molecular motor Eg5/KIF11, a kinesin-5 family member well known for its role in the assembly of the mitotic spindle during cell division (see (Ferenz et al., 2010) for review), is required for the transport of CARTS from the Golgi to the cell surface (Wakana et al., 2013).

Other members of the kinesin-1 family (KIF5A, KIF5C), kinesin-3 (KIF13A, KIF13B) and kinesin-14 (KIFC3) have also been implicated in the transport of Golgi-derived carriers to the cell surface in non-polarized cells or to the apical surface in polarized cells (Astanina and Jacob, 2010; Burgo et al., 2012; Jaulin et al., 2007; Nakagawa et al., 2000; Yamada et al., 2014).

In this study, we sought to understand which other kinesin motors contribute to the transport of Rab6 secretory vesicles. We focused on the members of the kinesin-3 family, and found that KIF13B is present on Rab6 vesicles. KIF13B has been reported to have functions in axonal and dendritic transport in neurons, endocytosis, mitotic spindle orientation and anterograde transport during angiogenesis (Horiguchi et al., 2006; Jenkins et al., 2012; Kanai et al., 2014; Lu and Prehoda, 2013; Yamada et al., 2014). Is has been shown that KIF13B and its *Drosophila* counterpart Kinesin-73, are super-processive kinesins *in vitro* and drive long distance cargo transport in cells (Huckaba et al., 2011; Soppina et al., 2014). We show that KIF13B promotes transport of Rab6 and PAUF-positive vesicles along MTs from the vicinity of the Golgi apparatus to the plasma membrane and explore possible molecular mechanisms of KIF13B targeting to Rab6 vesicles. We exploit the fact that fluorescently tagged KIF13B can be clearly detected on the vesicles to investigate the motor distribution on the individual carriers. Our data provide some general insights in the functioning of multimotor systems responsible for transport of cellular cargo.

Results and discussion

Rab6 vesicles and CARTS are the same Golgi-derived carriers

To understand if CARTS are the same Golgi carriers as the Rab6A-positive exocytotic vesicles, the transport of which we have described in our previous studies (Grigoriev et al., 2007; Schlager et al., 2014), we analyzed the colocalization between PAUF-mRFP and endogenous Rab6 (which in non-neuronal cells is represented by the Rab6A and Rab6A' isoforms that will be collectively called Rab6) (Fig. 1A, B). We found that approximately 80% of PAUF vesicles were positive for Rab6 staining, in agreement with the published data (Wakana et al., 2012). Colocalization between PAUF-mRFP and GFP-Rab6A was also observed in live cells, where the movement of PAUF/Rab6A-positive vesicles could be readily detected (Fig. 1C, D). However, only a sub-population of Rab6-positive vesicles contained PAUF (~ 60% and 50% in fixed and live cells, respectively) (Fig. 1E). This suggests that Rab6 vesicles may serve alternative exocytotic routes, with PAUF utilizing one of these routes. In line with this view, less than 20% of PAUF vesicles contained the classic secretion marker, the temperature-sensitive VSV-G in secretion assays (Wakana

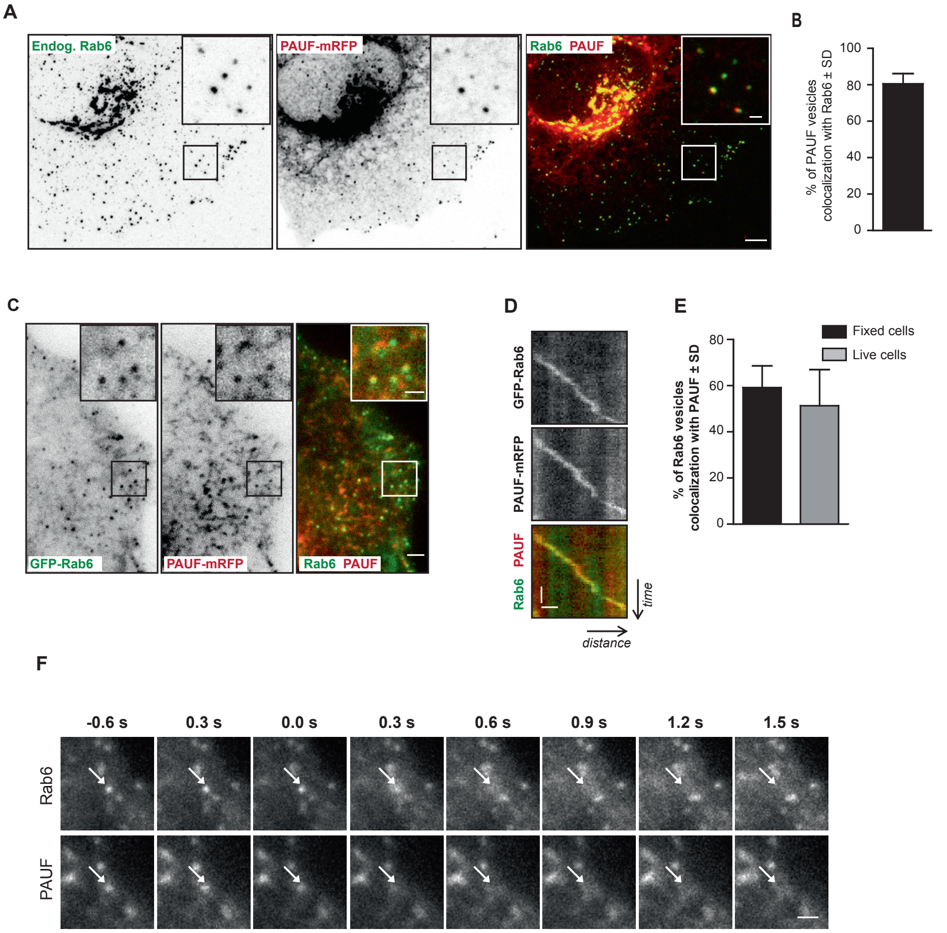
A
Endog. Rab6
PAUF-mRFP
Rab6 PAUF
B
% of PAUF vesicles colocalization with Rab6 ± SD
100
80
60
40
20
0
C
GFP-Rab6
PAUF-mRFP
Rab6 PAUF
D
GFP-Rab6
PAUF-mRFP
PAUF
Rab6
time
distance
E
% of Rab6 vesicles colocalization with PAUF ± SD
80
60
40
20
0
Fixed cells
Live cells
F
-0.6 s
0.3 s
0.0 s
0.3 s
0.6 s
0.9 s
1.2 s
1.5 s
Rab6
PAUF

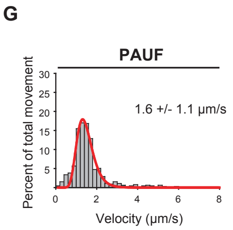

Figure 1. PAUF is a cargo of Rab6 secretory vesicles.
(A) Image of a HeLa cell expressing PAUF-mRFP and stained for endogenous Rab6. Scale bar: 5 μm. The insets correspond to magnified views of the boxed areas (scale bar: 1 μm).
(B) Quantification of the percentage of PAUF-mRFP positive vesicles colocalizing with endogenous Rab6 in HeLa cells. n= 10 cells
(C) A single frame of a movie of a HeLa cell transfected with GFP-Rab6A and PAUF-mRFP. Scale bar: 5 μm. The insets correspond to magnified views of the boxed areas (scale bar: 1 μm).
(D) Kymographs illustrating the movement of a vesicle labeled with GFP-Rab6A and PAUF-mRFP. Scale bars: horizontal, 1 μm, vertical, 1 s.
(E) Quantification of the percentage of GFP-Rab6A (live cells) or endogenous Rab6 (fixed) vesicles colocalizing with PAUF-mRFP in HeLa cells. Fixed cells, n= 11; Live cells, n= 6
(F) Live TIRFM images showing the behavior of GFP-Rab6A and PAUF-mRFP-labeled vesicles before and during fusion with the plasma membrane. 0 s corresponds to the sharp increase of fluorescent signal associated with the vesicle fusion. Scale bar: 1 μm.
(G) Distribution of PAUF-mRFP vesicle velocities in HeLa cells, measured manually using kymographs. n= 654, 20 cells. Error bars indicate SD.

et al., 2012), while a high degree of colocalization of VSV-G and Rab6 has been observed (Grigoriev et al., 2007). Another possibility is that we are underestimating colocalization, due to the relatively poor contrast of the PAUF-mRFP signal caused by its significant accumulation in the endoplasmic reticulum.

Next, we have analyzed the fusion of the PAUF/Rab6A vesicles with the plasma membrane by dual color total internal reflection fluorescence microscopy (TIRFM) (Fig. 1F). We could observe simultaneous fusion of GFP-Rab6A and PAUF-mRFP with the plasma membrane, confirming that PAUF is indeed an exocytotic cargo of Rab6 vesicles. Interestingly, the PAUF-mRFP signal disappeared before the GFP-Rab6A signal, suggesting that PAUF is secreted into the medium upon fusion of the vesicle with the plasma membrane, in agreement with a previous study, which could detect secreted PAUF in cell culture medium (Wakana et al., 2012). These data also fit with our previous observations for other secreted exocytotic markers, like NPY and BDNF (Grigoriev et al., 2007). We observed that PAUF vesicles moved with a speed of ~ 1.6 μm/sec, in the range of what we have observed for Rab6 (Schlager et al., 2014) (Fig. 1G). Taken together, our results show CARTS are Rab6-positive secretory vesicles, which transport PAUF to the plasma membrane.

The kinesin-3 family member KIF13B associates with Rab6-positive secretory carriers

We have previously shown that the kinesin-3 family members KIF1B and KIF1C are involved in the transport of Rab6 vesicles but that additional kinesins might be involved (Schlager et al., 2014). We hypothesized that other kinesin-3's could also be required for Rab6 vesicle transport. In mammals, kinesin-3 family includes KIF1A (which is a neuronal molecule), KIF1B, KIF1C, KIF13A, KIF13B, KIF14, KIF16A and KIF16B (Hirokawa et al., 2009). Here, we have focused of KIF13 and KIF14 motors. We found that KIF13A displayed little binding to Rab6 vesicles (Fig. 2A, B), in line with the previous work, which showed that KIF13A specifically binds to recycling endosomes by associating with the Rab11 family members Rab11A, Rab11B and Rab25 (Delevoye et al., 2014). KIF14, another member of the kinesin-3 family, which until now has mainly been studied for its function in cytokinesis (Carleton et al., 2006; Gruneberg et al., 2006), could not be detected on GFP-Rab6A vesicles at all (Fig. 2C). In contrast, KIF13B was abundantly present on Rab6A-positive vesicles in live cells, as confirmed by kymograph analysis (Fig. 2D, E). This co-localization required the tail but not the motor of KIF13B (Fig. 2E, and see below). In addition, GFP-KIF13B was present in numerous punctate cytoplasmic structures, which did not contain Rab6; some of these structures co-localized with the markers of early and recycling endosomes, GFP-Rab5A and Rab11A (Fig. 2F).

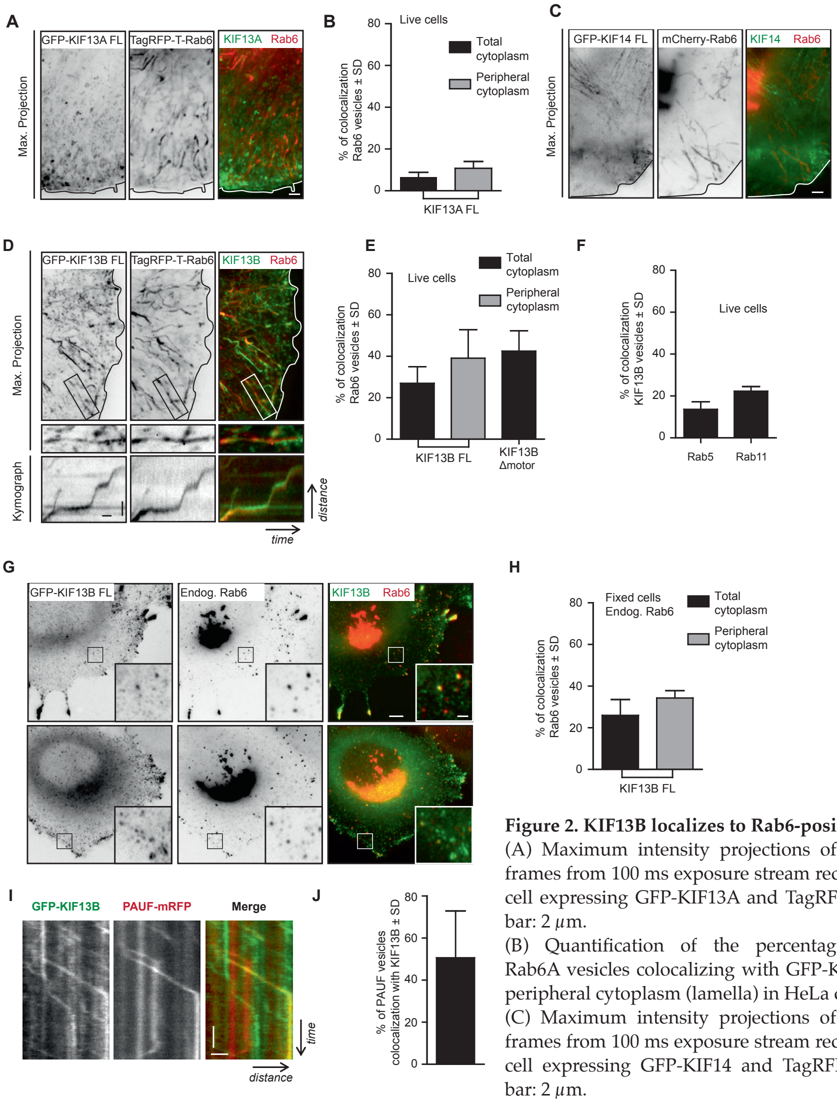
A
GFP-KIF13A FL
TagRFP-T-Rab6
KIF13A Rab6
Max. Projection
B
Live cells
Total cytoplasm
Peripheral cytoplasm
% of colocalization Rab6 vesicles ± SD
0
20
40
60
80
KIF13A FL
C
GFP-KIF14 FL
mCherry-Rab6
KIF14 Rab6
Max. Projection
D
GFP-KIF13B FL
TagRFP-T-Rab6
KIF13B Rab6
Max. Projection
Kymograph
distance
time
E
Live cells
Total cytoplasm
Peripheral cytoplasm
% of colocalization Rab6 vesicles ± SD
KIF13B FL
KIF13B Δmotor
F
Live cells
% of colocalization KIF13B vesicles ± SD
Rab5
Rab11
G
GFP-KIF13B FL
Endog. Rab6
KIF13B Rab6
H
Fixed cells Endog. Rab6
Total cytoplasm
Peripheral cytoplasm
% of colocalization Rab6 vesicles ± SD
KIF13B FL
I
GFP-KIF13B
PAUF-mRFP
Merge
time
distance
J
% of PAUF vesicles colocalization with KIF13B ± SD

Figure 2. KIF13B localizes to Rab6-positive vesicles.

(A) Maximum intensity projections of 250 consecutive frames from 100 ms exposure stream recording of a HeLa cell expressing GFP-KIF13A and TagRFP-T-Rab6A. Scale bar: 2 μm.

(B) Quantification of the percentage of TagRFP-T-Rab6A vesicles colocalizing with GFP-KIF13A in total or peripheral cytoplasm (lamella) in HeLa cells. n= 5 cells.

(C) Maximum intensity projections of 100 consecutive frames from 100 ms exposure stream recording of a HeLa cell expressing GFP-KIF14 and TagRFP-T-Rab6A. Scale bar: 2 μm.

(D) Maximum intensity projections of 300 consecutive frames from 100 ms exposure stream recording of a HeLa cells expressing GFP-KIF13B and TagRFP-T-Rab6A. Scale bar: 2 μm. The boxed areas are magnified. Kymographs below illustrate the movement of vesicles labeled with GFP-KIF13B and TagRFP-T-Rab6 (scale bars: horizontal, 1 s, vertical, 1 μm).

(E) Quantification of the percentage of TagRFP-T-Rab6A vesicles colocalizing with the indicated GFP tagged kinesin constructs in the total or peripheral cytoplasm in HeLa cells. n=6 in all conditions.

(F) Quantification of the percentage of GFP-Rab5A or GFP-Rab11A vesicles colocalizing with mCherry-KIF13B. n=8 (colocalization with Rab5) or n=7 (colocalization with Rab11).

(G) Image of a HeLa cell expressing GFP-KIF13B and stained for the endogenous Rab6. Scale bar: 5 μm. The insets correspond to magnified views of the boxed areas (scale bar: 1 μm).

(H) Quantification of the percentage of endogenous Rab6 vesicles colocalizing with GFP-KIF13B in the total or peripheral cytoplasm in HeLa cells. n=6 cells.

(I) Kymographs illustrating the movement of vesicles labelled with GFP-KIF13B and PAUF-mRFP. Scale bars: horizontal, 1 μm, vertical, 2 s.

(J) Quantification of the percentage of PAUF-mRFP vesicles colocalizing with GFP-KIF13B. n= 10 cells.

Error bars indicate SD.

The co-localization between GFP-KIF13B and Rab6 was confirmed in fixed cells: ~30% of endogenous Rab6 vesicles showed co-localization with GFP-KIF13B (Fig. 2G,H). Also the Rab6 vesicle cargo, PAUF, co-localized with KIF13B, as ~ 50% of PAUF-mRFP-positive vesicles were labeled with GFP-KIF13B, and kymograph analysis of PAUF / Rab6-positive vesicles clearly showed that they move together (Fig. 2I,J). These results suggest that KIF13B is involved in the transport of secretory vesicles containing both PAUF and Rab6. By performing fluorescence recovery after photobleaching (FRAP) experiments, we could observe that GFP-KIF13B does not exchange on exocytotic vesicles (Fig. 3A, B), similar to what we have previously observed for Rab6 and Rab8 (Grigoriev et al., 2007; Grigoriev et al., 2011). Analysis of vesicle fusion with the plasma membrane by TIRFM revealed that KIF13B persists on the vesicles until the actual fusion event takes place and then spreads out over the plasma membrane together with the Rab6A signal (Fig.3C). We conclude that motor detachment from the vesicles is not required to allow their fusion with the plasma membrane.

Characterization of the interaction of KIF13B with Rab6 vesicles

To understand how KIF13B is recruited to Rab6 vesicles, we tested which region of KIF13B is responsible for the binding to Rab6 vesicles. KIF13B contains an N-terminal motor domain, a forkhead-associated (FHA) domain that binds to centaurin-α1 (Venkateswarlu et al., 2005), a MAGUK binding stalk (MBS) responsible for the interaction with membrane-associated guanylate kinase (MAGUK) human Disks large homolog 1(hDlg1) (Hanada et al., 2000), a C-terminal cytoskeleton-associated protein-glycine-rich (CAP-Gly) domain and several coiled coils, the functions of which are still unclear. We generated a series of KIF13B deletion mutants and tested their ability to bind to Rab6 vesicles in live cells. As shown in Fig. 4A-B, the MBS and a C-terminal region containing a coiled coil and two predicted domains of unknown function (DUF3694) were required for the binding to Rab6 vesicles. Deletion of the motor or the CAP-Gly domain did not affect the recruitment of the kinesin to Rab6-positive vesicles (Fig. 4A,B).

We have next attempted to find out how KIF13B binds to Rab6 vesicles. KIF13A was shown to bind to two endocytic Rabs, Rab11 and Rab25 (Delevoye et al., 2014), and we therefore set out to test if KIF13B is also subject to Rab-mediated membrane recruitment. However, using pull down assays with proteins overexpressed in HEK293T cells, we were not able to show a direct interaction between Rab6A and KIF13B (Fig.5A).

We have also tested the potential interaction between KIF13B and Rab8A, because our previous study has shown that Rab8 is present on Rab6 secretory vesicles and is required for their docking and fusion with the plasma membrane (Grigoriev et al., 2011). We found no interaction between Rab8A and KIF13B in pull down assays (Fig. 5B). In line with these data, the depletion of Rab8A did not affect the recruitment of KIF13B to Rab6 vesicles (Fig. 5C). We conclude that KIF13B does not seem to be recruited to secretory vesicles by the two Rabs present on these vesicles.

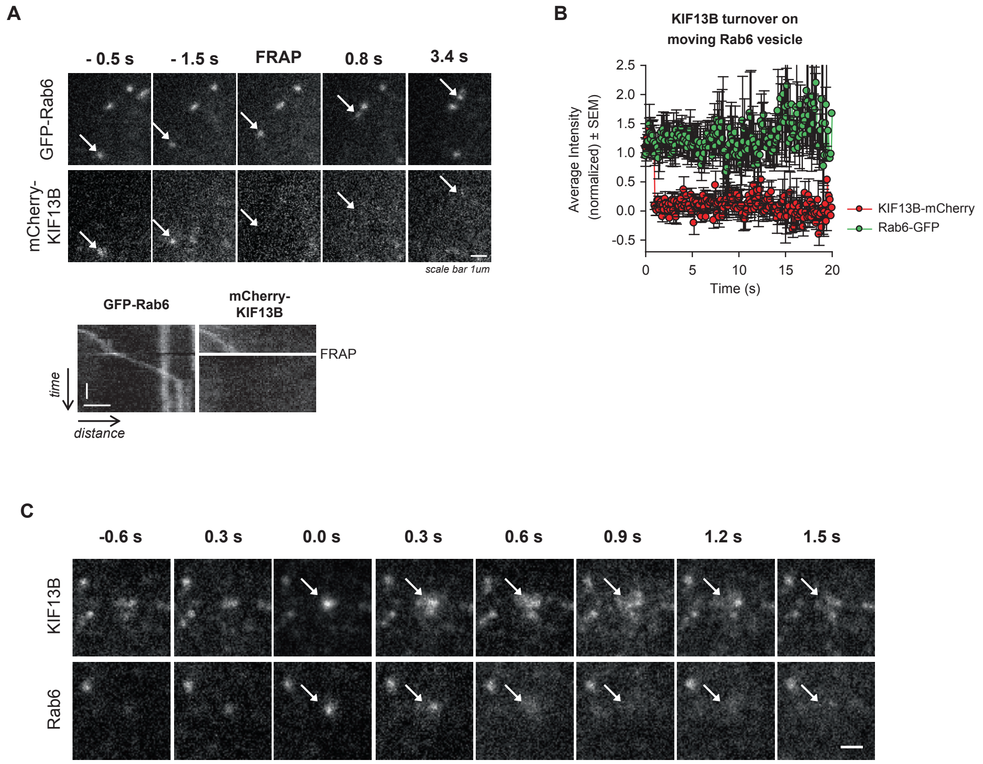
A
- 0.5 s
- 1.5 s
FRAP
0.8 s
3.4 s
GFP-Rab6
mCherry-KIF13B
scale bar 1um
GFP-Rab6
mCherry-KIF13B
FRAP
time
distance
B
KIF13B turnover on moving Rab6 vesicle
Average Intensity (normalized) ± SEM)
2.5
2.0
1.5
1.0
0.5
0.0
-0.5
0
5
10
15
20
Time (s)
KIF13B-mCherry
Rab6-GFP
C
-0.6 s
0.3 s
0.0 s
0.3 s
0.6 s
0.9 s
1.2 s
1.5 s
KIF13B
Rab6

Figure 3. KIF13B does not turn over on Rab6 vesicles.

(A) Frames from a two-color confocal movie of exocytotic vesicles labeled for GFP-Rab6A and mCherry-KIF13B. In the third shown frame, the mCherry signal was bleached in a small part of the cell by five iterations of 561 nm laser (100% of power). Arrows indicate the same vesicle over time. Scale bar: 1 μm. Kymographs are shown to illustrate the absence of fluorescence recovery of the vesicle (scale bars: horizontal, 1 μm, vertical, 2 s).

(B) Quantification of the FRAP data obtained as in (A). Error bars indicate SEM.

(C) Frames from a TIRFM movie showing the behavior of GFP-KIF13B and TagRFP-T-Rab6A vesicles before and during fusion. 0 s corresponds to the sharp increase of fluorescent signal associated with vesicle fusion. Scale bar: 1 μm.

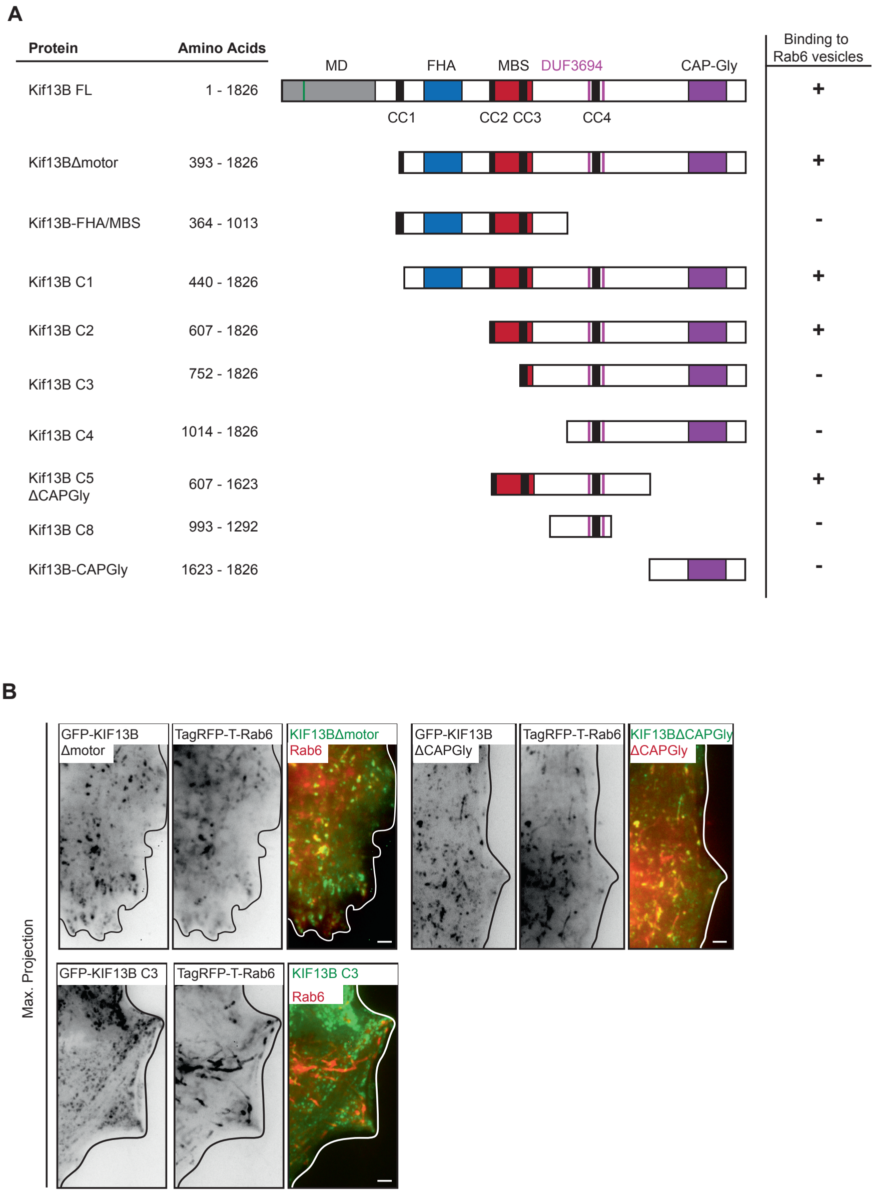
A
Protein
Amino Acids
Binding to Rab6 vesicles
MD
FHA
MBS
DUF3694
CAP-Gly
CC1
CC2 CC3
CC4
Kif13B FL
1 - 1826
+
Kif13BΔmotor
393 - 1826
+
Kif13B-FHA/MBS
364 - 1013
-
Kif13B C1
440 - 1826
+
Kif13B C2
607 - 1826
+
Kif13B C3
752 - 1826
-
Kif13B C4
1014 - 1826
-
Kif13B C5 ΔCAPGly
607 - 1623
+
Kif13B C8
993 - 1292
-
Kif13B-CAPGly
1623 - 1826
-
B
Max. Projection
GFP-KIF13B Δmotor
TagRFP-T-Rab6
KIF13BΔmotor
Rab6
GFP-KIF13B ΔCAPGly
TagRFP-T-Rab6
KIF13BΔCAPGly
ΔCAPGly
GFP-KIF13B C3
TagRFP-T-Rab6
KIF13B C3
Rab6

Figure 4. Mapping of the domain of KIF13B responsible for the interaction with Rab6 vesicles.
(A) A scheme of the GFP-KIF13B deletion constructs used in this study. The constructs were transfected in HeLa cells and the binding to Tag-RFP-T-Rab6A-positive vesicles was determined by live cell imaging (+, binding; -, no binding. The amino acid positions in KIF13B are indicated. MD, motor domain; FHA, forkhead-associated domain, MBS, MAGUK binding stalk; DUF, domain of unknown function; CC, coiled coil.
(B) Maximum intensity projections of 300 frames of a movie (collected with a 100 s interval) of a HeLa cell overexpressing TagRFP-T-Rab6A and the indicated GFP-KIF13B deletion constructs. The position of the cell edge is indicated with a white line. Scale bar: 2 μm.

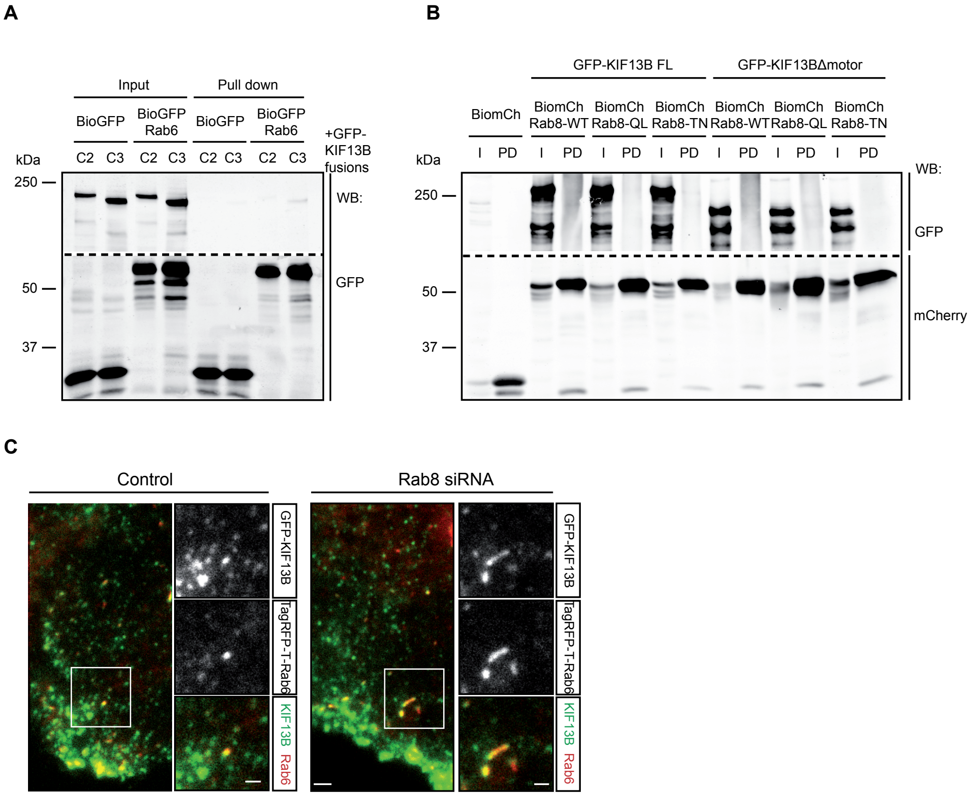
A
Input
Pull down
BioGFP
BioGFP Rab6
BioGFP
BioGFP Rab6
+GFP-KIF13B fusions
kDa
C2
C3
C2
C3
C2
C3
C2
C3
250
50
37
WB:
GFP
B
GFP-KIF13B FL
GFP-KIF13BΔmotor
BiomCh
BiomCh Rab8-WT
BiomCh Rab8-QL
BiomCh Rab8-TN
BiomCh Rab8-WT
BiomCh Rab8-QL
BiomCh Rab8-TN
kDa
I
PD
250
50
37
WB:
GFP
mCherry
C
Control
Rab8 siRNA
GFP-KIF13B
TagRFP-T-Rab6
KIF13B Rab6

Figure 5. KIF13B does not interact with Rab6A or Rab8A.
(A) Streptavidin pull down assays from lysates of HEK293T cells coexpressing BioGFP or BioGFP-Rab6A together with BirA and the indicated GFP-tagged KIF13B constructs. Western blots were performed with anti-GFP antibodies.
(B) Streptavidin pull down assays from lysates of HEK293T cells coexpressing the indicated Bio-mCherry-Rab8A constructs together with BirA and the indicated GFP-tagged KIF13B constructs. Western blots were performed with anti-GFP antibodies.
(C) Live images of HeLa cells expressing GFP-KIF13B and TagRFP-T-Rab6A and transfected with the indicated siRNAs for 72 hrs. Scale bar: 2 μm. The boxed areas are magnified on the right (scale bar: 1 μm).

We next searched for interacting partners of KIF3B that could mediate its binding to Rab6 vesicles by using streptavidin pull-down assays with biotinylation and GFP-tagged (BioGFP) KIF13B constructs combined with mass spectrometry (Fig. 6A, Table 1). For this analysis, we used the deletion mutants BioGFP-KIF13B C2, which binds to Rab6 vesicles, and BioGFP-KIF13B C3, which does not contain the MBS and does not bind to Rab6 vesicles (Fig.4A). We reasoned that putative molecular links between KIF13B and secretory vesicles should be enriched in the pull down with the C2 deletion mutant. We identified several significant hits that had a higher number of peptides in the sample with the C2 mutant compared to the C3 mutant (Table 1). These included the already known KIF13B binding partners hDlg1, which binds to the MBS (Yamada et al., 2007), together with its three known interaction partners MPP7, LIN7C and CASK (Bohl et al., 2007; Lee et al., 2002), and utrophin, a large cytoskeletal adaptor, which was recently shown to bind to KIF13B in a complex that mediates endocytosis of the low density lipoprotein receptor-related protein 1 (LRP1) (Kanai et al., 2014). Known binding partners of utrophin, syntrophin (Kramarcy et al., 1994) and dystrobrevins (Peters et al., 1997), were also present in the pull down. The most prominent potential novel binding partners of KIF13B, which showed a significantly stronger association with the C2 compared to the C3 deletion mutant, were the kinase D-interacting substrate of 220kDa (KIDINS220, also known as ankyrin repeat-rich membrane spanning (ARMS)), a conserved transmembrane molecule implicated in different signaling pathways (Neubrand et al., 2012), and an adaptor protein belonging to the motin family, angiomotin (Moleirinho et al., 2014) (Table 1). Other significant hits in the screen (>4 unique peptides) which were enriched in the pull down with the C2 mutant relative to the C3 mutant were heterogeneous nuclear ribonucleoprotein H, 40S ribosomal protein S11, regulatory subunit B of the serine/threonine-protein phosphatase 2A and mitochondrial pyruvate dehydrogenase phosphatase, which were all unlikely to mediate kinesin recruitment to secretory vesicles.

By performing a streptavidin pulldown, we could confirm the interaction between BioGFP-KIF13B and HA-KIDINS220 (Fig. 6B), but the knockdown of KIDINS220 did not affect the binding of KIF13B to Rab6 vesicles (Fig. 6C,F). We also performed siRNA-mediated depletion of utrophin, hDlg1 and angiomotin, as well as the combined depletions of hDlg1 and utrophin and KIDINS220 and utrophin, but none of these treatments significantly affected the recruitment of KIF13B to Rab6 vesicles (Fig. 6D,E,F). Since triple protein knockdowns are typically not very efficient, we could not investigate whether there are more complex redundancies between these proteins for the KIF13B recruitment. We conclude that using the approaches described above, we were not able to find how KIF13B is recruited to Rab6-positive vesicles. We focused on the more significant hits, but it is possible that a protein that is less abundantly present in the list of potential KIF13B partners is relevant for the binding. It is also possible that we failed to isolate the relevant protein because of its poor solubility in the conditions used for our pull down. Another possibility is that the kinesin recruitment is mediated by multiple mechanisms that might include an interaction with multiple proteins or lipids. Further investigation is required to unveil the molecular mechanisms mediating the binding of KIF13B to Rab6 vesicles.

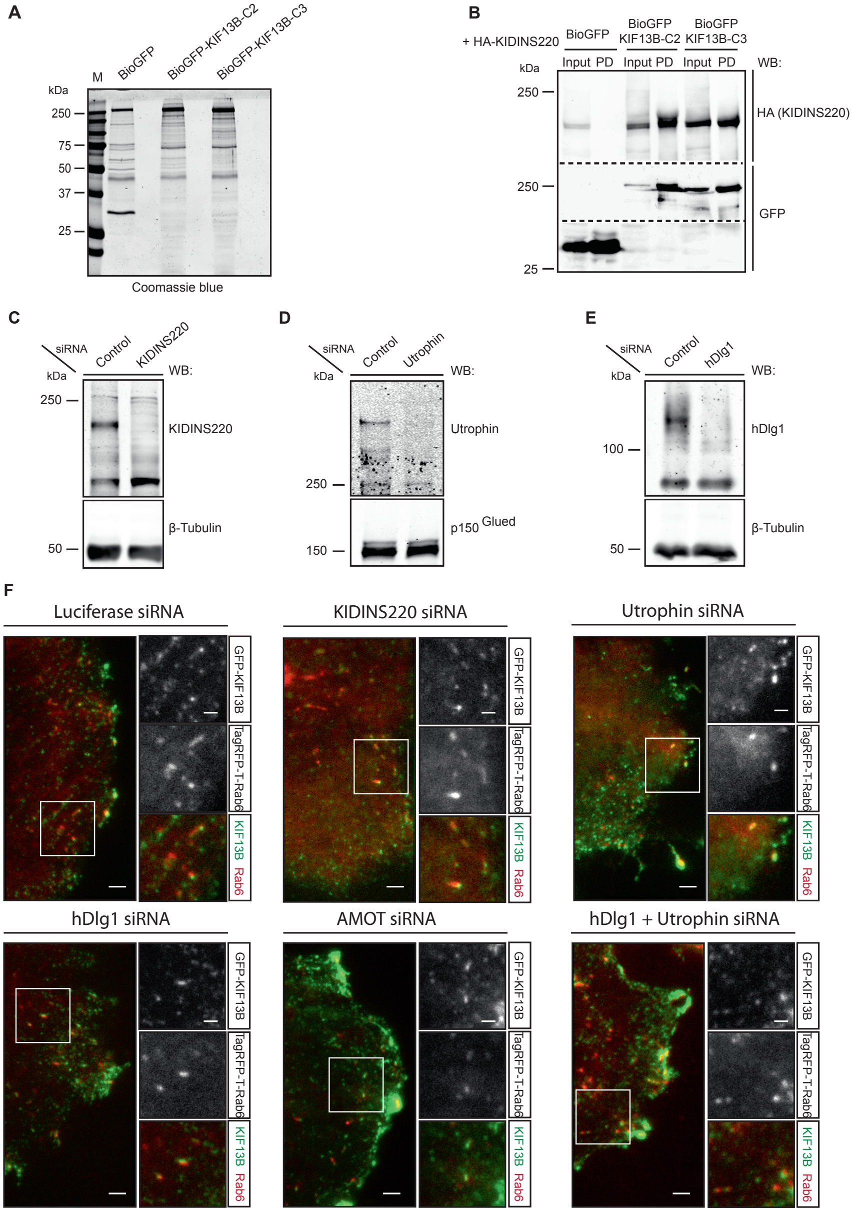
A
M
BioGFP
BioGFP-KIF13B-C2
BioGFP-KIF13B-C3
kDa
250
75
50
37
25
Coomassie blue
B
+ HA-KIDINS220
BioGFP
BioGFP KIF13B-C2
BioGFP KIF13B-C3
kDa
Input PD Input PD Input PD
WB:
250
HA (KIDINS220)
250
GFP
25
C
siRNA
Control
KIDINS220
kDa
WB:
250
KIDINS220
β-Tubulin
50
D
siRNA
Control
Utrophin
kDa
WB:
Utrophin
250
p150 Glued
150
E
siRNA
Control
hDlg1
kDa
WB:
hDlg1
100
β-Tubulin
50
F
Luciferase siRNA
KIDINS220 siRNA
Utrophin siRNA
hDlg1 siRNA
AMOT siRNA
hDlg1 + Utrophin siRNA
GFP-KIF13B
TagRFP-T-Rab6
KIF13B Rab6

Figure 6. Identification of KIF13B binding partners and analysis of their role in motor recruitment to Rab6 vesicles.
(A) Coomassie-stained gel of streptavidin pull down assays performed with lysates of HEK293T cells transiently expressing the biotin ligase BirA together with BioGFP or the indicated BioGFP tagged KIF13B constructs.
(B) Streptavidin pull-down assays from extracts of HEK293T cells coexpressing BirA, BioGFP or the indicated BioGFP-KIF13B constructs and HA-KIDINS220. BioGFP proteins were detected with anti-GFP antibodies and KIDINS220 with antibodies against KIDINS220 N terminus. 2.5% of the input and 10% of the precipitate was loaded on gel.
(C-E) Western blots showing the depletion of KIDINS220 (C), utrophin (D) and hDlg1 (E) in HeLa cells 72 hrs after transfection with the indicated siRNAs. β-tubulin or p150$^{\text{Glued}}$ serve as loading controls.
(F) Live images of HeLa cells expressing GFP-KIF13B and TagRFP-T-Rab6A and transfected with the indicated siRNAs for 72 hrs. Scale bar: 2 μm. The boxed areas are magnified on the right (scale bar: 1 μm).

Table 1: Binding partners of the indicated BioGFP-KIF13B constructs in HEK293T cells identified by mass spectrometry analysis

		KIF13B C2		KIF13B C3	
Gene name	Protein ID	Unique Peptide	PSM	Unique Peptide	PSM
KIF13B	Q9NQT8	147	294	102	177
MOV10	Q9HCE1	27	27	24	24
MARK2	Q7KZI7	26	31	17	19
HSPA5	P11021	22	24	16	18
KIDINS220	**Q9ULH0**	**22**	**22**	**8**	**8**
HADHA	P40939	20	21	11	11
UTRN	**P46939**	**19**	**19**	**2**	**2**
LRPPRC	P42704	17	17	10	10
MARK3	P27448	16	18	17	18
CUL3	Q13618	16	17	12	13
DLG1	**Q12959**	**15**	**16**	**0**	**0**
AMOT	**Q4VCS5**	**14**	**15**	**0**	**0**
MARK1	Q9P0L2	12	12	6	6
HADHB	P55084	11	12	10	10
ATAD3C	Q5T2N8	11	11	10	11
SNTB2	**Q13425**	**11**	**11**	**4**	**4**
NCL	P19338	9	9	9	9
MPP7	**Q5T2T1**	**9**	**9**	**0**	**0**
KLHL12	Q53G59	8	9	7	7
OSBPL8	Q9BZF1	8	9	5	5
PPP2R1A	P30153	5	5	4	4
ILF2	Q12905	5	7	3	3
CCT6A	P40227	5	5	3	3
TCP1	P17987	5	5	3	3
HNRNPH1	**P31943**	**5**	**5**	**2**	**2**
RPS11	**P62280**	**5**	**5**	**1**	**1**
PPP2R2A	**P63151**	**5**	**6**	**1**	**1**
CCT4	P50991	4	4	4	4
HNRNPA1	P09651	4	4	4	4
PKN3	Q6P5Z2	4	4	4	4
CSNK2A1	P68400	4	4	3	3
DDX6	P26196	4	4	3	3
LRRC59	Q96AG4	4	4	2	2
LIN7C	**Q9NUP9**	**4**	**4**	**0**	**0**
PDP1	**Q9P0J1**	**4**	**4**	**0**	**0**
CASK	**O14936**	**4**	**4**	**0**	**0**
KLHL7	Q8IXQ5	3	3	2	2
FAM98A	Q8NCA5	3	3	2	2
CCT7	Q99832	3	4	1	1
AIFM1	O95831	3	3	1	1
IRS4	O14654	3	3	1	1
DDX3X	O00571	3	3	1	1
DTNB	**O60941**	**3**	**4**	**0**	**0**

FBXW11	Q9UKB1	3	3	0	0
XPR1	Q9UBH6	3	3	0	0
DTNA	**Q9Y4J8**	**3**	**3**	**0**	**0**
CEP104	O60308	3	3	0	0
GLG1	Q92896	3	3	0	0
C14orf166	Q9Y224	2	2	4	4
PSPC1	Q8WXF1	2	2	3	3
KHSRP	Q92945	2	2	2	2
PPIA	P62937	2	2	2	2
MARK4	Q96L34	2	2	2	2
ABCF1	Q8NE71	2	2	2	2
NEDD8	Q15843	2	3	1	2
PRKDC	P78527	2	2	1	1
CCT2	P78371	2	2	1	1
CCT5	P48643	2	2	1	1
XRCC6	P12956	2	2	1	1
HS2ST1	Q7LGA3	2	2	1	1
DDX21	Q9NR30	2	2	1	1
CLTC	Q00610	2	2	1	1
SLIRP	Q9GZT3	2	2	0	0
DNAJA1	P31689	2	2	0	0
DRG1	Q9Y295	2	2	0	0
KPNA2	P52292	2	2	0	0
BTBD9	Q96Q07	2	2	0	0
OSBPL5	Q9H0X9	2	2	0	0
GTF2I	P78347	2	2	0	0
COL18A1	P39060	2	2	0	0
BAG2	O95816	1	1	1	1
MOGS	Q13724	1	1	1	1
GNB2L1	P63244	1	1	1	1
CACYBP	Q9HB71	1	1	1	1
EIF3C	Q99613	1	1	1	1
TARDBP	Q13148	1	1	1	1
STAU1	O95793	1	1	1	1
EWSR1	Q01844	1	1	1	1
TTC30A	Q86WT1	1	1	1	1
DHX36	Q9H2U1	1	1	1	1
PHB	P35232	1	1	0	0
VDAC2	P45880	1	2	0	0
PAM16	Q9Y3D7	1	1	0	0
RAB10	P61026	1	1	0	0
MIB1	Q86YT6	1	1	0	0

KIF13B is required for the transport of Rab6 vesicles from the Golgi to the plasma membrane

We next set out to investigate the functional involvement of KIF13B in Rab6 vesicle transport using siRNA-mediated protein depletion. A previous study suggested that PAUF-positive carriers are transported by Eg5 (Wakana et al., 2013), a microtubule plus end-directed motor best known for its function in antiparallel microtubule sliding required for the formation of the bipolar mitotic spindle (Ferenz et al., 2010), and we included the depletion of this kinesin in our analysis. We transfected HeLa cells stably expressing GFP-Rab6A with siRNAs against Eg5 or KIF13B, collected live imaging data of GFP-Rab6A vesicle movement and performed their automated analysis (Fig.7,8). The knockdown of Eg5 effectively blocked cells in mitosis by inducing monopolar spindles (data not shown). Therefore, to record vesicle motility in interphase cells, we prevented mitotic entry by treating cells with 2 mM thymidine for 24 hrs before imaging (Fig.7).

KIF13B depletion, the efficiency of which was confirmed by Western blotting (Fig.8F), had no obvious effect on cell viability or proliferation (data not shown). Vesicle tracking and extraction of directional runs was performed as described in Experimental Procedures. We found that the depletion of Eg5 had no effect on the number of directional runs to or from the plasma membrane, on the ratio of inward and outward runs or on the GFP-Rab6A vesicle velocity (Fig.7, Fig.10A). Furthermore, treatment of cells with the Eg5 inhibitor S-Trityl-L-cysteine (STLC) (Skoufias et al., 2006) did not inhibit transport of Rab6 vesicles (data not shown). These data seem to contradict the previous study, which demonstrated the involvement of Eg5 in PAUF vesicle movement (Wakana et al., 2013). This difference is likely to be due to different methodology. In the previous work, the depletion of Eg5 and the application of the Eg5 inhibitor monastrol were only used to show a reduction in the bulk secretion of PAUF. The actual analysis of PAUF vesicle movement was performed only in conditions of strong overexpression of a Eg5-T112N mutant, which is deficient in ATP hydrolysis but binds to microtubules, induces their strong bundling (Wakana et al., 2013) and might thus have unspecific effects on vesicle motility. Our data do not support the view that Eg5 is a major player in the motility of Rab6-positive secretory vesicles, indicating that the inhibitory effect of its depletion on PAUF secretion requires additional explanations.

The depletion of KIF13B also did not arrest Rab6 vesicle motility but did have an effect on the pattern of the movements (Fig.8A-C). While the number of directional runs was not changed in the Golgi area, the number of runs in the peripheral part of the cytoplasm was strongly reduced (Fig.8D). This reduction was due to fewer outward runs, while the number of inward runs was not altered, and, therefore, the fraction of outward runs was reduced (Fig.8D,E). HeLa cells have a reasonably radial microtubule system, with many microtubule minus ends clustered in the central cell region, although microtubules with

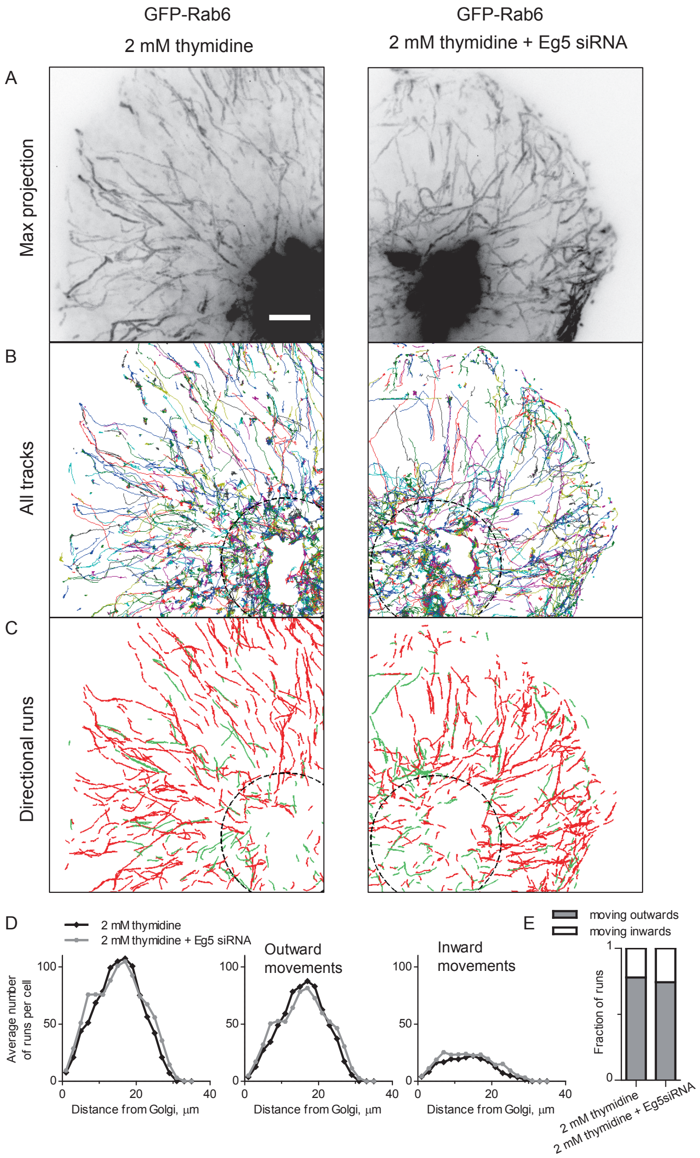
GFP-Rab6
2 mM thymidine
GFP-Rab6
2 mM thymidine + Eg5 siRNA
A
Max projection
B
All tracks
C
Directional runs
D
2 mM thymidine
2 mM thymidine + Eg5 siRNA
Average number of runs per cell
100
50
0
0
20
40
Distance from Golgi, µm
Outward movements
Inward movements
E
moving outwards
moving inwards
Fraction of runs
1
0
2 mM thymidine
2 mM thymidine + Eg5siRNA

Figure 7. Analysis of the effect of KIF11/Eg5 depletion on Rab6 vesicle movement.

(A) Maximum intensity projections of 500 consecutive frames from 100 ms exposure stream recordings of cells expressing GFP-Rab6A, transfected with the control (Luciferase) or Eg5 siRNA for 72 hrs and treated with 2 mM thymidine. Scale bar: 5 μm.

(B) GFP-Rab6A vesicle trajectories obtained from the live imaging data shown in (A). Position of the Golgi complex is highlighted by a dashed black oval.

(C) Segments of Rab6 trajectories, shown in (B), where directional vesicle motion was observed, color-coded by the average direction of movement: inward, towards cell center (green) and outward, towards cell boundary (red).

(D) Distributions of directional vesicle runs along the cell radius. The average number of directional runs per cell as a function of distance from the Golgi complex for all runs (left panel), directed outwards (middle panel) and inwards (right panel). 10 control and 12 KIF11-depleted cells were analyzed.

(E) Fractions of runs directed outwards and inwards.

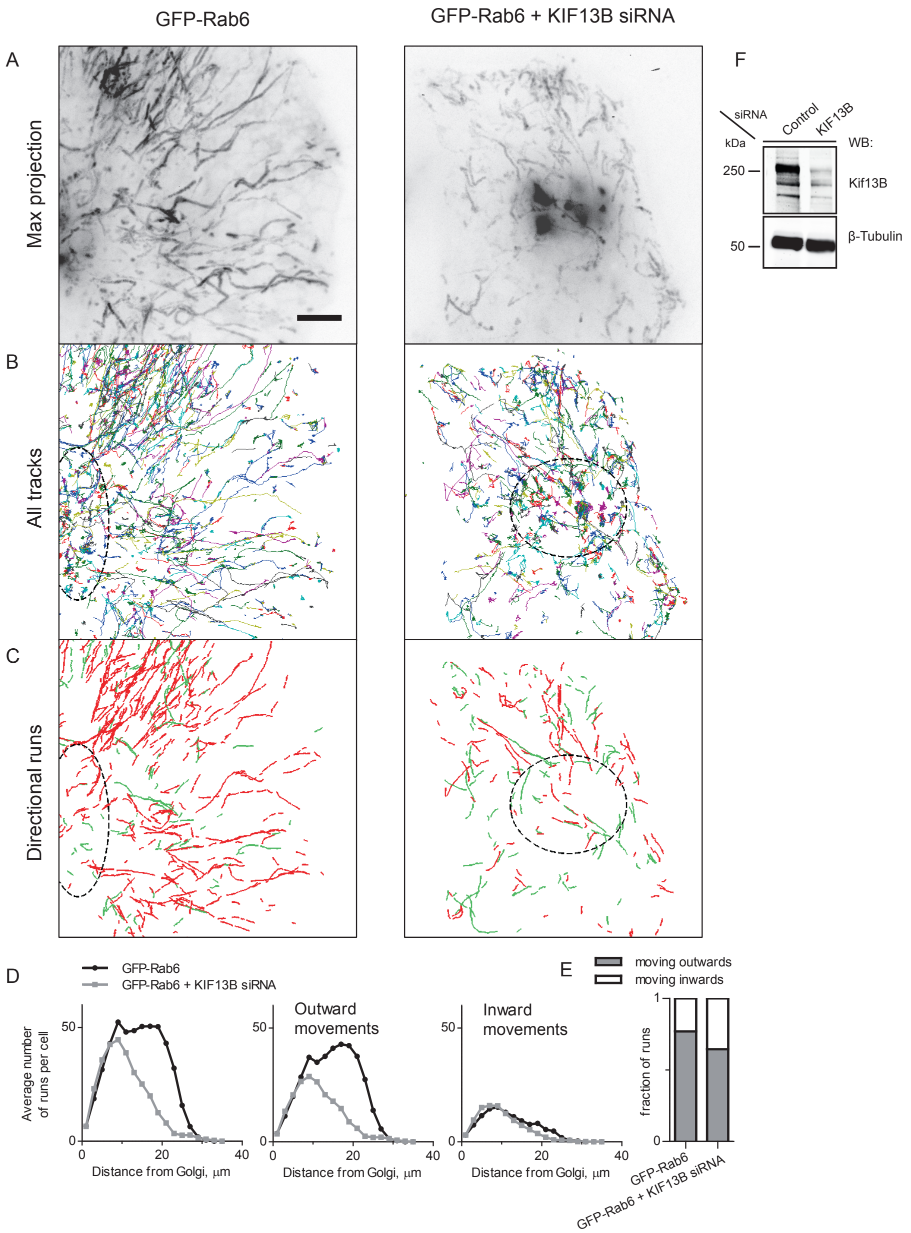
GFP-Rab6
GFP-Rab6 + KIF13B siRNA
A
Max projection
B
All tracks
C
Directional runs
F
siRNA
kDa
Control
KIF13B
WB:
250
Kif13B
50
β-Tubulin
D
GFP-Rab6
GFP-Rab6 + KIF13B siRNA
Average number of runs per cell
50
0
20
40
Distance from Golgi, µm
Outward movements
Inward movements
E
moving outwards
moving inwards
fraction of runs
1
GFP-Rab6
GFP-Rab6 + KIF13B siRNA

Figure 8. Analysis of the effect of KIF13B depletion on Rab6 vesicle movement.
(A-E) Maximum intensity projections of cell recordings, GFP-Rab6A vesicle trajectories, directional runs, their distributions along the cell radius and the fraction of inward/outward runs as described for Fig. 7. Cells expressing GFP-Rab6A were transfected with the control (Luciferase) or KIF13B siRNA for 72 hrs. 19 control cells and 31 KIF13B-depleted cells were analyzed.
(F) Western blots showing of depletion of KIF13B in HeLa cells 72 hrs after transfection with the indicated siRNAs. β-tubulin serves as a loading control.

their minus ends at the cell periphery are also present (Jiang et al., 2014). It is thus likely that a significant proportion of inward runs is driven by the minus end directed motor cytoplasmic dynein. Analysis of the overall vesicle velocities demonstrated an increase in fast long runs in KIF13B-depleted cells (Fig.10A,B). This is in agreement with our previous data, which showed that the depletion of KIF5B, KIF1B and KIF1C led to the acceleration of the residual vesicle motility due to an increased share of dynein-mediated movements, which are faster than those driven by kinesins (Schlager et al., 2014). Our results indicate that KIF13B is one of the kinesin motors contributing to the movement of Rab6 vesicles towards the plasma membrane.

We have also investigated whether the tail of KIF13B, which efficiently binds to Rab6 vesicles (Fig. 2E, Fig.4A,B) would act as a dominant negative. We have transfected HeLa cells with TagRFP-T-Rab6A either alone or together with KIF13BΔmotor and analyzed vesicle motility. We found that this treatment caused a strong arrest of vesicle motility, as the number of directional runs was dramatically reduced throughout the cell (Fig.9A-D). Both the outward and the inward runs were affected, although the number of the latter ones was diminished to a lesser degree, resulting in a reduced fraction of the outward runs (Fig.9D,E). The observed effect was much stronger than that of KIF13B depletion. This could be due to the fact that KIF13B depletion was incomplete, but might also be caused by the displacement of kinesins other than KIF13B from Rab6 vesicles. This would suggest that at least some if not all kinesins present on Rab6 vesicles use common receptors for their binding. The co-dependence of the activities of opposite polarity motors on each other, which appears to be a general property of bidirectional microtubule-based motility (Gross, 2004; Hoeprich et al., 2014), might explain why this leads to the overall inhibition of Rab6 vesicle motility including the dynein-mediated movements.

Detailed analysis of KIF13B driven Rab6 vesicle movement

While the depletion of KIF13B resulted in an increased fraction of fast long runs and therefore an increase in the average vesicle velocity (Fig. 10A,B), the mild overexpression of KIF13B used to detect it on the vesicles by live cell imaging had no effect on the speed of vesicle movement (Fig. 10B,C). Interestingly, the numerous KIF13B-labeled particles that were not colocalized with Rab6 displayed somewhat faster velocities than the Rab6-positive one (Fig. 10C). It is possible that this is due to the presence of a slower but more dominant KIF5B motor on these vesicles (Arpag et al., 2014; Norris et al., 2014; Schlager et al., 2014). The motor domain of KIF13B alone moved even faster (Fig. 10D), indicating that KIF13B is slowed down when bound to cargo, but the extent of speed reduction might be different for different cargos.

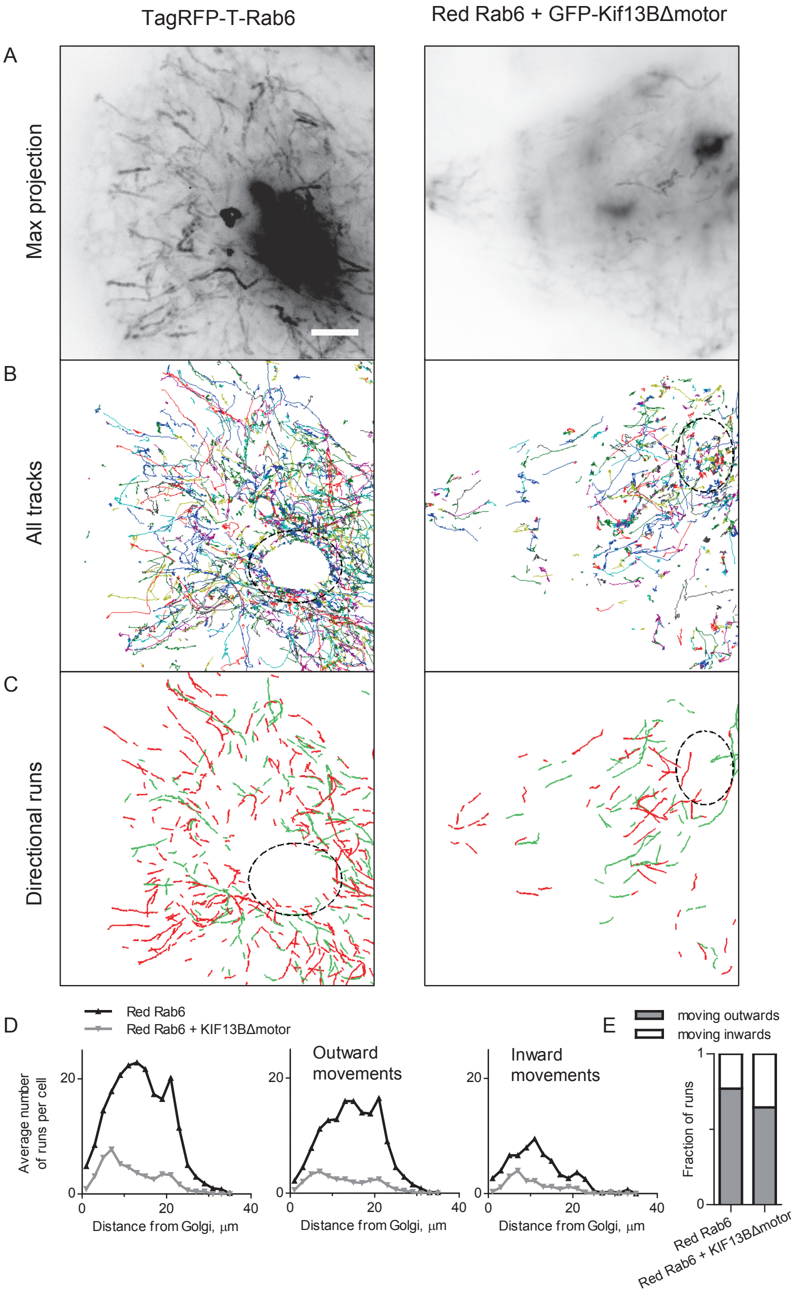
TagRFP-T-Rab6
Red Rab6 + GFP-Kif13BΔmotor
A
Max projection
B
All tracks
C
Directional runs
D
Red Rab6
Red Rab6 + KIF13BΔmotor
Average number of runs per cell
20
0
0
20
40
Distance from Golgi, μm
Outward movements
Inward movements
E
moving outwards
moving inwards
Fraction of runs
1
0
Red Rab6
Red Rab6 + KIF13BΔmotor

Figure 9. Analysis of the effect of the expression of KIF13B tail on Rab6 vesicle movement. (A-E) Maximum intensity projections of cell recordings, Tag-RFP-T-Rab6A vesicle trajectories, directional runs, their distributions along the cell radius and the fraction of inward/outward runs as described for Fig. 7. Cells expressing Tag-RFP-T-Rab6 either alone or together with GFP-KIF13B-Δmotor were analyzed one day after transfection. 6 control cells and 9 GFP-KIF13B-Δmotor-expressing cells were analyzed.

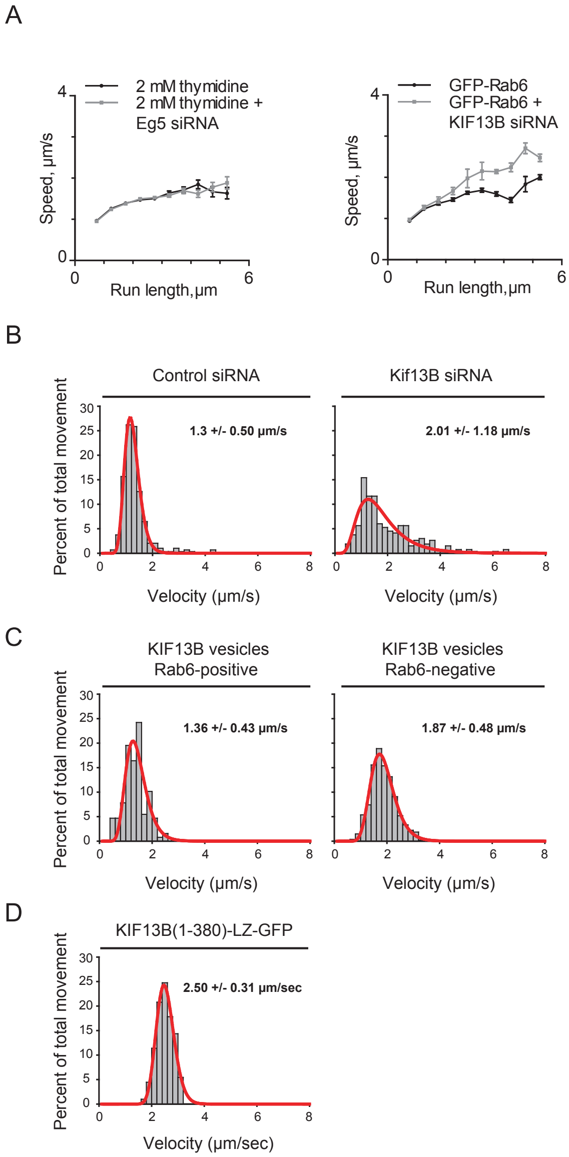

Figure 10. Analysis of velocities of Rab6 and KIF13B movements.
(A) The average velocity of directional vesicle runs as a function of the distance traveled during run. The datasets were the same as shown in Fig. 7 and 8. Error bars indicate SEM.
(B) Distributions of GFP-Rab6A vesicle velocities in control and KIF13B-depleted HeLa cells, measured manually using kymographs. Control, n= 294, 5 cells; KIF13B siRNA, n= 266, 5 cells.
(C) Distributions of velocities of GFP-KIF13B structures, which were either positive or negative for mCherry-Rab6A. Velocities were measured manually using kymographs. n= 128, 5 cells (Rab6-positive); n= 540, 5 cells (Rab6-negative).
(D) Distribution of velocities of single KIF13B motors (amino acids 1-380) dimerized using the leucine zipper (LZ) from GCN4 protein. n= 202, 5 cells.

Finally, we made use of our ability to detect the fluorescent KIF13B motors on Rab6 vesicles in order to investigate the motor distribution on the vesicle membrane during movement. First, we focused on the motor distribution on elongated tubules, which can be detected at low frequency in GFP-Rab6A-expressing cells. These tubules invariably had an accumulation of KIF13B at the front tip (Fig.11A). Similar accumulation of KIF13A has been previously reported at the tips of tubular endosomes (Delevoye et al., 2014).

Since elongated tubules represent atypical secretory carriers in HeLa cells, we next analyzed the distribution of GFP-KIF13B on regular-sized TagRFP-T-Rab6A vesicles by simultaneous two color imaging. As a control, we used the vesicle cargo, PAUF-mRFP, the position of which was compared to that of GFP-Rab6A. The positions of the two fluorescent signals on the vesicle were determined with sub-pixel localization precision using 2D Gaussian fitting. The alignment of the two fluorescent channels and the sub-pixel correction of chromatic aberrations were performed using fluorescent beads, as described in Experimental Procedures. Vesicle trajectories were separated into directional runs and phases of random movement as described in Experimental Procedures (Fig.11B-D), and only the periods of directional runs were used for further analysis. To determine whether and how the two fluorescent signals are displaced relative to each other during movement, we determined the distance between the two fluorescent signals on the vesicle projected on the velocity vector (Fig. 11E). As could be expected, the projected distance between Rab6A and PAUF was close to zero (Fig. 11F,G). In contrast, the projected distance between KIF13B and Rab6A was strongly skewed towards positive values, with an average of 80 nm (Fig.11F,G). The angles between the line connecting the centers of the two fluorescent signals (the distance vector) and the velocity vector were distributed randomly when the positions of Rab6A and its cargo, PAUF, were analyzed (Fig. 11H), while in the case of Rab6A and KIF13B the angles close to zero predominated, as can be expected if the kinesins were accumulating at the front of the moving vesicle. Analysis of individual vesicles showed that the maximal separation of the Rab6A and KIF13B signal varied per vesicle (from 80 to 400 nm) (Fig.11 I), as can be expected because different vesicles can have different sizes. We could not detect any dependence of the distance between Rab6A and KIF13B on the vesicle velocity. We conclude that the distance between Rab6A and KIF13B signals, which can be expected to be sensitive to the changes in motor distribution and the vesicle geometry, cannot be easily related to vesicle acceleration and deceleration.

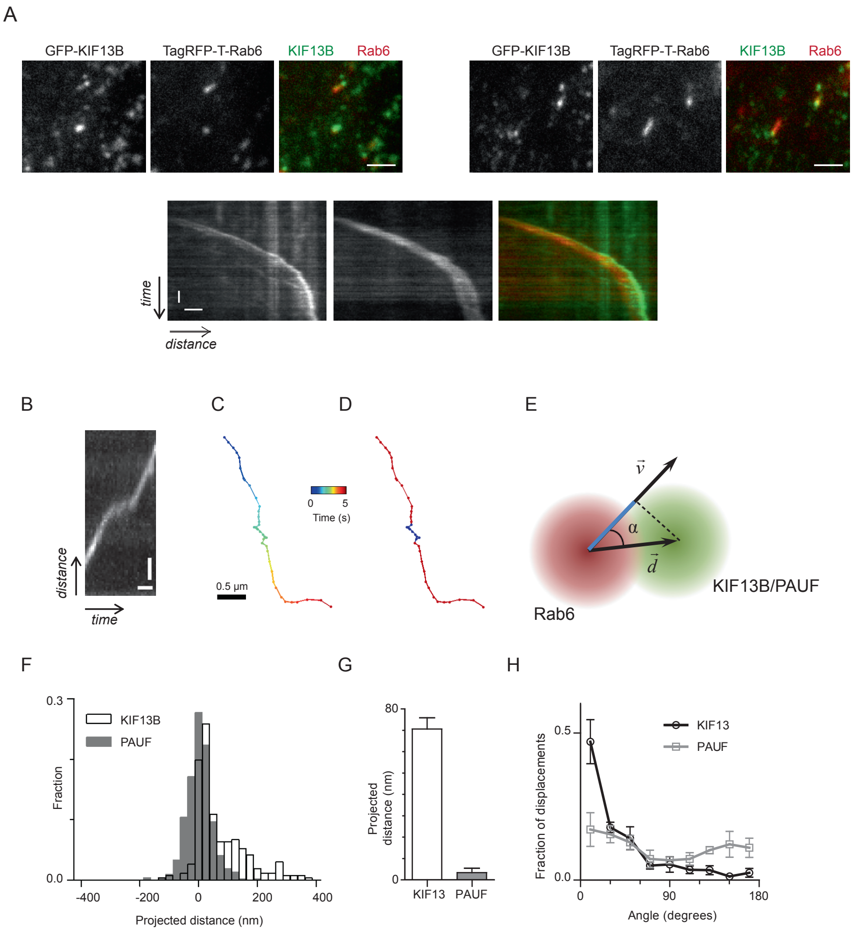

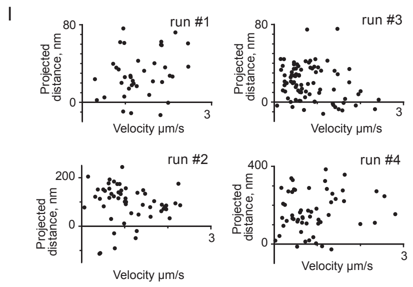

Figure 11. KIF13B localizes at the front of the moving vesicles.
(A) Images (top) and kymographs (bottom) of moving TagRFP-T-Rab6A labeled tubules. Scale bar top: 2 μm. Scale bars kymographs: horizontal, 1 μm, vertical 1 s.
(B) An example of a kymograph of TagRFP-T-Rab6A vesicle movement. Scale bars: horizontal, 1 μm, vertical 1 s.
(C) Vesicle trajectory shown in (B) with color-coded time. Scale bars: 0.5 μm.
(D). The same trajectory as in (B,C), with random motions colored blue and directional motions in red.
(E) Schematic representation of the fluorescent signals of TagRFP-T-Rab6A vesicle (red) and GFP-KIF13B or PAUF-mRFP (green). The projected distance between the signals (blue segment) is defined as a projection of the distance vector $\vec{d}$ between centers of spots localized with sub-pixel precision onto the Rab6 instant velocity vector $\vec{v}$.
(F) Distribution of the distances between the centers of Rab6A signal and KIF13B or PAUF signal projected onto Rab6A trajectory (4 tracks for each condition, n=267 and 519 frames, respectively).
(G) Average projected distance values for the data shown in (F).
(H) Distribution of the angles α (panel E) between the distance and the velocity vectors for the data shown in (F).
(I) Plots of the projected distance between Rab6A and KIF13B signals against velocity for four different vesicles.
Error bars represent SEM.

The observed asymmetry of KIF13B distribution both on the vesicles and on tubules argues for its frequent engagement and active movement along the microtubule. The drag force exerted by the vesicle is likely to cause motor redistribution to the front of the carrier. The presence of slower motors, such as KIF5B, might be an important contributing factor, which could promote membrane tubule extension: the faster KIF13B motors would accumulate at the leading extremity of the membrane tubule and exert a pulling force, while the slower KIF5B motors would accumulate at the rear and induce stretching of the Rab6 tubule along the microtubule. These ideas can be tested by depleting KIF5B or by inducible recruitment of additional KIF5B motors to Ra6 vesicles. It would also be interesting to induce switching of the direction of Rab6 vesicle motility by recruiting an excess of dynein motors, as we have described previously (Splinter et al., 2012), and investigate how the KIF13B will be distributed when the vesicles are pulled in the opposite direction.

To conclude, we have shown that KIF13B, a kinesin previously predominantly implicated in the transport of endosomes, also contributes to the transport of the carriers of constitutive secretion to the cell periphery. Fluorescently tagged full length KIF13B can be readily detected on the vesicles, providing interesting experimental possibilities to study the behavior of individual motors on cargo in the context of multimotor transport.

Acknowledgements

We thank Dr. Giampietro Schiavo, Dr. Vivek Malhotra and Dr. Rene Medema for sharing reagents. We thank Dr. Kenneth Schou and Stine Morthorst for suggestions on the project. This work was supported by Fundação para a Ciência e a Tecnologia fellowship (A.S-M.) and by the Netherlands Organization for Scientific Research (NWO) ALW-VICI grant and the European Research Council (ERC) Synergy grants to A.A., and by NWO-CW ECHO grant to A.A. and A.J.R.H.

Experimental procedures

Antibodies and reagents

The following primary and secondary antibodies were used in this study: mouse monoclonal antibodies against Rab6A/Rab6A' (Matanis et al., 2002); rabbit anti-GFP (Abcam), mouse anti-β-tubulin (Santa Cruz), mouse anti-HA (Covance), mouse anti-$p150^{Glued}$ (BD Biosciences). The rabbit anti-KIDINS220 antibody was a gift from Dr. Giampietro Schiavo (Cancer Research UK, London).

The anti-KIF13B polyclonal antibody was produced by immunizing rabbits with a purified GST-KIF13B protein (amino acids 1096–1143) expressed in BL21 *Escherichia coli* using the pGEX-5X-3 vector (GE Healthcare).The antiserum was affinity purified using the antigen coupled to Dyna M-280 Streptavidin beads (Life Technologies).

For immunofluorescence experiments we used Alexa488- and Alexa568-conjugated secondary antibodies (Invitrogen). For Western blotting we used IRDye 800CW goat anti-mouse and anti-rabbit antibodies, which were detected using Odyssey Infrared Imaging system (Li-Cor Biosciences).

Expression constructs, siRNAs and cell lines

GFP-Rab6A construct was described previously (Matanis et al., 2002). GFP-KIF13B deletion constructs were prepared by PCR-based strategy using GFP-KIF13B full length construct (a gift from Dr. Athar Chishti, University of Illinois College of Medicine, Chicago, USA). Subsequently, PCR products were subcloned in pEGFP expression vectors. HA-KIDINS220 was a gift from Dr. Giampietro Schiavo (Cancer Research UK, London), PAUF-mRFP a gift from Dr. Vivek Malhotra (Centre for Genomic Regulation, Barcelona, Spain) and TagRFP-T-Rab6A a gift from Dr. Yuko Mimori-Kiyosue (RIKEN Center for Developmental Biology, Japan). The siRNAs used in this study were synthesized by Sigma and were directed against the following sequences: Luciferase 5′-CGTACGCGGAATACTTCGA-3′;
KIF13B 5′-CCGAAGGTGTTTGCTTATGAT-3′;
KIDINS220 5′- GTCAACTGCTCTGATAAGT-3′;
utrophin 5′-CCATCAGAACCAGCTAGAAATATTT-3′;
hDlg1 5′-AGAAGTTACTCATGAAGAA-3′. The siRNA sequence against AMOT, 5′-GGCTTACAAAAGGGAATAG-3′, was synthetized by Ambion (siRNA ID: 129069). The siRNA against Rab8 was previously described (Grigoriev et al., 2011).

Streptavidin pulldown assays

HEK293 cells were cultured in DMEM/Ham's-F10 (50/50%) medium containing 10% FCS and 1% penicillin/streptomycin and were transfected using Polyethylenimine

(PEI; Mw 2500; Polysciences) at a 3:1 PEI:DNA ratio (w/w). Cells were harvested 24 hours after transfection, by scraping the cells in ice-cold PBS and lysing cell pellets in the lysis buffer (20 mM Tris-HCl, pH 7.5, 100 mM NaCl, 1.0% Triton X-100, and protease inhibitors; Roche). Supernatants and pellet fractions were separated by centrifugation at maximum speed for 20 minutes. Supernatants were mixed with an equal amount of Dyna M-280 Streptavidin beads (Life Technologies). Samples were incubated for 2 hours while rotating at 4°C, collected with a magnet and pellets were washed 5-7 times with the wash buffer (20 mM Tris-HCl, pH 7.5, 100 mM NaCl, 0.1 % Triton X-100). Samples were eluted in the SDS sample buffer, equally loaded onto SDS-PAGE gels and subjected to Western blotting. Blots were blocked with 2% bovine serum albumin/0.07% Tween 20 in PBS and incubated with primary antibodies at 4°C overnight. Blots were washed with 0.07% Tween 20 in PBS three times for 10 min at room temperature and incubated with either IRDye 800CW goat anti-mouse and anti-rabbit secondary antibodies, which were detected using Odyssey Infrared Imaging system (Li-Cor Biosciences).

Analysis of KIF13B binding partners by mass spectrometry

30 μl of each sample was run on a 12% Bis-Tris 1D SDS-PAGE gel (Biorad) for 1 cm and stained with colloidal Coomassie dye G-250 (Gel Code Blue Stain Reagent, Thermo Scientific). Each lane was cut into 1 band, which were treated with 6.5 mM dithiothreitol (DTT) for 1 hour at 60 °C for reduction and 54 mM iodoacetamide for 30 min for alkylation. The proteins were digested overnight with trypsin (Promega) at 37°C. The peptides were extracted with acetonitrile (ACN) and dried in a vacuum concentrator.

The data were acquired using an Orbitrap Q Exactive mass spectrometer. Peptides were first trapped (Dr Maisch Reprosil C18, 3 μm, 2 cm x 100 μm) before being separated on an analytical column (Zorbax SB-C18, 1.8 μm, 40 cm x 50 μm), using a gradient of 60 min at a column flow of 150 nl min-1. Trapping was performed at 8 μl/min for 10 min in solvent A (0.1 M acetic acid in water) and the gradient was as follows 7- 30% solvent B (0.1 M acetic acid in acetonitrile) in 31 min, 30-100% in 3 min, 100% solvent B for 5 min, and 7% solvent B for 13 min. Full scan MS spectra from m/z 350 – 1500 were acquired at a resolution of 35.000 at m/z 400 after accumulation to a target value of 3e6. Up to ten most intense precursor ions were selected for fragmentation. HCD fragmentation was performed at normalized collision energy of 25% after the accumulation to a target value of 5e4. MS/MS was acquired at a resolution of 17.500. In all cases nano-electrospray was performed at 1.7 kV using an in-house made gold-coated fused silica capillary (o.d. 360 μm; i.d. 20 μm; tip i.d. 10 μm).

Raw files were processed using Proteome Discoverer 1.3 (Thermo Scientific, Bremen, Germany). The database search was performed against the Swissprot human database, taxonomy (version November 2012) using Mascot (version 2.3, Matrix Science, UK) as search engine. Carbamidomethylation of cysteines was set as a fixed modification and oxidation of methionine was set as a variable modification. Trypsin was specified as enzyme and up to two miss cleavages were allowed. Data filtering was performed using percolator, resulting in 1% false discovery rate (FDR). Additional filter was Mascot ion score >20. Raw files corresponding to one sample were merged into one result file.

Transfection and immunofluorescence staining of cultured HeLa, Vero and MRC5 cells

HeLa cells were cultured in DMEM/Ham's F10 (50/50%) medium containing 10% FCS, 100 U/mL Penicilium and 100 µg/mL Streptomycin. One day before transfection, cells were plated on glass coverslips. Cells were transfected with FuGene 6 (Promega) or Polyfect (Qiagen) according to the manufacturer's protocol and incubated overnight. Stable GFP-Rab6A HeLa clones were selected with fluorescence activated cell sorting (FACS) and cultured in the presence of 0.4 mg/ml G418 (Roche) (Grigoriev et al., 2007). Cells were transfected with 10 nM siRNAs with HiPerFect (Qiagen) and analyzed 3 days after transfection. Cells were either mounted for live imaging or fixed in 4% paraformaldehyde for 10 min at room temperature followed by 10 min incubation in 0.15% Triton X-100 in PBS. Slides were blocked in 2% bovine serum albumin/0.07% Tween 20 in PBS and labeled with primary antibody for 1 hour at room temperature. Slides were washed three times with 0.07% Tween-20 in PBS, labeled with secondary antibodies for 1 hour at room temperature, washed three times with 0.07% Tween20 in PBS and mounted using Vectashield mounting medium (Vector laboratories).

Image acquisition of fixed and live cells

Images of fixed cells were collected with a Nikon Eclipse 80i microscope equipped with a Plan Apo VC 100x N.A. 1.40 oil objective and Chroma ET-DAPI (49000), Chroma ET-GFP (49002), Chroma ET-mCherry (49008) and Chroma ET-GFP/mCherry (59022) filters and a Photometrics CoolSNAP HQ2 CCD camera or with a confocal LSM 700 microscope equipeded with a 63x (oil) objective. Live cell imaging was performed on an inverted research microscope Nikon Eclipse Ti-E (Nikon) with perfect focus system (PFS) (Nikon), equipped with Nikon CFI Apo TIRF 100x 1.49 N.A. oil objective (Nikon), Photometrics Evolve 512 EMCCD (Roper Scientific) and controlled with MetaMorph 7.7.5 software (Molecular Devices). The 16-bit images were projected onto the CCD chip with intermediate lens 2.5X (Nikon C mount adapter 2.5X) at a magnification of 0.063 µm/pixel. To keep cells at 37°C we used stage top incubator (model INUBG2E-ZILCS Tokai Hit). The microscope was equipped with TIRF-E motorized TIRF illuminator modified by Roper Scientific France/PICT-IBiSA, Institut Curie. For regular imaging we used Mercury lamp HBO-103W/2 (Osram) for excitation or 491nm 100mW Calypso (Cobolt) and 561nm 100mW Jive (Cobolt) lasers. We used ET-GFP filter set (Chroma) for imaging of proteins tagged with GFP; ET-mCherry filter set (Chroma) for imaging of proteins tagged with mCherry. For simultaneous imaging of green and red fluorescence we used triple-band TIRF polychroic ZT405/488/561rpc (Chroma) and triple-band laser emission filter ZET405/488/561m (Chroma), mounted in the metal cube (Chroma, 91032) together with Optosplit III beamsplitter (Cairn Research Ltd, UK) equipped with double emission filter cube configured with ET525/50m, ET630/75m and T585LPXR (Chroma).

Image analysis

Automated vesicle tracking

To track and characterize movements of individual vesicles we used TrackMate plugin (v.2.5.0) for FIJI with subpixel LoG detector and "Simple LAP tracker" option (Schindelin et al., 2012). The resulting trajectories were exported to MTrackJ ImageJ plugin (Meijering et al., 2012) for the manual inspection and correction. To achieve sub-pixel localization precision, each fluorescent spots detection was further fitted with 2D Gaussian with the initial parameters corresponding to the microscope point spread function as described earlier (Yau et al., 2014). Only tracks longer than 10 frames were selected for the further analysis.

Two color track correction

For the simultaneous two color imaging, the signals from each channel where detected and tracked separately. The sub-pixel correction of chromatic aberrations in the imaging path was performed using microscope camera field of view calibration with TetraSpeckTM beads. A sample containing beads non-specifically immobilized on the coverslip was imaged simultaneously in both channels at the beginning of each imaging session. Microscope stage was moved in x and y directions to homogeneously cover the whole field of view with approximate density of 2.5-3 beads per square micrometer. We used these stacks to calculate two consecutive corrections. First, a rigid translational correction accounting for the x and y displacement of one color channel with respect to another was performed. Maximum projection images of beads in two separate channels were aligned using subpixel registration (Guizar-Sicairos et al., 2008). Second, a non-rigid "deformation" within the field of view was performed using Gaussian-fitted positions of beads. We used a point-based registration of 32x32 cells containing a B-spline grid (Rueckert et al., 1999) (http://www.mathworks.com/matlabcentral/fileexchange/20057-b-spline-grid--image-and-point-based-registration), which allows correcting chromatic aberrations with an average error of about 10 nm for the described bead density. The coordinates of all trajectories in one channel were registered using transformations obtained from this calibration.

Filtering of directional vesicle movements

Extraction of segments of persistent directional movement from the trajectories of Rab6 vesicles was performed using directional autocorrelation. First, an array of instant velocity vectors was generated as a difference between two positions of a vesicle in two consecutive frames divided by the time between frames. A cosine of the angle between two consecutive velocity vectors was used as a directional correlation measure. For every trajectory we filtered segments where its value was above defined threshold. To find runs we used the lower threshold value of 0.6, corresponding to approximately 100° cone looking in the direction of movement. Only runs longer than 0.5 seconds were taken into account. To determine "outward" or "inward" direction of runs we calculated the angle between the average velocity vector and the vector drawn from the center of the Golgi to the average coordinate position of a run. If the absolute value of angle was below or equal to 90°, the run was considered to be directed "outwards", otherwise it was considered as an "inward" movement. For the calculation of "projected distance" in two-color imaging between the Rab6A and KIF13B/PAUF signal we used only segments the segments with directional motion, which were filtered in the same manner.

References

Arpag, G., S. Shastry, W.O. Hancock, and E. Tuzel. 2014. Transport by populations of fast and slow kinesins uncovers novel family-dependent motor characteristics important for in vivo function. *Biophysical journal*. 107:1896-1904.

Astanina, K., and R. Jacob. 2010. KIF5C, a kinesin motor involved in apical trafficking of MDCK cells. *Cellular and molecular life sciences : CMLS*. 67:1331-1342.

Bergbrede, T., N. Chuky, S. Schoebel, W. Blankenfeldt, M. Geyer, E. Fuchs, R.S. Goody, F. Barr, and K. Alexandrov. 2009. Biophysical analysis of the interaction of Rab6a GTPase with its effector domains. *The Journal of biological chemistry*. 284:2628-2635.

Bohl, J., N. Brimer, C. Lyons, and S.B. Vande Pol. 2007. The stardust family protein MPP7 forms a tripartite complex with LIN7 and DLG1 that regulates the stability and localization of DLG1 to cell junctions. *The Journal of biological chemistry*. 282:9392-9400.

Burgo, A., V. Proux-Gillardeaux, E. Sotirakis, P. Bun, A. Casano, A. Verraes, R.K. Liem, E. Formstecher, M. Coppey-Moisan, and T. Galli. 2012. A molecular network for the transport of the TI-VAMP/VAMP7 vesicles from cell center to periphery. *Developmental cell*. 23:166-180.

Carleton, M., M. Mao, M. Biery, P. Warrener, S. Kim, C. Buser, C.G. Marshall, C. Fernandes, J. Annis, and P.S. Linsley. 2006. RNA interference-mediated silencing of mitotic kinesin KIF14 disrupts cell cycle progression and induces cytokinesis failure. *Molecular and cellular biology*. 26:3853-3863.

Chavrier, P., R.G. Parton, H.P. Hauri, K. Simons, and M. Zerial. 1990. Localization of low molecular weight GTP binding proteins to exocytic and endocytic compartments. *Cell*. 62:317-329.

Delevoye, C., S. Miserey-Lenkei, G. Montagnac, F. Gilles-Marsens, P. Paul-Gilloteaux, F. Giordano, F. Waharte, M.S. Marks, B. Goud, and G. Raposo. 2014. Recycling endosome tubule morphogenesis from sorting endosomes requires the kinesin motor KIF13A. *Cell reports*. 6:445-454.

Ferenz, N.P., A. Gable, and P. Wadsworth. 2010. Mitotic functions of kinesin-5. *Seminars in cell & developmental biology*. 21:255-259.

Girod, A., B. Storrie, J.C. Simpson, L. Johannes, B. Goud, L.M. Roberts, J.M. Lord, T. Nilsson, and R. Pepperkok. 1999. Evidence for a COP-I-independent transport route from the Golgi complex to the endoplasmic reticulum. *Nature cell biology*. 1:423-430.

Grigoriev, I., D. Splinter, N. Keijzer, P.S. Wulf, J. Demmers, T. Ohtsuka, M. Modesti, I.V. Maly, F. Grosveld, C.C. Hoogenraad, and A. Akhmanova. 2007. Rab6 regulates transport and targeting of exocytotic carriers. *Developmental cell*. 13:305-314.

Grigoriev, I., K.L. Yu, E. Martinez-Sanchez, A. Serra-Marques, I. Smal, E. Meijering, J. Demmers, J. Peranen, R.J. Pasterkamp, P. van der Sluijs, C.C. Hoogenraad, and A. Akhmanova. 2011. Rab6, Rab8, and MICAL3 cooperate in controlling docking and fusion of exocytotic carriers. *Current biology : CB*. 21:967-974.

Gross, S.P. 2004. Hither and yon: a review of bi-directional microtubule-based transport. *Physical biology*. 1:R1-11.

Grosshans, B.L., D. Ortiz, and P. Novick. 2006. Rabs and their effectors: achieving specificity in membrane traffic. *Proceedings of the National Academy of Sciences of the United States of America*. 103:11821-11827.

Gruneberg, U., R. Neef, X. Li, E.H. Chan, R.B. Chalamalasetty, E.A. Nigg, and F.A. Barr. 2006. KIF14 and citron kinase act together to promote efficient cytokinesis. *The Journal of cell biology*. 172:363-372.

Guizar-Sicairos, M., S.T. Thurman, and J.R. Fienup. 2008. Efficient subpixel image registration algorithms. *Optics letters*. 33:156-158.

Hanada, T., L. Lin, E.V. Tibaldi, E.L. Reinherz, and A.H. Chishti. 2000. GAKIN, a novel kinesin-like protein associates with the human homologue of the Drosophila discs large tumor suppressor in T lymphocytes. *The Journal of biological chemistry*. 275:28774-28784.

Hirokawa, N., Y. Noda, Y. Tanaka, and S. Niwa. 2009. Kinesin superfamily motor proteins and intracellular transport. *Nature reviews. Molecular cell biology*. 10:682-696.

Hoeprich, G.J., A.R. Thompson, D.P. McVicker, W.O. Hancock, and C.L. Berger. 2014. Kinesin's neck-linker determines its ability to navigate obstacles on the microtubule surface. *Biophysical journal*. 106:1691-1700.

Horiguchi, K., T. Hanada, Y. Fukui, and A.H. Chishti. 2006. Transport of PIP3 by GAKIN, a kinesin-3 family protein, regulates neuronal cell polarity. *The Journal of cell biology*. 174:425-436.

Huckaba, T.M., A. Gennerich, J.E. Wilhelm, A.H. Chishti, and R.D. Vale. 2011. Kinesin-73 is a processive motor that localizes to Rab5-containing organelles. *The Journal of biological chemistry*. 286:7457-7467.

Hutagalung, A.H., and P.J. Novick. 2011. Role of Rab GTPases in membrane traffic and cell physiology. *Physiological reviews*. 91:119-149.

Jasmin, B.J., B. Goud, G. Camus, and J. Cartaud. 1992. The low molecular weight guanosine triphosphate-binding protein Rab6p associates with distinct post-Golgi vesicles in Torpedo marmorata electrocytes. *Neuroscience*. 49:849-855.

Jaulin, F., X. Xue, E. Rodriguez-Boulan, and G. Kreitzer. 2007. Polarization-dependent selective transport to the apical membrane by KIF5B in MDCK cells. *Developmental cell*. 13:511-522.

Jenkins, B., H. Decker, M. Bentley, J. Luisi, and G. Banker. 2012. A novel split kinesin assay identifies motor proteins that interact with distinct vesicle populations. *The Journal of cell biology*. 198:749-761.

Jiang, K., S. Hua, R. Mohan, I. Grigoriev, K.W. Yau, Q. Liu, E.A. Katrukha, A.F. Altelaar, A.J. Heck, C.C. Hoogenraad, and A. Akhmanova. 2014. Microtubule minus-end stabilization by polymerization-driven CAMSAP deposition. *Developmental cell*. 28:295-309.

Kanai, Y., D. Wang, and N. Hirokawa. 2014. KIF13B enhances the endocytosis of LRP1 by recruiting LRP1 to caveolae. *The Journal of cell biology*. 204:395-408.

Kramarcy, N.R., A. Vidal, S.C. Froehner, and R. Sealock. 1994. Association of utrophin and multiple dystrophin short forms with the mammalian M(r) 58,000 dystrophin-associated protein (syntrophin). *The Journal of biological chemistry*. 269:2870-2876.

Lee, S., S. Fan, O. Makarova, S. Straight, and B. Margolis. 2002. A novel and conserved protein-protein interaction domain of mammalian Lin-2/CASK binds and recruits SAP97 to the lateral surface of epithelia. *Molecular and cellular biology*. 22:1778-1791.

Lu, M.S., and K.E. Prehoda. 2013. A NudE/14-3-3 pathway coordinates dynein and the kinesin Khc73 to position the mitotic spindle. *Developmental cell*. 26:369-380.

Martinez, O., C. Antony, G. Pehau-Arnaudet, E.G. Berger, J. Salamero, and B. Goud. 1997. GTP-bound forms of rab6 induce the redistribution of Golgi proteins into the endoplasmic reticulum. *Proceedings of the National Academy of Sciences of the United States of America*. 94:1828-1833.

Martinez, O., A. Schmidt, J. Salamero, B. Hoflack, M. Roa, and B. Goud. 1994. The small GTP-binding protein rab6 functions in intra-Golgi transport. *The Journal of cell biology*. 127:1575-1588.

Matanis, T., A. Akhmanova, P. Wulf, E. Del Nery, T. Weide, T. Stepanova, N. Galjart, F. Grosveld, B. Goud, C.I. De Zeeuw, A. Barnekow, and C.C. Hoogenraad. 2002. Bicaudal-D regulates COPI-independent Golgi-ER transport by recruiting the dynein-dynactin motor complex. *Nature cell biology*. 4:986-992.

Meijering, E., O. Dzyubachyk, and I. Smal. 2012. Methods for cell and particle tracking. *Methods in enzymology*. 504:183-200.

Moleirinho, S., W. Guerrant, and J.L. Kissil. 2014. The Angiomotins--from discovery to function. *FEBS letters*. 588:2693-2703.

Nakagawa, T., M. Setou, D. Seog, K. Ogasawara, N. Dohmae, K. Takio, and N. Hirokawa. 2000. A novel motor, KIF13A, transports mannose-6-phosphate receptor to plasma membrane through direct interaction with AP-1 complex. *Cell*. 103:569-581.

Neubrand, V.E., F. Cesca, F. Benfenati, and G. Schiavo. 2012. Kidins220/ARMS as a functional mediator of multiple receptor signalling pathways. *Journal of cell science*. 125:1845-1854.

Norris, S.R., V. Soppina, A.S. Dizaji, K.I. Schimert, D. Sept, D. Cai, S. Sivaramakrishnan, and K.J. Verhey. 2014. A method for multiprotein assembly in cells reveals independent action of kinesins in complex. *The Journal of cell biology*. 207:393-406.

Peters, M.F., M.E. Adams, and S.C. Froehner. 1997. Differential association of syntrophin pairs with the dystrophin complex. *The Journal of cell biology*. 138:81-93.

Rueckert, D., L.I. Sonoda, C. Hayes, D.L. Hill, M.O. Leach, and D.J. Hawkes. 1999. Nonrigid registration using free-form deformations: application to breast MR images. *IEEE transactions on medical imaging*. 18:712-721.

Schindelin, J., I. Arganda-Carreras, E. Frise, V. Kaynig, M. Longair, T. Pietzsch, S. Preibisch, C. Rueden, S. Saalfeld, B. Schmid, J.Y. Tinevez, D.J. White, V. Hartenstein, K. Eliceiri, P. Tomancak, and A. Cardona. 2012. Fiji: an open-source platform for biological-image analysis. *Nature methods*. 9:676-682.

Schlager, M.A., L.C. Kapitein, I. Grigoriev, G.M. Burzynski, P.S. Wulf, N. Keijzer, E. de Graaff, M. Fukuda, I.T. Shepherd, A. Akhmanova, and C.C. Hoogenraad. 2010. Pericentrosomal targeting of Rab6 secretory vesicles by Bicaudal-D-related protein 1 (BICDR-1) regulates neuritogenesis. *The EMBO journal*. 29:1637-1651.

Schlager, M.A., A. Serra-Marques, I. Grigoriev, L.F. Gumy, M. Esteves da Silva, P.S. Wulf, A. Akhmanova, and C.C. Hoogenraad. 2014. Bicaudal d family adaptor proteins control the velocity of Dynein-based movements. *Cell reports*. 8:1248-1256.

Short, B., C. Preisinger, J. Schaletzky, R. Kopajtich, and F.A. Barr. 2002. The Rab6 GTPase regulates recruitment of the dynactin complex to Golgi membranes. *Current biology: CB*. 12:1792-1795.

Skoufias, D.A., S. DeBonis, Y. Saoudi, L. Lebeau, I. Crevel, R. Cross, R.H. Wade, D. Hackney, and F. Kozielski. 2006. S-trityl-L-cysteine is a reversible, tight binding inhibitor of the human kinesin Eg5 that specifically blocks mitotic progression. *The Journal of biological chemistry*. 281:17559-17569.

Soppina, V., S.R. Norris, A.S. Dizaji, M. Kortus, S. Veatch, M. Peckham, and K.J. Verhey. 2014. Dimerization of mammalian kinesin-3 motors results in superprocessive motion. *Proceedings of the National Academy of Sciences of the United States of America*. 111:5562-5567.

Splinter, D., D.S. Razafsky, M.A. Schlager, A. Serra-Marques, I. Grigoriev, J. Demmers, N. Keijzer, K. Jiang, I. Poser, A.A. Hyman, C.C. Hoogenraad, S.J. King, and A. Akhmanova. 2012. BICD2, dynactin, and LIS1 cooperate in regulating dynein recruitment to cellular structures. *Molecular biology of the cell*. 23:4226-4241.

Utskarpen, A., H.H. Slagsvold, T.G. Iversen, S. Walchli, and K. Sandvig. 2006. Transport of ricin from endosomes to the Golgi apparatus is regulated by Rab6A and Rab6A'. *Traffic*. 7:663-672.

Venkateswarlu, K., T. Hanada, and A.H. Chishti. 2005. Centaurin-alpha1 interacts directly with kinesin motor protein KIF13B. *Journal of cell science*. 118:2471-2484.

Wakana, Y., J. van Galen, F. Meissner, M. Scarpa, R.S. Polishchuk, M. Mann, and V. Malhotra. 2012. A new class of carriers that transport selective cargo from the trans Golgi network to the cell surface. *The EMBO journal*. 31:3976-3990.

Wakana, Y., J. Villeneuve, J. van Galen, D. Cruz-Garcia, M. Tagaya, and V. Malhotra. 2013. Kinesin-5/Eg5 is important for transport of CARTS from the trans-Golgi network to the cell surface. *The Journal of cell biology*. 202:241-250.

Wanschers, B., R. van de Vorstenbosch, M. Wijers, B. Wieringa, S.M. King, and J. Fransen. 2008. Rab6 family proteins interact with the dynein light chain protein DYNLRB1. *Cell motility and the cytoskeleton*. 65:183-196.

White, J., L. Johannes, F. Mallard, A. Girod, S. Grill, S. Reinsch, P. Keller, B. Tzschaschel, A. Echard, B. Goud, and E.H. Stelzer. 1999. Rab6 coordinates a novel Golgi to ER retrograde transport pathway in live cells. *The Journal of cell biology*. 147:743-760.

Yamada, K.H., T. Hanada, and A.H. Chishti. 2007. The effector domain of human Dlg tumor suppressor acts as a switch that relieves autoinhibition of kinesin-3 motor GAKIN/KIF13B. *Biochemistry*. 46:10039-10045.

Yamada, K.H., Y. Nakajima, M. Geyer, K.K. Wary, M. Ushio-Fukai, Y. Komarova, and A.B. Malik. 2014. KIF13B regulates angiogenesis through Golgi to plasma membrane trafficking of VEGFR2. *Journal of cell science*. 127:4518-4530.

Yamada, M., K. Kumamoto, S. Mikuni, Y. Arai, M. Kinjo, T. Nagai, Y. Tsukasaki, T.M. Watanabe, M. Fukui, M. Jin, S. Toba, and S. Hirotsune. 2013. Rab6a releases LIS1 from a dynein idling complex and activates dynein for retrograde movement. *Nature communications*. 4:2033.

Yau, K.W., S.F. van Beuningen, I. Cunha-Ferreira, B.M. Cloin, E.Y. van Battum, L. Will, P. Schatzle, R.P. Tas, J. van Krugten, E.A. Katrukha, K. Jiang, P.S. Wulf, M. Mikhaylova, M. Harterink, R.J. Pasterkamp, A. Akhmanova, L.C. Kapitein, and C.C. Hoogenraad. 2014. Microtubule minus-end binding protein CAMSAP2 controls axon specification and dendrite development. *Neuron*. 82:1058-1073.

Young, J., T. Stauber, E. del Nery, I. Vernos, R. Pepperkok, and T. Nilsson. 2005. Regulation of microtubule-dependent recycling at the trans-Golgi network by Rab6A and Rab6A'. *Molecular biology of the cell*. 16:162-177.

5

KIDINS220 links KIF13B to the Dystrophin Associated Protein Complex

Andrea Serra-Marques[1], Cátia Frias[1], Casper Hoogenraad[1] and Anna Akhmanova[1]

[1] Cell Biology, Faculty of Science, Utrecht University, Utrecht, The Netherlands.

Abstract

Eukaryotic cells contain a broad variety of motor proteins, which can transport different organelles, vesicles and macromolecular complexes along cytoskeletal filaments and thus ensure their proper subcellular distribution. The connections between motors and cargos are complex: transport of each cargo is the result of collective activity of different motors, while the same molecular motor can be involved in movement of multiple types of cargo. Here we focus on how a member of kinesin-3 family, KIF13B, is connected to Dystrophin Associated Protein Complex (DAPC), a large transmembrane assembly involved in linking the cytoskeleton to the extracellular matrix (ECM) in muscles and other tissues. We find that the connections are mediated by an adaptor molecule KIDINS220 (Kinase D-Interacting Substrate of 220 kDa), but also likely involve the direct interaction between DAPC and KIF13B. Our previous work showed that KIF13B is present on exocytotic vesicles positive for the small GTPase Rab6, and here we show that in cultured cells, DAPC is localized to the cortical sites where the complexes responsible for the tethering and docking of Rab6 vesicles to the plasma membrane are located. We conclude that KIF13B and KIDINS220 likely form a part of a vesicular trafficking route for delivery and concentration of DAPC at specific cortical sites that might be important for the organization of cell-ECM adhesions, podosomes and synaptic sites in muscles and neurons.

Introduction

Vesicle trafficking is an essential cellular process responsible for the correct delivery of cellular components to specific sites in the cell or to the extracellular space. Molecular motors, the actin and the microtubule cytoskeletons are major players in this process. The myosin family of proteins moves along actin filaments, while the transport powered by kinesins and dyneins occurs along microtubules. Most kinesins transport cargo towards microtubule plus ends, while the transport in the minus-end direction is mainly performed by dynein (Hirokawa et al., 2009; Vale, 2003). Specific kinesins have been implicated in the transport of membrane organelles or messenger RNAs (mRNAs), positioning of organelles such as the endoplasmic reticulum and the organization of the mitotic spindle (Gumy et al., 2014; Hirokawa and Noda, 2008; Hirokawa et al., 2009). However, we still lack a full description of the motor proteins involved in the transport of any specific organelle or vesicle type; conversely, we do not have a complete list of cargos associated with any particular kinesin.

We have recently identified KIF13B, a kinesin-3 family member, as one of the kinesins involved in the transport of constitutive exocytotic carriers (Serra-Marques et al., in preparation). KIF13B was first identified in lymphocytes under the name GAKIN (Guanylate Kinase Associated Kinesin) (Hanada et al., 2000). It has been reported to participate in the establishment of mitotic spindle orientation in *Drosophila* (Lu and Prehoda, 2013; Siegrist and Doe, 2005) and to mediate the anterograde transport of VEGF receptor during angiogenesis (Yamada et al., 2014). Additionally, KIF13B is responsible for the transport of TRPV1 (Transient Receptor Potential Vanilloid 1) from the Golgi to the plasma membrane of sensory neurons (Xing et al., 2012). In hippocampal neurons, it is responsible for the transport of PIP3-containing vesicles along the axon and regulation of the establishment of neuronal polarity (Horiguchi et al., 2006). Recent work shows that KIF13B can also translocate into dendrites and transport specific dendritic cargo (Huang and Banker, 2012; Jenkins et al., 2012). KIF13B has also been implicated in the transport and endocytosis of LRP1 (low-density lipoprotein (LDL) Receptor–related Protein 1) (Kanai et al., 2014).

KIF13B comprises an N-terminal motor domain, an FHA (Forkhead-Associated) domain, a MAGUK Binding Stalk (MBS), a CAP-Gly domain and several predicted coiled coils. The C-terminal region containing coiled coils mediates the binding to utrophin (Kanai et al., 2014), a protein which forms part of the Dystrophin Associated Protein Complex (DAPC). The DAPC has been extensively studied in muscle cells, where it is essential for the stability of the muscle fiber by forming connections between the extracellular matrix (ECM) and the actin cytoskeleton (Ervasti and Campbell, 1993; Haenggi and Fritschy, 2006). Recently, this complex has also been shown to participate in microtubule organization (Belanto et al., 2014). This large assembly is comprised of multiple proteins, including dystrophin, the protein absent in patients with Duchenne muscular dystrophy (Hoffman et al., 1987), or utrophin, the autosomal homologue of dystrophin. These large proteins associate with multiple families of proteins, including dystroglycans, syntrophins and dystrobrevins, working as a scaffold and a signaling complex. The DACP is also expressed in non-muscle cells, including the nervous system and tissues with a secretory function, where utrophin and small isoforms of dystrophin are normally predominantly expressed (Haenggi and Fritschy, 2006).

In a previous study aiming to find KIF13B binding partners responsible for the recruitment of KIF13B to Rab6-positive exocytotic carriers (Serra-Marques et al., in preparation), we have performed mass spectrometry analysis of KIF13B -associated proteins and identified utrophin as an interactor of KIF13B, as previously reported (Kanai et al., 2014). In the same analysis, we identified KIDINS220 (Kinase D-Interacting Substrate of 220 kDa), also known as ARMS (Ankyrin Repeat-rich Membrane Spanning protein) as a new binding partner of KIF13B (Serra-Marques et al., in preparation). KIDINS220 was first identified as a kinase-D substrate in the PC12 neuronal cell line. It is a downstream effector for neurotrophin and ephrin tyrosine kinase receptors (Iglesias et al., 2000; Kong et al., 2001) and a platform for sustained MAP kinase signaling by neurotrophins (Arevalo et al., 2006; Arevalo et al., 2004).

KIDINS220 is a transmembrane protein containing four transmembrane regions and several domains that mediate interaction with multiple binding partners (Neubrand et al., 2012). The cytoplasmic N-terminal domain of KIDINS220 contains 11 Ankyrin repeats, which mediate the binding to the RhoGEF Trio, inducing activation of Rac1 and promoting neurite outgrowth (Neubrand et al., 2010). This region also binds to SCG10 and SCLIP (SCG10-like protein) (Higuero et al., 2010), members of the Stathmin family of proteins that bind to tubulin in a phospho-dependent manner (Chauvin and Sobel, 2014). Interestingly, other microtubule-associated proteins, such as MAP1a, MAP1b and MAP2, also bind to the C-terminus of KIDINS220/ARMS (Higuero et al., 2010). KIDINS220 has been shown to regulate the phosphorylation of these different MAPs known to control neuronal morphogenesis, supporting a role for KIDINS220 in neuronal polarity and development (Higuero et al., 2010; Poulain and Sobel, 2010). The kinesin-1 motor protein has been shown to bind to the kinesin light chain (KLC)-interacting motif (KIM) of KIDINS220 and implicated in the transport of KIDINS220 to neurite tips in PC12 cells (Bracale et al., 2007). Furthermore, KIDINS220 has also been implicated in regulation of dendritic branching and spine stability in mouse hippocampal neurons (Wu et al., 2009). Interestingly, the PDZ domain of KIDINS220 binds to the DAPC protein α1-syntrophin (Luo et al., 2005), which in concert with other DAPC proteins has been detected in postsynaptic density preparations (Haenggi and Fritschy, 2006).

In this work, we sought to explore the connection between KIF13B, KIDINS220 and the DAPC identified in our KIF13B interactome mass spectrometry analysis. We show that the cytoplasmic domains of KIDINS220 mediate its binding to KIF13B. Additionally, we also investigated whether KIF13B could bind DAPC proteins other than utrophin. Our results suggest that the DAPC proteins identified in our mass spectrometry-based analysis of KIF13B interactome are connected to KIF13B through utrophin and KIDINS220. Additionally, we provide evidence for the presence of the DAPC in specific cortical structures located in proximity of focal adhesions, and discuss a possible role for the KIF13B-DAPC association in podosomes, specialized organelles involved in the attachment and degradation of ECM. Finally, we demonstrate that KIF13B and Rab6-positive vesicles localize to the tips of neurites and to dendrites in hippocampal neurons, suggesting a possible role in dendritic transport. With these preliminary data, we discuss and propose future experiments to be performed in neurons, where KIF13B-KIDINS220 interaction may play a role in the delivery of DAPC into neurites.

Results and Discussion

KIDINS220 binds to KIF13B through the N- and C- terminus

In our previous mass spectrometry analysis of KIF13B interactome, we identified and characterized KIDINS220 as a direct binding partner of KIF13B (Serra-Marques et al., in preparation). In order to better understand how KIDINS220 interacts with KIF13B, we designed BioGFP-KIDINS220 deletion constructs (Fig. 1A) and analyzed their binding to a KIF13B deletion mutant used for the mass spectrometry analysis (GFP-KIF13B C2; Fig. 1B) by performing streptavidin pull down assays (Fig. 1C). As expected, no binding was found between the transmembrane domains of KIDINS220 and KIF13B (Figure 1C, lane 10, 11, 12). A weak binding was observed between the C-terminus (BioGFP-KIDINS220-C) and N-terminus (BioGFP-KIDINS220/ARMS-N) (Figure 1C, lanes 8,9) of KIDINS220 and GFP-KIF13B-C2, suggesting that both regions might be required for efficient binding to KIF13B. Previous reports have shown that the KIM domain of KIDINS220, present at the C-terminal region of the protein, mediates the binding to kinesin-1. Our results now show that both the C- and N-terminal regions of KIDINS220 might be required for the binding to another kinesin. It would be interesting to finely map the region of KIF13B which is necessary and sufficient for binding to KIDINS220 and perform experiments to understand if both C- and N- terminal regions of KIDINS220 bind to the same domain of KIF13B.

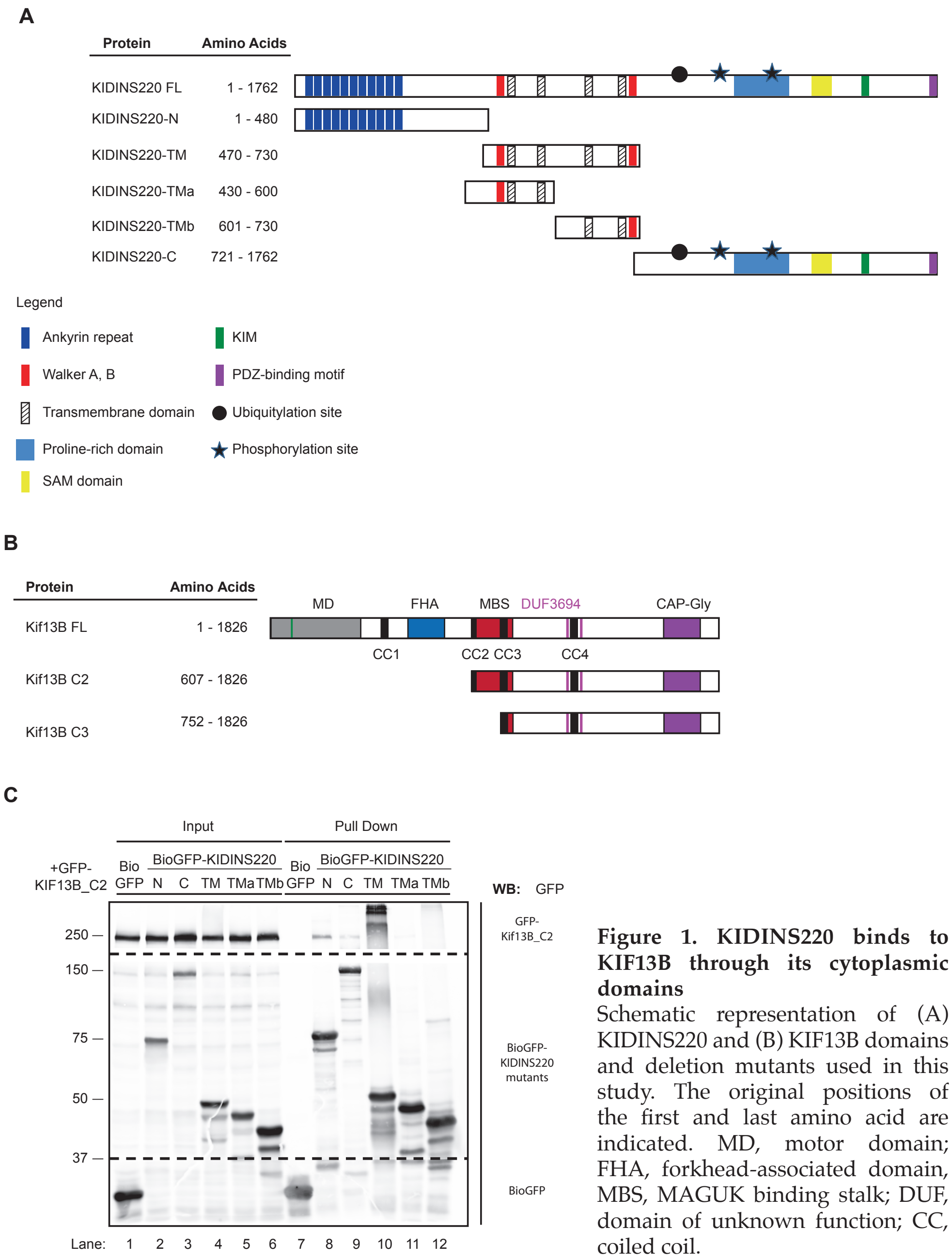
A
Protein
Amino Acids
KIDINS220 FL
1 - 1762
KIDINS220-N
1 - 480
KIDINS220-TM
470 - 730
KIDINS220-TMa
430 - 600
KIDINS220-TMb
601 - 730
KIDINS220-C
721 - 1762
Legend
Ankyrin repeat
Walker A, B
Transmembrane domain
Proline-rich domain
SAM domain
KIM
PDZ-binding motif
Ubiquitylation site
Phosphorylation site
B
Protein
Amino Acids
Kif13B FL
1 - 1826
Kif13B C2
607 - 1826
Kif13B C3
752 - 1826
MD
FHA
MBS
DUF3694
CAP-Gly
CC1
CC2 CC3
CC4
C
Input
Pull Down
+GFP-KIF13B_C2
Bio GFP
BioGFP-KIDINS220
N C TM TMa TMb
Bio GFP
BioGFP-KIDINS220
N C TM TMa TMb
WB: GFP
250 —
150 —
75 —
50 —
37 —
GFP-Kif13B_C2
BioGFP-KIDINS220 mutants
BioGFP
Lane: 1 2 3 4 5 6 7 8 9 10 11 12

Figure 1. KIDINS220 binds to KIF13B through its cytoplasmic domains
Schematic representation of (A) KIDINS220 and (B) KIF13B domains and deletion mutants used in this study. The original positions of the first and last amino acid are indicated. MD, motor domain; FHA, forkhead-associated domain, MBS, MAGUK binding stalk; DUF, domain of unknown function; CC, coiled coil. (C) Streptavidin pull-down assays from extracts of HEK293T cells coexpressing BirA, GFP-KIF13B-C2 and BioGFP or the indicated BioGFP-KIIDINS220 mutants. BioGFP and GFP-tagged proteins were detected with anti-GFP antibodies. 2.5% of the input and 10% of the precipitate was loaded on gel.

KIDINS220 binds the DAPC and mediates the link to KIF13B

In our previous mass spectrometry analysis of KIF13B interactome, we identified utrophin and other proteins from the DAPC (namely α1-syntrophin and α1-dystrobrevin) as potential KIF13B partners (Chapter 4, Table 1). As the interaction between the N-terminus of utrophin and the C-terminal part of KIF13B has been recently validated by Kanai and colleagues (Kanai et al., 2014), we tested the binding between KIF13B and the proteins α1-syntrophin and α1-dystrobrevin. HEK293T cells were transfected with BioGFP-α1-syntrophin or BioGFP-α1-dystrobrevin and different GFP-KIF13B (C2 or C3) deletion mutants, followed by streptavidin pull down assays. As shown in Fig. 2A, both KIF13B deletion mutants could bind to Bio-GFP-α1-syntrophin and Bio-GFP-α1-dystrobrevin, but the interaction was weak (Fig. 2A, compare lanes 9, 10, 11, 12). This result suggests that the interaction is indirect. Previous studies have shown that the PDZ domain of KIDINS220 mediates binding to α1-syntrophin (Luo et al., 2005). To confirm this interaction, we transfected cells with BioGFP-α1-dystrobrevin, BioGFP-α1-syntrophin or BioGFP-β2-syntrophin (another protein from the same complex detected by the mass spectrometry analysis) and HA-KIDINS220, and performed streptavidin pull downs (Figure 2B). We observed that all proteins bind HA-KIDINS220, with the strongest interaction mediated by α1-syntrophin (Figure 2B, lane 7), in line with the previous observations. These results suggest that α1-syntrophin and α1-dystrobrevin are connected to KIF13B through their direct binding to utrophin and/or KIDINS220. Since the GFP-KIF13B-C3 deletion mutant does not contain the MBS, we can predict that this domain is not essential for this interaction. According to Kanai and colleagues (Kanai et al., 2014), utrophin binds to a C-terminal region of KIF13B that does not include the MBS. Taken together, our data suggest that KIF13B, KIDINS220 and DAPC can form a complex that is held together by multiple interactions.

Proteins from the Dystrophin Associated Protein Complex are localized in patches at the cell cortex

To get insight into the potential function of the link between the DAPC and KIF13B, we first analyzed the distribution of DAPC subunits found in our KIF13B interactome in HeLa cells, either by antibody immunostaining or overexpression of fluorescently tagged proteins. Antibody staining of utrophin showed a plasma membrane and peripheral cytoplasmic localization, as depicted in Figure 3A (1 and 2). Overexpression of α1-syntrophin and α1-dystrobrevin showed a similar distribution (Fig. 3B), which was expected, as several studies showed that all DAPC subunits are required for the proper localization of the others (Bhat et al., 2013). These results suggest that these proteins might localize to the same sites as LL5β and ELKS, known cortical proteins important for microtubule stabilization and fusion of Rab6-positive exocytotic carriers with the

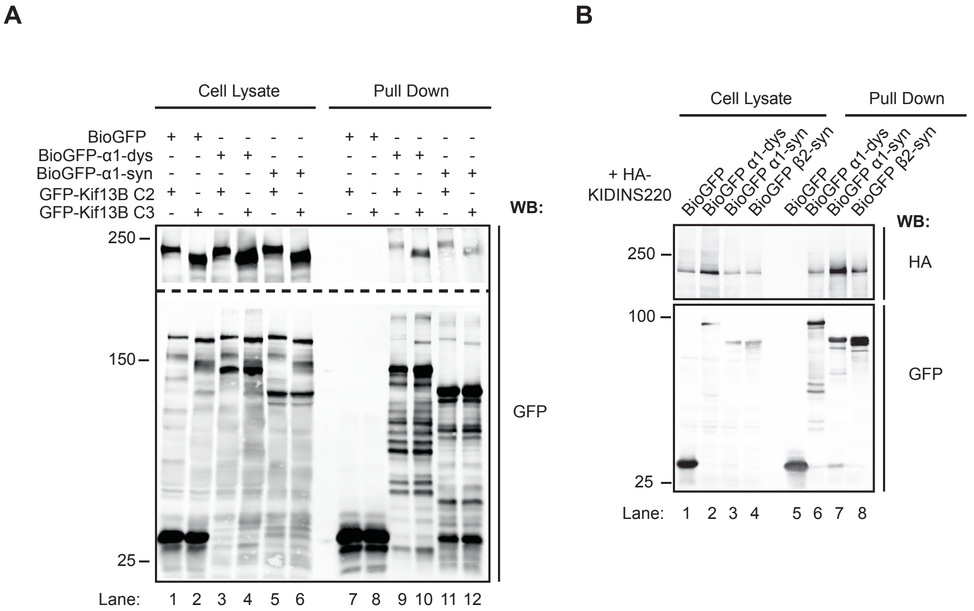
A
Cell Lysate
Pull Down
BioGFP + + - - - - + + - - - -
BioGFP-α1-dys - - + + - - - - + + - -
BioGFP-α1-syn - - - - + + - - - - + +
GFP-Kif13B C2 + - + - + - + - + - + -
GFP-Kif13B C3 - + - + - + - + - + - +
WB:
250
150
25
GFP
Lane: 1 2 3 4 5 6 7 8 9 10 11 12
B
Cell Lysate
Pull Down
+ HA-KIDINS220
BioGFP
BioGFP α1-dys
BioGFP α1-syn
BioGFP β2-syn
BioGFP
BioGFP α1-dys
BioGFP α1-syn
BioGFP β2-syn
WB:
250
HA
100
GFP
25
Lane: 1 2 3 4 5 6 7 8

Figure 2. KIDINS220 binds the DAPC and mediates the link to KIF13B
(A) Streptavidin pull-down assays from extracts of HEK293T cells coexpressing BirA, BioGFP or the indicated BioGFP proteins and the indicated GFP-KIF13B mutants. All proteins were detected with anti-GFP antibodies. 2.5% of the input and 10% of the precipitate was loaded on gel.
(B) Streptavidin pull-down assays from extracts of HEK293T cells coexpressing BirA, BioGFP or the indicated BioGFP proteins and HA-KIDINS220. BioGFP-tagged proteins were detected with anti-GFP antibodies and HA-KIDINS220 was detected with anti-HA antibodies. 2.5% of the input and 10% of the precipitate was loaded on gel.

plasma membrane (Grigoriev et al., 2011; Lansbergen et al., 2006). To test this idea, we overexpressed TagRFP-T-ELKS or RFP-LL5β and different GFP-tagged DAPC proteins. As observed in Figure 3C, overexpressed α1-dystrobrevin and α1-syntrophin colocalized with ELKS and LL5β. The same was observed when GFP-β2-syntrophin and TagRFP-T-ELKS were co-transfected. It is interesting to note that α1-syntrophin could also be detected in structures that resemble focal adhesions (or focal adhesion delimiting areas) when expressed at high levels, and in these conditions colocalization with ELKS could not be observed or was strongly reduced (Fig. 3C, a).

Recent studies from our laboratory have shown that the scaffolding proteins liprin-α1 and liprin-β1, LL5β and ELKS are all part of a cortical microtubule attachment complex required for microtubule stabilization (van der Vaart et al., 2013). Moreover, in a search for liprin-α1 binding partners using pull-down assays combined with mass spectrometry (van der Vaart et al., 2013), we identified DAPC components as putative liprin-α1 associated proteins (Fig. 3D). By performing streptavidin pull-down experiments using

BioGFP-β2-syntrophin and HA-tagged liprin-α1 or liprin-β1, we observed that β2-syntrophin could pull down liprin-α1 (Fig. 3E, lane 7) and, to a lower extent, liprin-β1 (Fig. 3E, lane 8). These results provide further evidence for a link between the cortical microtubule attachment complex and the DAPC.

The observed colocalizations argue for a functional overlap between the complexes containing LL5β, liprins and ELKS, the DAPC and KIF13B. Previous work showed that LL5β forms a complex with the microtubule plus end tracking proteins CLASP1/2, contributing to the capture and stabilization of cortical microtubules (Lansbergen et al., 2006). This interaction was also shown to be important to prevent epithelial-to-mesenchymal transition of epiblast cells during chicken embryonic development; in this system, the CLASP-LL5β complex stabilizes basal microtubules and binds to dystroglycan, a DAPC component that regulates the interaction between the microtubule cytoskeleton and the basal membrane (Nakaya et al., 2013). Additionally, LL5β has been reported to be present at the neuromuscular junction, a structure the formation of which also involves dystroglycan function (Peng et al., 1999). LL5β was shown to mediate the anchoring of CLASP2-decorated MT plus tips at the postsynapse, promoting the local transport of vesicles containing Acetylcholine Receptors (AChRs), the most abundant receptors at the postsynaptic membrane (Basu et al., 2015). LL5β was also demonstrated to be one of the key components of postsynaptic podosomes, actin-rich organelles involved in postsynaptic maturation and extracellular matrix remodeling at the AChRs clusters (Kishi et al., 2005; Proszynski et al., 2009). When myotubes are formed, AChRs are organized into a plaque-shaped cluster, which matures into a complex and pretzel-like structure (Sanes and Lichtman, 2001). Importantly, DAPC proteins, including dystroglycan and α-dystrobrevin, have also been implicated in this process (Grady et al., 2003; Jacobson et al., 2001), and evidence has been provided for the presence of dystroglycan at podosomes and for its degradation at the sites of active podosomes (Proszynski et al., 2009; Thompson et al., 2008). Additionally, we have identified angiomotin as a putative binding partner of KIF13 by mass spectrometry analysis (Chapter 4, Table 1), and a protein from the same family, Amotl2, has recently been reported to regulate organization of synaptic podosomes and remodeling of AChRs clusters (Moleirinho et al., 2014; Proszynski and Sanes, 2013). Taken together, these data support a strong functional link between LL5β and DAPC at the cortex.

Here we show that components of the DAPC are present at LL5β-containing cortical microtubule attachment complexes, the preferred sites for Rab6 vesicle fusion (Grigoriev et al., 2007). Moreover, our work showed that KIF13B transports Rab6 vesicles, and is strongly connected to DAPC. It is hence tempting to speculate about a possible function for KIF13B in the targeted transport of Rab6-positive exocytotic vesicles or other carriers to the cortical sites of DAPC accumulation, to promote their formation, maintenance

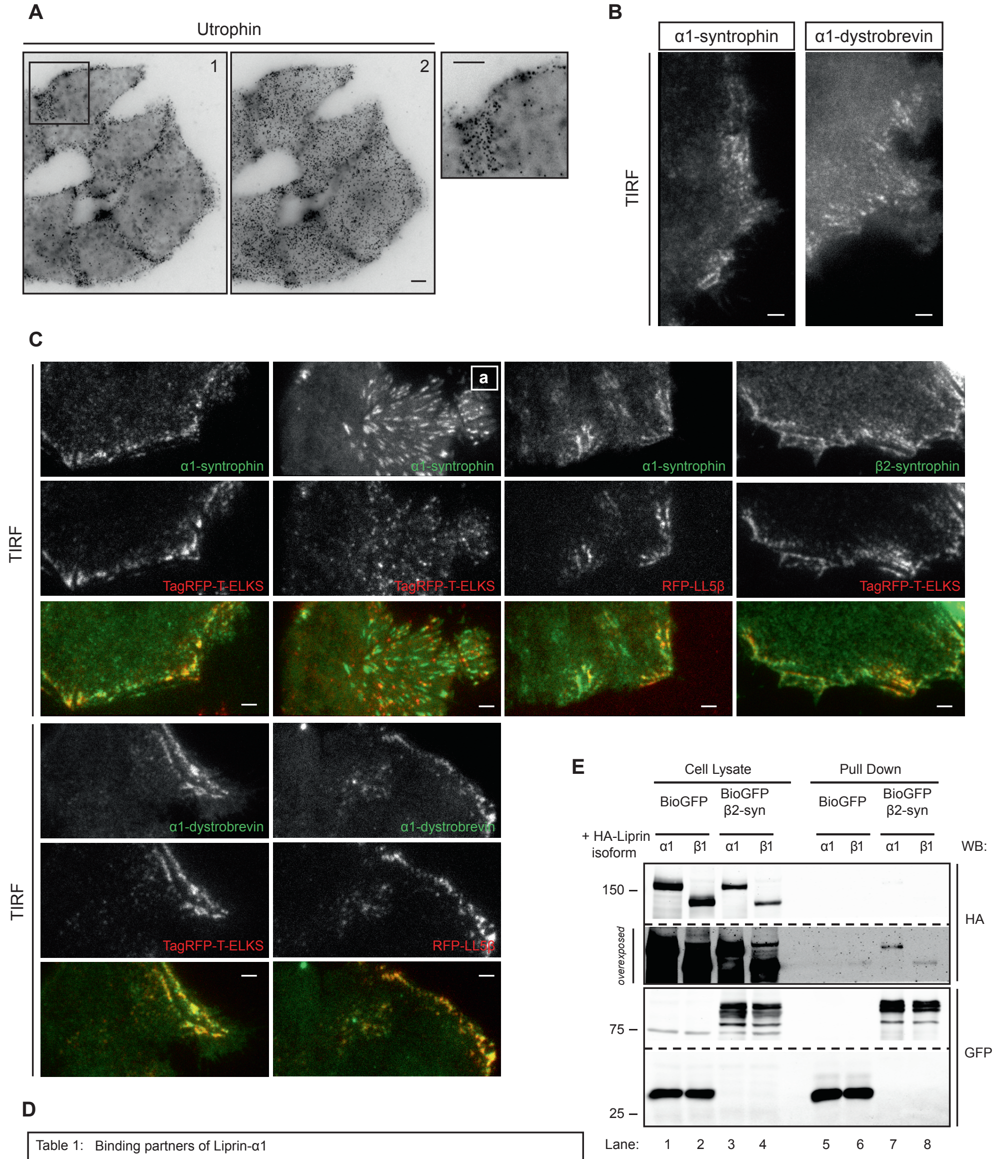
A
Utrophin
1
2
B
α1-syntrophin
α1-dystrobrevin
TIRF
C
TIRF
a
α1-syntrophin
α1-syntrophin
α1-syntrophin
β2-syntrophin
TagRFP-T-ELKS
TagRFP-T-ELKS
RFP-LL5β
TagRFP-T-ELKS
TIRF
α1-dystrobrevin
α1-dystrobrevin
TagRFP-T-ELKS
RFP-LL5β
E
Cell Lysate
Pull Down
BioGFP
BioGFP β2-syn
BioGFP
BioGFP β2-syn
+ HA-Liprin isoform
α1
β1
α1
β1
α1
β1
α1
β1
WB:
150 –
HA
overexposed
75 –
GFP
25 –
Lane:
1
2
3
4
5
6
7
8

D

Table 1: Binding partners of Liprin-α1

		Control			Liprin-α1		
Gene name	**Prot. ID**	**Mascot score**	**Peptides**	**Unique peptides**	**Mascot score**	**Peptides**	**Unique peptides**
PPFIA1	Q13136	0	0	0	3763	565	43
SNTB2	Q13425	0	0	0	417	8	7
DTNB	O60941	0	0	0	172	2	2
DMD	P11532	0	0	0	278	6	5

Figure 3. Dystrophin Associated Protein Complex localizes to cortical patches
(A) Representative image of a HeLa cell stained for the endogenous utrophin (scale bar: 5 μm). 1 and 2 represent different focal planes of the same cell. The inset corresponds to magnified view of the boxed area in 1. Scale bar: 5 μm.

See rest of legend on next page

or dynamics. Podosome formation and maintenance presents an interesting model system where such molecular connections could be tested. Podosomes are present in various cell types, including macrophages, fibroblasts, epithelial cells, dendritic cells and osteoclasts, where they have been implicated in multiple functions, including cell migration, adhesion and bone resorption (Murphy and Courtneidge, 2011; Proszynski and Sanes, 2013). Another kinesin-3 family member, KIF1C, has already been implicated in the regulation of podosome dynamics (Kopp et al., 2006), and our work has shown that KIF1C is also involved in Rab6 vesicle transport (Schlager et al., 2014). It would be interesting to test whether Rab6-dependent delivery of exocytotic cargo by these kinesin-3 family members contributes to podosome function and behavior.

KIF13B and Rab6 localize to the dendrites of hippocampal neurons

KIF13B is highly expressed in neurons, and different studies have described its role in axonal and dendritic transport and in the establishment of neuronal polarity (Horiguchi et al., 2006; Huang and Banker, 2012; Jenkins et al., 2012). To better understand the role of KIF13B in neuronal systems, we overexpressed GFP-KIF13B in hippocampal neurons at stage 2 and analyzed its distribution and the distribution of Rab6-positive vesicles (Fig. 4A). GFP-KIF13B could be detected along and at the tip of neurites of young neurons, at a time when the neuronal polarity is not yet completely established. Rab6 was detected at the same locations, suggesting that KIF13B can be involved in the transport of Rab6-positive vesicles, like we have previously described in non-neuronal cells (Serra-Marques et al., in preparation). Rab6-vesicle transport has been previously implicated in axon outgrowth (Schlager et al., 2010; Schlager et al., 2014), but its relevance in dendrites has never been properly studied. To confirm that Rab6 and KIF13B can be detected in dendrites of hippocampal neurons, we stained endogenous KIF13B and Rab6, but also MAP2, a specific marker of dendrites. We observed that Rab6 and KIF13B are indeed present in MAP2 positive neurites of 4 DIV hippocampal neurons (Fig. 4B). These results indicate that Rab6-vesicles might be as well involved in the transport of dendritic cargos and that KIF13B can be involved in that process. Live imaging of hippocampal neurons coexpressing Rab6 and KIF13B will be necessary to understand if Rab6 cargo can be transported by KIF13B in neurons. It is also important to investigate if there is

(B) HeLa cells were transfected with GFP-α1-syntrophin or GFP-α1-dystrobrevin and imaged by TIRF microscopy. The images correspond to one frame of a movie. Scale bar: 2 μm.

(C) HeLa cells were transfected with the indicated constructs and imaged by TIRF microscopy. The images correspond to one frame of a movie. Scale bar: 2 μm.

(D) Binding partners of HA-liprin-α1 in HEK293 cells identified by mass spectrometry.

(E) Streptavidin pull-down assays from extracts of HEK293T cells coexpressing BirA, BioGFP or BioGFP-β2-syntrophin and the indicated HA-liprin isoforms. BioGFP-tagged proteins were detected with anti-GFP antibodies and HA-liprins were detected with anti-HA antibodies. 2.5% of the input and 10% of the precipitate was loaded on gel.

a functional relevance for the interaction between KIF13B and KIDINS220 in dendritic transport. Previous studies have implicated KIDINS220 in the regulation of dendritic branching and dendrite and axon development (Higuero et al., 2010; Wu et al., 2009) and the DAPC has been associated to important postsynaptic functions in neurons (Haenggi and Fritschy, 2006). Therefore, it will be interesting to further investigate whether the DAPC is functionally related to the activities of KIF13B and KIDINS220 in neuronal systems.

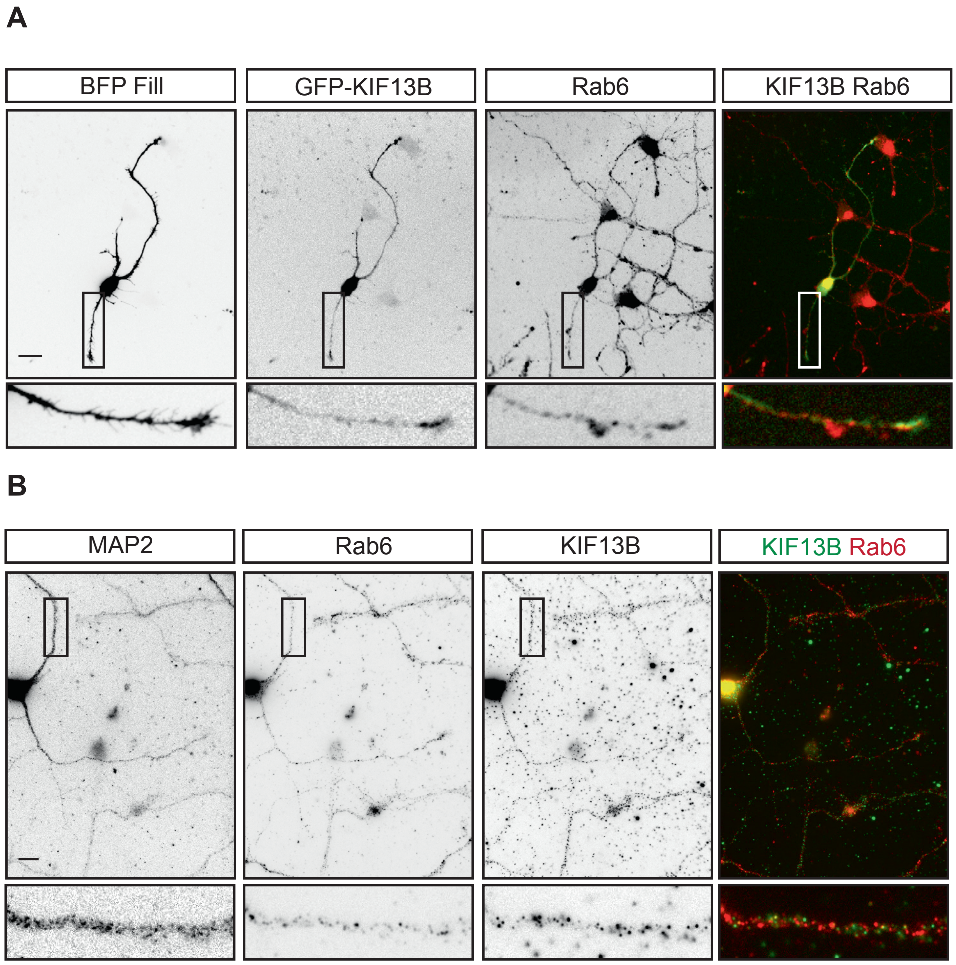

Figure 4. KIF13B and Rab6 localize to the dendrites of hippocampal neurons
(A) Representative images of 2 DIV hippocampal neurons expressing TagBFP and GFP-KIF13B and immunostained for endogenous Rab6. Enlarged boxed areas correspond to a region of a neurite. Scale bar: 10 μm.
(B) Representative images of 4 DIV hippocampal neurons stained for endogenous MAP2, KIF13B and Rab6. Enlarged boxed areas correspond to a dendrite. Scale bar: 10 μm.

Acknowledgements

We thank Dr. Marvin Adams, Dr. Athar Chishti and Dr. Giampietro Schiavo for sharing reagents. We thank Dr. Ines Ferreira and Marta Esteves da Silva for suggestions. This work was supported by Fundação para a Ciência e a Tecnologia fellowship (A.S-M.) and by the Netherlands Organization for Scientific Research (NWO) ALW-VICI grant and the European Research Council (ERC) Synergy grants to A.A.

Experimental procedures

Antibodies and reagents

The following primary and secondary antibodies were used in this study: mouse monoclonal antibodies against Rab6A/Rab6A' (Matanis et al., 2002); rabbit anti-GFP (Abcam), mouse anti-HA (Covance); mouse anti-Utrophin (Santa Cruz), chicken anti-MAP2.

The anti-KIF13B polyclonal antibody was produced by immunizing rabbits with a purified GST-IF13B protein (1096–1143) expressed in BL21*Escherichia coli* using the pGEX-5X-3 vector (GE Healthcare). The antiserum was affinity purified using a BioGFP-KIF13B protein coupled to Dyna M-280 Streptavidin beads (Life Technologies).

For immunofluorescence experiments we used Alexa488-, and Alexa568-conjugated secondary antibodies (Invitrogen). For Western blotting we used IRDye 800CW goat anti-mouse and anti-rabbit antibodies, which were detected using Odyssey Infrared Imaging system (Li-Cor Biosciences).

Expression constructs

KIF13B deletion constructs were prepared by PCR-based strategy using GFP-KIF13B full length construct (a gift from Dr. Athar Chishti, University of Illinois College of Medicine, Chicago, USA). Subsequently, PCR products were subcloned in pEGFP expression vectors. The KIDINS220 deletion constructs were prepared by PCR-based strategy using HA-KIDINS220, which was a gift from Dr. Giampietro Schiavo (London Research Institute, United Kingdom). Subsequently, PCR products were subcloned in pEGFP expression vectors. TagRFP-T-Rab6 was a gift from Dr. Yuko Mimori-Kiyosue (RIKEN Center for Developmental Biology, Japan). RFP-LL5β was previously described (Lansbergen et al., 2006). cDNAs for α1-dystrobrevin, α1-syntrophin and β2-syntrophin were a gift from Dr. Marvin Adams (Department of Physiology and Biophysics, University of Washington, Seattle, USA). Subsequent PCR amplification was used to introduce specific restriction sites to subclone in pEGFP expression vectors.

Streptavidin pulldown assays

HEK293 cells were cultured in DMEM/Ham’s-F10 (50/50%) medium containing 10% FCS and 1% penicillin/streptomycin and were transfected using Polyethylenimine (PEI; Mw 2500; Polysciences) at a 3:1 PEI:DNA ratio (w/w). Cells were harvested 24 hours after transfection, by scraping the cells in ice-cold PBS and lysing cell pellets in lysis buffer (20 mM Tris-HCl, pH 7.5, 100 mM NaCl, 1.0% Triton X-100, and protease inhibitors; Roche). Supernatants and pellet fractions were separated by centrifugation at maximum speed for 20 minutes. Supernatants were mixed with an equal amount of Dyna M-280 Streptavidin beads (Life Technologies). Samples were incubated for 2 hours while rotating at 4°C, collected with a magnet and the pellets were washed 5-7 times with the wash buffer (20 mM Tris-HCl, pH 7.5, 100 mM NaCl, 0.1 % Triton X-100). Samples were eluted in SDS sample buffer, equally loaded onto SDS-PAGE gels and subjected to Western blotting. Blots were blocked with 2% bovine serum albumin/0.07% Tween 20 in PBS and incubated with primary antibodies at 4°C overnight. Blots were washed with 0.07% Tween 20 in PBS three times for 10 min at room temperature and incubated with either IRDye 800CW goat anti-mouse and anti-rabbit secondary antibodies, which were detected using Odyssey Infrared Imaging system (Li-Cor Biosciences).

Cell culture, transfection and immunofluorescence cell staining

HeLa cells were cultured in DMEM/Ham’s F10 (50/50%) medium containing 10% FCS and 1% penicillin/streptomycin. One day before transfection, cells were plated on glass coverslips. Cells were transfected with FuGene6 (Promega) according to the manufacturer’s protocol and incubated overnight. Cells were either mounted for live imaging or fixed in 4% paraformaldehyde for 10 min at room temperature followed by 10 min in 0.15% Triton X-100 in PBS. Slides were blocked in 2% bovine serum albumin/0.07% Tween 20 in PBS and labeled with primary antibody for 1 hour at room temperature. Slides were washed three times with 0.07% Tween20 in PBS, labeled with secondary antibodies for 1 hour at room temperature, washed three times with 0.07% Tween20 in PBS and mounted using Vectashield mounting medium (Vector laboratories).

Primary hippocampal cultures were prepared from embryonic day 18 (E18) rat brains (Hoogenraad et al., 2005). Cells were plated on coverslips coated with poly-L-lysine (30 µg/ml) and laminin (2 µg/ml) at a density of 75,000/well. Hippocampal cultures were grown in Neurobasal medium (NB) supplemented with B27, 0.5 mM glutamine, 12.5 µM glutamate and penicillin/streptomycin. 6 hours or 2 day after plating, hippocampal neurons were transfected using Lipofectamine 2000 (Invitrogen). Briefly, DNA (3.6 µg /well) was mixed with 3 µl Lipofectamine 2000 in 200 µl NB, incubated for 30 minutes and then added to the neurons in NB at 37°C in 5% CO2 for 45 min. Next, neurons were washed with NB and transferred in the original medium at 37°C in 5% CO2 for 2 days. Neurons were fixed for 10 min with 4% paraformaldehyde (PFA)/4% sucrose in PBS at room temperature or 10 min with ice-cold methanol 100% containing 1mM EGTA at -20°C. After fixation cells were washed 3 times for 5 min in PBS at room temperature and incubated with the primary-antibody mix in GDB buffer (0.2% BSA, 0.8M NaCl, 0.5% Triton X-100, 30mM phosphate buffer, pH 7.4) overnight at 4°C. Next the neurons were washed 3 times for 5 min in PBS at room temperature and incubated with the secondary-antibody mix in GDB buffer for at most 1 hour at room temperature. Neurons were then washed 3 times for 5 min in PBS at room temperature and subsequently mounted on slides in Vectashield mounting medium (Vector Laboratories).

Image acquisition and time-lapse live cell imaging

Images of fixed cells were collected with a Nikon Eclipse 80i microscope equipped with a Plan Fluor 10x N.A. 0.30 objective, Chroma ET-GFP (49002) filter and a Photometrics CoolSNAP HQ2 CCD camera. Live cell imaging was performed on an inverted research microscope Nikon Eclipse Ti-E (Nikon) with perfect focus system (PFS) (Nikon), equipped with Nikon CFI Apo TIRF 100x 1.49 N.A. oil objective (Nikon), Photometrics Evolve 512 EMCCD (Roper Scientific) and controlled with MetaMorph 7.7.5 software (Molecular Devices). The 16-bit images were projected onto the CCD chip with intermediate lens 2.5X (Nikon C mount adapter 2.5X) at a magnification of 0.063 μm/pixel. To keep cells at 37°C we used stage top incubator (model INUBG2E-ZILCS Tokai Hit). The microscope was equipped with TIRF-E motorized TIRF illuminator modified by Roper Scientific France/PICT-IBiSA, Institut Curie. For regular imaging we used mercury lamp HBO-103W/2 (Osram) for excitation or 491nm 100mW Calypso (Cobolt) and 561nm 100mW Jive (Cobolt) lasers. We used ET-GFP filter set (Chroma) for imaging of proteins tagged with GFP; ET-mCherry filter set (Chroma) for imaging of proteins tagged with mCherry. For simultaneous imaging of green and red fluorescence we used triple-band TIRF polychroic ZT405/488/561rpc (Chroma) and triple-band laser emission filter ZET405/488/561m (Chroma), mounted in the metal cube (Chroma, 91032) together with Optosplit III beamsplitter (Cairn Research Ltd, UK) equipped with double emission filter cube configured with ET525/50m, ET630/75m and T585LPXR (Chroma).

References

Arevalo, J.C., D.B. Pereira, H. Yano, K.K. Teng, and M.V. Chao. 2006. Identification of a switch in neurotrophin signaling by selective tyrosine phosphorylation. *J Biol Chem*. 281:1001-7.

Arevalo, J.C., H. Yano, K.K. Teng, and M.V. Chao. 2004. A unique pathway for sustained neurotrophin signaling through an ankyrin-rich membrane-spanning protein. *EMBO J*. 23:2358-68.

Basu, S., S. Sladecek, Y.V.I. Martinez de la Pena, M. Akaaboune, I. Smal, K. Martin, N. Galjart, and H.R. Brenner. 2015. CLASP2-dependent microtubule capture at the neuromuscular junction membrane requires LL5beta and actin for focal delivery of acetylcholine receptor vesicles. *Mol Biol Cell*.

Belanto, J.J., T.L. Mader, M.D. Eckhoff, D.M. Strandjord, G.B. Banks, M.K. Gardner, D.A. Lowe, and J.M. Ervasti. 2014. Microtubule binding distinguishes dystrophin from utrophin. *Proc Natl Acad Sci U S A*. 111:5723-8.

Bhat, H.F., M.E. Adams, and F.A. Khanday. 2013. Syntrophin proteins as Santa Claus: role(s) in cell signal transduction. *Cell Mol Life Sci*. 70:2533-54.

Bracale, A., F. Cesca, V.E. Neubrand, T.P. Newsome, M. Way, and G. Schiavo. 2007. Kidins220/ARMS is transported by a kinesin-1-based mechanism likely to be involved in neuronal differentiation. *Mol Biol Cell*. 18:142-52.

Chauvin, S., and A. Sobel. 2014. Neuronal stathmins: A family of phosphoproteins cooperating for neuronal development, plasticity and regeneration. *Prog Neurobiol*.

Ervasti, J.M., and K.P. Campbell. 1993. A role for the dystrophin-glycoprotein complex as a transmembrane linker between laminin and actin. *J Cell Biol*. 122:809-23.

Grady, R.M., M. Akaaboune, A.L. Cohen, M.M. Maimone, J.W. Lichtman, and J.R. Sanes. 2003. Tyrosine-phosphorylated and nonphosphorylated isoforms of alpha-dystrobrevin: roles in skeletal muscle and its neuromuscular and myotendinous junctions. *J Cell Biol*. 160:741-52.

Grigoriev, I., D. Splinter, N. Keijzer, P.S. Wulf, J. Demmers, T. Ohtsuka, M. Modesti, I.V. Maly, F. Grosveld, C.C. Hoogenraad, and A. Akhmanova. 2007. Rab6 regulates transport and targeting of exocytotic carriers. *Dev Cell*. 13:305-14.

Grigoriev, I., K.L. Yu, E. Martinez-Sanchez, A. Serra-Marques, I. Smal, E. Meijering, J. Demmers, J. Peranen, R.J. Pasterkamp, P. van der Sluijs, C.C. Hoogenraad, and A. Akhmanova. 2011. Rab6, Rab8, and MICAL3 cooperate in controlling docking and fusion of exocytotic carriers. *Curr Biol*. 21:967-74.

Gumy, L.F., E.A. Katrukha, L.C. Kapitein, and C.C. Hoogenraad. 2014. New insights into mRNA trafficking in axons. *Dev Neurobiol*. 74:233-44.

Haenggi, T., and J.M. Fritschy. 2006. Role of dystrophin and utrophin for assembly and function of the dystrophin glycoprotein complex in non-muscle tissue. *Cell Mol Life Sci*. 63:1614-31.

Hanada, T., L. Lin, E.V. Tibaldi, E.L. Reinherz, and A.H. Chishti. 2000. GAKIN, a novel kinesin-like protein associates with the human homologue of the Drosophila discs large tumor suppressor in T lymphocytes. *J Biol Chem*. 275:28774-84.

Higuero, A.M., L. Sanchez-Ruiloba, L.E. Doglio, F. Portillo, J. Abad-Rodriguez, C.G. Dotti, and T. Iglesias. 2010. Kidins220/ARMS modulates the activity of microtubule-regulating proteins and controls neuronal polarity and development. *J Biol Chem*. 285:1343-57.

Hirokawa, N., and Y. Noda. 2008. Intracellular transport and kinesin superfamily proteins, KIFs: structure, function, and dynamics. *Physiol Rev*. 88:1089-118.

Hirokawa, N., Y. Noda, Y. Tanaka, and S. Niwa. 2009. Kinesin superfamily motor proteins and intracellular transport. *Nat Rev Mol Cell Biol*. 10:682-96.

Hoffman, E.P., R.H. Brown, Jr., and L.M. Kunkel. 1987. Dystrophin: the protein product of the Duchenne muscular dystrophy locus. *Cell*. 51:919-28.

Horiguchi, K., T. Hanada, Y. Fukui, and A.H. Chishti. 2006. Transport of PIP3 by GAKIN, a kinesin-3 family protein, regulates neuronal cell polarity. *J Cell Biol*. 174:425-36.

Huang, C.F., and G. Banker. 2012. The translocation selectivity of the kinesins that mediate neuronal organelle transport. *Traffic*. 13:549-64.

Iglesias, T., N. Cabrera-Poch, M.P. Mitchell, T.J. Naven, E. Rozengurt, and G. Schiavo. 2000. Identification and cloning of Kidins220, a novel neuronal substrate of protein kinase D. *J Biol Chem*. 275:40048-56.

Jacobson, C., P.D. Cote, S.G. Rossi, R.L. Rotundo, and S. Carbonetto. 2001. The dystroglycan complex is necessary for stabilization of acetylcholine receptor clusters at neuromuscular junctions and formation of the synaptic basement membrane. *J Cell Biol*. 152:435-50.

Jenkins, B., H. Decker, M. Bentley, J. Luisi, and G. Banker. 2012. A novel split kinesin assay identifies motor proteins that interact with distinct vesicle populations. *J Cell Biol*. 198:749-61.

Kanai, Y., D. Wang, and N. Hirokawa. 2014. KIF13B enhances the endocytosis of LRP1 by recruiting LRP1 to caveolae. *J Cell Biol*. 204:395-408.

Kishi, M., T.T. Kummer, S.J. Eglen, and J.R. Sanes. 2005. LL5beta: a regulator of postsynaptic differentiation identified in a screen for synaptically enriched transcripts at the neuromuscular junction. *J Cell Biol*. 169:355-66.

Kong, H., J. Boulter, J.L. Weber, C. Lai, and M.V. Chao. 2001. An evolutionarily conserved transmembrane protein that is a novel downstream target of neurotrophin and ephrin receptors. *J Neurosci*. 21:176-85.

Kopp, P., R. Lammers, M. Aepfelbacher, G. Woehlke, T. Rudel, N. Machuy, W. Steffen, and S. Linder. 2006. The kinesin KIF1C and microtubule plus ends regulate podosome dynamics in macrophages. *Mol Biol Cell*. 17:2811-23.

Lansbergen, G., I. Grigoriev, Y. Mimori-Kiyosue, T. Ohtsuka, S. Higa, I. Kitajima, J. Demmers, N. Galjart, A.B. Houtsmuller, F. Grosveld, and A. Akhmanova. 2006. CLASPs attach microtubule plus ends to the cell cortex through a complex with LL5beta. *Dev Cell*. 11:21-32.

Lu, M.S., and K.E. Prehoda. 2013. A NudE/14-3-3 pathway coordinates dynein and the kinesin Khc73 to position the mitotic spindle. *Dev Cell*. 26:369-80.

Luo, S., Y. Chen, K.O. Lai, J.C. Arevalo, S.C. Froehner, M.E. Adams, M.V. Chao, and N.Y. Ip. 2005. {alpha}-Syntrophin regulates ARMS localization at the neuromuscular junction and enhances EphA4 signaling in an ARMS-dependent manner. *J Cell Biol*. 169:813-24.

Matanis, T., A. Akhmanova, P. Wulf, E. Del Nery, T. Weide, T. Stepanova, N. Galjart, F. Grosveld, B. Goud, C.I. De Zeeuw, A. Barnekow, and C.C. Hoogenraad. 2002. Bicaudal-D regulates COPI-independent Golgi-ER transport by recruiting the dynein-dynactin motor complex. *Nat. Cell Biol.* 4:986-92.

Moleirinho, S., W. Guerrant, and J.L. Kissil. 2014. The Angiomotins--from discovery to function. *FEBS Lett*. 588:2693-703.

Murphy, D.A., and S.A. Courtneidge. 2011. The 'ins' and 'outs' of podosomes and invadopodia: characteristics, formation and function. *Nat Rev Mol Cell Biol*. 12:413-26.

Nakaya, Y., E.W. Sukowati, and G. Sheng. 2013. Epiblast integrity requires CLASP and Dystroglycan-mediated microtubule anchoring to the basal cortex. *J Cell Biol*. 202:637-51.

Neubrand, V.E., F. Cesca, F. Benfenati, and G. Schiavo. 2012. Kidins220/ARMS as a functional mediator of multiple receptor signalling pathways. *J Cell Sci*. 125:1845-54.

Neubrand, V.E., C. Thomas, S. Schmidt, A. Debant, and G. Schiavo. 2010. Kidins220/ARMS regulates Rac1-dependent neurite outgrowth by direct interaction with the RhoGEF Trio. *J Cell Sci*. 123:2111-23.

Peng, H.B., H. Xie, S.G. Rossi, and R.L. Rotundo. 1999. Acetylcholinesterase clustering at the neuromuscular junction involves perlecan and dystroglycan. *J Cell Biol*. 145:911-21.

Poulain, F.E., and A. Sobel. 2010. The microtubule network and neuronal morphogenesis: Dynamic and coordinated orchestration through multiple players. *Mol Cell Neurosci*. 43:15-32.

Proszynski, T.J., J. Gingras, G. Valdez, K. Krzewski, and J.R. Sanes. 2009. Podosomes are present in a postsynaptic apparatus and participate in its maturation. *Proc Natl Acad Sci U S A*. 106:18373-8.

Proszynski, T.J., and J.R. Sanes. 2013. Amotl2 interacts with LL5beta, localizes to podosomes and regulates postsynaptic differentiation in muscle. *J Cell Sci*. 126:2225-35.

Sanes, J.R., and J.W. Lichtman. 2001. Induction, assembly, maturation and maintenance of a postsynaptic apparatus. *Nat Rev Neurosci*. 2:791-805.

Schlager, M.A., L.C. Kapitein, I. Grigoriev, G.M. Burzynski, P.S. Wulf, N. Keijzer, E. de Graaff, M. Fukuda, I.T. Shepherd, A. Akhmanova, and C.C. Hoogenraad. 2010. Pericentrosomal targeting of Rab6 secretory vesicles by Bicaudal-D-related protein 1 (BICDR-1) regulates neuritogenesis. *EMBO J*. 29:1637-51.

Schlager, M.A., A. Serra-Marques, I. Grigoriev, L.F. Gumy, M. Esteves da Silva, P.S. Wulf, A. Akhmanova, and C.C. Hoogenraad. 2014. Bicaudal d family adaptor proteins control the velocity of Dynein-based movements. *Cell Rep*. 8:1248-56.

Siegrist, S.E., and C.Q. Doe. 2005. Microtubule-induced Pins/Galphai cortical polarity in Drosophila neuroblasts. *Cell*. 123:1323-35.

Thompson, O., I. Kleino, L. Crimaldi, M. Gimona, K. Saksela, and S.J. Winder. 2008. Dystroglycan, Tks5 and Src mediated assembly of podosomes in myoblasts. *PLoS One*. 3:e3638.

Vale, R.D. 2003. The molecular motor toolbox for intracellular transport. *Cell*. 112:467-80.

van der Vaart, B., W.E. van Riel, H. Doodhi, J.T. Kevenaar, E.A. Katrukha, L. Gumy, B.P. Bouchet, I. Grigoriev, S.A. Spangler, K.L. Yu, P.S. Wulf, J. Wu, G. Lansbergen, E.Y. van Battum, R.J. Pasterkamp, Y. Mimori-Kiyosue, J. Demmers, N. Olieric, I.V. Maly, C.C. Hoogenraad, and A. Akhmanova. 2013. CFEOM1-associated kinesin KIF21A is a cortical microtubule growth inhibitor. *Dev Cell*. 27:145-60.

Wu, S.H., J.C. Arevalo, F. Sarti, L. Tessarollo, W.B. Gan, and M.V. Chao. 2009. Ankyrin Repeat-rich Membrane Spanning/Kidins220 protein regulates dendritic branching and spine stability in vivo. *Dev Neurobiol*. 69:547-57.

Xing, B.M., Y.R. Yang, J.X. Du, H.J. Chen, C. Qi, Z.H. Huang, Y. Zhang, and Y. Wang. 2012. Cyclin-dependent kinase 5 controls TRPV1 membrane trafficking and the heat sensitivity of nociceptors through KIF13B. *J Neurosci*. 32:14709-21.

Yamada, K.H., Y. Nakajima, M. Geyer, K.K. Wary, M. Ushio-Fukai, Y. Komarova, and A.B. Malik. 2014. KIF13B regulates angiogenesis through Golgi to plasma membrane trafficking of VEGFR2. *J Cell Sci*. 127:4518-30.

6

Characterization of docking and fusion machineries for Rab6-secretory vesicles

Andrea Serra-Marques[1], Qingyang Liu[1,2], A. F. Maarten Altelaar[2],
Albert J. R. Heck[2] and Anna Akhmanova[1]

[1]Cell Biology, Faculty of Science, Utrecht University, Utrecht, The Netherlands; [2]Biomolecular Mass Spectrometry and Proteomics, Bijvoet Center for Biomolecular Research, Utrecht Institute for Pharmaceutical Sciences and The Netherlands Proteomics Centre, Utrecht University, Utrecht, the Netherlands.

Abstract

Constitutive exocytosis is an essential cellular process responsible for transport of newly synthesized proteins and other cellular components to the plasma membrane. It is mediated by Golgi-derived vesicles, which move along cytoskeletal filaments and fuse with the plasma membrane. We have previously shown that the small GTPase Rab6 marks the carriers of constitutive secretion, regulating their transport and fusion with the plasma membrane. Vesicular carriers utilize a complex network of factors, which promote their specific interactions and fusion with the target membranes. Among these factors, a family of proteins called soluble N-ethylmaleimide-sensitive factor (NSF) adaptor proteins receptors (SNAREs) are considered essential. These are generally divided into v-SNAREs (vesicle SNAREs) and t-SNAREs (target membrane SNAREs), which are required for specific fusion steps between different compartments. Previous studies in our laboratory have shown that the flavoprotein monooxygenase MICAL-3, the small GTPase Rab8 and the coiled coil protein ELKS/Rab6IP2, which resides in cortical patches localized at the leading edges of migrating cells, form a complex and promote docking and fusion of Rab6 vesicles. Interestingly, in the absence of Rab6, the fusion of secretory carriers is accelerated but is much less selective with respect to cell location. This suggests that ELKS/Rab6IP2 and Rab6 cooperate in some specific way with the membrane fusion machinery. We tested the involvement of specific SNAREs in the fusion of Rab6-positive vesicles and found the specific members of the VAMP (v-SNARE), and SNAP (t-SNARE) families, which participate in fusion of exocytotic carriers. We also found that inhibition of Rab8 function impairs fusion, arresting vesicles at cortical sites enriched in ELKS. We have searched for putative molecular links between the docking and fusion machineries, but our results suggest that they might not be physically connected to each other. Furthermore, we have found that proteins from the endocytic EHD family are recruited to Rab6 vesicles when they dock at the plasma membrane, opening an exciting avenue of research for the role of endocytic proteins in constitutive exocytosis.

Introduction

Constitutive exocytosis is an essential cellular process responsible for the transport of newly synthesized proteins and other cellular components to the plasma membrane (Burgess and Kelly, 1987). It is mediated by Golgi-derived vesicles, which bud from the donor organelle, move along cytoskeletal filaments and fuse with the plasma membrane, in a sequence of events typical of a classical vesicle transport cycle (Bonifacino and Glick, 2004). Vesicular carriers utilize a complex network of factors, which promote their specific interactions and fusion with the target membranes (Cai et al., 2007).

The large family of small Rab GTPases regulates several aspects of the vesicle life cycle, being particularly relevant for the control of docking and tethering steps between membrane compartments and for connecting membranes to the cytoskeleton during different trafficking processes (Barr and Lambright, 2010; Hutagalung and Novick, 2011). They exist in their inactive GDP form in the cytoplasm, associated with the GDP-dissociation inhibitor (GDI), which occludes the hydrophobic C-terminal prenyl anchor of the Rab. Rabs are recruited to the membranes with the aid of a GDF (GDI displacement factor) and anchored to the membrane via a prenyl group (Dirac-Svejstrup et al., 1997). The membrane-anchored Rab is subsequently activated by a GEF (guanine nucleotide exchange factor) that will replace the bound GDP by GTP (Soldati et al., 1994; Ullrich et al., 1994). Once activated, the Rab interacts with downstream effectors and is inactivated when GTP is hydrolyzed, an irreversible reaction mediated by a GAP (GTPase-activating protein) (Rybin et al., 1996). An accurate Rab activity depends on specific membrane targeting and coordinated action of GEFs and GAPs.

Our lab has previously shown that the small GTPase Rab6 is a marker of constitutive exocytotic vesicles, stimulating their processive transport along microtubules and their fusion at sites in the plasma membrane enriched in cortical proteins, such as ELKS/Rab6IP2 (Grigoriev et al., 2007). Another Rab involved in this pathway is Rab8, an important factor in vesicular transport between the Trans Golgi Network (TGN) and the basolateral membrane in MDCK cells (Huber et al., 1993). In line with this, we have shown that Rab8 is stably recruited to exocytotic vesicles in a Rab6-dependent manner and associates with ELKS through MICAL-3, a member of the MICAL family of flavoprotein monooxygenases. Although Rab8 is not necessary for the movement of the vesicles, it is required for proper docking and fusion (Grigoriev et al., 2011).

Once docking and tethering of a vesicle are completed, fusion can take place, and a family of proteins called soluble N-ethylmaleimide-sensitive factor (NSF) adaptor proteins receptors (SNAREs) are considered essential at this step (Sollner et al., 1993; Sudhof and Rothman, 2009). SNAREs are small coiled-coil membrane-anchored proteins present on both vesicle (v-SNAREs) and target membranes (t-SNAREs). When in close proximity, they form a four-helix bundle complex to overcome the dehydration forces associated with bringing two lipid bilayers together in an aqueous environment, driving membrane fusion (Bassham and Blatt, 2008; Sutton et al., 1998; Trimble et al., 1988). The core (coiled-coil) domains of SNARE proteins are highly conserved, and they are classified in Q-SNAREs or R-SNAREs, depending on whether they have a glutamine (Q) or an arginine (R) at the center of the core domain, respectively (Fasshauer et al., 1998). The neuronal SNARE complex is formed by one R-SNARE and two Q-SNAREs: the R-SNARE VAMP1 and the Q-SNARE syntaxin-1 contribute one helix each, while the Q-SNARE SNAP-25 contributes 2 helices. Other organizations of the SNARE complexes are possible; for example, in many cases four SNARE proteins contribute only one helix and the 1R-3Q symmetry is not strictly necessary (Bassham and Blatt, 2008; Brunger, 2005). The SNARE cycle typically starts with the opening of the closed SNARE conformation by a Sec/Munc-like protein. Then, one v-SNARE interacts with 2 or 3 t-SNAREs, forming a complex and pulling the membranes toward each other, driving membrane lipid bilayer fusion. After the fusion, the SNARE complexes left on the membrane will be recycled by the action of SNAP and NSF, and individual SNAREs are free for a new cycle of fusion (Bassham and Blatt, 2008). The yeast SNAREs required for constitutive secretion are well characterized (Pelham, 1999). In mammalian cells, the SNAREs required for ER-to-Golgi trafficking are also known, consisting of syntaxin-5, GS27, Bet1(Q-SNAREs) and Sec22b (R-SNARE) (Jahn and Scheller, 2006). More recently, the SNAREs syntaxin-5, syntaxin-17, syntaxin-18, GS27, SLT1, Sec20, Sec22b, YKT6, SNAP-29 and syntaxin-19 were identified in a screen for proteins involved in constitutive secretion (Gordon et al., 2010).

In this study we sought to understand the molecular link between the docking and fusion machineries responsible for the fusion of exocytotic carriers with the plasma membrane. We show that the v-SNARE VAMP4 and the t-SNARE SNAP-29 are involved in the fusion of Rab6 vesicles. Using TIRF microscopy we show that VAMP4 and Rab6 colocalize during vesicle fusion with the plasma membrane. Furthermore, by using an inactive form of Rab8, the dominant negative mutant Rab8-T22N which is constitutively bound to GDP, we observed that fusion of Rab6 vesicles is impaired, suggesting that an accurate activation and inactivation of Rab8 is essential for proper fusion. Additionally, we have found that endocytic proteins are recruited to Rab6 vesicles upon vesicle docking, what opens a new avenue of research on the crosstalk between the endocytic and exocytotic pathways.

Results and Discussion

The SNARE proteins VAMP4 and SNAP29 mediate fusion of Rab6-secretory vesicles with the plasma membrane

In order to understand which SNAREs are involved in the fusion of Rab6 secretory vesicles with the plasma membrane, we transfected HeLa cells with siRNAs against a subset of SNAREs which were previously implicated in post-Golgi processes. This subset included SNAP-29 and syntaxin 19, because a previous study showed that transfection of HeLa cells with siRNAs against these two SNAREs reduced the secretion of an inducible fluorescent reporter that was based on chemically reversible aggregation of mutant FKBP proteins in the ER (Gordon et al., 2010). We have also included in the analysis the four post-Golgi R-SNARES, VAMP3, VAMP4, VAMP7 and VAMP8, which could previously be detected in HeLa cells by immunoblotting (Gordon et al., 2010). We found that only the depletion of VAMP4 and SNAP29 induced an accumulation of Rab6 vesicles at the plasma membrane compared to control (Fig. 1A-C), suggesting that vesicle fusion was delayed, while the depletion of the other SNARES had not detectable effect on the Rab6 vesicle abundance. The effect of SNAP29 depletion was in line with the previous study, which showed that the depletion of this SNARE caused an accumulation of secretory vesicles under the plasma membrane and reduced the number of vesicle fusion events (Gordon et al., 2010). VAMP4 was not found in the previous screen, and its depletion had no effect on the secretion of the inducible reporter even when combined with knockdown of VAMP3, VAMP7 and VAMP8 (Gordon et al., 2010). The discrepancy with our results could be due to the use of a different marker for secretory vesicles. On the other hand, we failed to observe any significant effect of syntaxin 19 depletion (data not shown); again, this might be due to experimental differences. We note, however, that the expression of syntaxin 19 might be weak in HeLa cells, as it could only be detected by RT-PCR (Gordon et al., 2010), and, therefore, other syntaxins might contribute to vesicle fusion in our system.

We next attempted to determine which syntaxins might cooperate with SNAP29 and VAMP4 in Rab6 vesicle fusion with the plasma membrane. We employed mass spectrometry analysis to identify the binding partners of VAMP4 and SNAP29 using streptavidin pull down assays from HEK293T cells co-transfected with biotinylation and GFP-tagged (BioGFP) version of these SNAREs together with the biotin ligase BirA (Table 1). We identified SNAP29 as a binding partner in the mass spectrometry analysis of BioGFP-VAMP4, and VAMP4 in the mass spectrometry analysis of BioGFP-SNAP29 (Table 1). However, the specificity of this assay was low: a broad array of different syntaxins was found in both pull downs. Furthermore, different VAMPs, including VAMP2, VAMP3, VAMP7 and VAMP8, as well as other SNAREs were found in SNAP29 pull down. Conversely, in addition to SNAP29, also its homologue SNAP23 was identified in VAMP4 pull down. The results of mass spectrometry analysis were confirmed by immunoblotting: BioGFP-VAMP4 co-precipitated endogenous SNAP29, and BioGFP-SNAP29 co-precipitated endogenous VAMP4 (Fig.1D). We have also tested the binding of these SNAREs to syntaxin 3 and syntaxin 4 and found that both endogenous SNAREs could co-precipitate with BioGFP-syntaxin 3 and BioGFP-syntaxin 4, with VAMP4 having a somewhat higher affinity for syntaxin 3 (Fig.1D). Taken together, our data suggest that VAMP4 and SNAP29 might indeed form a complex with each other and with one of the syntaxins to promote Rab6 vesicle fusion with the plasma membrane, but the conventional pull down assays with overexpressed tagged proteins cannot be used to unravel the SNARE specificity in this system.

Table 1: Binding partners of the indicated BioGFP-SNAP29 and BioGFP-VAMP4 constructs in HEK293T cells identified by mass spectrometry analysis.

		SNAP29		***VAMP4***	
Gene name	Protein ID	*Unique peptides*	*PSM*	*Unique Peptides*	*PSM*
EHD1	Q9H4M9	47	162	1	1
SNAP29	**O95721**	**42**	**421**	**27**	**96**
EHD4	Q9H223	41	169	5	5
MYH9	P35579	32	40	16	17
DNAJC13	O75165	27	35	4	4
VPS45	Q9NRW7	25	42	26	59
SCFD1	Q8WVM8	23	49	0	0
EHD3	Q9NZN3	22	65	0	0
STX18	Q9P2W9	21	43	17	30
SEC22B	O75396	19	97	10	16
STX5	Q13190	18	42	21	54
MYH10	P35580	18	19	9	10
VAMP7	P51809	18	40	9	11
NAPA	P54920	16	34	27	108
GOSR1	O95249	16	26	11	18
YKT6	O15498	16	39	4	7
STX17	P56962	14	21	6	6
STX12	Q86Y82	10	27	11	40
MLLT4	P55196	10	10	1	1
STX4	Q12846	9	24	12	35
STX7	O15400	9	16	10	31
STX10	O60499	9	17	12	38
VPS51	Q9UID3	8	10	0	0
STX16	O14662	8	16	7	10
STX6	O43752	8	14	15	33
SNAP23	O00161	8	17	23	66
STXBP5	Q5T5C0	7	8	0	0
VAMP8	Q9BV40	7	17	1	1

Table 1: Continued

		SNAP29		***VAMP4***	
Gene name	Protein ID	*Unique peptides*	*PSM*	*Unique Peptides*	*PSM*
VAMP3	Q15836	7	42	6	9
VAMP2	P63027	7	34	4	6
VTI1B	Q9UEU0	7	11	10	21
EHD2	Q9NZN4	6	21	0	0
NAPG	Q99747	6	6	22	35
SMARCA5	O60264	6	6	8	8
TMPO	P42167	6	8	7	7
TCOF1	Q13428	6	6	0	0
AP2M1	Q96CW1	5	5	3	5
NUP205	Q92621	5	6	22	28
GLG1	Q92896	5	5	9	9
TMPO	P42166	5	7	3	3
DSG2	Q14126	5	5	1	1
SUN2	Q9UH99	5	5	13	22
FKBP8	Q14318	5	5	1	1
BCAP31	P51572	5	8	14	31
AGL	P35573	5	5	1	1
MYH11	P35749	5	8	4	4
NAPB	Q9H115	4	9	7	21
SKA1	Q96BD8	4	4	0	0
COPG2	Q9UBF2	4	4	2	2
VTI1A	Q96AJ9	4	8	6	11
NDRG1	Q92597	4	4	0	0
CCDC124	Q96CT7	4	6	3	4
GAPVD1	Q14C86	4	4	0	0
ASPH	Q12797	4	4	4	4
LARP1	Q6PKG0	4	4	0	0
DBN1	Q16643	4	4	0	0
EIF5B	O60841	3	3	1	1
CORO1C	Q9ULV4	3	3	0	0
PPID	Q08752	3	3	0	0
STX8	Q9UNK0	3	5	13	29
GPS1	Q13098	3	5	3	3
TPM4	P67936	3	4	1	1
CTNND1	O60716	3	3	0	0
RACGAP1	Q9H0H5	3	3	0	0
CHMP2B	Q9UQN3	3	3	2	2
SSRP1	Q08945	3	3	0	0
ACTN4	O43707	3	3	0	0
BET1	O15155	3	4	1	1
STRN4	Q9NRL3	3	3	0	0
MYO1C	O00159	3	3	0	0
MYBBP1A	Q9BQG0	3	3	1	1
RRBP1	Q9P2E9	3	3	1	1

Table 1: Continued

		SNAP29		*VAMP4*	
Gene name	Protein ID	*Unique peptides*	*PSM*	*Unique Peptides*	*PSM*
UFL1	O94874	3	3	2	2
NDE1	Q9NXR1	3	3	0	0
NOP56	O00567	3	3	1	1
HLTF	Q14527	3	3	1	1
HS2ST1	Q7LGA3	3	3	6	9
SLC27A4	Q6P1M0	3	4	3	3
VPS26A	O75436	3	3	1	1
AP1G1	O43747	3	4	40	133
ASNS	P08243	3	3	1	1
BAG4	O95429	3	3	0	0
LBR	Q14739	3	3	8	11
MYL6	P60660	3	4	3	3
PUM1	Q14671	2	2	0	0
PYCRL	Q53H96	2	2	0	0
NOP58	Q9Y2X3	2	3	1	1
CCDC101	Q96ES7	2	2	0	0
PTPN11	Q06124	2	2	0	0
CKAP2	Q8WWK9	2	2	0	0
TOP1	P11387	2	3	0	0
CHD4	Q14839	2	2	1	1
CGN	Q9P2M7	2	2	0	0
DYNC1LI1	Q9Y6G9	2	3	0	0
FAM98A	Q8NCA5	2	2	1	1
EIF2A	Q9BY44	2	2	0	0
SEC23B	Q15437	2	2	1	1
TXLNA	P40222	2	2	0	0
XPO5	Q9HAV4	2	2	0	0
NUP155	O75694	2	2	5	5
ZC3HAV1L	Q96H79	2	2	0	0
LRRC47	Q8N1G4	2	2	0	0
SNX9	Q9Y5X1	2	2	0	0
COPS3	Q9UNS2	2	2	2	2
SH3GL1	Q99961	2	2	0	0
PPP2R1B	P30154	2	2	1	1
PEX19	P40855	2	2	1	1
SCAMP3	O14828	2	2	0	0
GEMIN4	P57678	2	2	0	0
KLC1	Q07866	2	2	0	0
PTPLAD1	Q9P035	2	2	7	9
BET1L	Q9NYM9	2	2	2	4
KIF2C	Q99661	2	2	1	1
ATXN10	Q9UBB4	2	2	2	2
ZC3H15	Q8WU90	2	2	4	4
TMEM134	Q9H6X4	2	2	0	0

Table 1: Continued

Gene name	Protein ID	***SNAP29*** *Unique peptides*	*PSM*	***VAMP4*** *Unique Peptides*	*PSM*
AP2A1	O95782	2	2	2	2
BRI3BP	Q8WY22	2	2	2	2
KTN1	Q86UP2	2	2	2	2
PIN1	Q13526	2	2	0	0
CCAR2	Q8N163	2	2	2	2
NCDN	Q9UBB6	2	2	0	0
SCRIB	Q14160	2	2	0	0
LARP4	Q71RC2	2	2	1	1
ZWINT	O95229	2	3	0	0
GLMN	Q92990	2	2	0	0
ZW10	O43264	2	2	0	0
TES	Q9UGI8	2	2	0	0
PRMT3	O60678	2	2	0	0
ADSS	P30520	2	2	0	0
DSP	P15924	2	2	3	3
BNIP1	Q12981	2	2	7	7
MTDH	Q86UE4	2	2	1	1
PAICS	P22234	2	2	3	3
SRP19	P09132	2	2	0	0
SEC23A	Q15436	2	3	2	2
POLDIP3	Q9BY77	2	2	0	0
B3GNT1	O43505	2	2	17	60
XRN2	Q9H0D6	2	2	1	1
GOSR2	O14653	2	2	3	4
EIF4E	P06730	2	2	2	2
TNPO2	O14787	2	3	5	5
NDUFB10	O96000	2	2	3	3
SGPL1	O95470	2	2	6	6
WDR6	Q9NNW5	2	2	0	0
SMU1	Q2TAY7	2	2	0	0
ZYX	Q15942	2	2	0	0
SMPD4	Q9NXE4	2	2	1	1
AP2A2	O94973	2	2	2	2
SSR4	P51571	1	1	5	11
RCC1	P18754	1	1	1	1
MCU	Q8NE86	1	1	1	1
RAB10	P61026	1	1	4	4
MKI67	P46013	1	1	8	9
BTAF1	O14981	1	1	9	11
KIAA2013	Q8IYS2	1	1	7	10
SEC63	Q9UGP8	1	1	2	2
CTNNA1	P35221	1	1	2	2
LSM12	Q3MHD2	1	2	0	0
VTA1	Q9NP79	1	1	0	0

Table 1: Continued

		SNAP29		***VAMP4***	
Gene name	Protein ID	*Unique peptides*	*PSM*	*Unique Peptides*	*PSM*
ALG6	Q9Y672	1	1	8	18
CFHR5	Q9BXR6	1	1	0	0
AP3D1	O14617	1	1	0	0
DYNC2H1	Q8NCM8	1	1	2	2
COPE	O14579	1	1	1	1
KIDINS220	Q9ULH0	1	1	0	0
ERP44	Q9BS26	1	1	5	8
TBC1D15	Q8TC07	1	1	0	0
MICALL1	Q8N3F8	1	1	0	0
MAPRE1	Q15691	1	1	1	1
FAF2	Q96CS3	1	1	2	2
PIK3R1	P27986	1	1	0	0
U2AF2	P26368	1	1	0	0
CSRP2	Q16527	1	1	0	0
MAP2K6	P52564	1	1	0	0
LRRC8C	Q8TDW0	1	1	0	0
DDOST	P39656	1	1	5	7
TRAPPC3	O43617	1	1	0	0
TMEM41B	Q5BJD5	1	1	0	0
NUP188	Q5SRE5	1	1	8	9
USE1	Q9NZ43	1	1	8	12
EMC2	Q15006	1	1	7	8
KIAA1715	Q9C0E8	1	1	3	3
ANO10	Q9NW15	1	1	8	16
LMBR1	Q8WVP7	1	1	5	10
SHQ1	Q6PI26	1	2	0	0
OPA1	O60313	1	1	2	2
TMED10	P49755	1	1	3	5
CTNNB1	P35222	1	1	4	4
SPTAN1	Q13813	1	1	2	2
EMC1	Q8N766	1	2	7	11
GORASP2	Q9H8Y8	1	1	0	0
PIGG	Q5H8A4	0	0	3	3
SOAT1	P35610	0	0	4	6
FLOT1	O75955	0	0	7	7
AP1S1	P61966	0	0	7	17
COX4I1	P13073	0	0	7	11
LAMP2	P13473	0	0	1	1
GNAI3	P08754	0	0	2	2
SLC39A14	Q15043	0	0	2	2
RAB11FIP1	Q6WKZ4	0	0	1	1
TMEM214	Q6NUQ4	0	0	2	2
TEX261	Q6UWH6	0	0	1	1
TFRC	P02786	0	0	1	1

Table 1: Continued

		SNAP29		***VAMP4***	
Gene name	Protein ID	*Unique peptides*	*PSM*	*Unique Peptides*	*PSM*
TMCO1	Q9UM00	0	0	4	9
PKD2	Q13563	0	0	2	2
GOLIM4	O00461	0	0	4	4
MBLAC2	Q68D91	0	0	21	73
FNDC3A	Q9Y2H6	0	0	1	1
TUBGCP2	Q9BSJ2	0	0	7	7
TXN	P10599	0	0	1	1
GNB1	P62873	0	0	1	1
SACM1L	Q9NTJ5	0	0	10	12
FAM20B	O75063	0	0	5	5
RAB1A	P62820	0	0	3	3
PBXIP1	Q96AQ6	0	0	1	1
EMC4	Q5J8M3	0	0	1	1
RAB5C	P51148	0	0	1	1
RAP1GDS1	P52306	0	0	1	1
DFFA	O00273	0	0	1	1
COG6	Q9Y2V7	0	0	4	4
SAAL1	Q96ER3	0	0	8	16
VAMP4	**O75379**	**6**	**9**	**16**	**67**
RABL3	Q5HYI8	0	0	1	2
CHCHD3	Q9NX63	0	0	3	3
STAG2	Q8N3U4	0	0	16	23
FLOT2	Q14254	0	0	2	2
FLG2	Q5D862	0	0	1	1
VPS4A	Q9UN37	0	0	1	1
CKAP4	Q07065	0	0	16	23
RER1	O15258	0	0	2	2
STOML2	Q9UJZ1	0	0	10	18
PREB	Q9HCU5	0	0	9	16
AP1S3	Q96PC3	0	0	2	3
DYM	Q7RTS9	0	0	4	4
UGT8	Q16880	0	0	1	1
COG2	Q14746	0	0	1	1
ZMPSTE24	O75844	0	0	5	7
COG8	Q96MW5	0	0	1	1
BSCL2	Q96G97	0	0	1	1
RAB6A	P20340	0	0	3	3
PDIA4	P13667	0	0	1	1
COX7A2L	O14548	0	0	2	2
PIGT	Q969N2	0	0	5	5
WDR64	B1ANS9	0	0	1	1
COG7	P83436	0	0	7	9
AP1S2	P56377	0	0	6	10
GOLM1	Q8NBJ4	0	0	1	1

Table 1: Continued

		SNAP29		***VAMP4***	
Gene name	Protein ID	*Unique peptides*	*PSM*	*Unique Peptides*	*PSM*
TMEM9	Q9P0T7	0	0	1	1
LCLAT1	Q6UWP7	0	0	1	1
SAMM50	Q9Y512	0	0	3	3
STOM	P27105	0	0	5	10
CLCC1	Q96S66	0	0	3	4
C14orf166	Q9Y224	0	0	2	2
CLASP2	O75122	0	0	1	1
TMEM205	Q6UW68	0	0	1	2
IGF2R	P11717	0	0	10	10
SPCS1	Q9Y6A9	0	0	1	1
TP53I11	O14683	0	0	2	2
WDFY2	Q96P53	0	0	2	2
COG4	Q9H9E3	0	0	6	6
MT-ND2	P03891	0	0	1	1
GTPBP4	Q9BZE4	0	0	1	1
NAT14	Q8WUY8	0	0	1	1
TNPO3	Q9Y5L0	0	0	6	6
SLC29A1	Q99808	0	0	1	1
TMEM160	Q9NX00	0	0	1	1
SLC30A6	Q6NXT4	0	0	2	2
PRKDC	P78527	0	0	52	69
SNCAIP	Q9Y6H5	0	0	1	1
SAR1A	Q9NR31	0	0	1	1
MBOAT7	Q96N66	0	0	2	2
COG5	Q9UP83	0	0	12	13
SCRN1	Q12765	0	0	1	1
KIF14	Q15058	0	0	5	6
TMEM192	Q8IY95	0	0	2	2
TRPM4	Q8TD43	0	0	3	3
SLC12A7	Q9Y666	0	0	30	53
ACP2	P11117	0	0	5	6
ESYT1	Q9BSJ8	0	0	6	7
RAB33B	Q9H082	0	0	1	1
SORT1	Q99523	0	0	11	15
LEMD2	Q8NC56	0	0	9	13
GPR180	Q86V85	0	0	2	2
CHP1	Q99653	0	0	4	4
ROCK2	O75116	0	0	1	1
KIAA1033	Q2M389	0	0	1	1
EMC3	Q9P0I2	0	0	3	3
DOCK1	Q14185	0	0	7	7
ERMP1	Q7Z2K6	0	0	3	3
EBP	Q15125	0	0	2	4
SEC22A	Q96IW7	0	0	1	1

Table 1: Continued

		SNAP29		***VAMP4***	
Gene name	Protein ID	*Unique peptides*	*PSM*	*Unique Peptides*	*PSM*
TMED7	Q9Y3B3	0	0	1	1
SFT2D2	O95562	0	0	1	1
SLC30A5	Q8TAD4	0	0	2	2
MMGT1	Q8N4V1	0	0	5	8
VAC14	Q08AM6	0	0	1	1
TM9SF4	Q92544	0	0	3	3
TM9SF3	Q9HD45	0	0	6	8
SLC12A4	Q9UP95	0	0	9	13
UQCC1	Q9NVA1	0	0	4	4
C16orf91	Q4G0I0	0	0	2	2
SNAP47	Q5SQN1	0	0	7	8
SMEK1	Q6IN85	0	0	1	1
ALG8	Q9BVK2	0	0	3	3
TMEM161A	Q9NX61	0	0	2	5
VANGL1	Q8TAA9	0	0	2	2
SDCBP	O00560	0	0	2	2
CLTA	P09496	0	0	1	1
JPH1	Q9HDC5	0	0	4	4
PPAP2B	O14495	0	0	1	1
GOLGA2	Q08379	0	0	1	1
SLC39A11	Q8N1S5	0	0	3	5
FAM168A	Q92567	0	0	1	1
STXBP1	P61764	0	0	1	1
RAB8A	P61006	0	0	2	2
TRIM4	Q9C037	0	0	11	13
COPZ1	P61923	0	0	2	2
TMEM165	Q9HC07	0	0	1	1
DLGAP4	Q9Y2H0	0	0	1	1
SLC12A2	P55011	0	0	2	2
TMED9	Q9BVK6	0	0	2	2
TMTC3	Q6ZXV5	0	0	1	1
PIGS	Q96S52	0	0	1	1
XPO6	Q96QU8	0	0	18	24
SEC11A	P67812	0	0	2	4
AP3S1	Q92572	0	0	1	1
SLC12A5	Q9H2X9	0	0	5	8
TMEM43	Q9BTV4	0	0	6	11

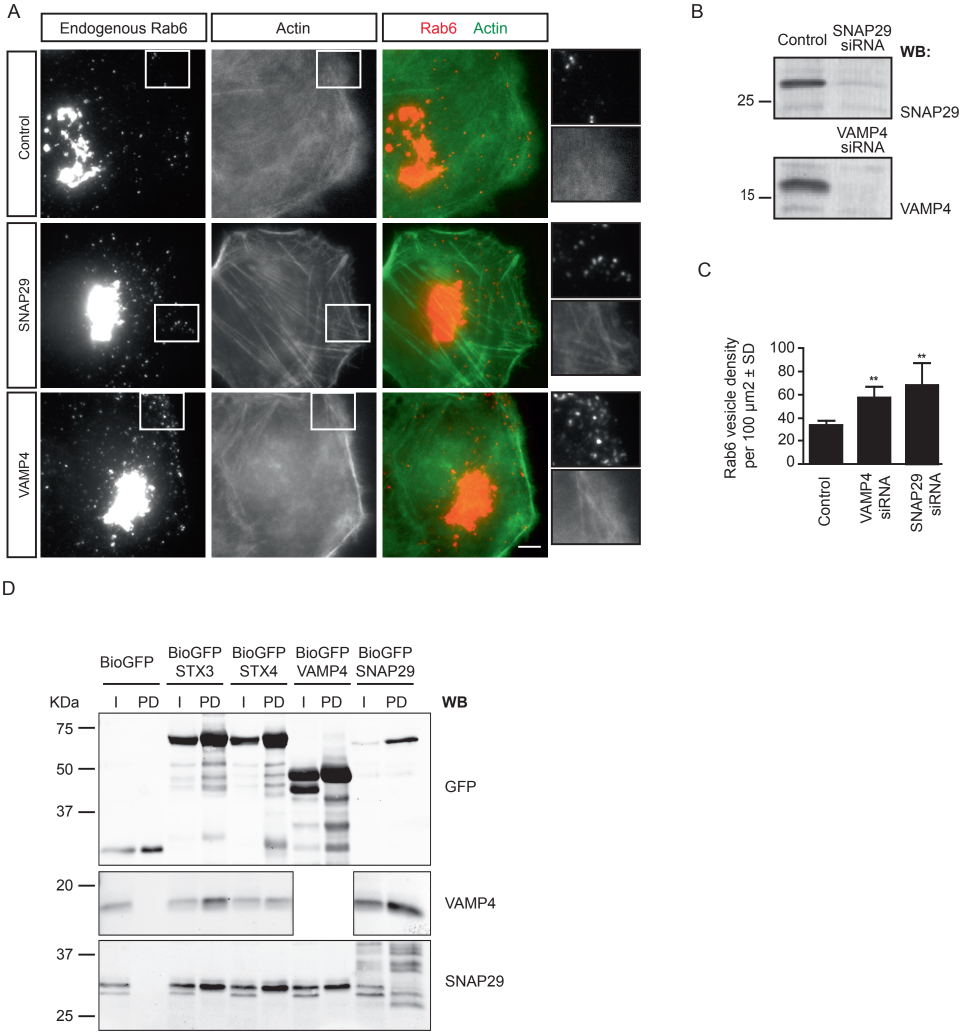
A
Endogenous Rab6
Actin
Rab6 Actin
Control
SNAP29
VAMP4
B
Control
SNAP29 siRNA
WB:
25
SNAP29
VAMP4 siRNA
15
VAMP4
C
Rab6 vesicle density per 100 µm2 ± SD
100
80
60
40
20
0
**
**
Control
VAMP4 siRNA
SNAP29 siRNA
D
BioGFP
BioGFP STX3
BioGFP STX4
BioGFP VAMP4
BioGFP SNAP29
KDa
I
PD
WB
75
50
37
GFP
20
VAMP4
37
25
SNAP29

Figure 1. VAMP4 and SNAP29 are involved in fusion of Rab6 secretory vesicles
(A) HeLa cells were transfected with siRNAs against VAMP4 or SNAP29 and immunostained for endogenous Rab6. Actin was detected with Phalloidin. Boxed areas are magnified. Scale bar: 5 μm.
(B) Western blots showing the depletion of VAMP4 and SNAP29 in HeLa cells three days after transfection.
(C) Quantification of Rab6 vesicle density in the cytoplasm per 100 μm^2 in control cells or cells transfected with siRNAs against VAMP4 or SNAP29. Error bars indicate standard deviation (SD). At least 1000 vesicles were analysed in 7-10 cells for each condition. ** $p<0.005$, Mann-Whitney test.
(D) Streptavidin pull-down assays from extracts of HEK293T cells coexpressing BirA, BioGFP or the indicated BioGFP-SNARE proteins (namely, BioGFP-syntaxin 3, BioGFP-syntaxin 4, BioGFP-VAMP4 and BioGFP-SNAP29). BioGFP proteins were detected with anti-GFP antibodies and VAMP4 and SNAP29 were detected with specific antibodies against VAMP4 and SNAP29. 2.5% of the input and 10% of the precipitate was loaded on gel.

To gain further support for the involvement of VAMP4 in Rab6 vesicle fusion, we next turned to microscopy-based assays. VAMP4 has been previously shown to localize to the trans-Golgi network (TGN) (Steegmaier et al., 1999), where Rab6 is also distributed (Antony et al., 1992). We tested if VAMP4 was present on Rab6 vesicles. We transfected cells with GFP-VAMP4 and TagRFP-T-Rab6, and by performing TIRF microscopy, which allows visualization of events occurring in close proximity to the plasma membrane, we observed that VAMP4 and Rab6 co-localized during vesicle fusion with the plasma membrane (Fig. 2A). Further, we have previously shown that Rab6-positive exocytotic vesicles display a fusion defect in the absence of ELKS and Rab8 and accumulate at the cell periphery (Grigoriev et al., 2011). To confirm that VAMP4 is present on Rab6 vesicles, we performed siRNA-mediated depletion of Rab8 and ELKS in cells stably expressing HA-VAMP4, and analyzed the co-localization between HA-VAMP4 and Venus-NPY, an exogenous cargo of Rab6 secretory vesicles (Grigoriev et al., 2007) (Fig. 2B). Accumulation of NPY-positive vesicles in the peripheral cytoplasm caused by the depletion of ELKS and Rab8 was accompanied by an accumulation of HA-VAMP4. These results support our data from live cells, and suggest that VAMP4 is a v-SNARE present on Rab6 vesicles. Altogether, our results suggest that VAMP4, SNAP29 and one of the yet to be identified syntaxins may form a SNARE complex responsible for the fusion of Rab6 vesicles with the plasma membrane.

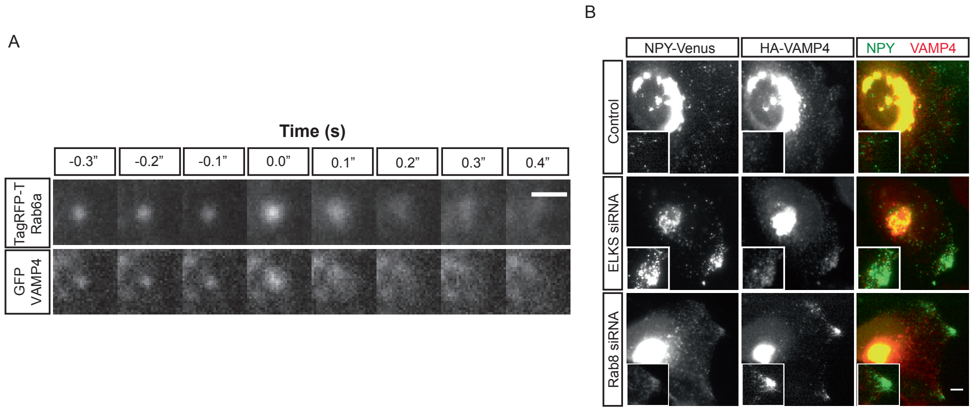

Figure 2. VAMP4 localizes to Rab6 secretory vesicles
(A) Frames from TIRFM movies showing the behavior of TagRFP-T-Rab6 and BioGFP-VAMP4 vesicles before and during fusion. Time is indicated in seconds. 0 sec corresponds to the sharp increase of fluorescent signal. Scale bar: 1 μm.
(B) HeLa cells stably expressing HA-VAMP4 were transfected with Venus-NPY and siRNAs against VAMP4 or SNAP29 and immunostained for the endogenous Rab6 and HA. Boxed areas are magnified. Scale bar: 5 μm.

Dominant negative Rab8 arrests secretory vesicles at the ELKS-positive cortical sites

We have reasoned that the finding of potential links between the ELKS-dependent machinery responsible for Rab6 vesicle docking at the cortex and the molecular complexes responsible for vesicle fusion might be facilitated by identifying a situation whereby Rab6 vesicles dock but fail to fuse. We have previously shown that depletion of Rab8 and overexpression of the GDP-bound Rab8-T22N mutant cause an increase in the number of vesicles at the cell periphery (Grigoriev et al., 2011). However, detailed analysis demonstrated that the behavior of the vesicles is very different in cells subjected to these treatments. In cells depleted of Rab8, Rab6 vesicles accumulated in the peripheral cell regions devoid of ELKS, and underwent extensive diffuse movements in these regions (Grigoriev et al., 2011). In contrast, in cells overexpressing the GDP-bound Rab8-T22N mutant, endogenous Rab6-vesicles strongly colocalized with ELKS-positive cortical patches (Fig. 3A). Live cell imaging demonstrated that GFP-Rab6 vesicles colocalized with mCherry-ELKS patches, where they were immobilized (Fig. 3B).

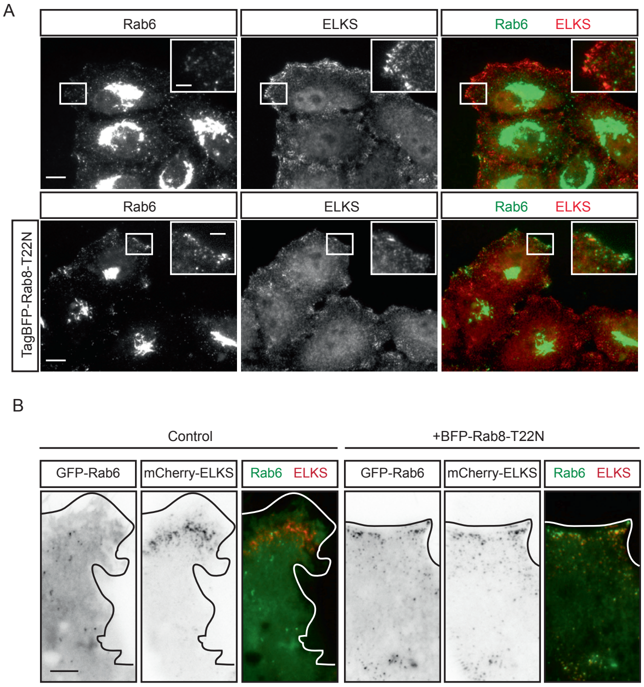

Figure 3. The GDP-bound Rab8-T22N mutant impairs fusion of Rab6 secretory vesicles
(A) HeLa cells were transfected with TagBFP-Rab8-T22N and immunostained for endogenous Rab6 and ELKS. Control cells are shown above. Scale bar: 10 μm. Boxed areas are magnified (Scale bar: 3 μm).
(B) HeLa cells were transfected with GFP-Rab6 and mCherry-ELKS. The images correspond to one frame of a movie. Scale bar: 5 μm.

We next wondered whether the interactions between Rab6, Rab8 and ELKS can occur on heterologous membranes which do not constitute a part of the secretory pathway. To test this, we have used the membrane targeting sequence (MTS) of the ActA protein of *Listeria monocytogenes* (Pistor et al., 1994). This domain targets heterologous proteins to the cytoplasmic side of the outer mitochondrial membrane and to the surface of peroxisomes (Hoogenraad et al., 2003). We have fused this domain to GFP-Rab6 (GFP-Rab6-MTS) and, as a control, to GFP (GFP-MTS). HeLa cells were then transfected with a construct expressing one of these two proteins together with different Rab8 constructs, namely the wild-type Rab8 (Rab8-WT), the constitutively active GTP-bound Rab8 (Rab8-Q67L) or the inactive GDP-bound Rab8 (Rab8-T22N), and the localization of Rab6-decorated membranes was tested. Both GFP-MTS and GFP-Rab6-MTS were efficiently targeted to mitochondrial and peroxisome membranes (Fig. 4 A-C). Endogenous ELKS was recruited to some of these structures, especially to the smaller ones, which, based on our previous experience, were peroxisomes (Fig. 4A-C). Interestingly, we could also observe that Rab8-WT and the GTP-bound Rab8-Q67L were recruited to GFP-Rab6-MTS membranes but not to GFP-MTS-labeled membranes (Fig. 4 A,B). The GDP-bound mutant Rab8-T22N was diffuse in the cytoplasm, and its recruitment to Rab6-positive membranes was less efficient (Fig. 4C). Additionally, Rab6-positive membranes partially localized with the cortical ELKS-positive sites at the cell periphery, an effect that was stronger when the inactive Rab8-T22N mutant was overexpressed (Fig.4C), resembling the effect of the expression of this Rab8 mutant on the endogenous Rab6 vesicles (Fig 3A). Our results show that Rab6 can recruit Rab8 to heterologous membranes and that these Rab6-decorated membranes can still be recruited to the cortical ELKS patches, especially when the inactive Rab8-T22N protein is expressed. These results suggest that the docking of Rab6 vesicles at the ELKS-positive sites requires interactions that are independent of the transmembrane proteins located in the secretory pathway, such as v-SNAREs.

Our results suggest that Rab8 GTPase lacking the ability to hydrolyze GTP promotes the docking of Rab6 vesicles but blocks their fusion with the plasma membrane. Therefore, Rab8 activity must be precisely regulated to ensure correct fusion of Rab6 secretory carriers with the plasma membrane. One possible explanation for the effect of the Rab8-T22N mutant effect is that it is mimicking the effect of a GAP (that inactivates GTPases by stimulating hydrolysis of the bound GTP) acting on Rab8. There are several GAPs with reported activity towards Rab8. AS160 is a GAP that in muscle cells is inactivated upon insulin stimulated phosphorylation, regulating GLUT4 translocation to the membrane (Sano et al., 2003). *In vitro*, AS160 displays a Rab-GAP activity towards the Rabs Rab2A, 8A, 8B, 10 and 14 (Miinea et al., 2005) and it was reported that Rab8A and Rab14 are physiological substrates of AS160, which cooperate to promote docking and fusion of GLUT4 vesicles in muscle cells (Ishikura et al., 2007; Randhawa et al., 2008). Rab8 was also reported as a target of the RabGAP XM_037557, which was identified in a screen for proteins involved in cilia formation (Yoshimura et al., 2007).

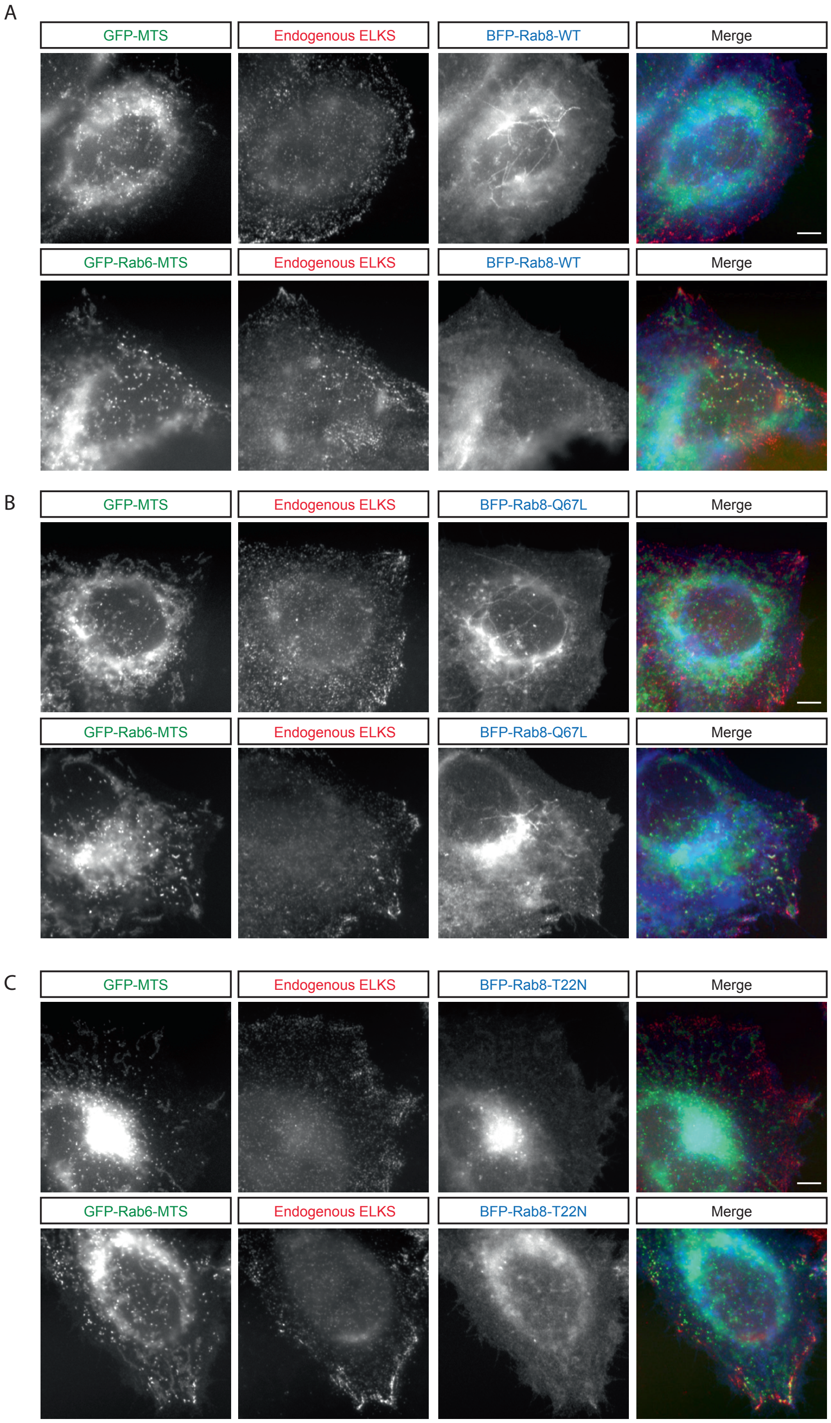
A
GFP-MTS
Endogenous ELKS
BFP-Rab8-WT
Merge
GFP-Rab6-MTS
Endogenous ELKS
BFP-Rab8-WT
Merge
B
GFP-MTS
Endogenous ELKS
BFP-Rab8-Q67L
Merge
GFP-Rab6-MTS
Endogenous ELKS
BFP-Rab8-Q67L
Merge
C
GFP-MTS
Endogenous ELKS
BFP-Rab8-T22N
Merge
GFP-Rab6-MTS
Endogenous ELKS
BFP-Rab8-T22N
Merge

See legend on next page

In order to test whether the effect of the Rab8-T22N on Rab6 vesicle fusion could be mimicked by the overexpression of a GAP with the reported activity towards Rab8, we overexpressed Flag-AS160, Flag-AS160-4P (non-phosphorylatable; constitutively active GAP mutant), Flag-AS160-RK (arginine to lysine mutation in the GAP domain, lacking the GAP activity), Flag-AS160-4PRK (inactive GAP activity) or GFP- XM_037557, and analyzed the distribution of endogenous Rab6 vesicles (Fig. 5A-E). None of the overexpressed GAPs produced an effect similar to that observed upon the overexpression of Rab8-T22N (Fig. 3A, B). Although AS160 and XM_037557 have been shown to have GAP activity towards Rab8 *in vitro* and in specific pathways, their overexpression does not have an effect on the docking or fusion of Rab6/Rab8 positive vesicles. Nevertheless, and because the intrinsic GTPase activity of Rab proteins is low (Scheffzek et al., 1998), GTPase activating proteins must be required in the majority of Rab cycles. It is possible that the GAP required for Rab8 inactivation in this pathway is still undiscovered or that multiple GAPs are required for the inactivation of Rab8. Another possible explanation for the effect of the inactive Rab8-T22N mutant could be an enhanced binding to Rabin8, the main activator of Rab8 (Hattula et al., 2002). It has been shown that Rab GEFs are major determinants for specific Rab membrane targeting (Blumer et al., 2013). Rab8-T22N mutant could display enhanced binding to Rabin8 and increased recruitment of Rab8, blocking downstream trafficking events. To test this possibility, we overexpressed GFP-Rabin8 but no differences were detected in the distribution of Rab6 vesicles (Fig. 5F). We thus conclude that although the results with the Rab8-T22N mutant confirm the importance of the proper GTPase cycle of Rab8 for the Rab6 vesicle docking and fusion at the cortex, all our attempts to identify the GAPs and GEFS involved so far have been unsuccessful.

Figure 4. Rab6 recruits Rab8 to heterologous membranes and the GDP-bound Rab8-T22N mutant arrests Rab6 membranes at cortical patches

(A-C) HeLa cells were transfected with GFP-fusion and TagBFP-fusion constructs and stained for the endogenous ELKS. An overlay of the imaged channels is shown. (A) Cells were transfected with GFP-MTS (upper panel) or GFP-Rab6-MTS (bottom panel) and TagBFP-Rab8-WT (wild type) and stained for the endogenous ELKS. (B) Cells were transfected with GFP-MTS (upper panel) or GFP-Rab6-MTS (bottom panel) and TagBFP-Rab8-Q67L and stained for the endogenous ELKS. (C) Cells were transfected with GFP-MTS (upper panel) or GFP-Rab6-MTS (bottom panel) and TagBFP-Rab8-T22N and stained for the endogenous ELKS. Scale bars: 5 μm.

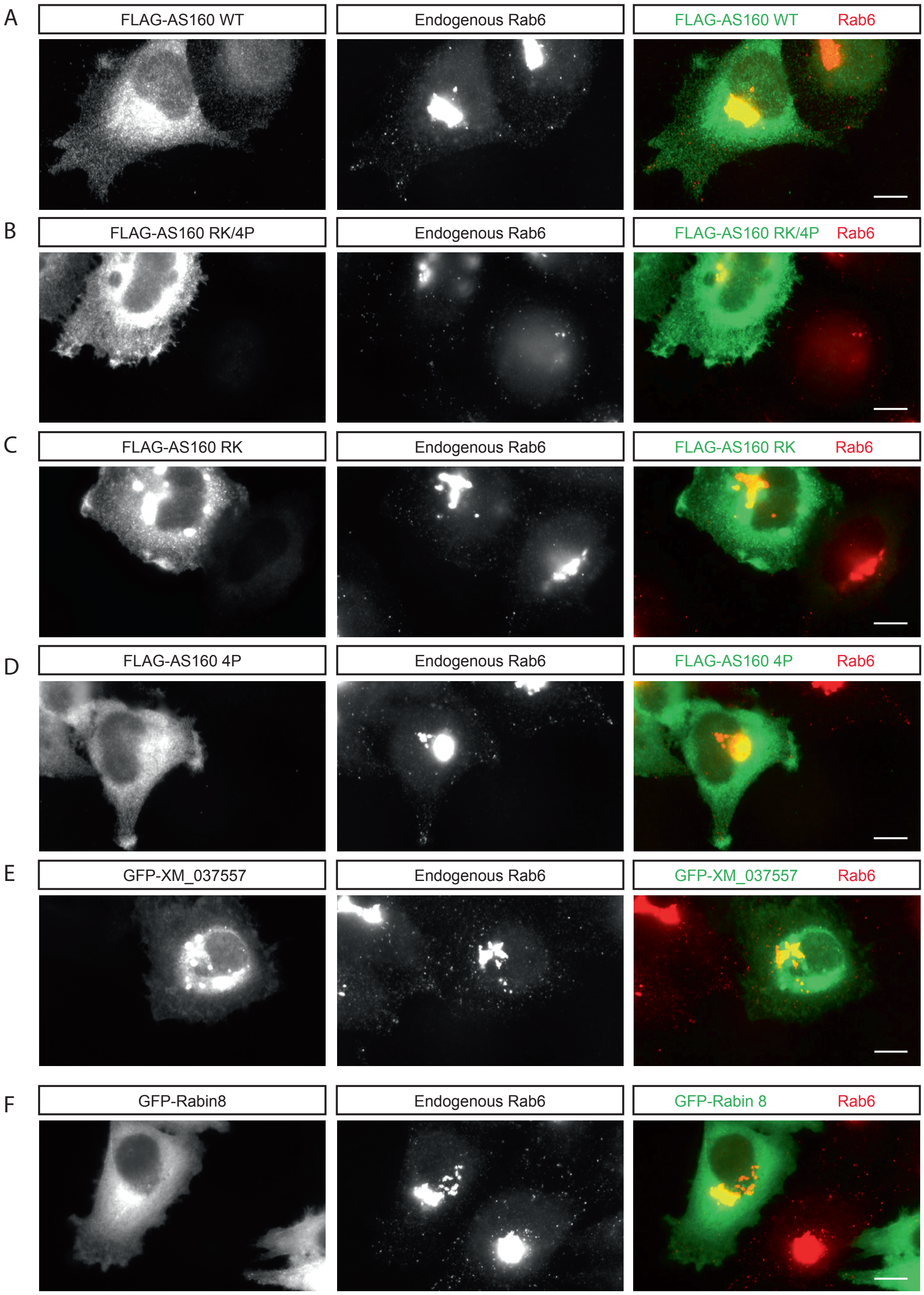
A
FLAG-AS160 WT
Endogenous Rab6
FLAG-AS160 WT Rab6
B
FLAG-AS160 RK/4P
Endogenous Rab6
FLAG-AS160 RK/4P Rab6
C
FLAG-AS160 RK
Endogenous Rab6
FLAG-AS160 RK Rab6
D
FLAG-AS160 4P
Endogenous Rab6
FLAG-AS160 4P Rab6
E
GFP-XM_037557
Endogenous Rab6
GFP-XM_037557 Rab6
F
GFP-Rabin8
Endogenous Rab6
GFP-Rabin 8 Rab6

See legend on next page

Crosstalk between the endocytic and exocytotic pathways

The function of different tethering and docking complexes in membrane fusion is to facilitate the engagement of SNAREs, to which such complexes can often bind (Cai et al., 2007)). Is there a direct molecular link between the ELKS complexes and SNAREs? Using streptavidin pull down assays with BioGFP-VAMP4 and BioGFP-SNAP29 from HEK293T cells, we searched for potential connections between the SNARE-associated protein machinery and ELKS-containing vesicle docking complexes. Among the highest hits in the mass spectrometry analysis of the potential BioGFP-SNAP29 binding partners were the members of the C-terminal Eps15 homology domain (EHD) family of proteins (Table 1). EHDs are endocytic regulatory proteins, and all four mammalian homologues have been implicated in the regulation of endocytic transport steps (Grant and Caplan, 2008). In our mass spectrometry analysis of SNAP29 interactome we also identified VPS-45, another protein known to interact with the EHD binding protein Rabenosyn-5 (Naslavsky et al., 2004). Interestingly, VPS-45 was also identified in the mass spectrometry analysis of VAMP4, a R-SNARE that binds to SNAP29 (Fig.1). To confirm these results we tested the binding between SNAP29 and EHD1 and EHD3. HEK293T cells were transfected with BioGFP-SNAP29 and GFP-myc-EHD1 or GFP-EHD3, followed by streptavidin pull down assays. As shown in Figure 6A, both EHD proteins could bind to BioGFP-SNAP29. This result is in line with previous studies, where SNAP29 was shown to bind to EHD1 (Xu et al., 2004). Interestingly, a mass spectrometry-based search for ELKS partners from HEK293T cells has also identified one of the EHD family members, EHD4 (K.L.Yu, personal communication).

We next transfected HeLa cells with GFP-myc-EHD1 and tested its colocalization with TagRFP-T-Rab6 (Fig. 6B, a). By performing live cell microscopy, we could observe that EHD1 localized to vesicle-like structures at the plasma membrane, but the colocalization with TagRFP-T-Rab6 was not obvious.

Figure 5. Rab8 GAPs do not block fusion of Rab6 secretory vesicles

(A-D) HeLa cells were transfected with Flag-AS160, Flag-AS160-RK/4P, Flag-AS160-RK or Flag-AS160-4P constructs and stained for the endogenous Rab6 and Flag tag.

(E-F) HeLa cells were transfected with GFP-XM_037557 (E) or GFP-Rabin8 (F) and stained for the endogenous Rab6. Scale bars: 10 μm.

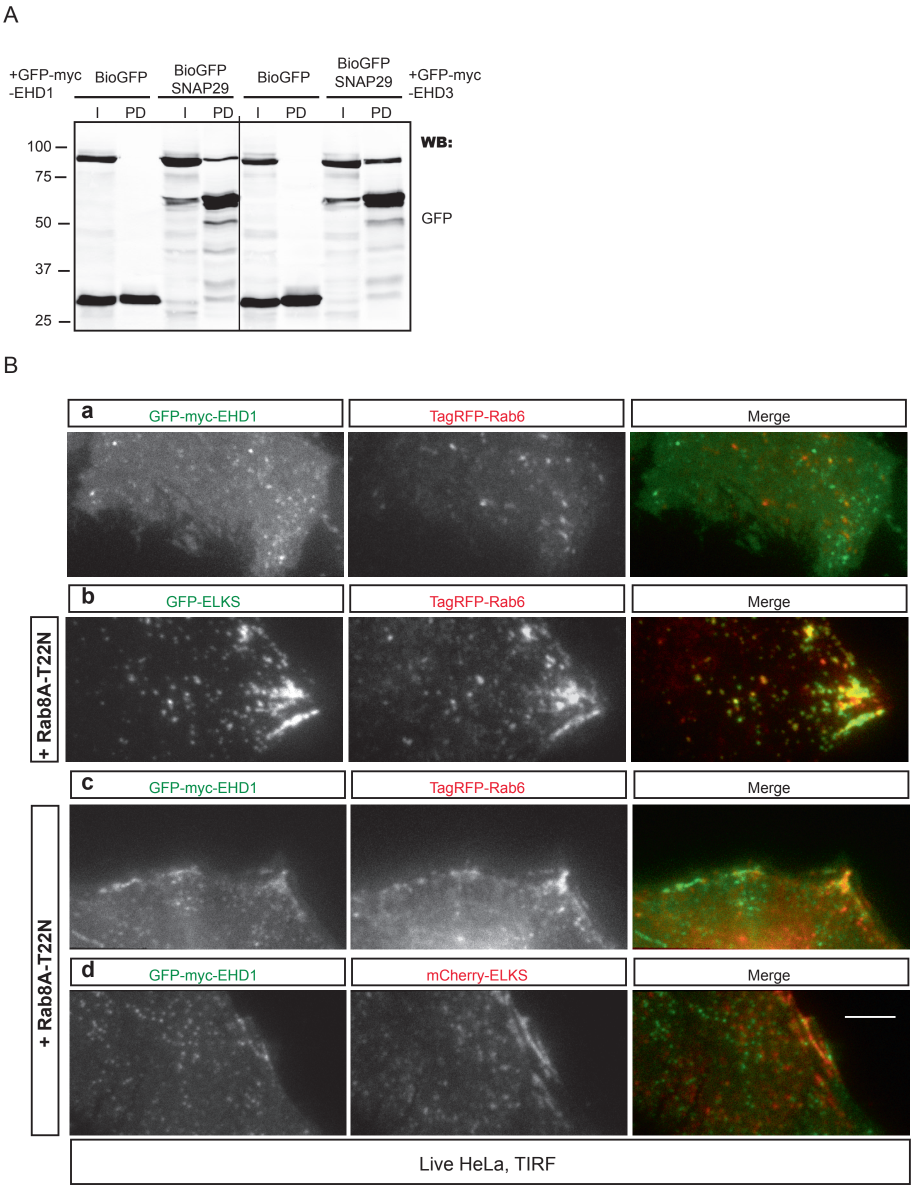
A
+GFP-myc
-EHD1
BioGFP
BioGFP
SNAP29
BioGFP
BioGFP
SNAP29
+GFP-myc
-EHD3
I
PD
I
PD
I
PD
I
PD
100
75
50
37
25
WB:
GFP
B
a
GFP-myc-EHD1
TagRFP-Rab6
Merge
b
GFP-ELKS
TagRFP-Rab6
Merge
+ Rab8A-T22N
c
GFP-myc-EHD1
TagRFP-Rab6
Merge
d
GFP-myc-EHD1
mCherry-ELKS
Merge
+ Rab8A-T22N
Live HeLa, TIRF

Figure 6. Members from the EHD family of proteins are linked to Rab6 mediated constitutive exocytosis

(A) Streptavidin pull-down assays from extracts of HEK293T cells coexpressing BirA, BioGFP or BioGFP-SNAP29 and GFP-myc-EHD1 or GFP-EHD3. All proteins were detected with anti-GFP antibodies. 2.5% of the input and 10% of the precipitate was loaded on gel.

(B) (a) HeLa cells were transfected with GFP-myc-EHD1 and TagRFP-T-Rab6. (b-d) HeLa cells were transfected with TagBFP-Rab8-T22N and (b) GFP-ELKS and TagRFP-T-Rab6 (c) GFP-myc-EHD1 and TagRFP-T-Rab6 (d) GFP-myc-EHD1 and mCherry-ELKS. The images correspond to one frame of a movie. Scale bar: 5 μm.

As we have previously discussed, overexpression of the GDP-bound Rab8A-T22N mutant induces accumulation of Rab6 positive vesicles at ELKS patches in the cell cortex. We observed that overexpression of Rab8A-T22N likewise caused accumulation of EHD1 at the cell periphery (Fig. 6B, b-d), suggesting a function for EHDs in Rab6 dependent exocytosis. Due to the poor co-localization between Rab6 and EHD1 on vesicles, we wondered whether EHD1 was specifically present on Rab6 vesicles when they were ready to fuse. Indeed, by looking at the fusion of individual vesicles by TIRF microscopy, we could observe recruitment of EHDs upon Rab6 vesicle docking (Figure 7A, B), what is particularly evident from the kymograph analysis depicted in figure 7B.

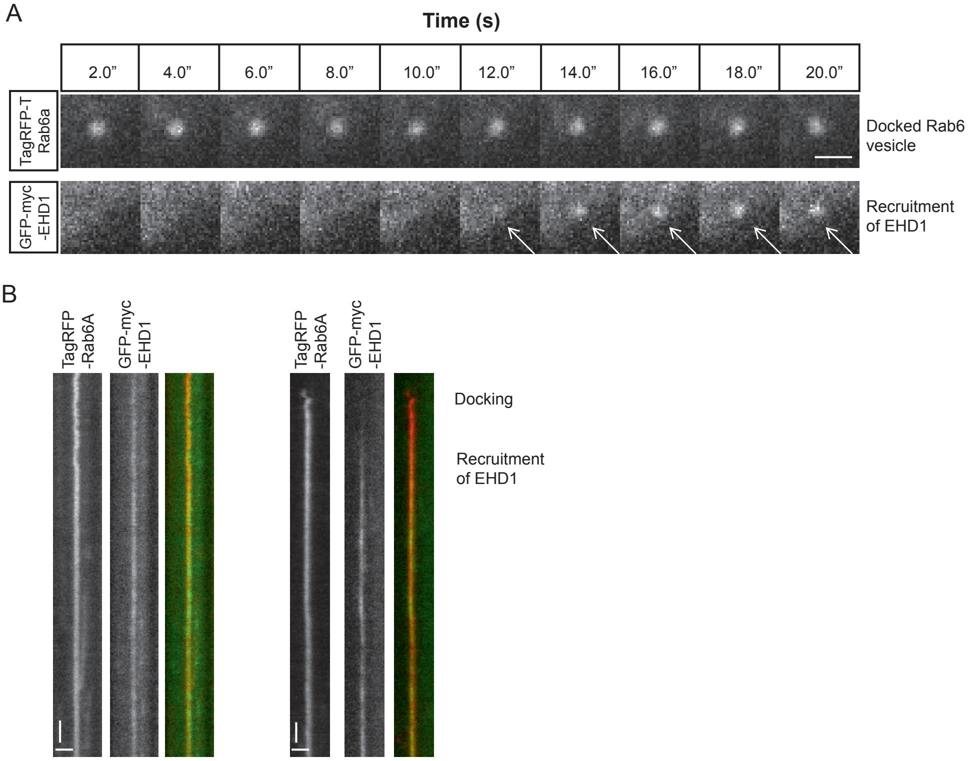
A
Time (s)
2.0”
4.0”
6.0”
8.0”
10.0”
12.0”
14.0”
16.0”
18.0”
20.0”
TagRFP-T Rab6a
Docked Rab6 vesicle
GFP-myc -EHD1
Recruitment of EHD1
B
TagRFP -Rab6A
GFP-myc -EHD1
TagRFP -Rab6A
GFP-myc -EHD1
Docking
Recruitment of EHD1

Figure 7. EHD1 is recruited to docked Rab6 vesicles
(A) Frames from TIRFM movies showing the behavior of TagRFP-T-Rab6 and GFP-myc-EHD1 vesicles during docking. Time is indicated in seconds. Scale bar: 1 μm.
(B) Kymographs illustrating the behavior of vesicles labelled with GFP-myc-EHD1 and TagRFP-T-Rab6. Horizontal bar: 1 μm. Vertical bar: 1s.

Altogether, our results suggest a new function for the EHD endocytic family of proteins in mediating the interplay between the docking and fusion machineries of constitutive exocytotic carriers. MICAL-L1, a protein from the Molecule Interacting with CasL

(MICAL) protein family, binds to EHD1 and recruits EHD1 and Rab8 to tubular recycling endosomes (Sharma et al., 2009). Interestingly, we have shown that the MICAL-L1 related protein MICAL-3, a monooxygenase, cooperates with Rab8 to promote docking and fusion of Rab6 secretory vesicles (Grigoriev et al., 2011).

We have tried to further investigate the function of EHD proteins in this pathway by testing the effect of different EHD mutants on Rab6 vesicle fusion, including GFP-EHD1-T94A (loss of ATPase activity), GFP-EHD1-I150Q (enhanced ATPase activity) and GFP-EHD1- ΔEH (lack of the EH domain, no binding to partners) (Naslavsky and Caplan, 2011; Naslavsky et al., 2006). Unfortunately, the results obtained with overexpression of the aforementioned mutants were not consistent and it was not possible to make solid interpretations or conclusions. siRNA transfection against these proteins was also inconclusive. Additional limitations, including the lack of specific antibodies for siRNA-mediated depletion efficiency validation and the possible redundancy between the four mammalian EHD homologues constitute challenges that need to be addressed in the future.

Conclusions and outlook

In this chapter, we have identified two SNAREs, VAMP4 and SNAP29, which contribute to the fusion of Rab6 vesicles with the plasma membrane. Further, we have shown that Rab8-T22N mutant arrests Rab6 vesicles on the ELKS-positive cortical sites. Since the phenotype is different from Rab8 depletion, where Rab6 vesicles fail to interact with ELKS-positive "patches", these data suggest that Rab8 in the GDP form can promote docking but inhibits the fusion step. The underlying mechanism is unclear, but might involve MICAL-3, which can bind to both ELKS and Rab8 (Grigoriev et al., 2011), a possibility which deserves further investigation. Further, we have identified EHDs, proteins well known for their multimerisation and ATPase-dependent membrane function in endocytosis (Naslavsky and Caplan, 2011) as potential players that might be connected to both SNAREs and ELKS. Our data suggest that EHDs might be recruited to the vesicle fusion sites, possibly to mediate some membrane remodeling steps associated with fusion.

Are there some other links between the SNAREs and the ELKS-containing cortical complexes? In neurons, ELKS and its homologue CAST are part of the cytomatrix at the active zone, an extensive scaffold responsible for docking of synaptic vesicles at the presynaptic membrane and their rapid fusion induced by calcium influx (Gundelfinger and Fejtova, 2012; Sudhof, 2012). At the presynapse, ELKS and CAST bind to RIM1 and Munc13, which are intimately involved in vesicle docking and priming, with Munc13 interacting with SNAREs and SM (Sec1/Munc18) proteins (Gundelfinger and Fejtova, 2012; Sudhof, 2012). However, the ubiquitously expressed ELKS isoform present in

HeLa cells and other cell lines lacks the C-terminal RIM1-binding domain (Wang et al., 2002). Mun13 proteins are specific for calcium-regulated exocytosis in neuronal and neuroendocrine cells, and their role in SNARE activation might be performed by other tethering factors (James and Martin, 2013). So far, we have not been able to identify these factors. For example, a logical candidate would be the exocyst, a large multi-subunit tethering complex, which regulates polarized exocytotic vesicle fusion with the plasma membrane in different organisms (Das and Guo, 2011). Until now, we have not found any biochemical connections between ELKS and the exocyst, and the depletion of Exo70, an exocyst component had only a mild effect, if any, on the distribution and abundance of rab6 vesicles (our unpublished data). It is also possible that ELKS-containing complexes exert their effect on Rab6 vesicle fusion without making direct contact with SNAREs, but rather by regulating the timing and localization of their interaction with the plasma membrane and thus indirectly facilitating SNARE engagement. Additional biochemical and imaging studies will be needed to reveal all the molecular details underlying the last steps of constitutive exocytosis.

Acknowledgements

We thank Dr. Andrew Peden, Dr. Steve Caplan, Dr. Francis Barr, Dr. A. Barnekow, Dr. Frauke Melchior and Dr. Amira Klip for sharing reagents and for discussions about the project. We thank Dr. V. Lupashin for the suggestion to use Rab6 recruitment to mitochondria as a tool to study Rab6-Rab8 membrane recruitment hierarchy. This work was supported by Fundação para a Ciência e a Tecnologia fellowship to A.S-M., by the Netherlands Organization for Scientific Research (NWO) ALW-VICI grant and the European Research Council (ERC) Synergy grants to A.A., and by NWO-CW ECHO grant to A.A. and A.J.R.H.

Experimental procedures

Antibodies and reagents

The following primary and secondary antibodies were used in this study: mouse monoclonal antibodies against Rab6A/Rab6A' (gift of Dr. A. Barnekow, University of Muenster, Germany, (Matanis et al., 2002) rabbit anti-GFP (Abcam), mouse anti-HA (Covance), rabbit anti-Flag (Sigma). The rabbit anti-ELKS antibody was a gift from Dr. F. Melchior (Heidelberg University, Germany). And the Rabbit antibodies against VAMP4 and SNAP29 were a gift from Dr. Andrew Peden (Gordon et al., 2010).

For immunofluorescence experiments we used Alexa488-, and Alexa568-conjugated secondary antibodies (Invitrogen) and Phalloidin-A488. For Western blotting we used IRDye 800CW goat and anti-rabbit antibodies, which were detected using Odyssey Infrared Imaging system (Li-Cor Biosciences).

Expression constructs, siRNAs and cell lines

We used the following previously described expression vectors: GFP-ELKS (Grigoriev et al., 2007), mCherry-ELKS (Grigoriev et al., 2011), NPY-Venus (Nagai et al., 2002), BirA (Lansbergen et al., 2006), GFP-MTS (Hoogenraad et al., 2003). Flag-AS160-WT, 4P, RK, RK/4P were a gift of Dr. Amira Klip (The Hospital for Sick Children, Toronto, Canada). GFP-myc-EHD1, GFP-EHD3 and GFP-myc-ΔEH were gifts of Dr. Steven Caplan (University of Nebraska Medical Center, Nebraska, USA). BioGFP-VAMP4, SNAP29, syntaxin 3 and syntaxin 4 were cloned as following: VAMP4, SNAP29, syntaxin 3 and syntaxin 4 were PCR amplified from HA-VAMP4, SNAP29, syntaxin 3 and syntaxin 4 (Gordon et al., 2010), respectively and subsequently cloned into a BioGFP vector. TagBFP-Rab8-WT, Q67L and T22N were cloned by replacing the GFP tag on previously described GFP-tagged constructs (Ang et al., 2003) by TagBFP. The GFP-EHD-T94A and GFP-EHD-I157Q constructs were prepared by PCR-based strategy using GFP-myc-EHD1 construct. Subsequently, PCR products were subcloned in pEGFP expression vectors. GFP-Rab6-MTS was generated by PCR-based strategy using GFP-Rab6 (Matanis et al., 2002). Rab6 was then subcloned into GFP-MTS. TagRFP-T-Rab6 was a gift of Dr. Yuko Mimori-Kiyosue (RIKEN Center for Developmental Biology, Japan).

The siRNAs used in this study were synthesized by Sigma and were directed against the following sequences: VAMP4 5'-GGAUGAAGUUAUUGAUGUC-3'; SNAP29 5'-GAAGCUAUAAGUACAAGUA-3'. The HeLa cell line stably expressing HA-VAMP4 was a gift of Dr. Andrew Peden (University of Sheffield, United Kingdom).

Streptavidin pulldown assays

HEK293 cells were cultured in DMEM/Ham's-F10 (50/50%) medium containing 10% FCS and 1% penicillin/streptomycin and were transfected using Polyethylenimine (PEI; Mw 2500; Polysciences) at a 3:1 PEI:DNA ratio (w/w). 24 hours after transfection, cells were incubated with N-ethylmaleimide (NEM;0.5 mM) for 30 min at 37^{0}C and harvested by scraping the cells in ice-cold PBS and lysing cell pellets in lysis buffer (20 mM Tris-HCl, pH 7.5, 100 mM NaCl, 1.0% Triton X-100, and protease inhibitors; Roche). Supernatants and pellet fractions were separated by centrifugation at maximum speed for 20 minutes. Supernatants were mixed with an equal amount of Dyna M-280 Streptavidin beads (Life Technologies). Samples were incubated 2 hours while rotating at 4°C, collected with magnet and pellets were washed 5-7 times with the wash buffer (20 mM Tris-HCl, pH 7.5, 100 mM NaCl, 0.1 % Triton X-100). Samples were eluted in SDS sample buffer, equally loaded onto SDS-PAGE gels and subjected to Western blotting. Blots were blocked with 2% bovine serum albumin/0.07% Tween 20 in PBS and incubated with primary antibodies at 4°C overnight. Blots were washed with 0.07% Tween 20 in PBS three times for 10 min at room temperature and incubated with either IRDye 800CW goat anti-mouse and anti-rabbit secondary antibodies, which were detected using Odyssey Infrared Imaging system (Li-Cor Biosciences).

Transfection and immunofluorescence of cultured HeLa cells

HeLa cells were cultured in DMEM/Ham's F10 (50/50%) medium containing 10% FCS and 1% penicillin/streptomycin. One day before transfection, cells were plated on glass coverslips. Cells were transfected with FuGene 6 (Promega) according to the manufacturer's protocol and incubated overnight. Cells were transfected with 10 nM siRNAs with HiPerFect (Qiagen) and analyzed 3 days after transfection. Cells were either mounted for live imaging or fixed in 4% paraformaldehyde for 10 min at room temperature followed by 10 min in 0.15% Triton X-100 in PBS. Slides were blocked in 2% bovine serum albumin/0.07% Tween 20 in PBS and labeled with primary antibody for 1 hour at room temperature. Slides were washed three times with 0.07% Tween20 in PBS, labeled with secondary antibodies for 1 hour at room temperature, washed three times with 0.07% Tween20 in PBS and mounted using Vectashield mounting medium (Vector laboratories).

Mass spectrometry and data analysis

30 μl of each sample was run on a 12% Bis-Tris 1D SDS-PAGE gel (Biorad) for 1 cm and stained with colloidal Coomassie dye G-250 (Gel Code Blue Stain Reagent, Thermo Scientific). Each lane was cut into 1 band, which were treated with 6.5 mM dithiothreitol (DTT) for 1 hour at 60 °C for reduction and 54 mM iodoacetamide for 30 min for alkylation.

The proteins were digested overnight with trypsin (Promega) at 37°C. The peptides were extracted with acetonitrile (ACN) and dried in a vacuum concentrator.

The data were acquired using an LTQ-Orbitrap coupled to an Agilent 1200 system. Peptides were first trapped (Dr Maisch Reprosil C18, 3 μm, 2 cm x 100 μm) before being separated on an analytical column (50 μm x 400 mm, 3 μm, 120 Å Reprosil C18-AQ). Trapping was performed at 5 μl/min for 10 min in solvent A (0.1 M acetic acid in water), and the gradient was as follows; 10 - 37% solvent B in 30 min, 37-100% B in 2 min, 100% B for 3 min, and finally solvent A for 15 min. Flow was passively split to 100 nl min^{-1}. Data was acquired in a data-dependent manner, to automatically switch between MS and MS/MS. Full scan MS spectra from m/z 350 to 1500 were acquired in the Orbitrap at a target value of 5e5 with a resolution of 60,000 at m/z 400. The five most intense ions were selected for fragmentation in the linear ion trap at a normalized collision energy of 35% after the accumulation of a target value of 10,000.

Raw files were processed using Proteome Discoverer 1.3 (Thermo Scientific, Bremen, Germany). The database search was performed against the Swissprot human database, taxonomy (version May 2012) using Mascot (version 2.3, Matrix Science, UK) as search engine. Carbamidomethylation of cysteines was set as a fixed modification and oxidation of methionine was set as a variable modification. Trypsin was specified as enzyme and up to two miss cleavages were allowed. Data filtering was performed using percolator, resulting in 1% false discovery rate (FDR). Additional filter was Mascot ion score >20. Raw files corresponding to one sample were merged into one result file.

Image acquisition and time-lapse live cell imaging

Images of fixed cells were collected with a Nikon Eclipse 80i microscope equipped with a Plan Fluor 10x N.A. 0.30 objective, Chroma ET-GFP (49002) filter and a Photometrics CoolSNAP HQ2 CCD camera. Live cell imaging was performed on an inverted research microscope Nikon Eclipse Ti-E (Nikon) with perfect focus system (PFS) (Nikon), equipped with Nikon CFI Apo TIRF 100x 1.49 N.A. oil objective (Nikon), Photometrics Evolve 512 EMCCD (Roper Scientific) and controlled with MetaMorph 7.7.5 software (Molecular Devices). The 16-bit images were projected onto the CCD chip with intermediate lens 2.5X (Nikon C mount adapter 2.5X) at a magnification of 0.063 μm/pixel. To keep cells at 37°C we used stage top incubator (model INUBG2E-ZILCS Tokai Hit). The microscope was equipped with TIRF-E motorized TIRF illuminator modified by Roper Scientific France/PICT-IBiSA, Institut Curie. For regular imaging we used mercury lamp HBO-103W/2 (Osram) for excitation or 491nm 100mW Calypso (Cobolt) and 561nm 100mW Jive (Cobolt) lasers. We used ET-GFP filter set (Chroma) for imaging of proteins tagged with GFP; ET-mCherry filter set (Chroma) for imaging of proteins tagged with mCherry. For simultaneous imaging of green and red fluorescence we used triple-band TIRF polychroic ZT405/488/561rpc (Chroma) and triple-band laser emission filter ZET405/488/561m (Chroma), mounted in the metal cube (Chroma, 91032) together with Optosplit III beamsplitter (Cairn Research Ltd, UK) equipped with double emission filter cube configured with ET525/50m, ET630/75m and T585LPXR (Chroma).

References

Ang, A.L., H. Folsch, U.M. Koivisto, M. Pypaert, and I. Mellman. 2003. The Rab8 GTPase selectively regulates AP-1B-dependent basolateral transport in polarized Madin-Darby canine kidney cells. *The Journal of cell biology*. 163:339-350.

Antony, C., C. Cibert, G. Geraud, A. Santa Maria, B. Maro, V. Mayau, and B. Goud. 1992. The small GTP-binding protein rab6p is distributed from medial Golgi to the trans-Golgi network as determined by a confocal microscopic approach. *Journal of cell science*. 103 (Pt 3):785-796.

Barr, F., and D.G. Lambright. 2010. Rab GEFs and GAPs. *Current opinion in cell biology*. 22:461-470.

Bassham, D.C., and M.R. Blatt. 2008. SNAREs: cogs and coordinators in signaling and development. *Plant physiology*. 147:1504-1515.

Blumer, J., J. Rey, L. Dehmelt, T. Mazel, Y.W. Wu, P. Bastiaens, R.S. Goody, and A. Itzen. 2013. RabGEFs are a major determinant for specific Rab membrane targeting. *The Journal of cell biology*. 200:287-300.

Bonifacino, J.S., and B.S. Glick. 2004. The mechanisms of vesicle budding and fusion. *Cell*. 116:153-166.

Brunger, A.T. 2005. Structure and function of SNARE and SNARE-interacting proteins. *Quarterly reviews of biophysics*. 38:1-47.

Burgess, T.L., and R.B. Kelly. 1987. Constitutive and regulated secretion of proteins. *Annual review of cell biology*. 3:243-293.

Cai, H., K. Reinisch, and S. Ferro-Novick. 2007. Coats, tethers, Rabs, and SNAREs work together to mediate the intracellular destination of a transport vesicle. *Developmental cell*. 12:671-682.

Das, A., and W. Guo. 2011. Rabs and the exocyst in ciliogenesis, tubulogenesis and beyond. *Trends in cell biology*. 21:383-386.

Dirac-Svejstrup, A.B., T. Sumizawa, and S.R. Pfeffer. 1997. Identification of a GDI displacement factor that releases endosomal Rab GTPases from Rab-GDI. *The EMBO journal*. 16:465-472.

Fasshauer, D., R.B. Sutton, A.T. Brunger, and R. Jahn. 1998. Conserved structural features of the synaptic fusion complex: SNARE proteins reclassified as Q- and R-SNAREs. *Proceedings of the National Academy of Sciences of the United States of America*. 95:15781-15786.

Gordon, D.E., L.M. Bond, D.A. Sahlender, and A.A. Peden. 2010. A targeted siRNA screen to identify SNAREs required for constitutive secretion in mammalian cells. *Traffic*. 11:1191-1204.

Grant, B.D., and S. Caplan. 2008. Mechanisms of EHD/RME-1 protein function in endocytic transport. *Traffic*. 9:2043-2052.

Grigoriev, I., D. Splinter, N. Keijzer, P.S. Wulf, J. Demmers, T. Ohtsuka, M. Modesti, I.V. Maly, F. Grosveld, C.C. Hoogenraad, and A. Akhmanova. 2007. Rab6 regulates transport and targeting of exocytotic carriers. *Developmental cell*. 13:305-314.

Grigoriev, I., K.L. Yu, E. Martinez-Sanchez, A. Serra-Marques, I. Smal, E. Meijering, J. Demmers, J. Peranen, R.J. Pasterkamp, P. van der Sluijs, C.C. Hoogenraad, and A. Akhmanova. 2011. Rab6, Rab8, and MICAL3 cooperate in controlling docking and fusion of exocytotic carriers. *Current biology : CB*. 21:967-974.

Gundelfinger, E.D., and A. Fejtova. 2012. Molecular organization and plasticity of the cytomatrix at the active zone. *Current opinion in neurobiology*. 22:423-430.

Hattula, K., J. Furuhjelm, A. Arffman, and J. Peranen. 2002. A Rab8-specific GDP/GTP exchange factor is involved in actin remodeling and polarized membrane transport. *Molecular biology of the cell*. 13:3268-3280.

Hoogenraad, C.C., P. Wulf, N. Schiefermeier, T. Stepanova, N. Galjart, J.V. Small, F. Grosveld, C.I. de Zeeuw, and A. Akhmanova. 2003. Bicaudal D induces selective dynein-mediated microtubule minus end-directed transport. *The EMBO journal*. 22:6004-6015.

Huber, L.A., S. Pimplikar, R.G. Parton, H. Virta, M. Zerial, and K. Simons. 1993. Rab8, a small GTPase involved in vesicular traffic between the TGN and the basolateral plasma membrane. *The Journal of cell biology*. 123:35-45.

Hutagalung, A.H., and P.J. Novick. 2011. Role of Rab GTPases in membrane traffic and cell physiology. *Physiological reviews*. 91:119-149.

Ishikura, S., P.J. Bilan, and A. Klip. 2007. Rabs 8A and 14 are targets of the insulin-regulated Rab-GAP AS160 regulating GLUT4 traffic in muscle cells. *Biochemical and biophysical research communications*. 353:1074-1079.

Jahn, R., and R.H. Scheller. 2006. SNAREs--engines for membrane fusion. *Nature reviews. Molecular cell biology*. 7:631-643.

James, D.J., and T.F. Martin. 2013. CAPS and Munc13: CATCHRs that SNARE Vesicles. *Frontiers in endocrinology*. 4:187.

Lansbergen, G., I. Grigoriev, Y. Mimori-Kiyosue, T. Ohtsuka, S. Higa, I. Kitajima, J. Demmers, N. Galjart, A.B. Houtsmuller, F. Grosveld, and A. Akhmanova. 2006. CLASPs attach microtubule plus ends to the cell cortex through a complex with LL5beta. *Developmental cell*. 11:21-32.

Matanis, T., A. Akhmanova, P. Wulf, E. Del Nery, T. Weide, T. Stepanova, N. Galjart, F. Grosveld, B. Goud, C.I. De Zeeuw, A. Barnekow, and C.C. Hoogenraad. 2002. Bicaudal-D regulates COPI-independent Golgi-ER transport by recruiting the dynein-dynactin motor complex. *Nature cell biology*. 4:986-992.

Miinea, C.P., H. Sano, S. Kane, E. Sano, M. Fukuda, J. Peranen, W.S. Lane, and G.E. Lienhard. 2005. AS160, the Akt substrate regulating GLUT4 translocation, has a functional Rab GTPase-activating protein domain. *The Biochemical journal*. 391:87-93.

Nagai, T., K. Ibata, E.S. Park, M. Kubota, K. Mikoshiba, and A. Miyawaki. 2002. A variant of yellow fluorescent protein with fast and efficient maturation for cell-biological applications. *Nature biotechnology*. 20:87-90.

Naslavsky, N., M. Boehm, P.S. Backlund, Jr., and S. Caplan. 2004. Rabenosyn-5 and EHD1 interact and sequentially regulate protein recycling to the plasma membrane. *Molecular biology of the cell*. 15:2410-2422.

Naslavsky, N., and S. Caplan. 2011. EHD proteins: key conductors of endocytic transport. *Trends in cell biology*. 21:122-131.

Naslavsky, N., J. Rahajeng, M. Sharma, M. Jovic, and S. Caplan. 2006. Interactions between EHD proteins and Rab11-FIP2: a role for EHD3 in early endosomal transport. *Molecular biology of the cell*. 17:163-177.

Pelham, H.R. 1999. SNAREs and the secretory pathway-lessons from yeast. *Experimental cell research*. 247:1-8.

Pistor, S., T. Chakraborty, K. Niebuhr, E. Domann, and J. Wehland. 1994. The ActA protein of Listeria monocytogenes acts as a nucleator inducing reorganization of the actin cytoskeleton. *The EMBO journal*. 13:758-763.

Randhawa, V.K., S. Ishikura, I. Talior-Volodarsky, A.W. Cheng, N. Patel, J.H. Hartwig, and A. Klip. 2008. GLUT4 vesicle recruitment and fusion are differentially regulated by Rac, AS160, and Rab8A in muscle cells. *The Journal of biological chemistry*. 283:27208-27219.

Rybin, V., O. Ullrich, M. Rubino, K. Alexandrov, I. Simon, M.C. Seabra, R. Goody, and M. Zerial. 1996. GTPase activity of Rab5 acts as a timer for endocytic membrane fusion. *Nature*. 383:266-269.

Sano, H., S. Kane, E. Sano, C.P. Miinea, J.M. Asara, W.S. Lane, C.W. Garner, and G.E. Lienhard. 2003. Insulin-stimulated phosphorylation of a Rab GTPase-activating protein regulates GLUT4 translocation. *The Journal of biological chemistry*. 278:14599-14602.

Scheffzek, K., M.R. Ahmadian, and A. Wittinghofer. 1998. GTPase-activating proteins: helping hands to complement an active site. *Trends in biochemical sciences*. 23:257-262.

Sharma, M., S.S. Giridharan, J. Rahajeng, N. Naslavsky, and S. Caplan. 2009. MICAL-L1 links EHD1 to tubular recycling endosomes and regulates receptor recycling. *Molecular biology of the cell*. 20:5181-5194.

Soldati, T., A.D. Shapiro, A.B. Svejstrup, and S.R. Pfeffer. 1994. Membrane targeting of the small GTPase Rab9 is accompanied by nucleotide exchange. *Nature*. 369:76-78.

Sollner, T., S.W. Whiteheart, M. Brunner, H. Erdjument-Bromage, S. Geromanos, P. Tempst, and J.E. Rothman. 1993. SNAP receptors implicated in vesicle targeting and fusion. *Nature*. 362:318-324.

Steegmaier, M., J. Klumperman, D.L. Foletti, J.S. Yoo, and R.H. Scheller. 1999. Vesicle-associated membrane protein 4 is implicated in trans-Golgi network vesicle trafficking. *Molecular biology of the cell*. 10:1957-1972.

Sudhof, T.C. 2012. The presynaptic active zone. *Neuron*. 75:11-25.

Sudhof, T.C., and J.E. Rothman. 2009. Membrane fusion: grappling with SNARE and SM proteins. *Science*. 323:474-477.

Sutton, R.B., D. Fasshauer, R. Jahn, and A.T. Brunger. 1998. Crystal structure of a SNARE complex involved in synaptic exocytosis at 2.4 A resolution. *Nature*. 395:347-353.

Trimble, W.S., D.M. Cowan, and R.H. Scheller. 1988. VAMP-1: a synaptic vesicle-associated integral membrane protein. *Proceedings of the National Academy of Sciences of the United States of America*. 85:4538-4542.

Ullrich, O., H. Horiuchi, C. Bucci, and M. Zerial. 1994. Membrane association of Rab5 mediated by GDP-dissociation inhibitor and accompanied by GDP/GTP exchange. *Nature*. 368:157-160.

Wang, Y., X. Liu, T. Biederer, and T.C. Sudhof. 2002. A family of RIM-binding proteins regulated by alternative splicing: Implications for the genesis of synaptic active zones. *Proceedings of the National Academy of Sciences of the United States of America*. 99:14464-14469.

Xu, Y., H. Shi, S. Wei, S.H. Wong, and W. Hong. 2004. Mutually exclusive interactions of EHD1 with GS32 and syndapin II. *Molecular membrane biology*. 21:269-277.

Yoshimura, S., J. Egerer, E. Fuchs, A.K. Haas, and F.A. Barr. 2007. Functional dissection of Rab GTPases involved in primary cilium formation. *The Journal of cell biology*. 178:363-369.

7

General Discussion

Intracellular trafficking controls numerous cellular functions by promoting the correct sorting, transport and delivery of different cargos in the cell. Multiple regulatory mechanisms acting at different trafficking steps rely on the dynamic microtubule system and associated molecular motors, dynein and kinesins, which need to be tightly controlled to ensure that all cargos are distributed with spatial and temporal precision. In this thesis, we sought to understand the mechanisms underlying cargo selection and cargo transport by microtubule motors and adaptor proteins and explored possible connections between the docking and fusion machineries essential for the delivery of cellular content.

7.1 Cargo selection and regulation of transport by adaptor proteins

In intracellular transport, one of the first premises that need to be assured is the correct and efficient attachment of molecular motors to cargos. As discussed in Chapter 1, there are different mechanisms mediating the recruitment of molecular motors to cellular cargos, and adaptor proteins are often involved in this process. Dynein is a classic example of a motor that interacts with a multitude of adaptor proteins in order to exert its numerous functions (Kardon and Vale, 2009), and the multisubunit complex dynactin is known as one of the main interactors of dynein, being required for most of its cellular activities (Schroer, 2004). Dynein and dynactin associate with each other through the interaction between the dynein intermediate chain (DIC) and the dynactin subunit p150glued (Karki and Holzbaur, 1995; King et al., 2003; Vaughan and Vallee, 1995), but several studies have suggested that the complexes are not tightly bound to each other and might associate only to promote dynein activity (Bingham et al., 1998; Habermann et al., 2001; Quintyne et al., 1999; Quintyne and Schroer, 2002). In Chapter 2, we confirm these previous observations and show that an N-terminal fragment of the adaptor protein BICD2 (BICD-N) forms a complex with dynein and dynactin, promoting a stable interaction between dynein and dynactin both *in vitro* and *in vivo*. By recruiting BICD-N to the membrane of a BICD2 cargo, Rab6 vesicles, using an inducible heterodimerization system (Pollock et al., 2000), we observed that BICD2-N recruits dynein to cargo, stimulating the transport to the minus-end of microtubules. These results already suggested that the stabilization of the dynein/dynactin complex by BICD2 could promote its activation. In line with these observations, recent studies demonstrated that the binding of BICD2-N to dynactin not only promotes the stabilization of the dynein/dynactin complex but also remarkably stimulates the activation of cytoplasmic dynein *in vitro*, making the motor processive (McKenney et al., 2014; Schlager et al., 2014). The same effect was shown for other cargo-specific adaptor proteins (McKenney et al., 2014), supporting the hypothesis that dynein becomes active upon binding to cargo. The principle of motor activation upon cargo binding is also true for several kinesins, which are in an autoinhibited folded state when not attached to cargo, with the autoinhibition released upon coupling to cargo (Verhey and Hammond, 2009). If we take an example from daily life, a car cannot move without at least one person to transport, and the same seems to apply to molecular motors, which become more active and processive when attached to a cargo that they need to move from one cellular location to the other. We can also see it as a general rule of energy spending – it should only occur when something is being produced, in this case, mechanical movement to drive transport of cellular components.

These recent discoveries solved the basic principle behind cytoplasmic dynein activation, but other questions still remain. For example, do all dynactin-cargo complexes equally activate cytoplasmic dynein? If not, how is that regulated? We have observed that the recruitment of BICD2-N to Rab6 vesicles promotes an increase in the frequency of minus-end directed transport, without significantly affecting the dynamics of transport, i.e., the velocity of transport in both the minus- and plus-end direction. Along this line, in Chapter 3 we have investigated how the BICD family adaptor proteins BICD2 and BICDR-1 differently regulate the velocity of transport. We showed that BICD2, consistent with the observations reported in Chapter 2, does not significantly change the velocity of Rab6 vesicle transport, while BICDR-1 induces a remarkable increase of speed in the microtubule minus end direction (Figure 1). This demonstrates that different adaptor proteins can differentially regulate the velocity of transport or processivity. Importantly, overexpression of BICDR-1, but not BICD2, in both hippocampal and DRG neurons caused a redistribution of Rab6 vesicles, culminating in reduced axon outgrowth. These data demonstrate the functional significance of the differences between the adaptors.

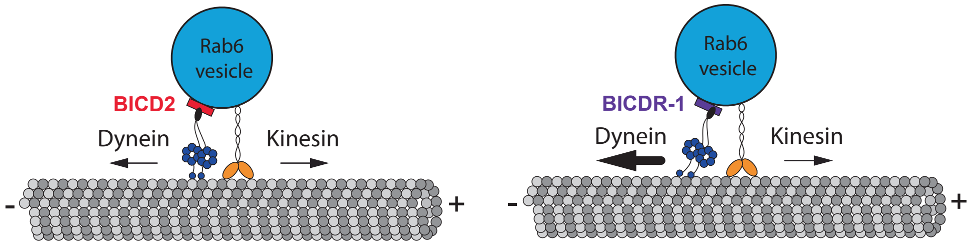

Figure 1: BICD proteins control the velocity of dynein-Based Movements
BICD proteins recruit the dynein motor to Rab6-positive vesicles thereby controlling the speed of transport. BICDR-1 induces a remarkable increase of cargo speed towards the minus-end of microtubules.

In light of the recent *in vitro* reconstitution studies mentioned above, it is tempting to speculate that the binding of different adaptor proteins to dynactin might induce different conformational changes on the dynein/dynactin complex and consequently differently modulate the motor activity. Interestingly, a recent study has proposed that when dynein is inactive, the motor heads are stacked together, and when the motor becomes active, the distance between the two heads increases (Torisawa et al., 2014). A possible explanation could be that the binding of the adaptor-dynactin complex to dynein promotes separation of the heads thus inducing activation of the dynein motor, and that the exact dynein conformation is different for different adaptors.

7.2 Transport by multiple motors and regulation of transport velocity

Most of cargos in the cell are transported bidirectionally along microtubules. While the minus-end directed transport is mainly driven by cytoplasmic dynein, the transport towards the plus-ends of microtubules is promoted by kinesins (Vale, 2003). There are two main models explaining the properties of bidirectional transport – the “tug-of-war” model, where opposite polarity motors compete with each other, and the “coordination” model, where the opposing motor activities are regulated to avoid competition and may even be mutually dependent (Gross, 2004; Hancock, 2014). One important question is what determines the velocity of transport and how the number of motors can influence transport. It is logical to think that, for instance, in a “tug-of-war” situation, one set of motors will “win” and drive transport. Nevertheless, *in vitro* studies have shown that the transport of lipid droplets by kinesin-1 does not depend on the number of motors (Shubeita et al., 2008). Furthermore, the size of a cargo and additional motors present on the cargo might also influence transport (Erickson et al., 2011). Dynein, the kinesin-1 KIF5B and the kinesin-3 KIF1C have been previously implicated in the motility of Rab6 vesicles (Grigoriev et al., 2007; Matanis et al., 2002; Schlager et al., 2010). In Chapter 3 we set out to understand how different kinesins can influence Rab6 vesicle transport. We demonstrated that the recruitment of KIF5B to Rab6 vesicles results in a slow transport, while the recruitment of the kinesin-3 family member KIF1C induces an increase of Rab6 vesicle velocity towards the plus-end of microtubules, without affecting the velocity of transport in the minus-end direction. These results clearly show that different kinesin motors can differentially modulate the velocity of cargos. This also indicates that velocity does not depend on the number of motors present on a cargo (similar in both conditions), but rather on the intrinsic properties of the molecular motors. Interestingly, the depletion of individual kinesin-1 and kinesin-3 motors or a combination of both does not completely impair the motility of Rab6 vesicles. The transport of Rab6 vesicles is thus driven by a team of motors with different intrinsic properties, and the final speed of a cargo is the result of their combined action (Figure 2).

In Chapter 4 we show that another kinesin-3 family member, KIF13B, robustly associates with Rab6 vesicles and promotes their movement towards the plasma membrane. We also have indications that dynein activity depends on kinesin function, what supports the coordination model of bidirectional transport (Gross, 2004; Hancock, 2014). Additionally, we demonstrate that KIF13B motor is slowed down on Rab6 vesicles, what probably reflects the action of a slower kinesin contributing to the transport, in line with our findings described in Chapter 3. One important question underlying these observations is how do multiple motors with different intrinsic properties, such as speed, run length, and force-dependence of unbinding, coordinate to promote efficient transport? Studies performed using melanosomes have shown that multiple motors of the same polarity cooperate during transport (Levi et al., 2006). Additionally, a recent study suggests that populations of faster and slower kinesins mechanically interact on a cargo, determining the final speed of transport (Arpag et al., 2014). The same work suggests that the relative contribution of a particular type of motor to motility within a team of motors strongly depends on its propensity to detach from the microtubule track when force is applied. Interestingly, the detachment of kinesin-1 is the least sensitive to load, while kinesin-3 motors dissociate from the microtubule more easily (Arpag et al., 2014). It is then interesting to hypothesize that, in the case of Rab6-vesicle transport, a mixed population of fast and slow kinesins is engaged and the slower motor kinesin-1, being more resistant to microtubule detachment, has a strong impact on the overall movement by reducing its velocity.

It is logical to think that the presence of different kinesins on a cargo might reflect different local requirements that only a subset of kinesins can respond to. It has been recently proposed that kinesin motors in a complex might be regulated by specific interactions with the microtubule network (Norris et al., 2014). It is known that microtubule posttranslational modifications or tubulin isotypes can affect the activity of certain kinesins (Dunn et al., 2008; Kaul et al., 2014; Konishi and Setou, 2009; Reed et al., 2006; Sirajuddin et al., 2014; Verhey and Hammond, 2009), and that specific microtubule associated proteins (MAPs) can also influence transport. For instance, KIF5B has been shown to bind to MAP7 on microtubules (Barlan et al., 2013). It is then possible that KIF5B promotes the transport of Rab6 vesicles along microtubules enriched in MAP7, while kinesin-3 family members promote transport on a subset of microtubules with a different identity. It will be interesting to analyze in more detail the distribution of different microtubules in the cell in relation to the speed of transport by specific kinesins (Figure 2).

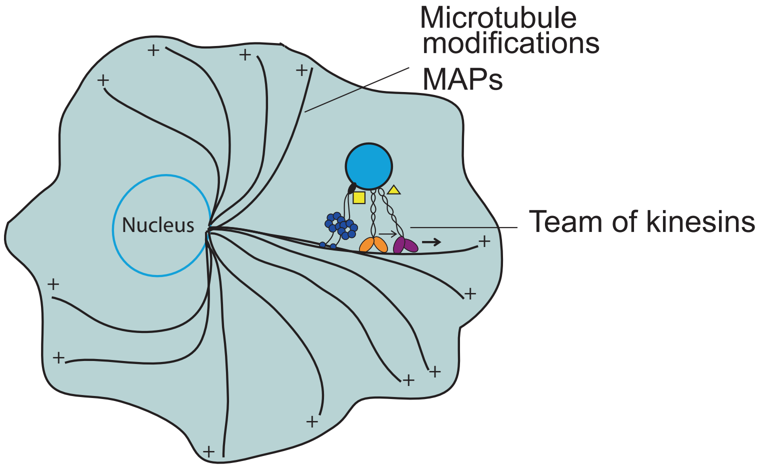

Figure 2: Regulation of Rab6-exocytotic vesicle transport by multiple motors.
The transport of Rab6 vesicles to the minus end of microtubules is driven by dynein, while the plus-end directed transport is powered by multiple kinesins. Kinesin-1 (orange) and kinesin-3 (purple) have different properties, and the final speed of transport depends on the combined action of both. Other factors, such as microtubule modifications, specific microtubule associated proteins (MAPs) and adaptor proteins (yellow) may also influence the velocity of transport.

7.3 KIF13B and its possible roles in cortical organization and neuronal function

In Chapters 4 and 5 we explore the interaction between KIF13B and the new identified interacting partner KIDINS220. KIDINS220 is a transmembrane protein, and we show that the cytoplasmic C- and N- termini of this molecule are probably required for the binding to KIF13B. At this moment we do not know which region of KIF13B is required for the interaction with KIDINS220, but the fact that we were able to identify KIDINS220 in the mass spectrometry analysis of the two KIF13B deletion mutants analyzed (Chapter 4, Table 1), indicates that the interaction must occur through the C-terminal region of KIF13B. Along with KIDINS220, we have identified several proteins from the Dystrophin Associated protein complex (DAPC), a large transmembrane assembly involved in linking the cytoskeleton to the extracellular matrix (ECM) in muscles, neurons and other systems (Ervasti and Campbell, 1993; Haenggi and Fritschy, 2006). We show that the DAPC subunit α1-syntrophin interacts with KIDINS220, in line with previous observations (Luo et al., 2005). Additionally, utrophin, the ubiquitous form of dystrophin, binds to several smaller subunits of the DAPC complex and has been recently shown to interact with KIF13B (Kanai et al., 2014). We observed that proteins from the DAPC are localized to specific cortical sites enriched in ELKS and LL5β, which are involved in microtubule organization (Lansbergen et al., 2006). Our lab has recently shown that the scaffolding proteins liprin-α1 and liprin-β1, LL5β and ELKS are all part of the same cortical microtubule attachment platform required for microtubule stabilization (van der Vaart et al., 2013). Mass spectrometry-based analysis of liprin-α1 interactome identified DAPC components as putative liprin-α1 interacting partners, and we could confirm these interactions. Our observations suggest a functional overlap between the cortical microtubule attachment complex, the DAPC and KIF13B.

LL5β binds to the plus end tracking proteins CLASP1/2, which induce cortical capture and stabilization of microtubules (Lansbergen et al., 2006). Recent studies have suggested that LL5β mediates the anchoring of CLASP2-decorated microtubule plus ends at the postsynapse in muscle cells, promoting local transport of vesicles containing Acetylcholine Receptors (AChRs), the most abundant receptors at the muscle postsynaptic membrane (Basu et al., 2015). Additionally, LL5β and DAPC proteins are key components of "synaptic podosomes", actin-rich organelles involved in postsynaptic maturation and extracellular matrix remodeling at the AChRs clusters (Grady et al., 2003; Jacobson et al., 2001; Kishi et al., 2005; Proszynski et al., 2009). Our results show that the DAPC colocalizes with LL5β-containing cortical microtubule attachment complexes, which are also the preferred sites for fusion of Rab6-labeled exocytotic vesicles with the plasma membrane (Grigoriev et al., 2007). In Chapter 4, we have shown that KIF13B is one of the kinesins transporting Rab6 vesicles. An attractive hypothesis is that KIF13B might be part of a transport route responsible for the directional delivery of DAPC in Rab6 vesicles to specific cortical sites along the microtubules stabilized at these sites, and thus promote the formation, maintenance or dynamics of DAPC-positive cortical assemblies.

Podosomes are an interesting model to study the functional interplay between KIF13B, the DAPC and LL5β. A recent study suggested that there is a focal adhesion-associated exocytosis pathway where Rab6-exocytotic vesicles fuse near focal adhesions (Stehbens et al., 2014), and several studies have demonstrated that podosomes also contain typical focal adhesion components, such as vinculin and talin (Proszynski et al., 2009). Furthermore, the kinesin-3 KIF1C, which we have shown to modulate Rab6-vesicle transport (Chapter 3), has been reported to regulate podosome dynamics (Kopp et al., 2006). It will be interesting to investigate whether KIF13B-mediated Rab6 vesicle transport plays a role in podosome formation and stability, and whether this process might be connected to DAPC function.

In Chapter 5 we also show preliminary data suggesting that KIF13B and KIDINS220 show some overlap in the dendrites of developing neurons. KIF13B was first implicated in the transport of PIP3-positive vesicles in axons, regulating neuronal polarity, but recent studies have suggested that it is also involved in the transport of dendritic cargos (Horiguchi et al., 2006; Huang and Banker, 2012; Jenkins et al., 2012). Additionally, KIDINS220 has also been implicated in the regulation of dendritic branching and dendrite and axon development (Higuero et al., 2010; Wu et al., 2009), and DAPC has been reported to play important postsynaptic functions in neurons (Haenggi and Fritschy, 2006). It will be interesting to investigate if KIF13B, KIDINS220 and Rab6 participate in the same transport pathways in neurons and whether this is relevant for the stability and function of DAPC at postsynaptic terminals.

7.4 Docking and fusion of Rab6 secretory vesicles with the plasma membrane

When membrane cargos reach their final destination in the cell, uncoupling from the transporting motors occurs, and the subsequent steps required for the delivery of vesicle content can take place. This normally involves docking on the target membrane and fusion of the cargo and target membranes (Cai et al., 2007). Docking is mediated by tethering complexes, while fusion is classically mediated by soluble N-ethylmaleimide-sensitive factor (NSF) adaptor proteins receptors (SNAREs) (Cai et al., 2007; Sollner et al., 1993; Sudhof and Rothman, 2009). We have previously shown that the small GTPase Rab8 present on Rab6 vesicles, together with the flavoprotein monooxygenase MICAL-3 and the Rab6-interacting protein ELKS, which reside at the cell cortex, form a complex to promote docking and fusion of Rab6-secretory vesicles with the plasma membrane (Grigoriev et al., 2007; Grigoriev et al., 2011). The interaction between ELKS and Rab6 is important for the speed and selectivity of fusion, suggesting that Rab6 and the docking machinery may cooperate with the fusion machinery. In Chapter 6, we found that the SNARE proteins VAMP4 (a v-SNARE present on the vesicle membrane) and SNAP29 (a t-SNARE present on the plasma membrane) are requited for proper fusion of Rab6 vesicles with the plasma membrane. We have performed mass spectrometry analysis of the interactome of SNAP29 and VAMP4 to identify putative SNARE partners but the specificity of the assay was rather low and multiple members of the SNARE family were found. Nevertheless, our biochemical data suggests that SNAP29 and VAMP4 might form a complex with syntaxin-3 what would allow the formation of a functional four-helix bundle complex required for membrane fusion.

We have previously reported that the depletion of Rab8 or overexpression of the GDP-bound Rab8 mutant (Rab8-T22N) induces accumulation of Rab6 vesicles at the cell periphery (Grigoriev et al., 2011). In Chapter 6 we show that the Rab8-T22N mutant causes accumulation of Rab6 vesicles at ELKS-positive cortical patches, indicating that the GTP hydrolysis-deficient mutant of Rab8 promotes docking of Rab6 vesicles but blocks their fusion with the plasma membrane. This effect could be explained by the involvement of a Rab GTPase activating protein (GAP), which stimulates GTPase hydrolysis leading to Rab inactivation. We have tested the effect of the overexpression of different proteins with reported GAP activity towards Rab8, but none of them affected the cellular distribution of Rab6 vesicles. Thus, although a proper GTPase cycle of Rab8 is important for Rab6 vesicle docking and fusion, the GAP protein involved in this process is still unknown.

In Chapter 6, we also show that the members of the C-terminal Eps15 homology domain (EHD) family of proteins, which have been previously shown to bind to SNAP29 (Xu et al., 2004), are recruited to the Rab6 vesicle docking sites before fusion. This is an interesting finding, since these proteins are very well known for their function in the endocytic transport and ATP-dependent fission of tubular endosomes, but have never been implicated in exocytosis (Grant and Caplan, 2008; Naslavsky and Caplan, 2011). During fusion, membranes need to be remodeled, and it is possible that the oligomerization of EHDs at the sites of exocytosis facilitates fusion. It will be interesting to further investigate the exact role of a classic endocytic family of proteins in the fusion of exocytotic carriers.

7.5 Future perspectives

In this thesis, we have used a combination of biochemical and live cell imaging techniques to study the role of adaptor proteins in cargo transport and have explored the mechanisms of multimotor cargo transport. In particular, we have provided strong cell biological evidence for the importance of adaptor proteins in dynein-based motility. This led to follow-up *in vitro* work that uncovered important principles of cytoplasmic dynein activation and regulation of its processivity (McKenney et al., 2014; Schlager et al., 2014). Nevertheless, how different dynactin-adaptor proteins differentially regulate dynein velocity and processive movement still needs to be further clarified. Understanding how different adaptor proteins cooperate with each other is another central question, the addressing of which will require a combination of high resolution live cell microscopy, electron microscopy, structural studies and *in vitro* reconstitution experiments.

Our current knowledge about bidirectional cargo motility and the transport by multiple kinesin motors mainly derives from *in vitro* reconstitution of motor/cargo complexes (Hancock, 2014; Shubeita et al., 2008). Simple reconstitutions with single or multiple motor proteins have been a great tool to understand the basic rules governing transport mechanisms. However, more complex reconstitution approaches mimicking the natural molecular links between motors and cargo will be needed to fully understand how multimotor systems function in cells. We can also expect advances in this field stemming from the rapidly developing microscopy methods, which will improve the speed and resolution of imaging revealing the details of transport steps and the relative distribution of the molecules involved. For example, super resolution techniques PALM (photo activated localization microscopy), STED (stimulated emission depletion) and SIM (structured illumination microscopy) have already been successfully applied to live cells (Fornasiero and Opazo, 2015). We expect that a combination of live super resolution imaging and *in vitro* reconstitution will provide a better understanding of the physical and mechanical properties of cellular transport.

The mechanisms underlying vesicle docking and fusion also require further investigation. We have used mass spectrometry based approaches to identify SNARE-binding partners that could be involved in the docking/fusion of secretory vesicles, but this method was inefficient. In future, it will be important to develop chemical crosslinking techniques that preserve SNARE complexes and adjacent complexes in the cell, which can be detected using biochemical and mass spectrometry techniques. *In vitro* reconstitution of artificial membrane vesicles with the intricate machinery required for the secretory vesicle docking and fusion might also provide further insight into the mechanisms of this complex process.

References

Arpag, G., Shastry, S., Hancock, W.O., Tuzel, E., 2014. Transport by populations of fast and slow kinesins uncovers novel family-dependent motor characteristics important for in vivo function. Biophysical journal 107, 1896-1904.

Barlan, K., Lu, W., Gelfand, V.I., 2013. The microtubule-binding protein ensconsin is an essential cofactor of kinesin-1. Current biology : CB 23, 317-322.

Basu, S., Sladecek, S., Martinez de la Pena, Y.V.I., Akaaboune, M., Smal, I., Martin, K., Galjart, N., Brenner, H.R., 2015. CLASP2-dependent microtubule capture at the neuromuscular junction membrane requires LL5beta and actin for focal delivery of acetylcholine receptor vesicles. Molecular biology of the cell.

Bingham, J.B., King, S.J., Schroer, T.A., 1998. Purification of dynactin and dynein from brain tissue. Methods in enzymology 298, 171-184.

Cai, H., Reinisch, K., Ferro-Novick, S., 2007. Coats, tethers, Rabs, and SNAREs work together to mediate the intracellular destination of a transport vesicle. Developmental cell 12, 671-682.

Dunn, S., Morrison, E.E., Liverpool, T.B., Molina-Paris, C., Cross, R.A., Alonso, M.C., Peckham, M., 2008. Differential trafficking of Kif5c on tyrosinated and detyrosinated microtubules in live cells. Journal of cell science 121, 1085-1095.

Erickson, R.P., Jia, Z., Gross, S.P., Yu, C.C., 2011. How molecular motors are arranged on a cargo is important for vesicular transport. PLoS computational biology 7, e1002032.

Ervasti, J.M., Campbell, K.P., 1993. A role for the dystrophin-glycoprotein complex as a transmembrane linker between laminin and actin. The Journal of cell biology 122, 809-823.

Fornasiero, E.F., Opazo, F., 2015. Super-resolution imaging for cell biologists: Concepts, applications, current challenges and developments. BioEssays : news and reviews in molecular, cellular and developmental biology.

Grady, R.M., Akaaboune, M., Cohen, A.L., Maimone, M.M., Lichtman, J.W., Sanes, J.R., 2003. Tyrosine-phosphorylated and nonphosphorylated isoforms of alpha-dystrobrevin: roles in skeletal muscle and its neuromuscular and myotendinous junctions. The Journal of cell biology 160, 741-752.

Grant, B.D., Caplan, S., 2008. Mechanisms of EHD/RME-1 protein function in endocytic transport. Traffic 9, 2043-2052.

Grigoriev, I., Splinter, D., Keijzer, N., Wulf, P.S., Demmers, J., Ohtsuka, T., Modesti, M., Maly, I.V., Grosveld, F., Hoogenraad, C.C., Akhmanova, A., 2007. Rab6 regulates transport and targeting of exocytotic carriers. Developmental cell 13, 305-314.

Grigoriev, I., Yu, K.L., Martinez-Sanchez, E., Serra-Marques, A., Smal, I., Meijering, E., Demmers, J., Peranen, J., Pasterkamp, R.J., van der Sluijs, P., Hoogenraad, C.C., Akhmanova, A., 2011. Rab6, Rab8, and MICAL3 cooperate in controlling docking and fusion of exocytotic carriers. Current biology : CB 21, 967-974.

Gross, S.P., 2004. Hither and yon: a review of bi-directional microtubule-based transport. Physical biology 1, R1-11.

Habermann, A., Schroer, T.A., Griffiths, G., Burkhardt, J.K., 2001. Immunolocalization of cytoplasmic dynein and dynactin subunits in cultured macrophages: enrichment on early endocytic organelles. Journal of cell science 114, 229-240.

Haenggi, T., Fritschy, J.M., 2006. Role of dystrophin and utrophin for assembly and function of the dystrophin glycoprotein complex in non-muscle tissue. Cellular and molecular life sciences : CMLS 63, 1614-1631.

Hancock, W.O., 2014. Bidirectional cargo transport: moving beyond tug of war. Nature reviews. Molecular cell biology 15, 615-628.

Higuero, A.M., Sanchez-Ruiloba, L., Doglio, L.E., Portillo, F., Abad-Rodriguez, J., Dotti, C.G., Iglesias, T., 2010. Kidins220/ARMS modulates the activity of microtubule-regulating proteins and controls neuronal polarity and development. The Journal of biological chemistry 285, 1343-1357.

Horiguchi, K., Hanada, T., Fukui, Y., Chishti, A.H., 2006. Transport of PIP3 by GAKIN, a kinesin-3 family protein, regulates neuronal cell polarity. The Journal of cell biology 174, 425-436.

Huang, C.F., Banker, G., 2012. The translocation selectivity of the kinesins that mediate neuronal organelle transport. Traffic 13, 549-564.

Jacobson, C., Cote, P.D., Rossi, S.G., Rotundo, R.L., Carbonetto, S., 2001. The dystroglycan complex is necessary for stabilization of acetylcholine receptor clusters at neuromuscular junctions and formation of the synaptic basement membrane. The Journal of cell biology 152, 435-450.

Jenkins, B., Decker, H., Bentley, M., Luisi, J., Banker, G., 2012. A novel split kinesin assay identifies motor proteins that interact with distinct vesicle populations. The Journal of cell biology 198, 749-761.

Kanai, Y., Wang, D., Hirokawa, N., 2014. KIF13B enhances the endocytosis of LRP1 by recruiting LRP1 to caveolae. The Journal of cell biology 204, 395-408.

Kardon, J.R., Vale, R.D., 2009. Regulators of the cytoplasmic dynein motor. Nature reviews. Molecular cell biology 10, 854-865.

Karki, S., Holzbaur, E.L., 1995. Affinity chromatography demonstrates a direct binding between cytoplasmic dynein and the dynactin complex. The Journal of biological chemistry 270, 28806-28811.

Kaul, N., Soppina, V., Verhey, K.J., 2014. Effects of alpha-tubulin K40 acetylation and detyrosination on kinesin-1 motility in a purified system. Biophysical journal 106, 2636-2643.

King, S.J., Brown, C.L., Maier, K.C., Quintyne, N.J., Schroer, T.A., 2003. Analysis of the dynein-dynactin interaction in vitro and in vivo. Molecular biology of the cell 14, 5089-5097.

Kishi, M., Kummer, T.T., Eglen, S.J., Sanes, J.R., 2005. LL5beta: a regulator of postsynaptic differentiation identified in a screen for synaptically enriched transcripts at the neuromuscular junction. The Journal of cell biology 169, 355-366.

Konishi, Y., Setou, M., 2009. Tubulin tyrosination navigates the kinesin-1 motor domain to axons. Nature neuroscience 12, 559-567.

Kopp, P., Lammers, R., Aepfelbacher, M., Woehlke, G., Rudel, T., Machuy, N., Steffen, W., Linder, S., 2006. The kinesin KIF1C and microtubule plus ends regulate podosome dynamics in macrophages. Molecular biology of the cell 17, 2811-2823.

Lansbergen, G., Grigoriev, I., Mimori-Kiyosue, Y., Ohtsuka, T., Higa, S., Kitajima, I., Demmers, J., Galjart, N., Houtsmuller, A.B., Grosveld, F., Akhmanova, A., 2006. CLASPs attach microtubule plus ends to the cell cortex through a complex with LL5beta. Developmental cell 11, 21-32.

Levi, V., Serpinskaya, A.S., Gratton, E., Gelfand, V., 2006. Organelle transport along microtubules in Xenopus melanophores: evidence for cooperation between multiple motors. Biophysical journal 90, 318-327.

Luo, S., Chen, Y., Lai, K.O., Arevalo, J.C., Froehner, S.C., Adams, M.E., Chao, M.V., Ip, N.Y., 2005. {alpha}-Syntrophin regulates ARMS localization at the neuromuscular junction and enhances EphA4 signaling in an ARMS-dependent manner. The Journal of cell biology 169, 813-824.

Matanis, T., Akhmanova, A., Wulf, P., Del Nery, E., Weide, T., Stepanova, T., Galjart, N., Grosveld, F., Goud, B., De Zeeuw, C.I., Barnekow, A., Hoogenraad, C.C., 2002. Bicaudal-D regulates COPI-independent Golgi-ER transport by recruiting the dynein-dynactin motor complex. Nature cell biology 4, 986-992.

McKenney, R.J., Huynh, W., Tanenbaum, M.E., Bhabha, G., Vale, R.D., 2014. Activation of cytoplasmic dynein motility by dynactin-cargo adapter complexes. Science 345, 337-341.

Naslavsky, N., Caplan, S., 2011. EHD proteins: key conductors of endocytic transport. Trends in cell biology 21, 122-131.

Norris, S.R., Soppina, V., Dizaji, A.S., Schimert, K.I., Sept, D., Cai, D., Sivaramakrishnan, S., Verhey, K.J., 2014. A method for multiprotein assembly in cells reveals independent action of kinesins in complex. The Journal of cell biology 207, 393-406.

Pollock, R., Issner, R., Zoller, K., Natesan, S., Rivera, V.M., Clackson, T., 2000. Delivery of a stringent dimerizer-regulated gene expression system in a single retroviral vector. Proceedings of the National Academy of Sciences of the United States of America 97, 13221-13226.

Proszynski, T.J., Gingras, J., Valdez, G., Krzewski, K., Sanes, J.R., 2009. Podosomes are present in a postsynaptic apparatus and participate in its maturation. Proceedings of the National Academy of Sciences of the United States of America 106, 18373-18378.

Quintyne, N.J., Gill, S.R., Eckley, D.M., Crego, C.L., Compton, D.A., Schroer, T.A., 1999. Dynactin is required for microtubule anchoring at centrosomes. The Journal of cell biology 147, 321-334.

Quintyne, N.J., Schroer, T.A., 2002. Distinct cell cycle-dependent roles for dynactin and dynein at centrosomes. The Journal of cell biology 159, 245-254.

Reed, N.A., Cai, D., Blasius, T.L., Jih, G.T., Meyhofer, E., Gaertig, J., Verhey, K.J., 2006. Microtubule acetylation promotes kinesin-1 binding and transport. Current biology : CB 16, 2166-2172.

Schlager, M.A., Hoang, H.T., Urnavicius, L., Bullock, S.L., Carter, A.P., 2014. In vitro reconstitution of a highly processive recombinant human dynein complex. The EMBO journal 33, 1855-1868.

Schlager, M.A., Kapitein, L.C., Grigoriev, I., Burzynski, G.M., Wulf, P.S., Keijzer, N., de Graaff, E., Fukuda, M., Shepherd, I.T., Akhmanova, A., Hoogenraad, C.C., 2010. Pericentrosomal targeting of Rab6 secretory vesicles by Bicaudal-D-related protein 1 (BICDR-1) regulates neuritogenesis. The EMBO journal 29, 1637-1651.

Schroer, T.A., 2004. Dynactin. Annual review of cell and developmental biology 20, 759-779.

Shubeita, G.T., Tran, S.L., Xu, J., Vershinin, M., Cermelli, S., Cotton, S.L., Welte, M.A., Gross, S.P., 2008. Consequences of motor copy number on the intracellular transport of kinesin-1-driven lipid droplets. Cell 135, 1098-1107.

Sirajuddin, M., Rice, L.M., Vale, R.D., 2014. Regulation of microtubule motors by tubulin isotypes and post-translational modifications. Nature cell biology.

Sollner, T., Whiteheart, S.W., Brunner, M., Erdjument-Bromage, H., Geromanos, S., Tempst, P., Rothman, J.E., 1993. SNAP receptors implicated in vesicle targeting and fusion. Nature 362, 318-324.

Stehbens, S.J., Paszek, M., Pemble, H., Ettinger, A., Gierke, S., Wittmann, T., 2014. CLASPs link focal-adhesion-associated microtubule capture to localized exocytosis and adhesion site turnover. Nature cell biology 16, 561-573.

Sudhof, T.C., Rothman, J.E., 2009. Membrane fusion: grappling with SNARE and SM proteins. Science 323, 474-477.

Torisawa, T., Ichikawa, M., Furuta, A., Saito, K., Oiwa, K., Kojima, H., Toyoshima, Y.Y., Furuta, K., 2014. Autoinhibition and cooperative activation mechanisms of cytoplasmic dynein. Nature cell biology 16, 1118-1124.

Vale, R.D., 2003. The molecular motor toolbox for intracellular transport. Cell 112, 467-480.

van der Vaart, B., van Riel, W.E., Doodhi, H., Kevenaar, J.T., Katrukha, E.A., Gumy, L., Bouchet, B.P., Grigoriev, I., Spangler, S.A., Yu, K.L., Wulf, P.S., Wu, J., Lansbergen, G., van Battum, E.Y., Pasterkamp, R.J., Mimori-Kiyosue, Y., Demmers, J., Olieric, N., Maly, I.V., Hoogenraad, C.C., Akhmanova, A., 2013. CFEOM1-associated kinesin KIF21A is a cortical microtubule growth inhibitor. Developmental cell 27, 145-160.

Vaughan, K.T., Vallee, R.B., 1995. Cytoplasmic dynein binds dynactin through a direct interaction between the intermediate chains and p150Glued. The Journal of cell biology 131, 1507-1516.

Verhey, K.J., Hammond, J.W., 2009. Traffic control: regulation of kinesin motors. Nature reviews. Molecular cell biology 10, 765-777.

Wu, S.H., Arevalo, J.C., Sarti, F., Tessarollo, L., Gan, W.B., Chao, M.V., 2009. Ankyrin Repeat-rich Membrane Spanning/Kidins220 protein regulates dendritic branching and spine stability in vivo. Developmental neurobiology 69, 547-557.

Xu, Y., Shi, H., Wei, S., Wong, S.H., Hong, W., 2004. Mutually exclusive interactions of EHD1 with GS32 and syndapin II. Molecular membrane biology 21, 269-277.

Summary

Samenvatting

Portfolio

Curriculum vitae

List of publications

Acknowledgements

Summary

Intracellular transport along cytoskeletal filaments is an essential cellular process that controls numerous cellular functions by promoting correct sorting, transport and delivery of different cargos in the cell. The microtubule system and associated molecular motors, dynein and kinesins, are essential components of this process, and their tight regulation is required to ensure the precise spatio-temporal distribution of cargos. In this thesis, we dissect the mechanisms underlying cargo selection and cargo transport by microtubule motors and adaptor proteins and investigate possible connections between the docking and fusion machineries essential for the delivery of cellular content into the extracellular space.

In chapter 1, we introduce molecular motors and focus on the current knowledge on the organization of microtubule-based transport.

The role of adaptor proteins in controlling cargo selection and motor activity is investigated in chapter 2, where we demonstrate that the adaptor protein BICD2 forms a triple complex with the dynein-dynactin complex and promotes a stable interaction between dynein and dynactin. Additionally, we provide evidence for the requirement of this triple stable complex for dynein activation and show that the interaction between dynein, dynactin and LIS1 is required for the BICD2-mediated recruitment of the dynein complex to cellular structures.

In chapter 3, we investigate the role of different kinesins and adaptor proteins in the transport of Rab6-positive secretory vesicles. We demonstrate that kinesin-1 and kinesin-3 differently influence the speed of transport of Rab6 vesicles. Additionally, we demonstrate that the Bicaudal D family proteins BICD2 and BICDR-1 differentially regulate the velocity of dynein-based movements. We show that BICDR-1 increases the velocity of transport of secretory vesicles towards microtubule minus ends and thereby controls the distribution of cellular cargos.

In chapter 4, we show that kinesin-3 family member KIF13B promotes the transport of constitutive secretory vesicles to the periphery of the cell. Additionally, we analyze the distribution of KIF13B on single Rab6 vesicles during active transport, a promising system to study multimotor transport mechanisms in the context of the cell.

In chapter 5, we demonstrate that KIDINS220, a novel KIF13B-interacting protein, links KIF13B to the Dystrophin-Associated Protein Complex (DAPC) and provide evidence for the presence of this complex at cortical structures in proximity of focal adhesions. Based on these results, we discuss the possible role for the KIF13B-DAPC complex in podosomes and neurons.

In chapter 6, we investigate the molecular link between the docking and fusion machineries for Rab6 vesicles. We found that the SNARE proteins VAMP4 and SNAP29 are involved in the fusion of Rab6 vesicles with the plasma membrane. Additionally, we propose a new function for the EHD endocytic family in the exocytosis of carriers of constitutive secretion.

In chapter 7, we discuss the general implications of our findings and the possible strategies for future experiments.

Samenvatting

Intracellulair transport via het cytoskelet is een essentieel proces dat verschillende cellulaire functies aanstuurt door te zorgen voor een correcte sortering, transport en aflevering van verschillende ladingen binnen de cel. Microtubuli en de geassocieerde motors, dyneïnes and kinesines, zijn essentiële spelers in dit proces en een strenge regulatie van deze eiwitten is nodig om de precieze verdeling van de getransporteerde ladingen te controleren. In dit proefschrift onderzoeken we de onderliggende mechanismen van de selectie en het transport van ladingen door motoren en adaptor eiwitten. Ook onderzoeken we de mogelijke connecties tussen de membraanfusie mechanismen die een rol spelen in het afleveren van cellulaire inhoud in de extracellulaire ruimte.

In hoofdstuk 1 introduceren we de moleculaire motoren en beschrijven we de huidige kennis over de organisatie van microtubuli-afhankelijk transport.

De rol van adaptor eiwitten in het reguleren van motor binding en activiteit is onderzocht in hoofdstuk 2 waar we laten zien dat het adaptor eiwit BICD2 een drievoudig complex vormt met dyneïne en dynactine en een stabiele interactie tussen dyneïne en dynactine stimuleert. Daarnaast laten we zien dat dit stabiele complex nodig is voor activatie van dyneïne en dat de interactie tussen dyneïne, dynactine en LIS1 nodig is voor de BICD2-afhankelijke rekrutering van het dyneïne complex naar cellulaire structuren.

In hoofdstuk 3 onderzoeken we de rol van verschillende kinesines en adaptor eiwitten in het transport van Rab6-positieve secretie vesikels. We laten zien dat kinesine-1 en kinesine-3 de transport snelheid van Rab6 vesikels verschillend beïnvloeden. Ook demonstreren we dat BICD2 en BICDR-1, eiwitten uit de Bicaudal D familie, de snelheid van het dyneïne-gedreven transport verschillend reguleren. We laten zien dat BICDR-1 de snelheid van transport van exocytose vesikels verhoogt in de richting van de microtubuli min-uiteinden en op deze manier de distributie van cellulaire ladingen reguleert.

In hoofdstuk 4 laten we zien dat KIF13B, een lid van de kinesine-3 familie, transport van constitutieve secretie vesikels naar de periferie van de cel stimuleert. We analyseren ook de distributie van KIF13B op afzonderlijke Rab6 vesikels gedurende het actieve transport. Dit is een veelbelovende methode waarmee het transport door verschillende motoren bestudeerd kan worden in de context van de cel.

In hoofdstuk 5 demonstreren we dat KIDINS220, een nieuw gevonden bindingspartner van KIF13B, een koppeling vormt tussen KIF13B en het Dystrophine-geassocieerde eiwit complex (DAPC). We geven ook bewijs voor de aanwezigheid van dit complex in de corticale structuren die zich dicht bij de integrine-afhankelijke adhesie complexen bevinden. Gebaseerd op deze resultaten bediscussiëren we de mogelijke rol van het KIF13B-DAPC complex in podosomen en in neuronen.

In hoofdstuk 6 onderzoeken we de moleculaire mechanismen van de fusie van Rab6 vesikels met de plasma membraan. We hebben gevonden dat de SNARE eiwitten VAMP4 en SNAP29 bij dit proces betrokken zijn. We introduceren ook een nieuwe functie voor de EHD eiwitten, tot nu toe bekend voor de rol in endocytose, in de exocytose van constitutieve secretie vesicles.

In hoofdstuk 7 bediscussiëren we de algemene implicaties van onze bevindingen en de mogelijke strategieën voor toekomstige experimenten.

Portfolio

Name PhD student: Andrea Margarita Afonso Serra Marques Research schools: Medical Genetics Center of South-West Holland (MGC), Erasmus MC Graduate School of Life Sciences, Institute of Biomembranes (IB)	PhD period: Oct 2009-Jun 2015 Promotor: Prof. Dr. Anna Akhmanova Supervisor: Prof. Dr. Anna Akhmanova
Courses	
- Cell and Developmental Biology, Erasmus MC	2010
- Biochemistry and Biophysics, Erasmus MC	2010
- Institute of Biomembranes course	2011
Conferences and Presentations **National**	
- 1st Intercity Young Scientist Meeting (IYSM). Heemskerk, The Netherlands *Poster*	2009
- 2nd Intercity Young Scientist Meeting (IYSM). Apeldoorn, The Netherlands *Poster*	2010
- Institute of Biomembranes conference. Utrecht, The Netherlands *Oral presentation*	2013
International	
- 17th Medical Genetics Center (MGC) Graduate Student Conference. Cologne, Germany *Poster*	2010
- Symposium *Mechanisms of Cytoskeleton Dynamics and Intracellular Trafficking*. Warsaw, Poland; *Poster*	2010
- 51st Annual Meeting of the American Society for Cell Biology (ASCB). Denver CO, USA; *poster*	2011
- Gordon Research Conference *Molecular Membrane Biology.* Andover NH, USA *Poster*	2013

Teaching activities	
- Supervision of Niels de Graaf, Master student from the Master's Programme Molecular and cellular life sciences of the University Utrecht.	2013-2014
- Supervision of Jonathan Marbun, undergraduate student from the HAN University of Applied Sciences.	2013
- Supervision of Jeske van Riel, Master student from the Master's Programme *Cancer, Genomics and Developmental Biology* of the University Utrecht	2012
Awards	
PhD scholarship from the Portuguese Foundation for Science and Technology	2010-2013

Curriculum vitae

Personal Information

Name: Andrea Margarita Afonso Serra Marques

Born: 1 November, 1985, Caracas, Venezuela

Education:

July 2011-present: PhD Student, Utrecht University, Utrecht, The Netherlands

Oct 2009- Jun 2011: PhD Student, Erasmus MC, Rotterdam, The Netherlands

2007-2009: Molecular and Cellular Biology (MSc), University of Coimbra, Portugal

2004-2007: Biology, University of Coimbra, Coimbra, Portugal

2003-2004: Psychology, University of Lisbon, Lisbon, Portugal

1995-2003: Pre University Education, Escola Dr. Manuel Ribeiro Ferreira, Alvaiázere, Portugal

List of publications

Serra-Marques A., Liu, Q., Katrukha, E., Grigoriev, I., Altelaar, A. F., Heck, A.J., Kapitein, L.C., Pedersen, L.B., Akhmanova, A. The kinesin-3 family member Kif13B promotes transport of exocytotic carriers. *In preparation*

Andrea Serra-Marques and Anna Akhmanova. New insights into microtubule-based transport. Review. *To be submitted*

Schou, K.B., Mogensen, J.B., Nielsen, B.S., Aleliunaite, A., Morthorst, S.K., **Serra-Marques, A**., Saunier, S., Veland, I.R., Akhmanova, A., Christensen, S.T., Pedersen, L.B. KIF13B is a novel RPGRIP1-type C2 family member that interacts with NPHP4 to establish a CAV1-enriched membrane micro domain at the ciliary transition zone required for regulation of ciliary length and signaling. *In preparation*

Serra-Marques A., Liu Q., Post H., Grigoriev I., Gordon E.D., Peden E.A., Altelaar M., Heck J.A., Akhmanova, A. Characterization of docking and fusion machinery for Rab6-secretory vesicles. *In preparation*

Schlager M.A.*, **Serra-Marques A.***, Grigoriev I., Gumy, L.F., Esteves da Silva, M., Wulf S.P., Akhmanova A., Hoogenraad C.C. Bicaudal D family adaptor proteins control the velocity of dynein-based movements. *Cell Rep.* 8, 1248-1256 (2014).

Splinter D., Razafsky D.S., Schlager M.A., **Serra-Marques A.**, Grigoriev I., Demmers J., Keijzer N, Jiang K., Poser I., Hyman A.A., Hoogenraad C.C., King S.J., Akhmanova A. BicD2, dynactin and Lis1 cooperate in regulating dynein recruitment to cellular structures. *Mol. Biol. Cell*. 23(21), 4226-41 (2012)

Logarinho E., Maffini S., Barisic M., **Marques A.**, Toso A., Meraldi P. and Maiato H. CLASPs prevent irreversible multipolarity by ensuring spindle-pole resistance to traction forces during chromosome alignment. *Nat. cell Biol.* 14(3), 295-303 (2012)

Grigoriev I., Yu K.L., Martinez-Sanchez E., **Serra-Marques A.**, Smal I., Meijering E., Demmers J., Peränen J., Pasterkamp R.J., van der Sluijs P., Hoogenraad C.C., Akhmanova A. Rab6, Rab8, and MICAL3 cooperate in controlling docking and fusion of exocytotic carriers. *Curr. Biol*. 21(11), 967-74 (2011)

*** Co-first author**

Acknowledgements

And it looks like it is time to start saying goodbye…

When I came to The Netherlands I didn't know how challenging and how amazing it would be! I came full of dreams, but what I really wanted was to grow as a person and as a scientist, and this I am pretty sure I achieved. All the good and bad things I had to face during my PhD had a profound impact on me and so had all the people I met during these last years. And for this, I want to thank everyone who has helped me getting all the way here and without whom nothing would have been possible.

First of all I would like to express my gratitude to my promotor and supervisor Anna Akhmanova. Anna, you are, with any doubt, the most clever and pragmatic woman I've ever met. I am always amazed by how in 99.99% of the cases you remember the tiniest details about experiments done 10 years ago, the position of that tube in that box ☺ and by how sapient you are. Thank you for sharing your vast knowledge and experience and for the great lessons I've learned from you and that will for sure help me in my future as a scientist. Thank you as well for your support and encouragement every time I came to your office because my projects were not going the way I expected and for the nice chats we had about life in general. There you also gave me very pragmatic and interesting opinions that I will always try to remember. Thank you!

To Casper Hoogenraad, the second biggest thank you! Casper, thank you very much for allowing me to work on the BICD proteins paper and for all the help with publishing it. It was very important to me and your support was exceptional. Thank you for the relaxed and nice discussions and for all the reagents I could use from your lab! Thank you as well for being part of my reading committee and for the nice suggestions for my scientific future!

To Ilya Grigoriev, a big thank you! Ilya, I always admired your work and how you always get the most beautiful movie (sometimes I think you fake it!! ☺) I am happy we managed to become very good colleagues and thank you for all the help during the last 2 years. I had a lot of fun working with you, discussing about DNA concentrations and making all kind of theories about Rab6 vesicle behavior! Thank you for your support while I was finishing my PhD and for all the effort you are putting on the KIF13B/multimotor transport paper!! All the best for you!

To all the people from the Cell Biology department in Erasmus MC, where I started my PhD, thank you for the nice environment and discussions. Thank you to Niels Galjart for the nice discussions about the PhD programme courses and to Rick Janssens for the nice chats and for showing me where things were!

To Lotte Pedersen, thank you for sending the kind student Stine to our lab with a very nice construct! The KIF13B story wouldn't have started without your help and collaboration, so thank you for that and for the suggestions on the project. Thank you as well for being part of my reading committee and I am very happy you are coming to The Netherlands for my defense!

To Erwin Peterman, Judith Klumperman and Ineke Braakman, thank you for being part of my reading committee.

To Max Schlager, thank you so much for all the tools and nice work you have generated and that I could follow up!

Now I want to thank my colleagues in the Akhmanova lab:
Kai, you were my bench supervisor and my greatest support when I joined the lab. I have learned so much with you, you are just a lab encyclopedia – "Kaipedia"!! ☺ Thank you for all the great discussions and useful tips you have given me and for being my Paranymph! I wish you all the success you deserve in science and I wish you, Shasha and your cute little girl all the best! And don't forget to invite me one day to visit your lab in China… ☺

To Qingyang, the sweetest Chinese girl, thank you for everything! Thank you for your collaboration on my projects, for all the great discussions we had about our projects and mass spec analysis, for being always willing to help with anything I needed. Thank you as well for your incredible support, friendship and all the fun we had together!

To Helma, thank you for being such a great colleague, for your friendship, constant support and for all the nice moments we have spent together in Utrecht and Den Bosh. I am really happy we met and I wish you good luck with finishing your PhD and all the best for the future! To both you and Qingyang: I will miss our chats in the office (always super short, of course) and our deep conversions about the good/bad/worth-following phenotypes and the great dinners in the amazing Italian restaurant! ☺

To Eugene, thank you so much for everything! Your incredible capacity to contribute to many people's projects in such a humble way really amazes me! Thank you for all the help with the tracking analysis, for the analysis on the vesicles / kinesin behavior and for the nice discussions and suggestions on my projects! Thank you as well for your friendship and for taking the girls to the parties of your physicist friends! ☺ I wish you all the best for your career and be happy!

To Amol, thank you for your support, for all the nice chats and conversations and for sharing your enthusiasm about science, movies and about the 1000 ways to kill yourself in an adventurous way before you turn 60! ☺ I wish you all the best for your future!

To Ben, thank you for the useful discussions about science, music and movies! I wish you all the best for your career!

To Ivar and Chingchao, you guys are awesome!! Thank you for the nice environment you've helped creating in the lab and good luck with your PhDs!

To all the other members, past and present, including Carol, Renu, Babet, Susana, Gert-Jan, Rick, Smiriti, Chris, Hari, Chao, Ruddi, Maud and Ankit, thank you for the nice chats and tips!

To my Master's students Jeske van Riel, Jonathan Marbun and Niels de Graaf (and also to Elisa Raineri and Daan Verhagen), I really enjoyed being your supervisor! Thank you for your help and I wish all of you all the best!

I also want to thank everybody in the labs of Casper, Esther, Corette and Lukas! Lukas, thank you for your suggestions and discussions about my project! Esther, thank you for your easy smile and for your great company during the ASCB meeting in Denver! Phebe, thank you for your incredible help with organizing our labs. I really value your work and I think every lab should have a Phebe! ☺ Mariella, thank you for your kindness and for the nice conversations and the best of luck with finishing your PhD! To Laura, thank you for your support, for all the nice moments and for your collaboration on the Cell Rep paper. I sincerely wish you all the luck and all the best for your future! To Marina and Martin, thank you very much for the great and useful scientific discussions! To all the other members, including Nanda, Bart (Arcade Fire rules!!), Margriet, Kah Wai, Bas, Sam, Petra, Max, Marleen, Dieudonnée, Michael, Hai Yin, Josta, Joanna, Riccardo, Cao, Roderick, Anne, Cátia, Marta, Marijn, Myrrhe, Robert, Karin, Harold, Philipp, Anaël, Lena, Helena, Amélie, Inês and Ricardo (the one who left but should have stayed☺), thank you for the nice environment, coffee corner chats, house warming parties and work discussions!

To Sander van den Heuvel, Paul van Bergen en Henegouwen, Mike Boxem and all the members of their labs and to Willie Geerts and Fons Cremers, thank you for the great Monday Lunch talks and the nice chats I had with you! To Rachid, the happiest person on Earth ☺, thank you for your always ready smile, I wish you all the best!

To my dear friend Antonio, thank you for your kindness, friendship, support and for our lunches in Antwerp to talk about the stuff that really matters… Good luck with finishing your PhD!

To Susana Gouveia, thank you for your help when I arrived in Rotterdam and for all the nice dinners we had together! Thank you also for introducing me to your friends and for all the fun every time we meet!!

To Cláudia and Tiago, thank you very much for your support and friendship. You were very important to me and I will always remember the nice moments we spent together in The Netherlands and in the UK!

To André and Claudia, thank you so much for your help when I moved to Utrecht, for the dinners at your place and for your kindness! To Ritinha, my Nashville and country music lover girl, thank you for your support, for the visits to Utrecht and for the super interesting nights we spent in interesting places in Amsterdam… ☺

To Sandra Videira, thank you for the patience and chocolates while I was writing my thesis ☺ and I wish you all the luck with finishing your PhD!!

To Elsa Logarinho, thank you so much for your support, your example as a scientist and a woman and for your friendship!

À Lilia, por te teres tornado uma amiga tão querida, pelo teu exemplo de força e tenacidade, pelas aventuras em NYC e por tudo o que temos partilhado nos últimos anos, obrigada! Desejo-te o maior sucesso na tua carreira e que, juntamente com o Miguel, o vosso bebé e as vossas famílias, sejas sempre muito feliz!

À Tanocas e à Joaninha, obrigada pela vossa amizade de tantos anos, pela vossa visita a Utrecht e por todo o apoio que sempre me deram!

To Cátia, thank you for your support, good energy and for sharing your enthusiasm about movies and music!!!! Good luck with your PhD and I wish you all the best Pimpolha! ☺ To Marta, or Martita, a very special thank you!! You arrived short after I started my PhD and we have been through so many things together… Thank you for your friendship, support, for the nice trips to Belgium, for the dinners, for the endless talks, for your help on the Cell Rep paper and for your pragmatic opinions about everything! I am pretty sure everything will turn out alright for you and I wish you all the luck with finishing your PhD and with everything else in your life!! ☺

To Ines, my chocolate buddy☺, thank you for everything! You joined Casper's lab only 2 years ago, but it looks like you've always been there. Thank you for your incredible support, friendship and for taking so good care of everyone! Thank you also for all the nice discussions about your pericentrin, I really enjoyed it! I wish you all the luck with your postdoc and with your new life with Roland!! I will for sure miss you girls …

To Daniel, Soraia and André, thank you for the amazing dinners and parties we had in Antwerp, Leuven and Utrecht and for our great night conversations!! All the best to you all !!!

À minha Amiga Ana Virgínia, obrigada pelo teu apoio, pela tua amizade incondicional, pelas férias e encontros sempre fantásticos, pelos chats diários no gmail e por tudo o que sempre fizeste por mim! Tens sido, mesmo à distância, um dos meus grandes pilares durante todos estes anos, e isso não tem preço! Gosto muito de ti ☺

Aos meus Padrinhos, pelo vosso apoio , pelas férias em Margarita e em Portugal e por tudo o que sempre fizeram por mim, obrigada! A todos os meus primos, obrigada pelos bons momentos em cada regresso a casa! Ao Rui, Cláudia, João Rui e Matilde, obrigada pelos dias fantásticos que passámos juntos na Holanda! Aos meus tios Quitas e Adriano, obrigada pelo carinho, pelos convívios em vossa casa e pelo apoio e orgulho em mim demonstrado ao longo de tantos anos! Aos meus tios Carminda e João (e à Lassie ☺), obrigada pelo vosso carinho e simpatia em casa regresso a casa!

Aos meus avós, obrigada pelo orgulho que sempre tiveram em mim.

À Inês e à São, obrigada pelo vosso apoio, carinho, por estarem sempre por perto e pela visita à Holanda! Gosto muito de vocês e agradeço-vos por toda a amizade! À minha Nocas, obrigada por seres a miúda mais fantástica do planeta e por seres como és! ☺

À minha Irmã Teresita, obrigada por tudo! Sempre foste um grande apoio e os últimos anos tornaram-te num dos meus grandes pilares! Obrigada por tudo o que tens feito por mim, pelo teu carinho incondicional e por tomares tão bem conta dos nossos pais... Admiro-te pela tua leveza e por tudo o que és e espero que possamos contar sempre uma com a outra! Obrigada por tudo... ☺ Aos meus pais, Gina e Carlos, o meu mais profundo agradecimento por tudo o que são para mim. Pai, obrigada por seres o meu castiço, pelo teu carinho e apoio incondicionais, pelas noites perdidas para me levares ao aeroporto e sempre bem disposto! Obrigada por seres o meu grande exemplo de luta, conquista e preserverança! Mãe, minha melhor Amiga, obrigada por tudo... viveste este doutoramente quase tão intensamente como eu, e isso, parecendo que não, tornou tudo mais leve. Houve momentos menos bons, mas aguentaste-te e nunca me falhaste, mesmo quando quem precisava de apoio eras tu. Obrigada por tudo o que fizeram e fazem por mim. Voces são o que de melhor tenho e prometo que um dia eu volto...

And now, as Daniel Plainview would say “I’m finished!” ☺

Thank you / Dank U / Obrigada,
Andrea